Waste Gasification for Hydrogen Production

Jirat Mankasem

Thesis submitted for Degree of Doctor of Philosophy

Supervisors:

Prof. Dr. Anh N. Phan

Prof. Dr. Thomas Curtis

School of Engineering, Newcastle University, United Kingdom

August 2024

Abstract

Hydrogen, vital in sectors like chemical production, polymer processing, and energy, is expected to see a demand surge to 450 million tonnes by 2050. Its importance in industry, transport, and power is growing, but current production, primarily from fossil fuels (95 million tonnes, 96% of total), significantly contributes to CO_2 emissions (3% of global annual total). To reduce emissions, research is shifting to low-carbon methods like renewable energy-powered water electrolysis and gasification processes. Challenges include the variability of solar and wind energy, nuclear energy's public acceptance and safety, and waste gasification's efficiency and heterogeneity. Effective waste gasification involves pre-treatment and a complex multi-stage process, with separate pyrolysis and gasification reactors improving syngas quality and gasifier efficiency. Addressing the increasing solid waste, responsible for 4.5% of global CO_2 emissions, is crucial, making waste gasification a key focus.

The aim of the PhD project was to investigate the effects of operating conditions on performance of two-stage gasification (TSG) of waste. Key parameters considered include steam to carbon ratio (S/C), stage temperature, heating rate, CO_2 concentration in the carrier gas, and residence time. Hydrogen production from waste via the TSG was also assessed for its environmental impact and sustainability to provide insights into the overall ecological footprint.

Combining CO_2 and steam as gasifying agents resulted in 30% increase in hydrogen content in the producer gas compared to theoretical amount of hydrogen in waste wood. In addition, CO_2/steam TSG reduced up to 93% tar (high molecular weight compounds) in the gas stream compared to steam gasification at the same operating condition (900°C for 1st stage and 1100°C for the 2nd stage at S/C of 5.7. These can be explained due to the synergy between Boudouard and water-gas shift reactions. Based on mass balance analysis, up to 34 wt% CO_2 in the gasifying agent was utilised in the process.

The optimization of the refuse-derived fuel pellets (RDF) TSG, leveraging the response surface methodology (RSM) for enhanced efficiency. This led to the discovery of optimal conditions for RDF-TSG: 1st stage temperature of 587°C, 2nd stage temperature of 924°C, S/C of 2.6, and a CO_2 flow rate of 100 cm^3/min. Under these conditions, it achieved a remarkable hydrogen yield of 93.4±1.2 mg/g RDF and a process efficiency of 67.0±0.7%.

The life cycle assessment (LCA) study revealed that RDF yielded 4-7 g CO_2 eq/kg H_2 through TSG. Local waste wood TSG resulted in emissions between 0.9-2.0 kg CO_2 eq/kg H_2. However, the origin and transportation of waste wood, especially from countries like the USA, Canada, Latvia, and the Netherlands, increased emissions to around 5 kg CO_2 eq/kg H_2, challenging its classification as UK low carbon hydrogen. With carbon capture and storage (CCS) technology, emissions from waste wood TSG were reduced to approximately -1.3 kg CO_2 eq/kg H_2, and RDF TSG to 0.4 kg CO_2 eq/kg H_2 in the UK context.

This thesis establishes a benchmark for multi-stage gasifier plant advancements, merging fundamental concepts with practical outcomes. It highlights the necessity for future research on blending RDF with waste wood to reduce environmental impacts and increase CO_2 utilization in carrier gas. It also encourages detailed studies on scaling up these technologies. The included LCA provides vital information for decision-makers in policy, industry, and academia, aiding in comparative analyses and shaping future hydrogen production strategies.

List of publications

List of publication from this thesis:

1. Mankasem, J., Prasertcharoensuk, P. and Phan, A.N., 2024. Intensification of two-stage biomass gasification for hydrogen production. International Journal of Hydrogen Energy. 49(A), 189-202.
2. Optimization of RDF gasification using CO_2 and steam for high hydrogen producer gas production, Fuel (in preparation)
3. Life cycle assessment of H_2 production system based on two-stage gasification (in preparation)

List of conference poster and oral presentations from this thesis:

1. Poster presentation titled "CO_2-steam Gasification with Wood Pellets Using Two-stage Gasifier to Produce Hydrogen-rich Syngas: A Study of Operational Factors" at the 13th Samaggi Academic Conference and Careers Fairs (SACC) 2021, Online, 21st February 2021.
2. Poster presentation titled "Gasification of Waste Biomass for Hydrogen Production: Effects of Gasification Parameters" at the 29th European Biomass Conference and Exhibition (EUBCE), Online, 28th April 2021.
3. Oral presentation titled "CO_2-steam Gasification with Waste Wood Pellets Using Two-stage Gasifier to Produce Hydrogen-rich Syngas: A Study of Operational Factors" at the 8th International Conference Sustainable Energy and Environment (SEE 2022), The Knowledge Xchange (KX), Bangkok, Thailand, 7-9 November 2022.
4. Oral presentation titled "Carbon dioxide steam gasification with wood pellets using two-stage gasifier to produce hydrogen-rich syngas: A Study of Operational Factors" at the International Symposium on Emerging Trends in Role and Production of Bioenergy for Sustainable Development (ETBSD) 2022, Korea republic, online presentation, 4-5 July 2022.
5. Oral presentation titled "Wood Pellets Two-stage Gasification using CO2-steam to Produce Hydrogen-rich Syngas" at the 31st European Biomass Conference and Exhibition (EUBCE), Bologna, Italy, 5-9 June 2023.
6. Oral presentation titled "Enhancing Hydrogen Production through Two-Step Wood and RDF Pellets Gasification with CO2- Steam as Gasifying Agent: An Optimization Study" at the 2nd Fuel and Energy Research Forum (FERIA), Sheffield, UK, 4-6 September 2023.

To myself

You tried

Acknowledgements

I would like to extend my sincere gratitude to the following individuals for their support and contributions during the course of my PhD thesis.

First and foremost, I would like to thank Professor Anh N. Phan for her invaluable guidance and support in developing this thesis.
Dr. Thomas Curtis for his guidance in both my thesis and life.
Dr. David A. Hernandez for his support in the computational fluid dynamics (CFD) modelling.
Dr. Paul Bilsborrow for introducing me to this research area and introducing me to Prof. Dr. Anh Phan.
Dr. Phuet Prasertcharoensuk for teaching me the necessary experiments and analysis.
Rob Dixon for providing me with important knowledge on hazards and safety in the lab.
Iain Strong for his help with equipment modification.
Dr. Long Duong for his assistance with GC-analysis and valuable knowledge in the field.
Bernard Bowler for his help with the TGA-MS analysis.
Dr. Alex Charlton for his help with C,H,N,S analysis and GC-MS analysis.
Catrona Beeney for providing me with the refuse-derived fuel for this study.
Nathan Hughes for providing me with the RDF pellets for this study.
Ashley Craig for helping with technician problems.
Chris Ottley for his help with the ICP.
Dr. Isabel Arce-Garcia for her help with the SEM-EDx.
Paul Sterling for his help in moving the gas cylinders.
Eric Gray for his assistance in modifying the reactor and equipment in this study.
Onos Esegbue for his help with the TGA-MS analysis.
Roy Proud for his help in fixing the heater and setting it up.
Robyn Hare for blowing the glassware for this study.
Nick Royston and Gerardo Martinez for his help with the RDF pyrolysis experiment.

Finally, I would like to extend my deepest gratitude to my parents and sister, Saroad Mankasem, Jeerawan Mankasem and Siriwan Mankasem, for their unwavering support and encouragement throughout my academic journey.

Table of contents

List of Figures

List of Tables

Nomenclature

ABS	Acrylonitrile butadiene
AWE	Alkaline water electrolysis
BET	Brunanuer-Emmett-Teller
BS	British standard
CCE	Carbon conversion efficiency
CCS	Carbon capture and storage
CFD	Computational fluid dynamics
CGE	Cold gas efficiency
CHP	Combined heat and power
C_p	Specific heat capacity
DSC	Differential scanning calorimetry
EDx	Energy-dispersive X-ray
FB	Fluidized bed
FC	Fixed carbon
FID	Flame ionisation detector
FT	Fischer-Tropsch
FTIR	Fourier-transform infrared spectroscopy
GC	Gas chromatography
GC-MS	Gas chromatography-mass spectrometry
HDPE	High-density polyethylene
HHV	Higher heating value
IC	Internal combustion
ICP-MS	Inductively coupled plasma-mass spectrometry
IEA	International Energy Agency
ISO	International Standard Organisation
LCA	Life cycle assessment
LDPE	Low-density polyethylene
LHV	Lower heating value
m/z	Mass to charge ratio
MSW	Municipal solid waste
PA	Polyamide or nylons
PAHs	Polycyclic aromatic hydrocarbons

PBT	Polybutylene terephthalate
PE	Polyethylene
PEM	Proton exchange membrane
PET	Polyethylene terephthalate
PM2.5	Particle matter below 2.5 micron
POX	Partial oxidation of oil products
PP	Polypropylene
PSA	Pressure swing adsorption
PVC	Polyvinyl chloride
RDF	Refused derived fuel
RSM	Response surface methodology
S/B	Steam to biomass waste ratio (kg/kg)
S/C	Steam to carbon ratio (mol/mol)
S/RDF	Steam to RDF ratio (kg/kg)
SEM	Scanning electron microscopy
SMR	Steam methane reforming
SOE	Solid oxide electrolysis
TCD	Thermal conductivity detector
TGA	Thermogravimetric analysis
TSG	Two-stage gasification
VM	Volatile matter
WGS	Water gas shift
WP	Wood pellets

Chapter 1 Introduction

Hydrogen is increasingly recognized as a pivotal energy carrier for the forthcoming century, owing to its high calorific value (120-142 MJ/kg) and the fact that its combustion yields no emissions (Rasul et al., 2022). Its role as a fundamental component in various industries, such as ammonia, methanol, liquid fuel production, and even in more traditional sectors like iron production, is noteworthy. However, a critical issue is that over 98% of current hydrogen production originates from fossil fuels (Ji and Wang, 2021), contributing approximately 900 million tonnes of CO_2 equivalent annually, accounting for 2-3% of global CO_2 emissions (Liu et al., 2022). Regarding policy development, by 2022, 32 countries had implemented hydrogen strategies focusing on increasing hydrogen production capacity, developing infrastructure for hydrogen storage and distribution, promoting research and development in hydrogen technologies, and encouraging the adoption of hydrogen in various sectors such as transportation, industry, and energy, establishing national objectives that vary between 160 and 210 gigawatts (International Energy Agency, 2023a).

An alternative method for producing hydrogen-rich gas is through gasification, a technology that has been known since World War II, because it offers a flexible and efficient way to convert various materials, including coal, biomass, and waste, into valuable syngas. Gasification is a complex process that transforms carbonaceous materials into producer gas through a series of stages (Basu, 2018). Initially, the feedstock is dried, followed by pyrolysis in the absence of oxygen, where it is decomposed using heat. The material then undergoes partial combustion before entering the final stage of gasification. This entire process takes place in a specialized reactor called a gasifier, which operates at temperatures ranging from 700°C to 1300°C (Rogoff and Screve, 2019). Various mediums like air, oxygen, steam, or carbon dioxide are used in the gasification process. The gas produced primarily consists of hydrogen (H_2) and carbon monoxide (CO), along with lesser amounts of carbon dioxide (CO_2), methane (CH_4), and other hydrocarbons (Cerone et al., 2016). The quality and characteristics of the gas are influenced by several factors, including the type of feedstock, the gasifying agent used, operational temperature and pressure, the design of the reactor, and the application of catalysts or sorbents (Karuppiah et al., 2022). Gasification has wide-ranging applications such as in the production of syngas, generation of heat and power, creation of biofuels, fertilizers, and char (Koppatz et al., 2009, Speight, 2014, Rogoff and Screve, 2019).

In light of COP28's recommendations, which emphasize the cessation of new fossil fuel-based projects to maintain global temperature increases below 1.5°C from pre-industrial levels (Birol, 2023), there is growing interest in utilizing biomass waste and municipal solid waste in the energy sector. However, conventional gasifiers like single stage gasifier face challenges in processing these materials due to their distinct properties. Biomass waste and municipal solid waste, despite their potentially high calorific value, present issues such as heterogeneity in size and composition, necessitating pre-treatment before gasification. This requirement has led to a more than 2-14% annual increase in waste pellet production (Fernandez, 2023). Pelletisation not only reduces heterogeneity but also helps control and maintain waste quality by providing uniform size and shape, reducing moisture content, and increasing bulk density, thereby mitigating operational issues in gasifiers such as blockages, irregular feedstock flow, and inefficient gasification processes (Simone et al., 2012).

Another challenge with waste material is the high ash and tar content post-gasification. Coal gasification typically occurs in a single reactor to maximize efficiency through energy transfer from the oxidation zone to other endothermic reactions (Shahabuddin, 2022). Coal's characteristics, notably its high fixed carbon content and slower reaction compared to the volatile matter abundant in biomass waste and plastic-rich waste, necessitate adjustments in processing (Waldheim, 2018).

To accommodate waste in gasifiers, pre-treatment to reduce moisture and volatile matter is essential. This can be achieved by integrating a pyrolysis reactor prior to the gasification reactor, a concept known as multi-stage gasification (Bui et al., 1994). Such pre-treatment reduces moisture and volatile matter, resulting in an increase in fixed carbon content. This modification renders waste characteristics more akin to fossil fuels, enabling the application of existing gasification technologies. Additionally, multi-stage gasification facilitates more extended reaction times between volatile matter, steam, and other gasifying agents within char, resulting in a syngas with lower tar content compared to traditional gasifiers (Gøbel et al., 2002).

However, segmenting the gasification process into multiple stages can reduce energy efficiency, as it necessitates external energy inputs. Fortunately, the global shift towards renewable energy, with its surplus energy potential, could be harnessed to power these multi-stage gasifiers, paving the way for producing purer and cleaner gas.

The primary objective of this study is to comprehensively analyse the impact of various operating conditions and the interplay of waste wood and Refuse-Derived Fuel (RDF) compositions in a two-stage steam gasification process, with a focus on optimizing hydrogen and syngas production. To systematically approach this goal, the study is structured around several key objectives:

1. **Analysis of operational condition:** This component entails a detailed study of how various operational parameters, such as temperature, steam input, carrier gas selection, residence time, and the specific characteristics of waste wood and RDF, influence the two-stage gasification process. By examining these factors, the study aims to identify optimal conditions for maximum yield and efficiency in hydrogen and syngas production.
2. **Examination of the thermal and chemical impact of waste composition:** This objective focuses on understanding how the unique composition of waste wood and RDFs affects their thermochemical behaviour during gasification. This analysis is vital for tailoring the gasification process to different feedstock compositions, thereby maximizing output and efficiency.
3. **Analyse the environmental implications of the two-stage gasification process for producing hydrogen utilizing waste materials:** This objective involves integrating laboratory data with literature-based models to construct a hydrogen production system. The study will then compare the environmental performance of this system with existing methods documented in the Ecoinvent database, focusing on sustainability and emission metrics.

Through these targeted objectives, the study seeks to advance the knowledge and technology of steam gasification, contributing to the development of more sustainable and efficient methods for hydrogen and syngas production from waste materials.

The novelty of the study lies in its demonstration of significantly enhanced hydrogen production from waste wood pellets through a two-stage gasification process, achieving up to 88 mg of hydrogen per gram, which exceeds theoretical yields. This is accomplished by recycling CO_2, improving carbon conversion efficiency by 3-12%, and reducing tar content by up to 93%. The process effectively utilizes CO_2, leading to higher efficiency and sustainability. Additionally, the use of CO_2 as a carrier gas in pyrolysis results in improved gas yields and reduced harmful chemicals. The study also optimizes RDF gasification using Response Surface Methodology, identifying conditions that maximize hydrogen production and process efficiency. Furthermore,

a life cycle assessment compares traditional and innovative hydrogen production methods, highlighting the environmental benefits and potential of CO_2 recycling and carbon capture and storage (CCS) in gasification processes.

This thesis is systematically organized into seven comprehensive chapters, each addressing distinct aspects of the research.

Chapter 1: Introduction - This chapter lays the foundational context for the study, articulating the motivation and background. It succinctly presents the overarching aim and specific objectives of the research, setting the stage for a detailed exploration of the subject matter.

Chapter 2: Literature review - An extensive literature review is presented, encapsulating three main areas: gasification technology (covering its history, principles, operational factors, types of reactors, applications of syngas, and associated challenges), waste gasification (exploring the problems and opportunities associated with waste, wood pellets, RDF pellets, and existing research in waste gasification), and the life cycle assessment (LCA) of hydrogen production technology (including the history of LCA, its principles, an overview of hydrogen as an energy carrier, a brief on various hydrogen production methods, and previous LCA studies).

Chapter 3: Materials, methodology, and calculations - This chapter delves into the materials used, specifically the characteristics of waste wood and RDF pellets, and outlines the detailed methodology, including various analysis methods such as Proximate analysis, C, H, N, S analysis, TGA, Inorganic compounds analysis, and SEM-EDx. It also describes the two-stage gasification process and the subsequent analysis of its products. Additionally, the chapter includes the calculations for mass balance, product yields, and efficiencies.

Chapter 4: Enhancing wood pellet gasification for increased hydrogen yield - Here, the focus is on enhancing the process of wood pellet gasification to boost hydrogen yield. It includes an analysis of the products at each stage (1^{st} and 2^{nd} stage) and examines the effects of varying operational factors within CO_2/steam gasification atmospheres.

Chapter 5: Optimization of RDF CO_2/steam two-stage gasification - This chapter describes the use of Response Surface Methodology (RSM) to optimize conditions for maximizing hydrogen yields from waste in RDF CO_2/steam two-stage gasification. It also details the use of

an isothermal process to simulate continuous stages, along with an analysis of the products at each stage.

Chapter 6: Life cycle assessment of hydrogen production processes - Based on lab data from Chapters 4 and 5, this chapter conducts a life cycle assessment of hydrogen production processes, comparing them with existing methods like steam methane reforming (SMR), fluidised bed gasification of coal, biomass waste, and RDF, Partial Oxidation of Oil Products (POX), and water electrolysis using various energy sources (coal, wind, solar, nuclear). The evaluation employs the Ecoinvent database alongside the ReCiPe2016 impact methodology to conduct a comprehensive analysis of environmental, human health, and resource impacts. This assessment follows a cradle-to-cradle approach, encompassing a time frame of 100 years.

Chapter 7: Conclusion - The final chapter concludes with key findings and offers recommendations for future research, providing a comprehensive closure to the study.
Each chapter builds upon the last, culminating in a thorough and methodical exploration of the gasification process, its optimization for hydrogen production, and its environmental impact.

Chapter 2 Literature review

This chapter provides an overview gasification technology, focusing on hydrogen production. Critical analysis of the current development and challenges of gasification for municipal solid waste and biomass waste is included. The chapter also analyses the sustainability of hydrogen production from various routes of hydrogen production methods.

2.1 Gasification

Gasification is a thermochemical process in limited air/oxygen in a temperature range of 700°C-1300 °C (Rogoff and Screve, 2019) to convert organic/carbonaceous materials into producer gas. The process involves several stages: drying, pyrolysis (known as devolatilization), gasification (Figure 2.1).

Depending upon gasifying agent (air, oxygen, steam, CO_2 or their combination), the gasification step can be divided into sub-steps: oxidation and reduction, where volatiles will be oxidised in the presence of oxygen (exothermic step) and then reactions between gas species and carbon (endothermic step). The producer gas will be cleaned and purified to producer synthetic gas (known as syngas) containing mainly hydrogen (H_2) and carbon monoxide (CO), with smaller amounts of carbon dioxide (CO_2), methane (CH_4), and other hydrocarbons (Cerone et al., 2016). The syngas, depending upon the ratio of H_2/CO and impurities can be used for energy production, hydrogen production, further processed for fuels and chemicals Basu (2018).

2.1.1 History and current gasification plant

In 1684, John Clayton made a significant discovery by heating coal in the absence of air, producing a previously unknown gas which he stored in a bladder. This early experiment in what is now known as pyrolysis was showcased at the British Royal Society, highlighting the flammability of the resulting 'producer gas'. In 1788, Robert Gardner proposed using the excess heat from this gas to enhance steam temperature, a concept considered the first gasification patent. By 1792, William Murdock introduced lighting in the UK using coal gas, marking a pivotal moment in gasification technology's application for lighting and heating, and later for electricity generation when connected to gas engines in 1878 (Kaupp and Goss, 1984).
Gasification technology saw extensive use during World War II as countries sought independence from fossil fuels, especially crude oil. Notably, in Sweden, 90% of cars were

converted to producer gas engines, with nearly half of the feedstock coming from biomass waste (Basu, 2018). However, post-war, with the decline in oil prices, biomass waste gasification technology waned as fossil fuel combustion and gasification gained prominence.

The 1973 oil crisis reignited interest in biomass waste gasification due to concerns over energy security. This led to a resurgence in coal gasification development, culminating in the operation of the first commercial gasification plant in the USA in 1977 (Russel, 1977). The turn of the millennium marked a heightened awareness of the impact of fossil fuels on global warming. Efforts to replace fossil fuels with renewable materials like biomass waste regained momentum, spurring renewed research into biomass waste gasification designs (Knoef, 2005). This shift represents a significant move towards sustainable energy solutions and a departure from the reliance on traditional fossil fuels.

The issue of waste management has become increasingly urgent, with only 45% of household waste being recycled in the UK as of 2020 (DEFRA, 2020). A significant portion of this waste includes plastics, which are notoriously difficult to degrade environmentally and often contribute to marine pollution (Shen et al., 2020). Compounding this challenge, various developing countries, including China, have ceased importing waste from Western nations, intensifying the need for efficient waste management solutions (Huang et al., 2020).

In response to this growing crisis, gasification plants are emerging as a viable solution. These facilities are increasingly utilizing municipal solid waste, industrial waste or biomass waste as alternatives to coal for the production of chemicals and syngas. A notable example is the Enerkem company, which processes 100,000 tonnes of refuse-derived fuel (RDF) annually to produce approximately 38 million litres of ethanol (Waldheim, 2018).

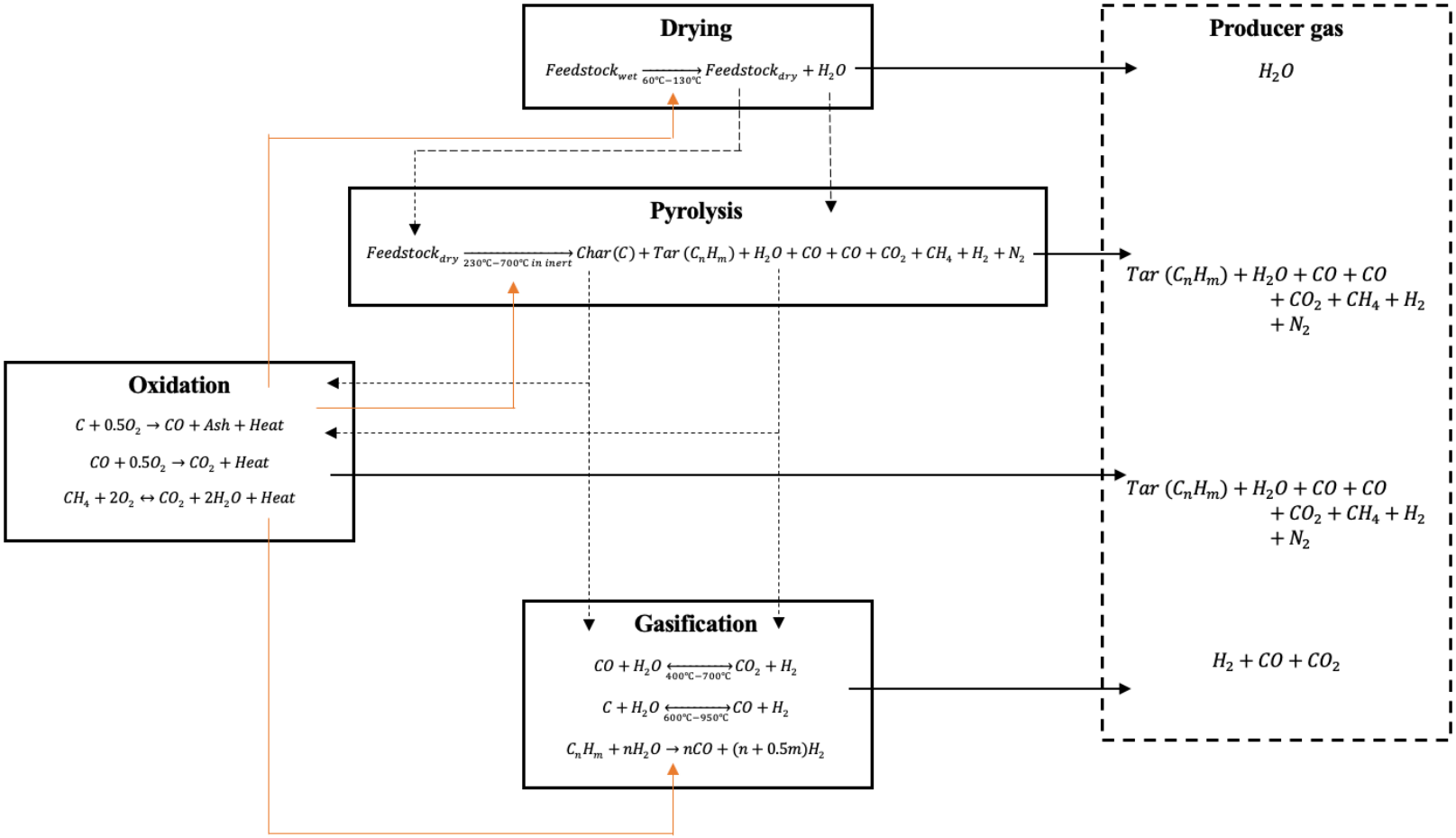

Figure 2.1: Stages in gasification (Luque and Clark, 2010). - The orange arrow symbolizes heat transfer from the oxidation process, while dash arrows indicate the movement of mediated products between processes. Black arrows represent the products generated in each process.

Given this context, recent research in gasification technology is pivoting towards the use of renewable materials and waste. This approach not only addresses waste reduction but also curtails reliance on fossil fuels. The versatility of gasification technology enables the conversion of these materials into valuable products such as heat, electricity, syngas, and chemicals, offering a promising path in both waste management and energy sustainability.

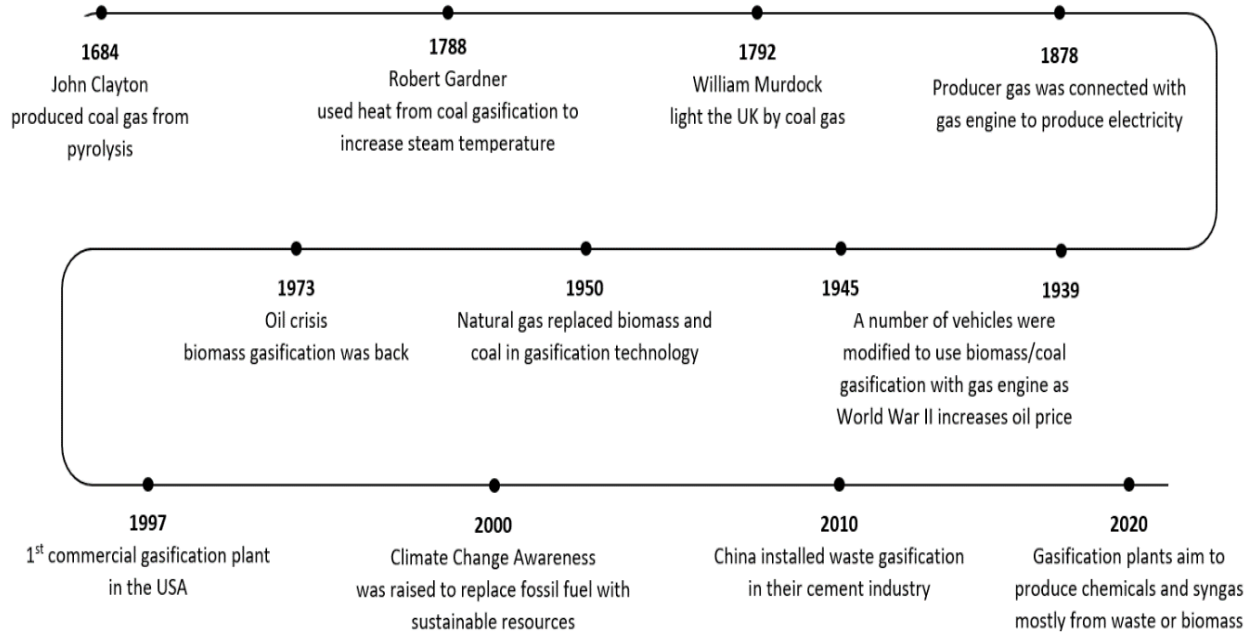

Figure 2.2: Evolution of gasification technology (1680s-2020s)

Approximately 315 gasification plants are operational, considering only those above 100 MW_{th}, with an additional 69 under construction and 155 in the planning stages (IEA, 2023, NETL, 2014, NERL, 2016). Notably, 32 plants are currently non-operational (see Figure 2.3(B)).

China leads globally with 187 gasification plants, followed by the USA, which has 65 (see other countries in Figure 2.3(A)). The field is marked by diversity in technology, with 12 commercial technologies prominent: GE Energy, ConocoPhillips E-Gas, Shell, Siemens, KBR Transport, British Gas Lurgi (BGL), Multi-Purpose (MPG) Gasifier, Lurgi Mark IV Gasifier, MHI Gasifier, U-Gas, High Temperature Winkler Gasifier, and PRENFLO Gasifier/Boiler (PSG). Detailed insights into each technology are available in Breault (2010).

These technologies are categorized based on reactor types are summarized in Table 2.3. In Europe, there are around 40 large-scale gasifiers (exceeding 3MWth), most of which are

transitioning from fossil fuels to biomass sources like waste wood, paper waste, wood chips, wood pellets, plastics, and RDF (Pio and Tarelho, 2021).

While small-scale gasifiers (10-200kW) are challenging to enumerate, their growing popularity is evident, as they enhance biomass waste resource efficiency and decentralize energy systems, fostering local energy access (Patuzzi et al., 2021). The comprehensive list of such small-scale gasifiers provided by Situmorang et al. (2020).

Gasification often integrates with combined heat and power (CHP) technology. Europe alone has over 1700 operational gasifiers. The synthesis of liquid fuels such as methanol, ammonia, hydrogen, or Fischer-Tropsch (FT) derivatives like diesel, kerosene, and petrol typically requires larger-scale gasifiers for economic viability (Hrbek et al., 2021).

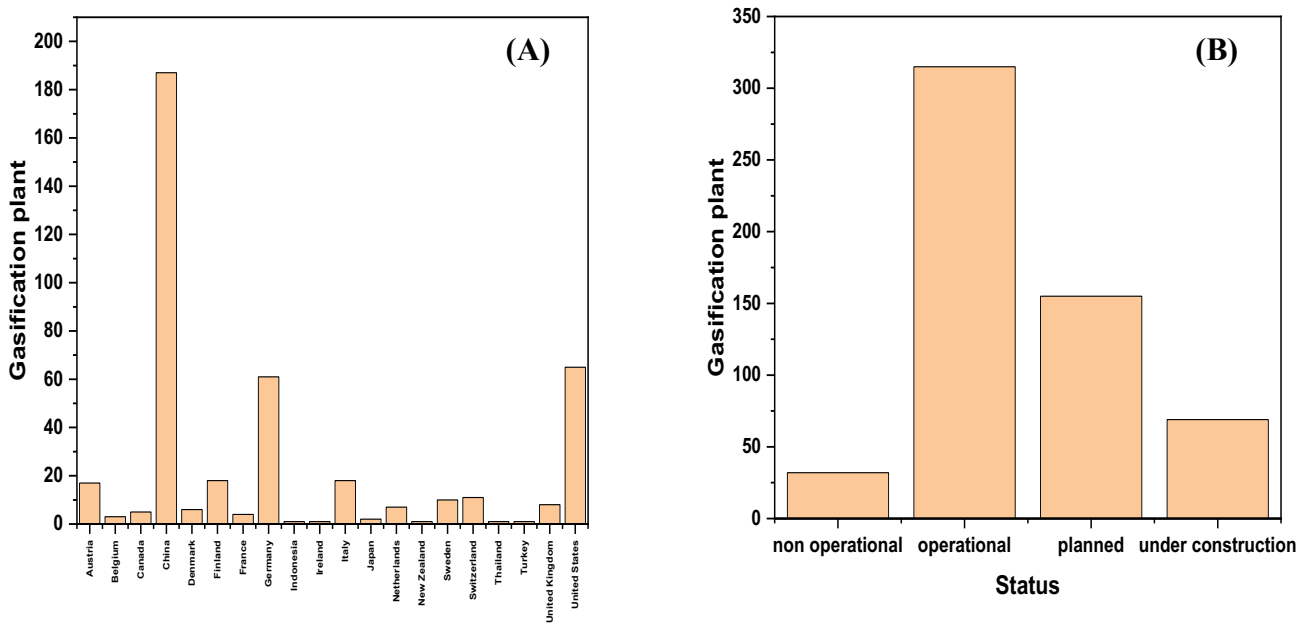

Figure 2.3: Global gasification plants (number of plants) with capacities greater than 100MW_{th} – (A) Distributions in each country and (B) Status (non-operational, operational, planned, and under construction) (IEA, 2023, NETL, 2014, NERL, 2016).

2.1.2 Principle and key reactions

Gasification efficiently preserves a higher proportion of energy in the form of product gases, unlike combustion which predominantly releases energy as heat. This process generates gases such as carbon monoxide (CO), hydrogen (H_2), and methane (CH_4). Unlike combustion,

gasification occurs in an oxygen-limited environment, leading to a distinct set of chemical reactions. These key reactions within the gasification process are detailed in Table 2.1. This lower oxygen atmosphere alters the chemical pathways, making gasification a more controlled and energy-efficient process compared to conventional combustion.
Gasification comprises four primary steps: drying, pyrolysis, partial combustion, and gasification itself.

I) Drying (60°C-130°C): The primary goal of drying is to reduce or eliminate the water content in the feedstock. Excessive moisture leads to energy loss in converting water to steam and can impede critical reactions, such as oxidation (Yuan et al., 2015). There are two types of water in the feedstock: bulk water, which is unbound and behaves like regular water, vaporizing easily; and bound water, absorbed by fibres or textiles, requiring the vaporization of bulk water first to transfer heat effectively (Gezici-Koç et al., 2017). While pure water boils at 100°C under standard atmospheric conditions, in feedstock, moisture vaporizes between 60°C and 130°C.

II) Pyrolysis (230°C-700°C): In an inert atmosphere, carbonaceous materials decompose into gas, liquid, and char. The product composition can be manipulated by adjusting the heating rate - a higher rate typically produces more gas (Chen et al., 2016a). Decomposition temperatures vary: biomass waste, containing hemicellulose, cellulose, and lignin, decomposes at 230°C-400°C and 400°C-700°C (Burhenne et al., 2013), while municipal solid waste, comprising plastics, paper, food, etc., has a broader decomposition temperature range. The exact decomposition temperatures for various materials have been experimentally determined using Thermogravimetric Analysis (TGA) (Aluri, 2018b). Pyrolysis involves heating carbonaceous materials in the absence of oxygen, breaking their bonds to form smaller molecules like acetylene, ethylene, methane, hydrogen, carbon monoxide, carbon dioxide, etc. The residual solid structure, not converted into liquid or gas, is termed char (Basu, 2018).

III) Partial Combustion (1200°C-1400°C): Partial oxidation provides the necessary energy for the process, and for economic reasons, air is typically used instead of pure oxygen (Franco et al., 2003). The temperature can dramatically increase to 1200°C due to highly exothermic reactions. Air is typically introduced in the middle of the reactor to facilitate other endothermic reactions (Siwal et al., 2020), which results in a lower heating value of the producer gas (8-15 MJ/kg biomass waste), compared to steam, as observed by Mishra and Upadhyay (2021). This reaction involves the combustion of char and volatiles with oxygen (see Table 2.1), which is exothermic and releases heat essential for drying, pyrolysis, and gasification reactions

(Mahinpey and Gomez, 2016). However, this combustion process generates harmful emissions, including NOx, SOx, Dioxins, acidic gases, and PM2.5 (Hasselriis and Licata, 1996). To mitigate these emissions, the substitution of this oxidation reaction with renewable energy sources such as wind, solar, or nuclear power is being considered. This approach could reduce emissions, but it's important to note that emissions might be displaced elsewhere, underscoring the need for further. Recent studies, like that of Fang et al. (2021), are exploring the use of solar thermal energy to drive endothermic reactions in small-scale gasifiers.

IV) Gasification (700°C-1300°C): Here, medium agents such as air, oxygen, steam, or CO_2 are introduced to facilitate the oxidation of carbon into gas, solid and liquid products. The composition of the resulting producer gas varies based on these agents. Using air, oxygen, and CO_2 typically results in higher CO and CO_2 content in the producer gas (Wang et al., 2020, Assima et al., 2019). Steam is preferable for hydrogen-rich gas production, reforming carbon into CO_2 and H_2 (Parthasarathy and Narayanan, 2014). Gasification involves complex phase reactions among hydrocarbon liquids, solid carbon char, permanent gases, and medium agents. Key reactions in this process are detailed in Table 2.1.

Table 2.1: Key reactions in gasification

Number	**Name**	**Reactions**	**Enthalpy, kJ/mol**	**References**
Pyrolysis				
R1	Devolatilization	$Biomass \rightarrow char + tar + C_xH_yO_z + H_2O + CO + CO_2 + CH_4 + H_2 + N_2$	Endothermic	(Ranzi et al., 2008)
	Tar reactions			

R2	Thermal cracking	$C_nH_m \rightarrow 0.25mCH_4 + (n - 0.25m)C$	-165 to -505	(Minh, 2018)
R3	Partial oxidation	$C_nH_m + 0.5O_2 \rightarrow nCO + 0.5mH_2$	-715 to -2538	(Glassman et al., 2014)
R4	Steam reforming	$C_nH_m + nH_2O \rightarrow nCO + (n + 0.5m)H_2$	+740 to +2302	(Minh, 2018)
R5	Dry reforming	$C_nH_m + nCO_2 \rightarrow 2nCO + 0.5mH_2$	+980 to +3112	(Gao et al., 2018)
R6		$CH_4 + CO_2 \leftrightarrow 2CO + 2H_2$	+247.3	(Chan et al., 2021)
R7	Hydrogenation	$C_nH_m + (2n - 0.5m)H_2 \rightarrow nCH_4$	-498 to -1815	(Minh, 2018)
Carbon reactions				
R8	Boudouard	$C + CO_2 \leftrightarrow 2CO$	+172	(Wiberg et al., 2001) (Lahijani et al., 2015)
R9	Steam gasification	$C + H_2O \leftrightarrow CO + H_2$	+131	Happened at between 600-950C (Siwal et al., 2020)
R10	Hydrogasification	$C + 2H_2 \leftrightarrow CH_4$	-74.8	(Saraceno et al., 2023)
Oxidation reactions				
R11	Char partial combustion	$C + 0.5O_2 \rightarrow CO$	-111	(Basu, 2018)

R12	Combustion	$C + O_2 \rightarrow CO_2$	-394	(Glassman et al., 2014)
R13	CO partial combustion	$CO + 0.5O_2 \rightarrow CO_2$	-284	(Basu, 2018)
R14	Methane combustion	$CH_4 + 2O_2 \leftrightarrow CO_2 + 2H_2O$	-803	(Lee and Trimm, 1995)
R15	H_2 partial combustion	$H_2 + 0.5O_2 \rightarrow H_2O$	-242	(Basu, 2018)
Methanation reactions				
R16		$2CO + 2H_2 \rightarrow CH_4 + CO_2$	-247	(Basu, 2018) (Wei and Jinlong, 2011)
R17		$CO + 3H_2 \leftrightarrow CH_4 + H_2O$	-206	(Basu, 2018)
R18		$CO_2 + 4H_2 \rightarrow CH_4 + 2H_2O$	-165	(Ashok et al., 2020)
Steam-Reforming reactions				
R19	Water-gas shift	$CO + H_2O \leftrightarrow CO_2 + H_2$	-41.2	(Basu, 2018)
R20	Water-methane shift	$CH_4 + H_2O \leftrightarrow CO + 3H_2$	+206	(Chan et al., 2021)
R21		$CH_4 + 0.5O_2 \rightarrow CO + 2H_2$	-36	(Basu, 2018)
Others				
R22	Methane cracking	$CH_4 \rightarrow 2H_2 + C$	+74.85	(Msheik et al., 2021)

2.1.3 Parameters affecting performances of gasification process

The effect of operational factors on the gasification process can significantly impact the production of syngas. Factors such as pyrolysis temperature, heating rate, and type of gasifying agent can affect the yield, quality, and composition of the syngas produced. The summary of these effects is presented in Table 2.2.

The temperature of the pyrolysis process affects the yield and composition of the solid char, liquid, and gas products produced (Yao et al., 2021). The heating rate can also impact the gas yield, but its effects on the properties of the products are limited (Hu et al., 2022). Different gasifying agents, such as air, oxygen, steam, and CO_2, have different impacts on the quality of the syngas produced. The steam to carbon ratio also affects the content of H_2, CO_2, CH_4, CO, and tar (Valizadeh et al., 2022). In biomass waste steam gasification, an increase in temperature initially increases H_2 and CO, but later leads to a drop in H_2 and a rise in CO_2 and CH_4, while also decreasing the carbon conversion efficiency and tar content (Babatabar and Saidi, 2021).

Table 2.2: Main effects of operational factors on gasification

Operational Factors	**Effect**
Pyrolysis temperature	• Low temperatures (<400°C) favour solid pyrolysis char production (53.6% feed) (Selvarajoo, 2022), higher temperatures (≥450°C-550°C) promote liquid production (49.0-50.3% feed) (de Almeida et al., 2022). • Elevation in temperature above 600°C leads to significant increase in gas yield from 11.2% to 43.2% as pyrolysis temperature is raised from 600 to 800°C (Yao et al., 2021). • Increase in pyrolysis temperature results in faster decomposition, release of volatile compounds, increased surface area (from 38.6m^2/g to 98.4m^2/g at 600°C to 900°C) (Prasertcharoensuk et al., 2019). • The liquid product composition changes with temperature, with some components decreasing (octane, esters, tridecane, xylene, butanone, and most hydrocarbons) and others (PAHs,

	acetic acid, phenolic compounds) increasing (Setter et al., 2020).
Heating rate	• High heating rates can lead to an increase in gas yield and a reduction in char and liquid fractions (Safdari et al., 2019). • Increasing heating rate over 25 °C/min has little impact on the properties of pyrolysis products, suggesting a limited influence of heating rate on their composition and characteristics (Hu et al., 2022).
Gasifying agents	Air • It is widely used as a gasifying agent due to its low cost but produces syngas with low calorific value (3.6-3.9 MJ/Nm^3) and high N_2 (over 52vol% in syngas) content (Antolini et al., 2019). • The high N_2 content requires a separation process, increasing capital and operational costs of the process (Cui et al., 2021). O_2 • Oxygen gasification produces medium calorific value syngas (9-10 MJ/Nm^3) (Niu et al., 2014). • High purity oxygen is expensive to generate (He et al., 2021). Steam • Steam produces high calorific value syngas (15-20 MJ/Nm^3) with high H_2 concentration (over 50vol% in syngas) (Karuppiah et al., 2022). • Requires energy for steam production, reducing process efficiency (Sidek et al., 2020). CO_2 • CO_2 gasification is a potential negative emissions technology that combines waste valorisation and CO_2 conversion to produce CO-rich syngas • high quality syngas (H_2/CO 0.63-1.49) with minimum impurities (<10 g/m^3) and ash residues (<2.4g/m^3) (Mauerhofer et al., 2019). • CO-rich syngas from CO_2-gasification can be mixed with H_2 to form syngas for downstream syntheses and applications

	such as methanol, DME, formaldehyde, ethanol, Fischer-Tropsch fuels, power generation, and hydrogen (Chan et al., 2021). • Lack of research on the effects of CO_2 with different feedstocks and interactions between CO_2 and steam on H_2/syngas production and process efficiency (Prasertcharoensuk, 2019).
Steam to carbon ratio	• Increasing the S/C ratio (0.3-1.9) increase H_2 and CO_2 content while reducing CH_4, CO, and tar formation (Tursun et al., 2016). • H_2 content maximised (52-72 g H_2/kg feed) at S/B ratio of 1.2-3.9 (Cao et al., 2020). • the H_2 content decreasing from 42 mol% to 38 mol% when the S/B ratio reached values of 2.4 and 3.0, respectively (Valizadeh et al., 2022). • An excessive amount of steam leads to a decrease in the gasification temperature by 50°C with the addition of 10ml/h of steam, and it interferes with chemical reactions (Zhang et al., 2022). • Heating value of producer gas decreased with increasing S/B ratio due to higher CO_2 and lower CH_4 in syngas (Li et al., 2021a).
Gasification temperature	• In biomass waste steam gasification, an increase in gasification leads to an initial increase in H_2 and CO, followed by a drop in H_2 and a continued rise in CO after reaching 780°C to 800°C. Conversely, CO_2 and CH_4 decrease during the process (Babatabar and Saidi, 2021). • The carbon conversion efficiency increases and tar content decreases with increasing gasification temperature (Hu et al., 2019).

2.1.4 Reactor types

A gasifier reactor, a critical component in gasification technology, is designed to convert organic or fossil fuel-based carbonaceous materials into carbon monoxide, hydrogen, and carbon dioxide. This is achieved through high-temperature processing with controlled amounts of oxygen and/or steam. There are various types of gasifier reactors, each with its unique advantages and disadvantages, catering to different scales and feedstock requirements (see Table 2.3).

In short, each gasifier reactor type offers unique advantages tailored to specific operational scales and feedstock characteristics. updraft and downdraft gasifiers are more suitable for small-scale operations, with specific preferences for moisture content and feedstock size. Fluidized bed and entrained flow gasifiers cater to larger-scale applications, balancing between high heat transfer rates and tar production. The two-stage gasifier stands out for its efficiency in producing high calorific value gas and its cost-effectiveness, though it necessitates further research for broader biomass waste applicability. The choice of gasifier ultimately depends on the specific requirements of the process, including scale, feedstock type, and desired syngas quality.

Table 2.3: Advantages and disadvantages of gasifier designs

Gasifier types	**Advantages**	**Disadvantages**	**References**
Updraft	High moisture feedstock is acceptable (max 50% by weight). It is suitable for small scale (<20MW) producing heat. Less carbon is in ash (nearly 100% of carbon conversion). Simple	The limitation of feed size and upscale. High tar and slagging production have been produced (up to 100g/m^3). The heating value of producer gas is lower.	(Beohar et al., 2012, Siedlecki et al., 2011)

Downdraft	It is suitable for small scale (<5MW). Low particulates and tar (less than 500 mg/m^3) Simple Dominant (75% of all types in commercial market)	The limitation of feed size and upscale (no longer than 30 cm depending on the size of throat). Moisture of feedstock need to be low (no more than 30% by weight). Producer gas heating value is lower.	(Beohar et al., 2012, Siedlecki et al., 2011)
Fluidized Bed	Large scale is acceptable (10-100MW). Direct or indirect heating can be used. High heat transfer rate. Flexibility	Medium tar production (8-12 g/m^3) High particulate matters (4-20 g/m^3)	(Siedlecki et al., 2011)
Entrained Flow	Large scale is acceptable (>100MW). Very low tar production (0.001-0.08 kg tar/kg biomass waste). High syngas quality (operating at 1200-1500°C which make the gases are close to equilibrium composition)	High particulate matters (0.1-0.2 kg soot/kg biomass waste)	(Billaud et al., 2016)
2-stage gasifier (pyrolysis unit and gasification unit)	Low tar (less than 500mg/m^3)	Need more studies with different types of biomass waste	(Pei et al., 2018, Heidenreich and Foscolo,

	Powder feedstock (lower than 10mm) is acceptable High calorific value of producer gas (1142-1256 kcal/Nm^3) Cheap ($182,690 for 1.5MW)		2015, Brandt et al., 2000)

The concept of multi-stage gasification, first introduced by Bui et al. (1994), marked a significant advancement in gasification technology. It was discovered that tar produced in the first zone (pyrolysis) could be more effectively cracked in the second zone (gasification), resulting in a tar amount 40 times lower than that of single-stage gasifiers. Niu et al. (2019) and Gøbel et al. (2002) both demonstrated the production of low-tar (0.0-1g/Nm3), higher heating value fuel gas (>11.1 MJ/Nm^3) using this method. The process involves physical separation of pyrolysis and gasification, with the volatiles from pyrolysis being partially oxidized and used as the gasification medium. This results in high energy efficiencies and low tar content in the gas.

Nilsson et al. (2012) further improved this process by developing a staged fluidized bed gasifier, which achieved a low concentration of tar, reduced from 31g/Nm^3 to 0.0g/Nm^3, and high process efficiency, increasing from 77% to 82% in CGE and 94% to 97% in CCE. Šulc et al. (2012) also found that a two-stage gasification system (670°C and 950°C) led to a substantial reduction in aromatic compounds and tar content, although it did result in a decrease in gas heating value.

Later, Gunarathne et al. (2016) integrated this multi-stage system, separating pyrolysis, gasification, and oxidation in different reactors, with a steel heat treatment furnace, boosting the total system efficiency by 13%. The concept of multi-stage gasification is drawn in the Figure 2.4.

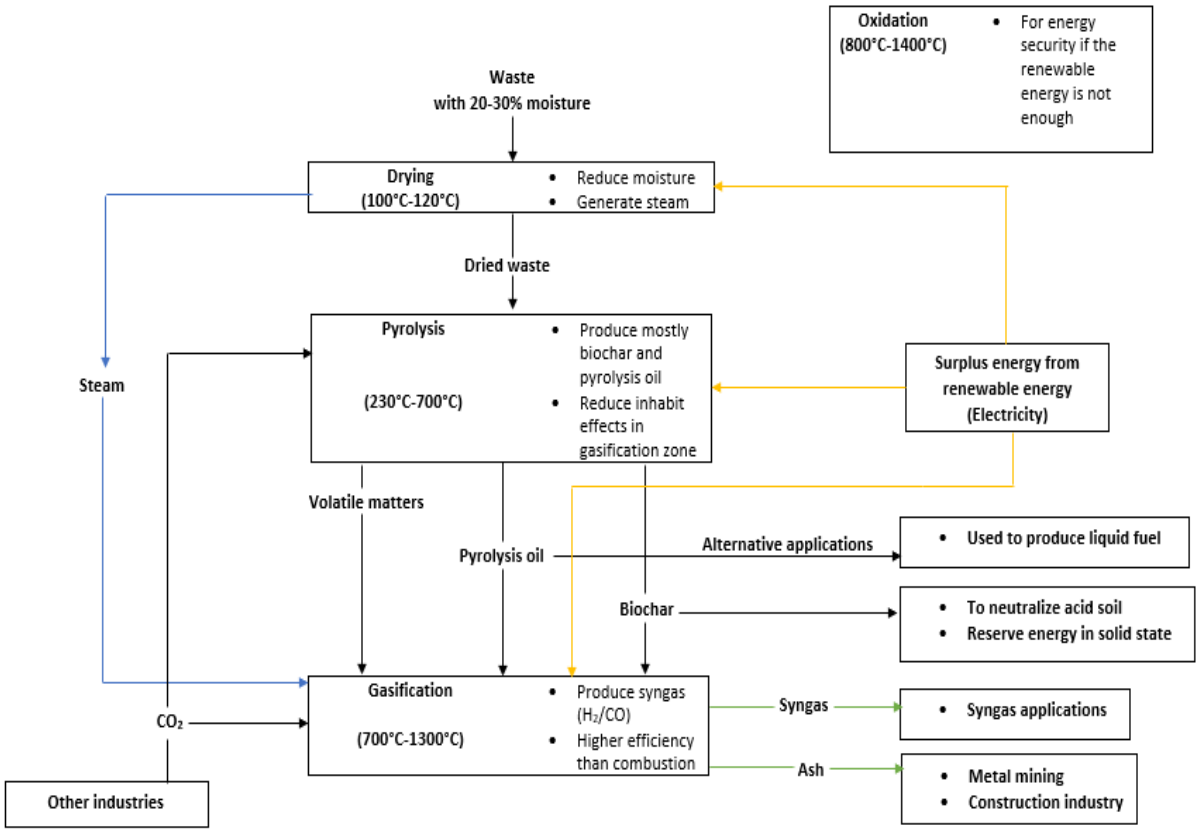

Figure 2.4: Concept of multi-stage gasification highlighting the applications of value added products and potential integrating of renewable energy sources (Bui et al., 1994).

The distinction of having separate pyrolysis and gasification reactors not only yields low-tar syngas but also enhances the efficiency of the gasifier system. A comprehensive review by Mednikov (2018) highlighted various multi-stage gasifiers (see Table 2.4), including two-stage Viking, three-stage FLETGAS, two-stage LT-CFB, two-stage Carbo-V, two-stage CW-700, three-stage WoodRoll, two-stage Stadtwerke Rosenheim, and three-stage BTG gasifiers. These systems have achieved remarkable results, producing tar below 50 mg/m³ and carbon conversion efficiencies over 96%, with hydrogen content reaching up to 58%.

However, despite these advancements, current gasifiers still rely on oxygen, air, or both to supply energy. The potential for producing purer syngas through the use of external, sustainable energy sources, without these oxygenated gasifying agents, remains a promising but under-researched area. Further studies are needed to explore this possibility, especially in a future where renewable energy sources are more readily accessible.

Table 2.4: Overview of multi-stage gasification processes in research, institutes, and companies including their process descriptions and performances

Developers/Institute/Company/etc	**Description**	**Performance**	**Ref**
Danish Technical University	2-stage gasifier which separate pyrolysis and gasification reaction in different reactor. Pyrolysis reactor (700°C-900°C) conveyed by screw feeder to a downdraft gasifier (900°C-1100°C) called "Viking gasifier"	Power: 75kW$_{th}$ Raw material: wood pellets Oxidising agent: Air Producer gas: 32% H_2, 16%CO, 4%CH_4, Tars: <15mg/Nm^3	(Gadsbøll et al., 2018)
University of Sevilla	Three stage gasification 1. Fluidised bed gasification (700°C-800°C) 2. Oxidation/reforming (1200C) 3. Catalytic filtration	Raw material: Sewage sludge Oxidising agent: Air/steam Producer gas: 12-21%H_2	(Cano, 2013)
DONG Energy Co.	Low-temperature circulating fluidised bed (LT-CFB) gasifier: 1. CFB pyrolysis reactor (650°C) 2. Bubbling FBG (730°C)	Power: 100-500kWth Tar: > 5000 mg/m^3 Raw material: Coal Oxidising agent: Air	(Thomsen et al., 2017)

	Note: low temperature at first stage is responsible for retention of alkaline in ash	Producer gas: 3.5%H_2, 16.3%CO, 16.9%CO_2 4.3%CH_4, 59%N_2	
FLETGAS	The FLETGAS system uses a three-stage process: First, oxidative pyrolysis at 700°C–800°C optimizes gas production. Second, pyrolysis gas undergoes tar decomposition at 1200°C. Finally, char is processed in a gasification reactor	Tar: <10 mg/Nm^3 Producer gas: 8%H_2, 13%CO, 15%CO_2 4%CH_4, 58%N_2 CCE: 83-96%	(Mednikov, 2018)
Choren Industries	This gasifier called "Carbo-V gasifier" Thet are 3-stage gasification process including pyrolysis (400°C-500°C), combustion (1400°C), and gasification of char (800°C)	Tar: 0 mg/Nm^3 (cannot detected) Producer gas: 31-33%H_2, 38-41%CO, 24-27%CO_2 <0.2%CH_4, 1-2%N_2 CCE: >99%	(Mednikov, 2018)
Cortus Energy	This gasifier called "WoodRoll gasifier" This involves three stages: drying (105°C),	Tar: <30 mg/Nm^3 Producer gas:	(Mednikov, 2018)

	pyrolysis in N_2 (400°C-500°C), and gasification with steam (1100°C).	55-58%H_2, 25-31%CO, 12-16%CO_2 <2%CH_4, 0%N_2 CCE: 84-94%	
SynCraft Engineering GmbH	This gasifier called "CW-700 gasifier" this two-stage gasification process involves drying biomass waste, followed by pyrolysis at 500°C, and then gasification at 850°C.	Tar: <50 mg/Nm^3 Producer gas: 18%H_2, 20%CO, 15%CO_2 2%CH_4, 45%N_2 CCE: 90%	(Mednikov, 2018)
Stadtwerke Rosenheim GmbH and Co. KG	This gasifier called "Stadtwerke Rosenheim gasifier" They involves a screw pyrolysis reactor at 700°C, followed by gasification in an air-blown fluidized-bed at 900°C–950°C.	Tar: 0 mg/Nm^3 Producer gas: 20%H_2, 22%CO, 10% CO_2 3%CH_4, 35%N_2 CCE: none	(Mednikov, 2018)
Biomass Technology Group (BTG)	This gasifier called "BTG gasifier" They involves fast ablation pyrolysis at 450°C-600°C, followed by combustion ad gasification (air-steam at 800°C-950°C) in a fluidized bed.	Tar: 0 mg/Nm^3 Producer gas: 18-25%H_2, 19-25%CO, 14-16%CO_2 4-5%CH_4, 12-35%N_2 CCE: none	(Mednikov, 2018)

Vikhrevye sistemy	This gasifier called "OOO Vikhrevye sistemy gasifier" They features a vertical stainless-steel housing with distinct parts for biomass waste pyrolysis and gasification. Air is heated to 300°C and fed into both zones, with the pyrolysis and gasification processes occurring at 580°C-600°C.	Tar: none Producer gas: 25%H_2, 32%CO, 0%CO_2 3%CH_4, 40%N_2 CCE: none	(Mednikov, 2018)

2.1.5 Gasification products and their application

The gasification of waste can yield a high-quality product gas (75-99% of waste), and pyrolysis char or residue (gasification char) (12-33%) (Zaini, 2019, Win, 2019, Schweitzer et al., 2018). The producer gas with increased hydrogen content, suitable for a range of applications including combined heat and power production, fuel cell operation, liquid fuel conversion, and synthetic natural gas and hydrogen generation (Koppatz et al., 2009, Speight, 2014, Rogoff and Screve, 2019). The syngas is a precursor for synthesis liquid fuels through the Fischer-Tropsch process. This technique transforms solid waste into valuable fuels like bio-oil, biodiesel, methanol, and ethanol, thereby converting waste materials into usable energy forms (Placido et al., 2018). The versatility of gasification in producing a range of gases and fuels underscores its significance in the transition towards more sustainable energy and chemical production.

However, challenges remain in gasification and downstream processing, particularly in understanding the effects of operating conditions on gasification reactions and optimizing product compositions (Kumar et al., 2009). Impurities such as tar, particulate matters, and poisonous gases produced during gasification can create problems in downstream applications, necessitating gas cleaning before utilization (Asadullah, 2014). The Table 2.5 shows the limitation and issues for each application for producer gas from gasification

Char, a product of gasification, exhibits porous characteristics and a high surface area, making it an effective catalyst for various processes (Leng et al., 2021). Notably, char serves as a solid form of energy storage. Its reduced density and increased H/O ratio enhance its calorific value, as detailed in Table 2.6. This transformation not only diminishes transportation costs but also augments grinding efficiency, especially when higher production rates are required (Widjaya et al., 2018). Conversely, ash, often considered an undesirable by-product of gasification, holds potential in the construction industry (Li et al., 2023). The utilization of ash from waste incineration in the construction industry can significantly reduce cement usage, with reductions ranging from 50-85% as detailed in Lam et al. (2010). Future prospects include extracting rare elements from this slag, aligning with the escalating demand for rare earth elements propelled by the renewable energy sector's growth (Fu et al., 2022).

Table 2.5: Limitation of syngas compounds categorized by downstream applications. All data is stated without reference, it is from (Waldheim, 2018).

Contaminants	**Applications**					
	Direct Combustion	**Gas Engine**	**Gas Turbine**	**Fuel Cell**	**FT Synthesis**	**Methanol Synthesis**
Challenges	No need for cleaning if the gas travel freely -Flue gas after combustion must be cleaned sufficiently to meet local emission requirements(Basu, 2018)	The gas must be cooled, which causes tar to condense. The piston-cylinder is not designed for solid particles (Basu, 2018).	Gas turbine sensitives to cleanliness (Basu, 2018)	Sensitive to cleanliness especially Proton Exchange membrane (PEM), use catalyst like Pt that are highly sensitive to impurities (S, NH_3, tar)	FT synthesis relies on Fe and Co based catalyst which are highly sensitive to S, N, and halides	Methanol synthesis relies on Cu- based catalyst which are highly sensitive to S, Cl, and heavy metals

Particles (mg/Nm^3)	No limit specified	< 50	< 10	< 0.1	< 0-0.1	< 1
Tar (mg/Nm^3)	No limit specified	< 50	< 10	n.a.	0.1-1	< 1
Sulphur (ppm)		< 20-50	< 20	< 1 SOFC < 0.06-10 PAFC < 50 MC < 0.5	< 1-0.01	< 1-0.1
Nitrogen (ppm)		< 80	< 50 (emission limit)	Not limited	< 1-0.02	< 0.1-10
Alkali (ppm)		< 0.025-0.1	< 0.025-0.1		< 0.01	n.a.
Halide, Cl, F, Br (ppm)		< 100	< 1	< 1	< 0.01	< 0.01-0.1

2.2 Waste gasification

The total worldwide generation of municipal solid waste (MSW) is increasing, with 2.02 billion tons generated in 2016, and predictions estimate an increase to 2.59 billion tons by 2030 and 3.4 billion tons by 2050. On a global scale, the average waste generation per person per day is 0.74 kilograms (see Figure 2.5(A)). The treatment of this waste varies globally, with an average from over 200 countries showing that 37% of waste goes to landfills, 33% is openly dumped, 19% is recovered through recycling and composting, and 11% is treated by incineration (see Figure 2.5(B)). These solid waste management were responsible for generating 1.6 billion tons of CO_2 equivalent, accounting for 4.5% of global emissions. The composition of the waste includes 44% food and green waste, 5% glass, 4% metal, 17% paper and cardboard, 12% plastic, 2% rubber and leather, 2% wood, and 14% from other sources (Kaza et al., 2018).

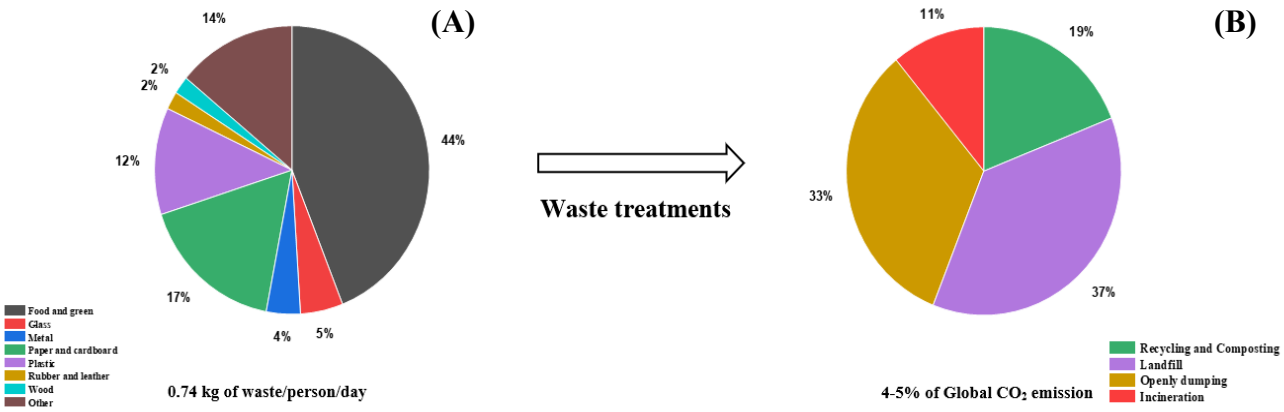

Figure 2.5: (A) Global composition proportions in municipal solid waste (wt% of waste) and (B) fractional distribution of waste treatment methods (wt% of waste) (Kaza et al., 2018).

The design challenges for gasifiers using waste materials, as opposed to coal or biomass waste, are primarily twofold (Waldheim, 2018). Firstly, waste material presents a heterogeneity in size and composition, comprising both combustible and non-combustible elements. The variable quality of waste is influenced by its origin, pre-treatment processes, seasonal changes, and a diverse composition including plastics, paper, and metals. This necessitates a gasifier that can efficiently process a range of material sizes and accommodate the varying quality of waste.

Secondly, Reinmöller et al. (2019) notes that RDF typically contains a significantly higher ash content, approximately 10-30wt%, compared to 1-2wt% in biomass waste and 1-16wt% in coal. Biomass waste gasification usually occurs at temperatures between 800°C and 900°C to ensure thorough burn-out and minimize tar production. However, at these temperatures, the high ash content in waste can combine with metals and hydrocarbons to form slag, leading to operational challenges and complicating the recovery of valuable metals. To mitigate this issue and prevent the oxidation of metals, waste gasifiers typically operate at lower temperatures, ranging from 400°C to 600°C.

Table 2.6: Comparison of proximate and ultimate analysis of agricultural and municipal waste and coal

Feedstock	Moisture	Fixed carbon	Volatile matter	Ash	Carbon	Hydrogen	Oxygen*	Nitrogen	Sulphur	HHV	References
	wt% as received				wt% dried ash free					MJ/kg	
Coal	1-5	46-78	14-51	1-16	52-94	3-6	1-21	0.3-3	0.3-0.6	12-36	(Basu, 2018)
Wood	7-23	10.7-15	74-80.5	0.9-2.3	41-50.7	6-6.7	41-43	0.1-3.0	0.1-3.0	15-21	(Schweitzer et al., 2018)
MSW	45-70	10.7-13.5	83-87	2.7-3.4	53-60	8-9.4	30-38	0.6-0.7	0.1-2	5-27	(Suriapparao, 2015)
RDF	4.2-26.7	2-10	70-77	11-30	43.5-56	0.9-7.1	20-37	0.6-7.1	0.2-2.1	13-24.3	(Efika et al., 2015, Tosti et al., 2019, Robinson et al., 2017)
Wood pellets	7-10	16-23	65-77	1-3	48-50	5-6	44-46	0.2-0.4	n.d.	15-17	(Brand et al., 2021, Kluska et al., 2020)
RDF pellets	5-8	3.6-13	65-72	10-26	47-51	5-12	20	0.4-1.1	0.3-1.5	12-20	(García et al., 2021, Laosena et al., 2022)
Pyrolysis char	3-5	31-38	43-58	2-4	65-71	5-6	29-33	n.d.	n.d.	20-27	(Yu et al., 2019)

*By difference

2.2.1 Wood pellets

Wood pellets, made from sawdust and woody materials such as pine, oak, and beech, are an important bioenergy source used in electricity generation (56.4%) and residential heating (43.6%), conforming to the ENplus standard (Goh et al., 2013, Strauss, 2023). Globally standardized under ISO 17225-2, wood pellets are seeing growing demand in both traditional and emerging markets.

Emerging applications in medium-scale heating and combined heat and power (CHP) systems are driving this demand, particularly as they help reduce overall emissions. The market expansion is evident from new countries entering the pellet industry; for example, in 2020, China expected to substitute 30 million tonnes of biomass waste pellets for 15 million tonnes of coal (Thrän et al., 2017). The global wood pellet production per year illustrated in the Figure 2.6(A). However, recent global developments, such as the Russia-Ukraine conflict, have disrupted the energy sector, impacting the wood pellet trade significantly. This has led to an increase in the cost of wood pellets, jumping from an average of $170/tonne (2009-2020) to $303/tonne (2021-2023) (Strauss, 2023).

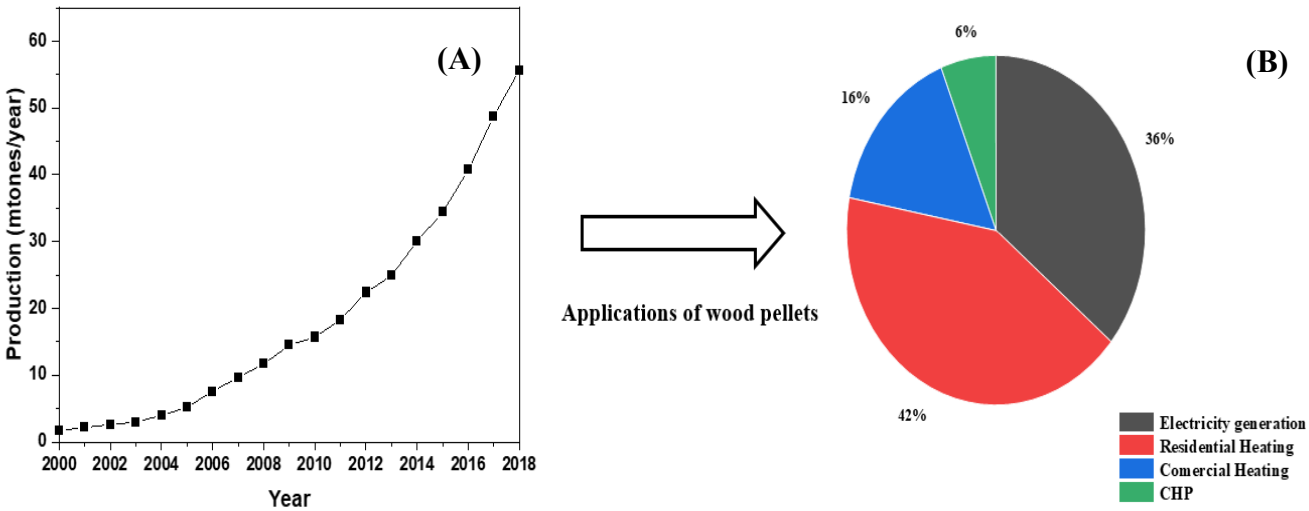

Figure 2.6: (A) Annual wood pellets production (mtones/year) (Fernandez, 2023) and (B) its various applications across the EU (% of total wood pellets) (Gauthier et al., 2017)

The wood pellets production follows a systematic process: drying wet sawdust (initial moisture content between 50-65wt%) to around 10wt%, size reduction using a hammer mill, and finally,

compacting the biomass waste into pellets in a press mill. These pellets are then cooled from 70°C -90°C to approximately 25°C for quality stabilization (Magelli et al., 2009).

Wood pellets are gaining attention in feedstock for gasification due to their high energy content (15-17 MJ/kg) and consistent composition (see Table 2.6). The properties of wood pellets are regulated by the ENplus standard, which ensures a set of stringent quality controls. These include limiting ash content to less than 2wt%, maintaining a diameter of 6-8 mm, and keeping moisture content below 10wt%. This standard elevates wood pellets to a promising future commodity, offering improved ease of operation compared to unprocessed biomass waste.

However, the downdraft gasification process (200kW with air) can lead to high and unstable pressure drops, reducing productivity and stability since rapid change in waste decomposition due to its high volatile matter in pyrolysis stage. Despite this, the gasification of wood pellets can still achieve good syngas compositions (H_2 17.2vol% and CO 21.2vol%) and high cold gas efficiency (68-70%) compared to waste wood without pelletisation (Simone et al., 2012). Additionally, the gasification process combining coal and wood pellets not only enhances fuel quality and mitigates tar formation—thanks to the interaction between the slow-reacting char from coal and the tar-rich biomass waste (synergistic reactions) as noted by Widjaya et al. (2018)—but also contributes to lower emissions like carbon dioxide. This is because wood pellets are considered a carbon-neutral, or in some cases, a carbon-negative feedstock (Lipiäinen et al., 2022).

The waste wood pellets, characterized by its high volatile matter (VM) content, reacts swiftly in the gasifier, leading to a rapid collapse of the bed structure. This behaviour contrasts with coal, which contains a high amount of fixed char and typically exhibits a slower rate of reaction. In future studies, it may be beneficial to compare the gasification rates of wood pellets, RDF, and coal to understand their distinct reaction rate. This variance in reaction rates underscores the need for a two-stage gasifier. In the first stage, the density of wood pellets and RDF is reduced to pyrolysis char, which, having a slower reaction rate, stabilizes the bed at the bottom of the gasifier and facilitates easier control and grinding ability. Many plants opt to co-gasify coal with biomass waste and RDF because of this (Widjaya et al., 2018). The high volatile matter content in wood pellets is the opposite of coal's properties, which contributes to the balance and efficiency in the co-gasification process.

Another notable challenge in this wood pellets gasification is the complexity of temperature control and reactor design (Schweitzer et al., 2018, Maneerung et al., 2018). Additionally, Efika et al. (2018)'s findings point to the influence of material properties, particularly how different heating rates can significantly alter the final product's characteristics.

On the opportunity front, the high hydrogen yield in wood pellet gasification offers a promising avenue for producing renewable hydrogen fuel (Cortazar et al., 2018). The efficient gasification of char pellets, as shown by Ding et al. (2018.), opens up new possibilities for utilizing the pyrolysis char. Moreover, the overall findings from these studies highlight the opportunity to convert waste biomass into valuable energy feedstock, underlining the role of wood pellet gasification in contributing to sustainable energy solutions and effective waste management.

2.2.2 RDF pellets

Refuse-Derived Fuel (RDF) is a by-product derived from the recycling of Municipal Solid Waste (MSW), typically consisting of household discards like paper, packaging, plastic bottles, and organic waste (Sprenger et al., 2018). Its composition varies based on factors such as geographic region, local population behaviour, and even seasonal changes. To enhance its energy content and minimize odour, MSW undergoes both mechanical and biological treatments.

The specific process for creating RDF can differ between facilities but generally includes three main stages: sorting, waste preparation, and biological treatment. The sorting process employs various techniques such as screening, magnets, cyclones, and optical separation to segregate different materials. Waste preparation then involves grinding or shredding the waste to homogenize it into smaller, more uniform sizes. Biological treatment, which can involve fermentation techniques or drying, serves to eliminate pathogens and reduce odours (Stapf et al., 2019).

The sequence of these processes is adaptable based on the specific requirements of the input waste. For instance, waste with a high organic content may initially undergo biological treatment as indicated by the 'Blue route' in Figure 2.7. Post-treatment, the material is classified as RDF. The general characteristics of MSW and RDF, including their differences and similarities, are detailed in Table 2.6. This systematic approach to processing waste not only creates a valuable fuel source but also contributes to more efficient and sustainable waste management.

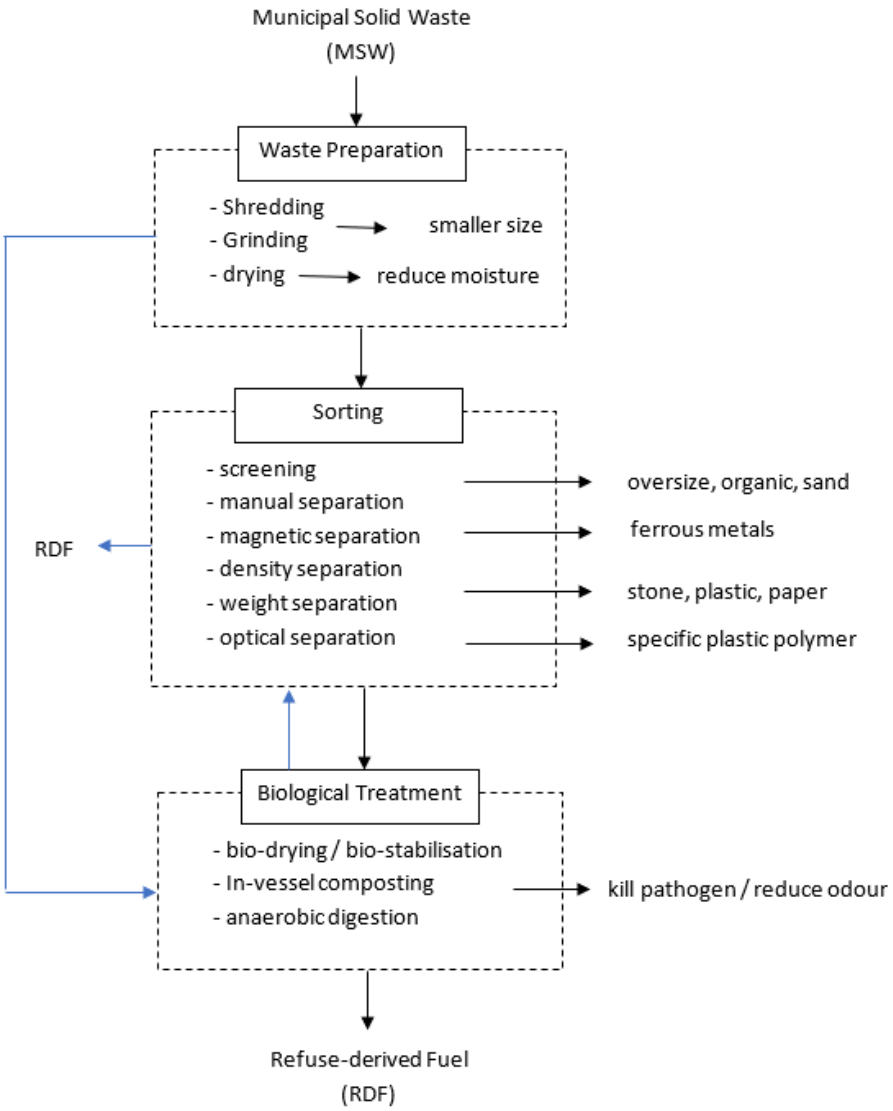

Figure 2.7: Detailed schematic of the RDF production process, adapted from Stapf et al. (2019)

The application of RDF in gasification presents several advantages. Firstly, RDF contains carbonaceous material necessary for gasification, leading to the generation of useful gases like H_2, CO, CH_4, and CO_2. While traditional combustion primarily yields heat and electricity,

gasification allows for the conversion of waste into liquid fuels, which are easier to store, or gas products. These can be used as building blocks in various industries, such as for producing methanol, ammonia, and synthetic natural gas (Waldheim, 2018). Additionally, RDF often includes unrecycled plastics, which contribute to a higher calorific value (24.3 MJ/kg) compared to other biomass waste (Ribeiro et al., 2017).

Using RDF in gasification, classified as a recovered energy technology, also helps waste dealers avoid landfill taxes, which have escalated significantly from £8 in 1996 to £104 in 2024 per tonne of waste (DEFRA, 2024). This economic pressure is driving waste management companies towards considering gasification as a viable future option.

Given that RDF is primarily sourced from community-generated municipal solid waste, gasification aligns well with the trend towards decentralized energy production. Implementing RDF gasification on a small to medium scale can provide power directly to the communities it originates from (Situmorang et al., 2020). This approach not only enhances energy security in the region but also plays a crucial role in minimizing waste.

The management and utilization of municipal solid waste (MSW) and refuse-derived fuel (RDF) vary significantly across different regions, reflecting diverse approaches to waste treatment and application.

In **Asia**, countries like Japan and Thailand actively convert MSW to RDF for energy and industrial applications. Japan processes 42.8 Mt of MSW annually, with 0.3-0.6 Mt used as RDF for local power and industry (Martignon, 2020). Thailand, with an annual MSW output of 27 Mt, turns 2.5 Mt into RDF (Intharathirat and Abdul Salam, 2015). China, with a substantial MSW volume of 203 Mt, primarily focuses on incineration (Y. et al., 2016). In India, out of 62 Mt of MSW produced, only 22-28% is treated or processed (Sambyal, 2018).

In **Africa**, Egypt's 12.2 Mt of MSW and 0.22 Mt of RDF find primary use in cement kilns, highlighting a focus on industrial applications of RDF (Martignon, 2020).

Europe presents a diverse picture. Austria processes 0.5 Mt of RDF for use in industrial facilities and cement kilns. Belgium, with 5.3 Mt of MSW and 0.4 Mt of RDF, leans towards incineration and recycling (34.2% and 61.6% respectively). The UK stands out for its substantial RDF export, producing 26.8 Mt of MSW and 3.0-3.2 Mt of RDF, with notable

percentages allocated to incineration, recycling, and landfilling. RDF consumption is significant, and a large portion is exported to countries like Germany and the Netherlands (Slow, 2019, Read, 2017, Martignon, 2020).

In **North America**, the United States processes a massive 251 Mt of MSW, with 34.5 Mt capacity in Waste-to-Energy facilities. A significant 65.3% of waste ends up in landfills and incineration (Aluri, 2018a, Reardon, 2018).

Overall, these global trends in MSW and RDF production and utilization reflect a mix of energy recovery, recycling, and landfilling practices. The conversion of MSW to RDF is a common strategy to harness waste for energy production, especially in power generation and industrial applications like cement kilns. However, the extent of RDF production and its subsequent use varies, influenced by regional waste management policies, infrastructure capabilities, and environmental considerations.

2.2.3 Waste gasification in research, challenges, and opportunities

Recent studies in waste gasification, primarily focusing on refuse-derived fuel (RDF) from municipal solid waste (MSW), indicate a growing interest in its application in various industrial processes. Sharma et al. (2022b), Sharma et al. (2022a) explore RDF's potential to partially replace traditional fuels like coal and pet coke in cement plant operations, with notable thermal substitution rates achievable in both calciners and kilns.

Similarly, Călin et al. (2021) investigates a combined heating, and power (CHP) system that integrates RDF gasification with solar thermal energy, aimed at improving district heating and cooling systems. It found that co-gasification of refuse-derived fuel (RDF) and straw in a fixed-bed gasifier significantly enhances gas yield, carbon conversion efficiency, and cold gas efficiency, particularly at an equivalence ratio (ER) of 0.2 and temperatures of 800-900°C, with potassium in the bottom ash favoring sulfur-containing compounds at higher temperatures and ER values, and calcium-rich small particles leading to melting agglomeration, which can be suppressed by adding straw.

The research by Alfè et al. (2022) takes a more laboratory-focused approach, examining the products of pyrolysis and gasification of MSW under various conditions, indicating a potential

application in the asphalt industry. Aluri et al. (2018) analyze the predictability of pyrolysis and gasification outcomes of model RDF, providing insights into the synergistic effects at play.

Śpiewak et al. (2021) found that increasing temperature (700-900°C) enhances RDF gasification in both steam and CO_2 atmospheres by improving the formation rates and yields of key gases (CO and H_2 for steam, CO for CO_2) and maximum carbon conversion degrees, while higher pressures (0.5-1.5 MPa) generally negatively affect these parameters, except at low temperatures (700-750°C) for CO_2 gasification, where pressure positively impacts CO formation rates and conversion degrees, with hydrogen being the dominant gas in steam gasification and carbon monoxide in CO_2 gasification, and the lower heating value of the resulting gas decreasing with higher temperature and pressure.

Salman and Omer (2020) explores the polygeneration of biofuels, heat, and power from MSW and RDF, emphasizing the potential of RDF due to its favourable composition. Nobre et al. (2020) looks into the use of RDF char as an additive for biomass waste pellets to improve gasification efficiency. Hongrapipat et al. (2022) investigates the co-gasification of RDF with wood chips, showcasing the adaptability of gasification processes. Zaini et al. (2019) and Ren et al. (2022) delve deeper into the kinetics and optimization of the gasification process, focusing on improving the reactivity and efficiency of gasification. Assima et al. (2018) and Sajid et al. (2022) highlight the utilization of waste-derived catalysts for tar reforming and the broader implications of gasification technology for sustainable waste management, respectively.

Despite the progress, several challenges persist in waste gasification. The variability in waste composition, particularly in MSW, poses a significant challenge, as seen in Sajid et al. (2022) and Zaini et al. (2019) studies. A key issue is the need for specific conditions, such as optimal particle size (Sharma et al., 2022a) and temperature control (Śpiewak et al., 2021, Cai et al., 2021), to ensure complete combustion and efficient gasification. The formation of tar and other by-products during gasification, as noted by Assima et al. (2018) and Nobre et al. (2020), requires additional processing and can complicate the operation of gasification systems. The high capital cost of systems like CHP (Cai et al., 2021) and the complexity of managing RDF's high ash content (Fazil et al., 2023) also pose significant barriers. Furthermore, the economic viability and technical limitations of large-scale applications, as observed in Salman and Omer (2020) study, are crucial hurdles that need to be addressed (Sharma et al., 2022b).

On the brighter side, waste gasification presents numerous opportunities. The ability of RDF to replace conventional fuels in cement plants (Sharma et al., 2022a, Sharma et al., 2022b) offers a pathway to more sustainable industrial practices. The integration of RDF gasification in district heating and cooling systems (Călin et al., 2021) and its potential use in the asphalt industry (Alfè et al., 2022) highlight its versatility. Furthermore, the co-gasification of RDF with biomass waste (Cai et al., 2021) opens up avenues for more efficient waste management and energy production. Optimizing the gasification process for hydrogen-rich syngas production demonstrates the potential of gasification in contributing to the renewable energy sector (Ren et al., 2022). The studies collectively suggest that with continued research and technological advancement, RDF gasification could significantly contribute to reducing landfill burden, mitigating CO_2 emissions, and advancing renewable energy applications.

Overall, current research in waste gasification is largely focused on enhancing the efficiency and applicability of RDF from MSW in various industrial processes. While challenges like technical requirements, high capital costs, and economic sensitivity exist, the opportunities for sustainable waste management and energy production are substantial and promising.

2.2.4 Summary

Gasification technology, which transforms waste into producer gas primarily composed of hydrogen (H_2) and carbon monoxide (CO), has evolved significantly since its development in the 1700s (Higman, 2008). Initially utilizing biomass waste and fossil fuels, it has expanded to include municipal solid waste, gaining global interest for its ability to convert waste into valuable syngas.

The process involves four main stages: drying, pyrolysis, oxidation, and gasification. Historically, gasification technology has been predominantly developed for fossil fuel-based systems. However, recent trends indicate a shift towards more sustainable approaches, including the study of new reactor designs, understanding waste characteristics that affect gasification performance, and exploring alternative gasifying agents like CO_2. This not only promotes the use of waste as feedstock but also aims to recycle CO_2, producing purer syngas with lower emissions.

Multi-stage gasification, noted for its flexibility in handling various types of waste, is emerging as a significant area of interest. This approach, involving separate pyrolysis and gasification reactors, results in low-tar syngas and improved efficiency. Notable multi-stage gasifiers have

achieved impressive results, including high carbon conversion efficiencies and significant hydrogen content.

Despite advancements, current gasification technologies primarily rely on oxygen and air as energy sources. The potential of using external, sustainable energy sources for purer syngas production is a promising yet underexplored area. Furthermore, the contrasting reaction rates of different feedstocks like wood, RDF pellets and coal highlight the need for tailored gasifier designs.

Opportunities in gasification technology are vast. High hydrogen yields from waste gasification present potential for renewable hydrogen fuel production. Research into RDF from MSW shows its applicability in industrial processes, including partial replacement of traditional fuels in cement plants and integration into CHP systems.

However, challenges remain. Variability in waste composition, necessitates specific operational conditions. Tar and by-product formation during gasification require additional processing. High capital costs and technical complexities in managing RDF's high ash content are significant barriers. For instance, ash can accumulate on the heat exchange surfaces, reducing the thermal efficiency of the boiler. This buildup requires frequent shutdowns for cleaning, which increases maintenance costs and downtime, thereby reducing the overall efficiency of the energy production process. Moreover, the ash can also contain harmful substances like heavy metals, which require additional treatment or disposal measures to prevent environmental contamination. Despite these challenges, the potential for RDF gasification to reduce landfill burden, mitigate CO_2 emissions, and contribute to renewable energy is substantial, warranting continued research and technological advancement.

2.3 Environmental sustainability of hydrogen production systems

The concept of quantification of resource requirements, emissions and waste flow was firstly used in 1969 (Hunt, 1974). However, there were not a standardised framework for quantifying for various processes until 1990s, which is also known as life cycle assessment (LCA). Applying the concept of LCA to evaluate the environmental impacts associated with all stages of a product's life cycle has significantly increased, as evidenced by the number of publications found in the Science Direct Database, which rose from fewer than 500 in 2000 to around 7000

in 2020. The ISO LCA standards (ISO 14040-14043) were available in between 1990-2000. In 2003, the European Union established a dedicated platform on LCA, further institutionalizing the practice. This was followed by updates to the (ISO 14040:2006) and (ISO 14044:2006) standards in 2006, reflecting the evolving nature of LCA methodologies.

2.3.1 Principle

The LCA study is structured into four distinct phases, as outlined by the (ISO 14040:2006) and (ISO 14044:2006) standards (see Figure 2.8). The first phase is the goal and scope definition. This initial stage sets the foundation for the LCA, determining the objectives, target audience, the specific aspects to be compared or disclosed, and the functional unit of the study. It also delineates the system boundaries, impact categories, data requirements, assumptions, limitations, and outlines the need for critical reviews and the format for reporting findings.
The second phase is the inventory analysis or Life Cycle Inventory (LCI) analysis. This stage involves the compilation and quantification of inputs and outputs for a product throughout its lifecycle, capturing the detailed data needed for assessment.

The third phase, known as the impact assessment or Life Cycle Impact Assessment (LCIA) phase, focuses on understanding and evaluating the potential environmental impacts of a product system throughout its lifecycle. This phase is crucial for identifying and quantifying the environmental effects associated with different stages of the product's life.

Finally, the interpretation phase is where the findings from the LCI or LCIA (or both) are analysed in the context of the initially defined goals and scope. This phase is essential for drawing conclusions, making informed recommendations, and providing a comprehensive understanding of the LCA results. This structured approach to LCA ensures that all aspects of a product's environmental impact are thoroughly examined and assessed, making it an invaluable tool in the pursuit of sustainability.

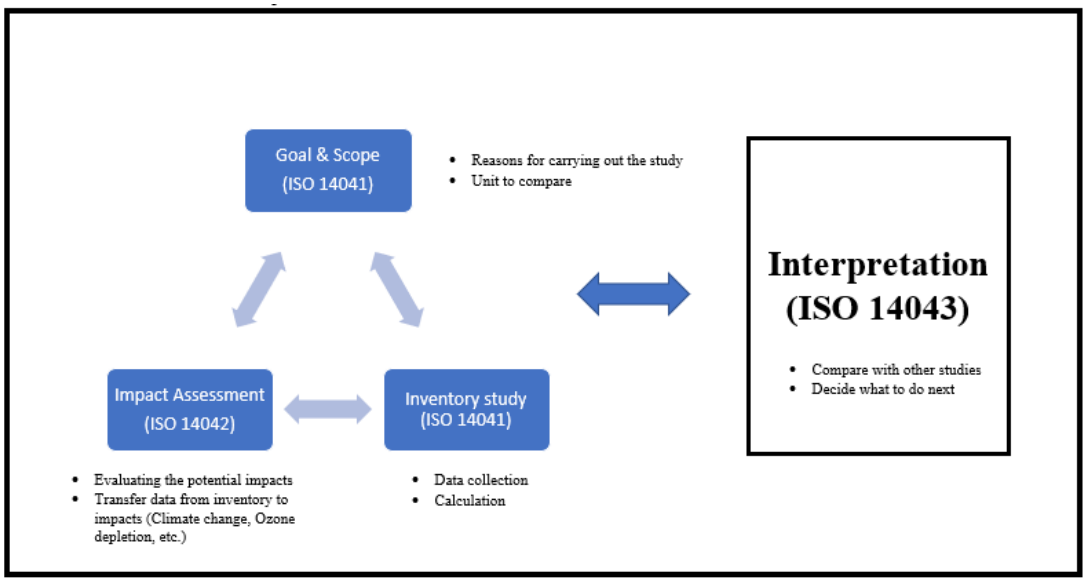

Figure 2.8: Detailed Illustration of the Life Cycle Assessment Framework, Adapted from ISO 14040 Standards

2.3.2 Overview of hydrogen as an energy carrier and its major production methods

Hydrogen, with its high lower heating value of around 120-142 MJ/kg (Rasul et al., 2022), stands as a potent energy carrier in today's world. In 2024, the global consumption of hydrogen projected to be approximately 120 Mt (Osman et al., 2022), signifying its growing importance in the energy sector. The production of hydrogen is predominantly achieved through various methods. About 48% is produced from steam methane reforming using natural gas, 18% from coal gasification, and 30% from by-products in oil products cracking. The remaining production comes from other sources and water electrolysis (Ji and Wang, 2021).

However, it's notable that low-emission hydrogen only accounted for a mere 0.7% of the total demand, as reported by International Energy Agency (2023a). The environmental impact of hydrogen production is significant. The sector contributes approximately 900 million tonnes of CO_2 per year (Lebrouhi et al., 2022), which is around 3% of the total annual CO_2 emissions of 34.9 giga tonnes (Liu et al., 2022). On the policy front, 32 countries had hydrogen strategies in place as of 2022, setting national targets ranging from 160-210 GW (International Energy Agency, 2023a). Figure 2.9 presents the comparative analysis of the costs and greenhouse gas emissions (measured in Global Warming Potential, GWP) associated with hydrogen production through various methods.

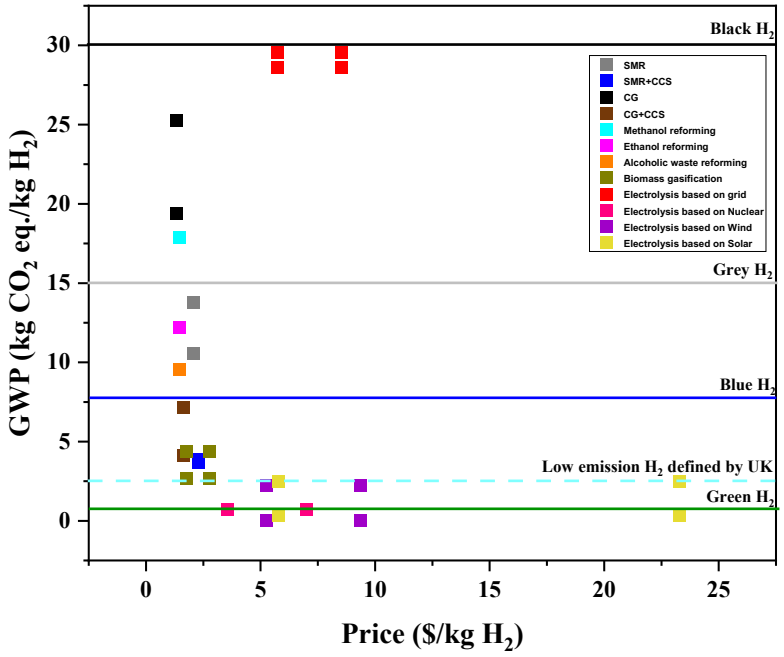

Figure 2.9: Comparative analysis of CO_2 emissions (kg CO_2 eq/kg H_2) versus production cost ($/kg H_2) across various hydrogen production technologies, based on (Ji and Wang, 2021)

Steam methane reforming (SMR)

Steam methane reforming (SMR) is a predominant industrial method for producing hydrogen gas (H_2). This process involves a reaction between methane (CH_4) and steam (H_2O) under high temperatures (850°C-950°C) (Nieva et al., 2014) and pressures (0.5-2.6 MPa), leading to the formation of hydrogen (H_2) and carbon dioxide (CO_2) (Faheem et al., 2021, Pashchenko, 2018). Figure 2.10 shows the SMR process to produce H_2. It begins with the desulfurization of natural gas, where sulfur compounds, which can poison the catalysts used later in the process, are converted to H_2S and removed with iron-based scrubber with efficiency of more than 95% (Muradov et al., 2010). The gas is then pre-heat (400°C-600°C) with steam to convert higher hydrocarbons into methane, ensuring that the feedstock entering the main reformer is predominantly methane. The steam to methane ratio at the pre-reformer inlet is maintained at 2-3.5 to optimize the process (Pashchenko, 2019, Pashchenko, 2018).

In the main reforming reactor, methane reacts with steam over a nickel/alumina-based catalyst to produce hydrogen and carbon monoxide (Van Beurden, 2004). This endothermic reaction requires an external energy source, which is commonly supplied by natural gas combustion unit

(Simpson and Lutz, 2007). Following this, a water gas shift (WGS) reaction is utilized to increase the hydrogen yield; CO reacts with water to form additional H_2 and CO_2.

The system is designed to be energy efficient, with high-pressure steam generated from heat integration within the process. This steam can be used to drive turbines, generating electricity which can then either be used for the plant's operations or sold back to the grid if there is an excess. The plant's energy requirements, both electrical and thermal, are met through the internal combustion of natural gas, with only a minor excess of electricity being produced (Katebah and Linke, 2022).

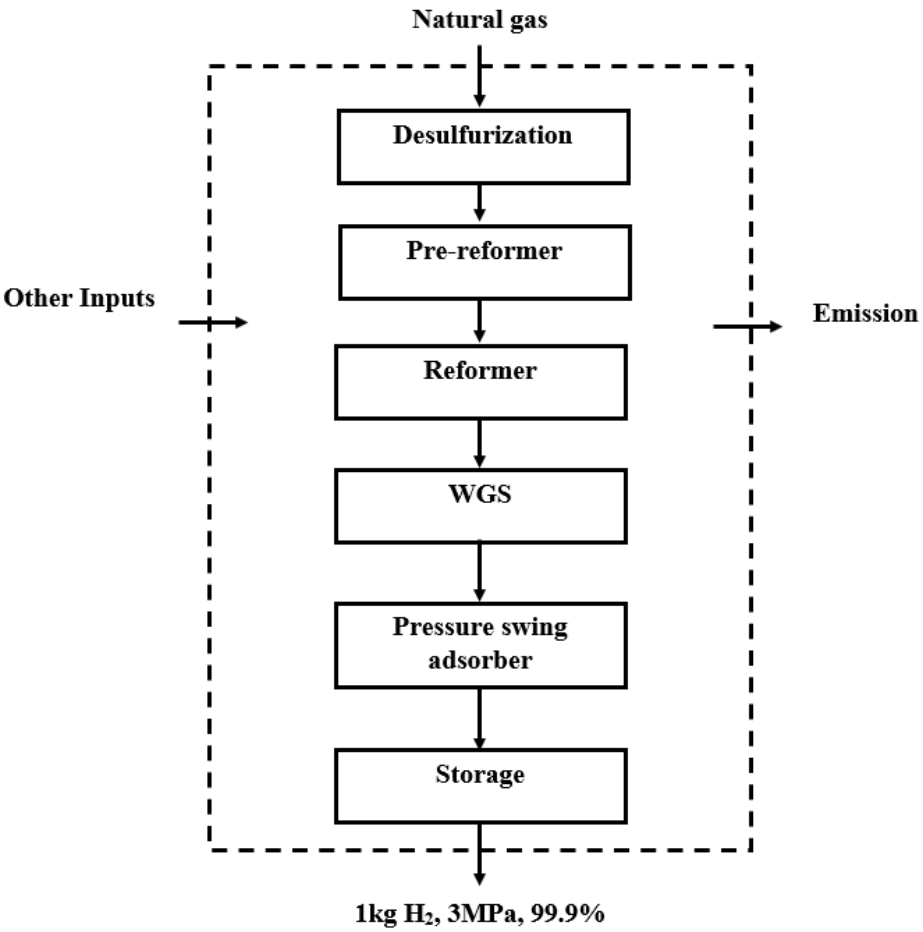

Figure 2.10: Schematic diagram of hydrogen production processes via Steam Methane Reforming (SMR)

The hydrogen produced through the SMR process is then purified to achieve a purity level of at least 99.9% and is compressed from 0.5 MPa to 3 MPa for storage and transportation. Pressure Swing Adsorption technology typically achieves a 90% hydrogen recovery rate (Molburg and Doctor, 2003). This highly pure hydrogen has a wide array of applications,

including in the chemical industry, petroleum refining, and as a potential clean energy carrier for fuel cells in vehicles. Despite its efficiency, the SMR process is also a significant source of carbon emissions due to the production of CO_2 as a by-product, an issue that is increasingly addressed by integrating carbon capture and sequestration technologies.

Conventional gasification

Conventional gasification is a versatile process that converts carbonaceous materials, such as coal, biomass waste, and municipal solid waste (MSW), into valuable products like synthetic gas (syngas), char, and condensate liquid. These products serve as important sources of energy and chemical feedstock. (Higman, 2008). The process begins with the transportation of these primary raw materials to the gasification facility (see Figure 2.11). Here, a critical pre-treatment step is undertaken, which typically involves milling or pulverizing the feedstock. This mechanical processing is crucial as it prepares the raw materials for effective gasification by ensuring uniformity and optimal reactivity (Dai et al., 2008).

Once milled to the proper size, coal, for instance, is mixed with water in a slurry tank to create a coal-water mixture. It allows the coal particle to rapidly heat-up in order to increase production rate (Smoot and Brown, 1987). This slurry is then fed into an entrained flow gasifier, a reactor where the actual gasification takes place. Within this high-temperature environment, often ranging between 1100°C and 1750°C (Kong et al., 2021), steam and oxygen are introduced. These reactants interact with the feedstock, inducing a series of complex chemical reactions that transform the solid feedstock into a gaseous mixture primarily composed of hydrogen and carbon monoxide (Mishra and Upadhyay, 2021).

After the gasification phase, first cooled down (to 250°C-400°C), which not only conserves energy but also conditions the gas for subsequent cleaning stages. The particulate scrubber is one such stage, designed to remove solid contaminants from the syngas. Additionally, a quench gas compressor may be utilized to adjust the syngas pressure to suitable levels for further processing (Ngo et al., 2021). To achieve the pure hydrogen, the cleaned syngas undergoes a purification process, which separates hydrogen from other components such as carbon monoxide, carbon dioxide, and residual water vapor. The resulting hydrogen, with its high purity, can be employed for various applications, including as a clean fuel or as a building block in the chemical industry (Cao et al., 2020).

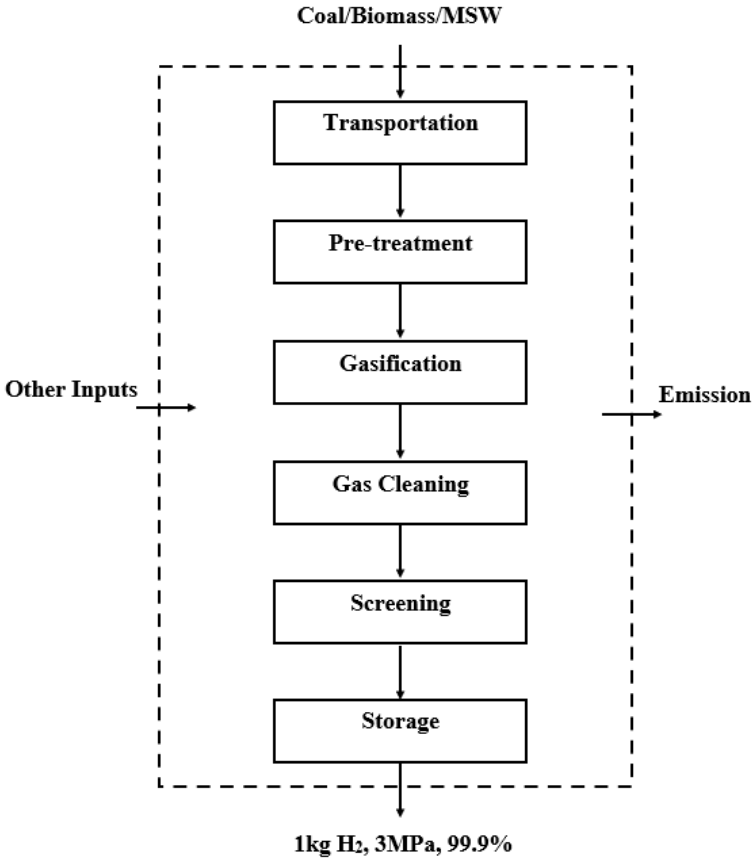

Figure 2.11: Schematic diagram of hydrogen production processes via waste gasification

Partial Oxidation of oil products (POX)

Hydrogen production through the partial oxidation of oil products, such as naphtha, is an essential industrial process, particularly for the synthesis of important petrochemicals like ethylene and propylene. Naphtha, a complex blend of hydrocarbons with n-hexane as a significant component, serves as the primary feedstock for this process (Ritter and Ebner, 2007).

The procedure begins by introducing naphtha into a cracking furnace, where it is subjected to extremely high temperatures ranging from 1200°C to 1500°C and pressure between 20-150 atm in the presence of steam (Makaryan et al., 2023). The steam acts as a diluent, enhancing the conversion rates of the hydrocarbons. This stage is crucial as it initiates the cracking reactions that break down the larger hydrocarbon molecules into smaller, more valuable ones (Lee and Elgowainy, 2018).

Following the cracking stage, the resultant product stream is at a very high temperature, around 800°C-1200°C, and must be cooled rapidly to 500°C-650°C—a process known as 'quenching'—to preserve the composition of the products obtained (Lee and Elgowainy, 2018). After quenching, the product mixture contains a variety of hydrocarbons, including heavier fractions that need to be removed. This is achieved through a process called fractionation, which separates the tar and oily materials from the desired products (Derrien, 1986). Subsequent to fractionation, a further cooling or 'screening' process isolates the heavier components from the lighter ones. The lighter fractions, which include hydrogen, are then refined using pressure swing adsorption (PSA) technology to achieve high purity levels of 99.9% hydrogen (Young et al., 2022). This showed in the Figure 2.12.

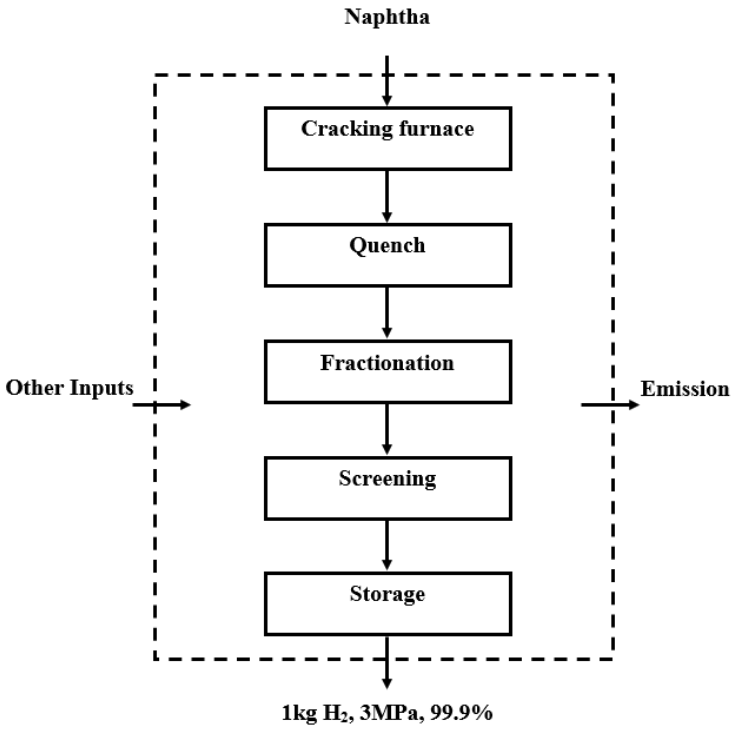

Figure 2.12: Schematic diagram of hydrogen production processes via naphtha cracking

Water electrolysis

Water electrolysis offers a sustainable method for producing pure hydrogen (see Figure 2.13), yet its widespread adoption is hindered by high energy requirements and the need for costly noble metal catalysts (Wang et al., 2021a). The process involves splitting water into hydrogen and oxygen gases using electricity, which can be sourced from renewable or nuclear energy (Chi and Yu, 2018).

Three primary technologies dominate the field of water electrolysis: alkaline water electrolysis (AWE), solid-oxide electrolysis (SOE), and proton exchange membrane (PEM) electrolysis (Anwar et al., 2021). AWE, a conventional and commercially viable technology, operates at temperatures of 65°C-100°C with KOH solutions and is the most cost-effective, although it has the lowest efficiency (70-80%) (Fortin et al., 2020). SOE, which operates at high temperatures (700°C-800°C) and doesn't require noble catalysts, is currently in the laboratory stage, showing potential for higher efficiency (>95%) and integration with industrial processes (Nechache and Hody, 2021).

PEM electrolysis stands out for its compact design and high efficiency (80-90%), functioning at <100°C (Ayers, 2019). However, it requires precious metal catalysts, making it more expensive ($3-$7.26/kg H_2) (Ayers, 2021, Wang et al., 2023). PEM's process involves several steps, starting with equipment setup and water circulation. The system stabilizes liquid levels in the hydrogen separator and the water tank, followed by energizing the PEM cell to initiate electrolysis. Hydrogen is separated and treated, while oxygen and excess water are discharged. The PEM system operates under differential pressure, allowing for efficient operation without gradual regulation (Guo et al., 2019).

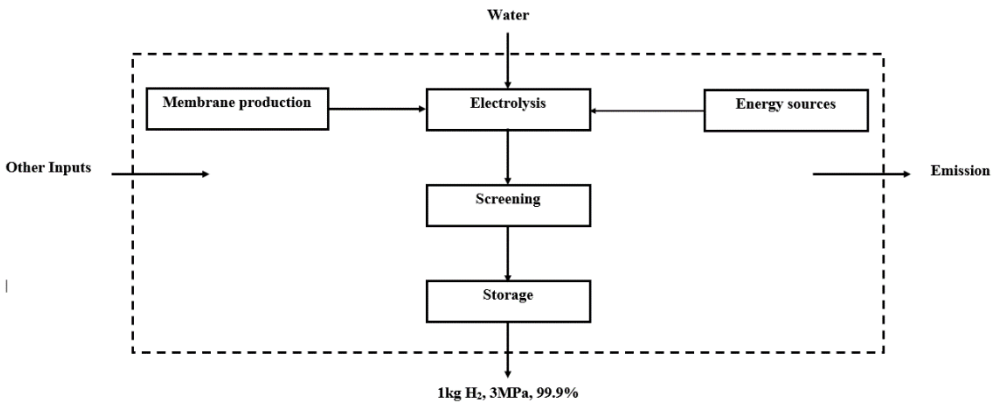

Figure 2.13: Schematic diagram of hydrogen production processes via water electrolysis

Despite challenges such as energy consumption and catalyst costs, water electrolysis, particularly through evolving technologies like AWE, SOE, and PEM, is a promising route towards a clean energy future. Its ability to integrate with renewable energy sources and the ongoing advancements in electrolysis technology underscore its potential as a key player in sustainable hydrogen production (Chi and Yu, 2018).

2.3.4 Case studies, key findings, challenges, and opportunities

The key findings in life cycle assessment (LCA) of hydrogen production systems include the variability of environmental impacts across different production methods like SMR, AWE, and electrolysis (Koroneos et al., 2004, Mehmeti et al., 2018). The energy source, particularly in electrolysis, plays a crucial role in determining environmental performance (Bareiß et al., 2019). Technological advancements, such as CCS, are shown to significantly enhance the environmental profiles of hydrogen production methods (Antonini et al., 2020).

A comprehensive overview of key findings from life cycle assessment (LCA) studies, along with their respective sources of raw data and methodologies employed shown in the Table 2.7. The challenges in these LCAs include inconsistencies and limitations in data, as highlighted by vague or outdated inventory data, which hinder accurate assessments (Bareiß et al., 2019). The focus on narrow impact categories in some studies could lead to overlooking other significant environmental impacts (Bareiß et al., 2019).

Additionally, the complexity in comparing different hydrogen production methods due to their varied efficiency and environmental impacts presents a significant challenge (Kalinci et al., 2012). The research on hydrogen (H_2) production systems previously faced a challenge due to the absence of a standardized functional unit for comparison. Different studies used varied functional units, leading to inconsistencies in the assessment of H_2 production methods. However, the UK has recently established a standard, stipulating that H_2 should be compared using the functional unit of 1 kg of H_2 at a purity of 99.9% and a pressure of 3 MPa. This standardization is a significant step towards harmonizing research methodologies and enabling more accurate comparisons across different hydrogen production studies (Department for Business, 2022a).

Opportunities arising from these studies include the promotion of cleaner hydrogen production methods, emphasizing the benefits of non-fossil and renewable energy sources (Mehmeti et al., 2018). The findings can guide policy decisions and economic strategies, encouraging sustainable practices in hydrogen production. Furthermore, identifying gaps in current research, these studies suggest future research directions such as integrating various energy sources in hydrogen production systems (Kalinci et al., 2012).

Table 2.7: Summary of research on Life Cycle Assessment (LCA) of hydrogen production: goals, database, methods, and principal findings

Objective	**Database and Methods**	**Key Findings**	**References**
Investigate environmental aspects of liquid hydrogen.	Not specify, Eco-indicator 95	PV-based hydrogen production has poor environmental performance due to inefficient module manufacturing.	(Koroneos et al., 2004)
Review impacts of hydrogen production pathways.	National Renewable Energy Laboratory, ReCiPe 2016	Non-fossil hydrogen better environmentally; wind-based electrolysis notably effective.	(Mehmeti et al., 2018)
Assess impacts of hydrogen via PEM in Germany.	Data from PEM Plant and ecoinvent database, ReCiPe 2016	Electricity mix crucial; PEM viable alternative to SMR; highlights need for updated data.	(Bareiß et al., 2019)
Study hydrogen from natural gas and biomethane.	Data from Brightway2 and ecoinvent database, ILCD 2.0 (2018)	CCS integration beneficial; biomethane offers significant climate advantages.	(Antonini et al., 2020)

Compare hydrogen production routes.	Ecoinvent database 2007, Green House Gases Emission Perspectives	SMR energy-intensive; potential in CGR with CCS and electrolysis; need for technological advances.	(Simons and Bauer, 2011)
Compare hydrogen from biomass waste gasification.	Literature review, no specified	Downdraft gasifier system more efficient and environmentally friendly than Circulating Fluidized Bed Gasifier (CFBG) system; further analysis planned.	(Kalinci et al., 2012)

Chapter 3 Material, methodology, and calculations

This chapter explores the gasification potential of three materials: RDF pellets, wood pellets, and RDF in shreds form, each presenting unique physical and chemical characteristics. The materials were prepared and characterized through a series of analyses, including thermogravimetric, proximate, and elemental assessments. Special attention was given to their diverse sizes, and elaborate preparations were conducted to reduce their dimensions for further analysis.

The research utilized various state-of-the-art techniques and instruments, such as Inductively Coupled Plasma Mass Spectrometry, SEM-EDx, and Netzsch Jupiter STA 449C TG-DSC analyser, to gain insights into the materials' inorganic composition, structure, and thermogravimetric properties. Furthermore, these materials were subjected to experimental procedures like pyrolysis and two-stage gasification, with product analysis conducted via gas chromatography and Karl-Fischer titration, among other methods. Finally, the calculation method used in this thesis like product yields, S/C, LHV of producer gas and efficiencies are provided.

3.1 Material

This study employs three different materials: RDF pellets, commercial wood pellets, and RDF in shreds form. Each of these materials originates from distinct sources and exhibits unique physical and chemical properties that make them suitable candidates for waste gasification.
RDF pellets, sourced from Knight Energy Service, derive from a range of waste materials that have been processed to yield a homogenous fuel. In contrast, the commercial wood pellets used are primarily made from by-products of the timber industry, such as sawdust and shavings. These wood pellets are commonly employed in boiler systems. Finally, the RDF in shreds form is an industrial by-product from Biffa company, which has been traditionally used for electricity generation.

In terms of physical properties, the RDF pellets exhibit a diameter of 8.9±0.2 mm and a length of 29.8±8.9 mm. Wood pellets are slightly smaller, with an average diameter of 6±0.1 mm and a length ranging between 19±6.2 mm. The size of the wood pellets aligns with the standard dimensions (6-8 mm diameter range and a 3-40 mm length range) established for wood pellets

in Europe (EN 14961-2) while a standardized size for RDF has not been established yet, given its inherently heterogeneous properties. The RDF shreds have an average width of 6.5±2.2 mm and an average length of 19.2±4.6 mm. Due to its irregular shape and texture, the size variation is considerable. RDF shreds was used for material properties comparison but was not utilized in the two-stage gasification due to the time constraints of this study.

Figure 3.1: Waste used in this study including A.) wood pellets, B.) RDF pellets, and C.) RDF shreds.

Table 3.1 Proximate and ultimate analysis of waste wood pellets and RDFs (based on 3 replicates)

Properties	**Wood pellets**	**RDF pellets**	**RDF shreds**
Diameter (mm)	6.0±0.1	8.9±0.2	Width: 6.5±2.2
Length (mm)	19.6±6.2	29.8±8.9	19.2±4.6
Proximate Analysis (wt%, as received)			
Moisture	8.9±0.0	1.7±0.0	2.2±1.6
Fixed Carbon	11.6±3.1	6.9±2.5	18.9±5.4
Volatile Matter	79.2±3.1	80.9±2.4	63.5±4.4
Ash	0.3±0.0	10.4±0.1	15.3±2.8
Ultimate Analysis (wt%, dry and ash free)			
C	46.3±0.2	57.7±0.5	72.3±0.8
H	6.5±0.0	8.2±0.1	10.9±0.1

O*	47.1±0.3	33.5±0.8	16.7±0.2
N	0.0±0.0	0.6±0.0	0.4±0.0
S	0.0±0.0	n.d.	n.d.
Empirical Formula	$C_6H_{10.13}O_{4.58}N$	$C_6H_{11.01}O_{2.60}N_{0.05}$	$C_6H_{10.89}O_{1.03}N_{0.02}$
HHV (MJ/kg)	18.0±0.7	19.2±0.6	20.5±0.8

* By difference

3.2 Analysis

3.2.1 Sample preparation for further analysis

Preparation and analysis of Wood and RDF, as depicted in Figures 3.2, involved several stages. Initially, the pellets were crushed using a mortar and then further reduced to a powder form by a laboratory blender operating at a low speed for a duration of 20-40 seconds.

Figure 3.2: A.) Refuse-Derived Fuel (RDF) and B.) Waste wood pellets (WP), which has been reduced to a size of 2 mm for subsequent analysis.

While this process yielded a fine powder for the wood pellets, the RDF pellets and shreds required further processing due to their larger size. The RDF was sieved and categorized into three main classes. The first class is in shred form, composed of textile and biomass waste fibre. The second class contains large solid particles primarily consisting of plastic, rocks, and metals. The final class comprises fine particles smaller than 0.2 mm.

Each of the three RDF types can be observed in Figure 3.2. To reduce their size, the first and second classes were cut with a knife and then mixed with the fine particles from the third class. Both the wood and RDF mix were subsequently stored in glass tubes at room temperature (15°C), pending further analysis. These analyses included thermogravimetric, proximate, and elemental assessments.

3.2.2 Proximate analysis

The proximate analysis was conducted based on British standards: moisture content was determined as per BS EN 14774-3: 2009 (British Standards, 2009), while ash and volatile matter were ascertained according to BS 1016-3 (British Standards, 1973). Fixed carbon was computed by difference.

For moisture content analysis, approximately 1 g of feedstock was placed in a dry crucible and then dried in an oven set at 105°C±2°C for a period of 2 hours. The loss of weight attributed to water evaporation was considered the moisture content.

For ash content determination, about 1 g of feedstock was combusted in a furnace at 815°C for a minimum of 1.5 hours, leaving behind solid particles referred to as ash.

To quantify volatile content, around 1 g of feedstock was subjected to decomposition in an inert atmosphere (N_2, 100ml/min) at 900°C for exactly 7 minutes. The weight loss observed during the experiment, minus the moisture percentage, was designated as volatile matter.

The proportions of moisture, ash, volatile matter, and fixed carbon were calculated using the following equations:

$$Moisture\ (\%) = \frac{M_2 - M_3}{M_2 - M_1} x100$$

$$Ash\ (\%) = \frac{M_3 - M_4}{M_2 - M_1} x100$$

$$Volatile\ (\%) = \left(\frac{M_2 - M_3}{M_2 - M_1} x100\right) - Moisture$$

$$Fixed\ Carbon\ (\%) = 100 - Moisture - Ash - Volatile$$

Where, M_1 = Weigh of crucible, M_2 = Weight of sample and crucible, M_3 = Weight of sample and crucible after dry, combustion or decomposition, M_4 = Weight of crucible after brushing all residue.

According to Table 3.1, wood pellets have a relatively high moisture content (8.9wt%) compared to RDF pellets (1.8wt%) and RDF shreds (2.2wt%), but it's still within acceptable limits for efficient gasification (less than 15.0wt%). While the RDF shreds show the highest fixed carbon content (18.9wt%), promising better energy efficiency, its high ash content (15.3wt%) could cause operational issues during gasification. Meanwhile, both wood and RDF pellets exhibit high volatile matter content (79.2wt% and 80.9wt% respectively), suggesting a potential for greater syngas yield. However, RDF pellets' lower fixed carbon content could limit their energy output. Each feedstock presents distinct advantages and challenges for gasification, and these need to be considered when optimizing the process.

3.2.3 C, H, N, and S element analysis

The primary elemental constituents of biomass waste, namely carbon (C), hydrogen (H), and nitrogen (N), were assessed using the automated Leco 628 instrument. This process adheres to the British standard (CEN/TS 15104:2005) (British Standards, 2005). Sulphur content was determined in accordance with CEN/TS 15289:2006 (British Standards, 2006). It is worth noting that the sample size, roughly around 2mm as prepared according to section 3.1, is slightly larger than the size recommendation specified by the standard CEN/TS 14780 (British Standards, 2011). The oxygen content was subsequently computed by difference.

RDF shreds, with the highest carbon (72.3wt%) and hydrogen content (10.9wt%), presents an exceptional energy potential for gasification, followed by RDF pellets and wood pellets. The high carbon content suggests a promising energy release during the gasification process, while the high hydrogen content can enhance the production of hydrogen-rich syngas. Oxygen, although essential for gasification, may decrease the calorific value when present in high amounts. Therefore, wood pellets, with their highest oxygen content (47.1wt%), might yield less energy output compared to RDF pellets and RDF shreds, which have lower oxygen levels. The low nitrogen content in all materials is favourable in minimizing harmful emissions during

gasification. Therefore, while all materials show potential for gasification, RDF shreds stand out due to its high carbon and hydrogen content, potentially offering superior syngas yield.

3.2.4 Thermogravimetric analysis (TGA)

The analysis of the samples was conducted using a combination of thermogravimetry (TG), differential scanning calorimetry (DSC), and quadrupole mass spectrometry (QMS), which facilitated the study of gases produced during thermal decomposition.

10g of samples underwent an overnight drying process at ambient temperature. A precisely measured subsample (roughly 11 mg) was then placed in an alumina crucible for examination using a Netzsch Jupiter STA 449C TG-DSC analyser. The gas evolving from the sample was sampled in real-time via a fused silica capillary transfer line, which connected to a Netzsch Aeolos 403C QMS.

The samples underwent a heating cycle from 25°C to 1000°C at different rates—10°C/min, 20°C/min, and 40°C/min—in a pure helium environment and a 20vol% oxygen-in-helium mix (purge gas flowing at 30 ml/min). A helium, carrier gas, was maintained at a 20 ml/min flow rate. The adapter heads and transfer lines (linking the Jupiter and Aeolos) were kept at a constant temperature of 150°C.

Data from TG and DSC were collected and managed with the help of Netzsch Proteus 61 software. The QMS operated in full scan mode over the range m/z 10-160, with mass spectrometric data gathered and processed via Aeolos software. Ions of significant interest during QMS analysis included:

m/z 12 representing carbon, m/z 18 indicating water, m/z 44 signifying carbon dioxide
Any ions displaying substantial deviation from baseline values were monitored and selected. To facilitate further analysis, the quantitative data regarding the selected ions' abundance in the evolved gas during heating were converted into ASCII format, then processed into Excel format.

3.2.5 Inductively Couple Plasma Mass Spectrometry (ICP-MS) for Inorganic compounds detection

The inorganic composition of the feedstock, pyrolysis and gasification char was detected using the Inductively Coupled Plasma Mass Spectrometry method, employing a high-resolution, fast-scanning instrument (Element2), a low-noise collision cell (Thermo XSERIES 2), and an Elan 6000.

3.2.6 SEM-EDx

The structure and form of both pyrolysis char and gasification char matter produced from the experiments were scrutinized using a Hitachi TM 3030 Environmental Scanning Electron Microscope (ESEM). This device is equipped with an EDAX Silicon Drift Detector for energy dispersive X-ray analysis (EDX) and operates at an accelerating voltage of 15 kV. The magnification range employed was between 38X and 5000X. To preserve the authenticity of the samples and assess them in their natural condition, the scanning process was executed without applying any conductive coating.

3.3 Experiments

3.3.1 Pyrolysis

A pyrolysis reactor was designed using an Inconel 600 tube, with dimensions of 33mm in diameter and 830mm in length. This reactor was indirectly heated by an external source. The reactor was filled with approximately 30g of the sample, and an inert atmosphere was created within it through the introduction of nitrogen, carbon dioxide, or a mixture at a rate of 100cm^3/min.

The reactor was programmed to heat at a rate of 20°C/min, aiming for a target temperature of 900°C. After the heating element was switched on, it took roughly 45 minutes to reach the desired temperature. This temperature was then sustained for an additional 15 minutes before the heater was turned off.

Gas products were gathered at five-minute intervals and stored in plastic sample bags. The flow of the producer gas was measured using a flow meter. Condensed by-products, such as pyrolysis

oil and water, were captured in 5 impingers (50ml) that were cooled and situated in an ice bath maintained between 0°C and 2°C. A 100ml conical flask was utilized as an additional water trap to ensure the absence of water in the producer gas.

Solid by-products, or pyrolysis char, were retrieved once the reactor's temperature dropped below 30°C. The pyrolysis char was analysed and reserved for future two-stage gasification experiments.

3.3.2 Two-stage gasification

The initial setup for the first stage and condensation unit follows that detailed in the pyrolysis section 3.3.1. The second stage, or the gasification phase, employs char generated from the pyrolysis experiment, situated centrally within the gasifier. The gasification zone's temperature was manipulated across a range of 700°C, 800°C, 900°C, 1000°C, and 1100°C.

Once the heater in the pyrolysis unit was activated, the gasification process commenced. After a period of 10 minutes - roughly correlating with a temperature of 200°C in the pyrolizer - steam was introduced into the second stage, maintaining a steam-to-carbon (S/C) ratio of 0-5.7. This aligns with the start of volatile matter release. The methodologies for product collection remained consistent with those implemented in the pyrolysis experiment.

3.3.3 Isothermal two-stage gasification

The operation closely mirrors the ramping process, with the key difference being that the temperature is initially set to the target value. Subsequently, the feedstock is inserted into the centre of the reactor. Once the feedstock is in place, the reaction commences. After a duration of 15 minutes, the reaction concludes, and the product is removed for analysis.
Producer gas samples were collected at several intervals for thorough analysis: 5s-10s, 25s-30s, 40s-45s, 55s-60s, 85s-90s, 145s-150s, 175s-180s, 295s-300s, 595s-600s, and finally, 895s-900s.

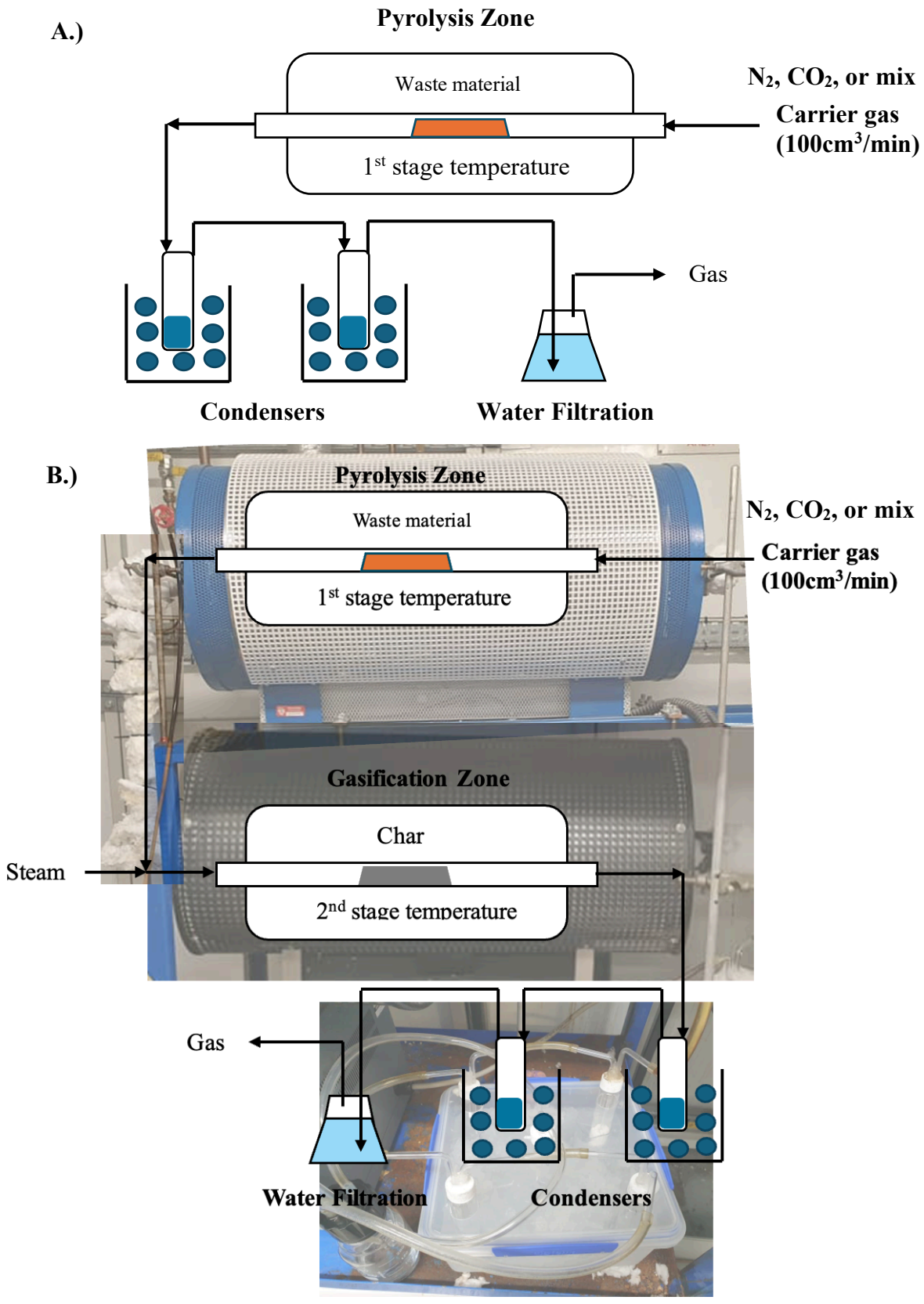

Figure 3.3: Schematic representation of a lab scale waste to syngas (A) pyrolysis, and (B) two-stage gasification reactor configuration

3.4 Products analysis

3.4.1 Gas analysis

The composition of the producer gas was determined using a Varian 450-GC gas chromatograph (GC) with Argon serving as the carrier gas for this analysis. The gas chromatograph is equipped with an array of three detectors, comprised of two Flame Ionization Detectors (FID) and one Thermal Conductivity Detector (TCD), and it operates in conjunction with five columns. The analytes, which included CO_2, H_2, O_2, N_2, CH_4, CO, C_2H_4, C_2H_6, and C_4H_8, were specifically identified through a combination of Molecular Sieve, Ultimate Metal, and Capillary columns. This comprehensive and multi-dimensional analytical approach allowed for precise determination of gas composition, further facilitating our understanding of the gasification process.

3.4.2 Condensates analysis

Water content was measured using Volumetric Karl-Fischer titration (915 KF Ti-Touch) with Hydranal Composite 5K as the titration reagent and a 3:1 methanol:chloroform solution as the solvent. Around 100.0 ± 0.1 mg of liquid sample and 45 ml of titration solvent were mixed in the titration cell to extract water. The water content was automatically determined, and the process was repeated three times for each sample.

For identifying and quantifying chemical compounds within the samples, a 7200 Accurate-Mass Q-TOF GC-MS in combination with a GC-FID was used. The GC-FID had a capillary column (14%-cyanopropylphenly-methylpolysiloxane, Restek Rtx-1707) and used helium as a carrier gas. Sample injections were conducted in split mode at a maintained temperature of 250°C.

A temperature program was employed in the GC oven, starting at 45°C and increasing to 250°C at a rate of 3°C/min. The MSD worked at 280°C in the electron ionization (EI) mode with ion source and quad temperatures set at 230°C and 150°C respectively.
The identification of compounds was based on the NIST spectral library and the Mass Bank high-resolution mass database. Quantification of major compounds was done through an external standard method, as detailed in Appendix B.

The gas chromatography preparation process involves several key steps. First, an internal standard solution is prepared by adding around 1.2 mg of 1-octanol to a 1.0 mL volumetric flask filled with acetonitrile. This solution is mixed and stored in a freezer. For the stock mixed standard, each of the standard compounds is weighed into a 25 mL volumetric flask and combined with acetonitrile. After an ultrasonic bath, the solution is stored in a freezer.
Calibration standards are prepared by adding specified volumes of the stock mixed standard, internal standard solution, and acetonitrile into labelled GC vials. Each solution is then shaken for proper mixing.

The procedure for liquid aliquots involves weighing approximately 400 mg of the condensed products into a labelled 8 mL vial. Internal standard solution (0.5 mL) and acetonitrile (5 mL) are added, and the solution is thoroughly shaken. This mixture is sonicated at 30°C for 20 minutes and then 1 mL of the mixture is transferred to a 1.5 mL GC vial. If there is a precipitate, the mixture is filtered and transferred to a GC vial. More details on the preparation of the internal standard and solution can be found in the Appendix B.

3.4.3 Pyrolysis char and gasification char analysis

The determination of C, H, N, and S content within the pyrolysis and gasification char is critical for validating the carbon conversion efficiency of the process. The analytical procedure should adhere to the British standard protocols specified in the elemental analysis section 3.4.

3.5 Calculations

The calculations in the gasification process include several key metrics to evaluate performance and efficiency. These metrics encompass mass balance, product yields derived from feedstock, gas yields (w/w feed), higher heating value (HHV), steam to carbon ratio (S/C), carbon conversion efficiency (CCE), cold gas efficiency (CGE), and process efficiency (PE).

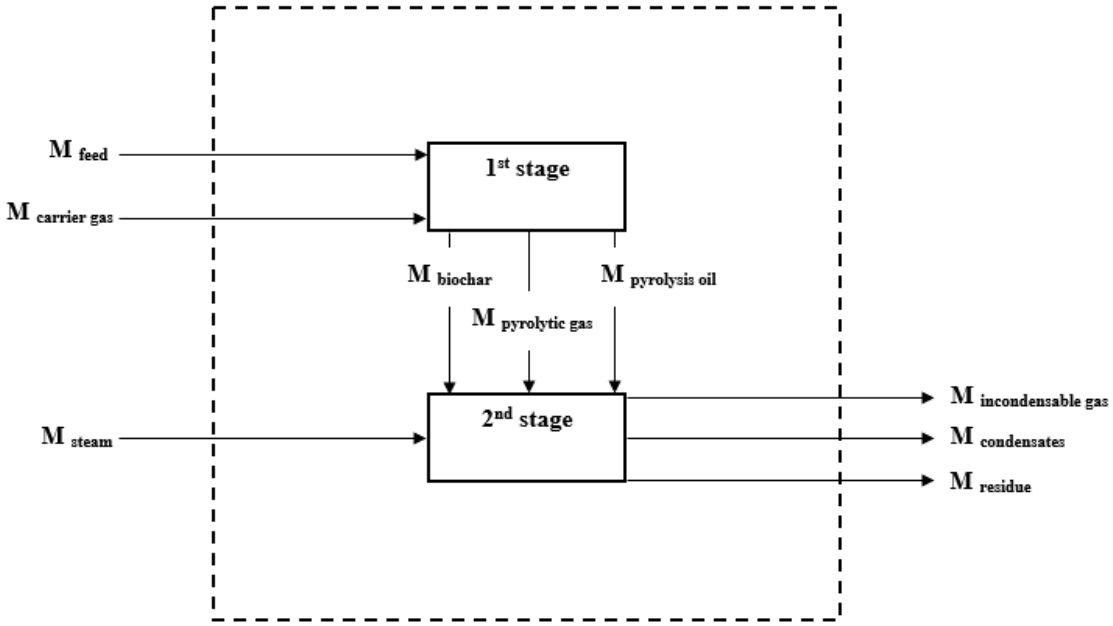

Figure 3.4: The mass balance in two-stage gasification

3.5.1 Mass balance in two-stage gasification

Mass balance calculations are crucial for evaluating the efficiency and performance of the two-stage gasification process. By analysing the input and output mass flow rates, we can determine the conversion efficiency of feed materials into syngas, biochar, and pyrolytic oil. Figure 3.4 illustrates the mass flow of materials through the gasification stages, providing a basis for this analysis.

$$M_{in} = M_{out} \tag{1}$$

$$M_{feed} + M_{carrier\ gas} + M_{steam} = M_{incondensable\ gas} + M_{condensates} + M_{residue} \tag{2}$$

$$M_{condensates} = M_{tars} + M_{wax} + M_{water} \tag{3}$$

Where M_{in} represents the total mass input, comprising the mass of the feedstock (M_{feed}), the mass of the carrier gas ($M_{carrier\ gas}$), and the mass of steam (M_{steam}). M_{out} symbolizes the total mass that exits the system, including the mass of condensates ($M_{condensates}$), the mass of solid residue (gasification char) ($M_{residue}$), and the mass of gases that cannot be condensed (M

incondensable gas). And M condensate is consisted of mass of tar (M tar), mass of waxy part (M wax), and mass of water (M water)

3.5.2 Products yield derived from feedstock.

Measuring product yields shows the efficiency of converting feedstock into syngas, biochar, and pyrolytic oil. This is crucial for optimizing the gasification process

$$Tar\ yield\ (wt\%) = \frac{M_{tar}}{M_{feed}} \quad (4)$$

$$Water\ yield\ (wt\%) = \frac{M_{water\ from\ feeds}}{M_{feed}} \quad (5)$$

$$Residue\ yield\ (wt\%) = \frac{M_{residue}}{M_{feed}} \quad (6)$$

$$Gas\ yield\ (wt\%) = 1 - \frac{M_{condensates} + M_{residue}}{M_{feed}} \quad (7)$$

3.5.3 Gas yields (w/w feed)

The total gas yields (w/w feed) measure the amount of gas produced per unit weight of feedstock, including contributions from both the steam and the carrier gas used in the gasification process.

$$M_{total\ gas}\ (mg/g\ feed) = \frac{M_{incondensate\ gas} + M_{used\ steam} + M_{carrier\ gas}}{M_{feed}} \quad (8)$$

$$Interested\ gas\ (mg/g\ feed) = \frac{mass\ percentage\ of\ interested\ gas \times M_{total\ gas}}{M_{feed}} \quad (9)$$

3.5.4 Higher heating value (HHV)

Another crucial aspect of the gasification process is the higher heating value (HHV). This value signifies the maximum amount of heat that can theoretically be produced from these feedstocks. Typically, the heat released from the feedstock is measured in a calorimeter, following the standards of BS EN 14918:2009. In this research, however, the HHV is estimated using a formula derived from the proximate analysis, as proposed by (Parikh, 2005). The formula is outlined as follows.

$$HHV\ (MJ/kg) = 0.3536FC + 0.1559VM - 0.0078ASH \quad (10)$$

Where HHV is High Heating Value (MJ/kg), FC is Fixed Carbon (wt% dry basis), VM is Volatile Matter (wt% dry basis), and ASH is Ash content (wt% dry basis).
It is noted that the average absolute error is 3.74wt% (1wt%≤FC≤wt91.5%, 0.92wt%≤VM≤90.6wt%, 0.12wt%≤ASH≤77.7wt%).

3.5.5 Steam to carbon ratio (S/C)

Steam to carbon ratio (S/C) is used to quantify the amount of steam in this work. It is the ratio of the amount of mole water in steam (n_{steam}) and moisture in the feedstock ($n_{water\ in\ feed}$) related with the mole of carbon in feedstock ($n_{C\ in\ feed}$).

$$S/C\ (mol/mol) = \frac{n_{steam} + n_{water\ in\ feed}}{n_{C\ in\ feed}} \quad (11)$$

It is noted that mol of carbon in the feedstock is given from elements analysis detailed in section 3.2.3.

3.5.6 Carbon conversion efficiency (CCE)

CCE is used to describe the efficiency of carbon in feedstock and carrier gas (CO_2 case) conversion to producer gas (Basu, 2018).

$$CCE = \frac{C_{in} - C_{out}}{C_{feed} + C_{carrier\ gas}} \times 100 \quad (12)$$

Where C_{in} is the total carbon inlet. C_{out} is the total carbon mass from outlet products including carbon from tar, wax, and solid residue (gasification char). C_{feed} is the total carbon mass of feedstock. $C_{carrier\ gas}$ is the total carbon mass of the carrier gas in CO_2 case. It is assumed that there is no other losses or gains of carbon through leaks, side reactions, or storage within the system that are not captured by these variables. The carbon content was measured in milligrams (mg).

3.5.7 Cold gas efficiency (CGE)

CGE is the term used to describe the proportion of the feedstock's chemical energy or heating value that remains in the resulting syngas product. The heating value of producer gas is given from the industrial data provided by (Waldheim, 2001). The lower heating value of CO is 12.63 MJ/Nm^3, for H_2 it is 10.78 MJ/Nm^3, for CH_4 it is 35.88 MJ/Nm^3, and for CO_2 it is 0 MJ/Nm^3. And y_{gas} is the mol fraction of the interested gas specie. This study utilizes steam operation, wherein the energy derives not solely from the feedstock but also from the hydrogen (H_2) and carbon monoxide (CO) produced via steam. Consequently, the energy expended to generate this steam (E_{steam}) will be included in the cumulative gross energy (CGE) calculation. $Y_{producer\ gas}$ is the total gas yield (Nm^3/kg feed).

$$LHV_{producer\ gas}(MJ/Nm^3 = y_{H_2} \times LHV_{H_2} + y_{CO} \times LHV_{CO} + (y_{CH_4} + y_{C1-C4}) \times LHV_{CH_4} \quad (13)$$

$$CGE\ (\%) = \frac{LHV_{producer\ gas} \times Y_{producer\ gas}}{LHV_{feed} + E_{steam}} \times 100 \quad (14)$$

3.5.8 Process efficiency (PE)

PE is the overall efficiency based on the energy produced from this process including energy from the producer gas (cold energy, $E_{cold\ energy}$) and sensible energy ($E_{sensible\ energy}$) compared with the input energy including feedstock (LHV_{feed}), heat for heating ($E_{heating}$), and heat for steam generation (E_{steam}).

$$E_{cold\ energy}(MJ/kg\ feed) = LHV_{producer\ gas} \times Y_{producer\ gas} \quad (15)$$

$$E_{sensible\ energy}(MJ/kg\ feed) = \sum n_{producer\ gas} h_{producer\ gas} \quad (16)$$

$$h_{\ producer\ gas}(J/mol) = h_0 + \int_{T_0}^{T} C_p dT \quad (17)$$

$$C_p\ (J/mol\ K) = A + BT + CT^2 + DT^3 \quad (18)$$

Table 3.2: The coefficients of constant pressure specific heat capacity from (Elliott and Lira, 2012).

	h_0 (J/mol)	A	B	C	D
H_2	8610	2.714E+1	9.274E-3	-1.381E-5	7.645E-9
CO	8700	3.087E+1	-1.285E-2	2.789E-5	-1.272E-8

CO_2	10 811	1.980E+1	7.344E-2	-5.602E-5	1.715E-8
CH_4 and C_2-C_4	10 601	19.25	5.213E-2	1.197E-5	-1.132E-8

$$PE\ (\%) = \frac{E_{cold\ energy} + E_{sensible\ energy}}{LHV_{feed} + E_{heating} + E_{steam}} \times 100 \quad (19)$$

Where $n_{producer\ gas}$ is the molar yield of producer gas (mol/kg feed). $h_{producer\ gas}$ (J/mol) is the specific enthalpy of producer gas at a selected temperature (T) and h_0 (J/mol) is those enthalpies of the producer gas at the room temperature, 25°C (T_0) (Zhang et al., 2021b). C_p is the constant pressure specific heat capacity (J/mol K). A, B, C, and D are the coefficient of Cp according to (Elliott and Lira, 2012) shown in Table 3.2.

Chapter 4 Enhancing the process of wood pellets gasification to increase hydrogen yield.

A study was conducted on the production of hydrogen from wood pellets using a two-stage gasification model. The findings revealed that a yield of 88 mg H_2/g of wood pellets, which is 1.3 times more than the theoretically expected amount of hydrogen from the feedstock (about 65 mg/g), was achieved at temperatures less than 1000^oC. A combination of CO_2 and steam as gasifying agents led to a 6wt% growth in the gas yield and a significant decrease in tar content, up to 93wt% (0.03g/Nm^3) compared to just steam gasification (0.5-0.7 g/Nm^3). Even though the quantity of hydrogen in the gas stream was similar for both steam and CO_2-steam gasification (88mg/g pellets), CO_2-steam gasification reduced the CO_2 content in the gas stream by 12wt%-17wt% compared to steam gasification alone. The H_2/CO ratio for steam gasification was 3.2-3.8 and 1.6-2.3 for CO_2-steam gasification. Due to a higher CO content in the gas, the cold gas efficiency (a measure comparing the calorific value of the products and that of the wood pellets) of CO_2-steam gasification was up to 6.8% more than that of steam gasification. In conclusion, the use of a CO_2-steam two-stage gasification process enhances overall efficiency and sustainability by making use of carbon sources in CO_2 emissions.

4.1 Thermal and chemical reactions of wood pellets under nitrogen and carbon dioxide conditions using TGA-MS study

This investigation examines the thermal decomposition, and chemical reactions of waste wood subjected to nitrogen and carbon dioxide atmospheres, utilizing Thermogravimetric Analysis coupled with Mass Spectrometry (TGA-MS). The objective is to delineate the specific degradation pathways and gas evolution profiles, thereby contributing to a better understanding of their applicability and environmental implications.

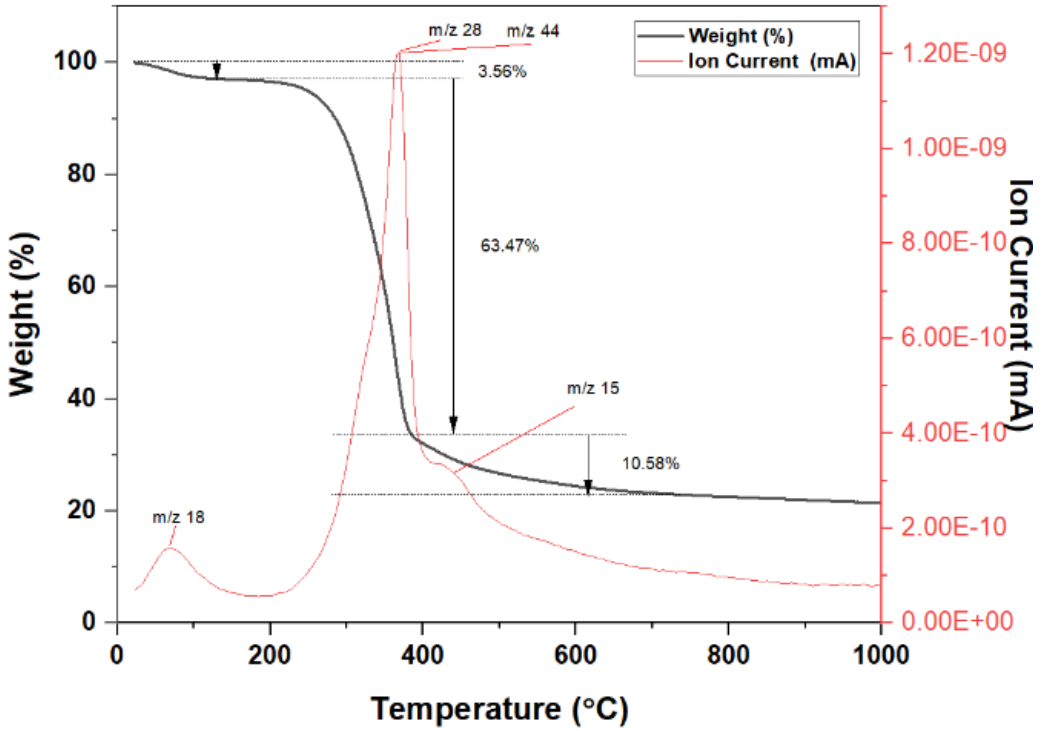

Figure 4.1: Analysis of the thermal degradation (TGA) of wood particles (150 µm - 250 µm) under a non-reactive (He) environment, with a steady temperature increase rate of 10°C/min (based on 3 replicates).

Figure 4.1 reveals that the drying process happens at temperatures under 200°C, as indicated by the absence of any gas other than water vapor (m/z 18). The weight decreased by 3.56wt% during this process. Notably, there is a significant weight loss of approximately 63.4 wt% within the 230°C to 400°C range. This is linked to the decomposition of cellulose/hemicellulose via decarboxylation and decarbonylation (Belgacem and Pizzi, 2016, Burhenne et al., 2013), coinciding with the highest concentrations of CO and CO_2 in the gas stream (as illustrated in Figure 4.2). A slower decomposition process (10.6 wt%) is evident at temperatures above 400°C due to the breakdown of lignin (Burhenne et al., 2013), resulting in the release of other gases like methane (m/z 15) and hydrogen (also seen in Figure 4.1). Biomass waste decomposition nearly ceases around 700°C, leaving about 22 wt% of solid residues (gasification char) (displayed in Figure 4.1). This solid fraction aligns well with the pyrolysis char yield from the pyrolysis process (as tabulated in Table 4.1).

Data in Figure 4.2 come from experiments in which 30 g of wood pellets underwent pyrolysis in both N_2 and CO_2 environments. The gas profile during pyrolysis, ranging from room

temperature to 900°C, was monitored to observe the evolution of permanent gases, as captured by gas chromatography (GC). Meanwhile, yields of pyrolysis oil, pyrolysis char, and gas were quantified between 500°C and 900°C (as depicted in Table 4.1) to study the temperature's effect on yield.

Figure 4.2 visualizes the gas evolution during the pyrolysis of wood pellets from room temperature to 900°C in both nitrogen and carbon dioxide environments. In nitrogen pyrolysis, no gases were detectable by GC between room temperature and 200°C. At 300°C, the main gases detected were CO_2 (nearly 0.2 mmol/g.min) and CO (0.1 mmol/g.min). Increasing temperature caused the quantities of CO_2 and CO to decrease, while CH_4 wasn't detected until temperatures exceeded 400°C, peaking at 0.1 mmol/g*min at 400°C, and then gradually declining with rising temperature. By 700°C, the quantities of CO_2, CO, and CH_4 had dropped below 0.0 mmol/g.min, whereas the H_2 quantity had increased, peaking at 0.1 mmol/g.min, and then steadily dropping with increased temperature. At 900°C, CO_2, CO, and CH_4 were undetectable, but H_2 was present at 0.8 mmol/g.min.

In contrast, during CO_2 pyrolysis, a sharp increase in CO concentration was noted after 600°C, along with a rapid decrease in CO_2, attributed to the Boudouard reaction (Lahijani et al., 2015). The gas yield at 900°C was 11.5wt% higher in CO_2 pyrolysis than in nitrogen pyrolysis, albeit at the expense of liquid oil and pyrolysis char. Additionally, a greater reduction in phenol derivatives was observed in CO_2 pyrolysis than in nitrogen pyrolysis (declined by 9.6wt%).

In the nitrogen environment pyrolysis of wood pellets (depicted in Figure 4.2(A)), a similar pattern is observed. No gas was identified at temperatures ≤200°C. Temperature elevations led to the release of CO_2 and CO as principal species, registering rates of 0.18 and 0.11 mmol/g min at 300°C, respectively. At 400°C, CO_2 declined to 0.0 mmol/g min, while CO remained approximately constant at 0.1 mmol/g min. CH_4 and H_2 were observed at temperatures above 300°C. As the temperature rose above 400°C, the levels of CO_2, CO, and CH_4 decreased, but H_2 peaked at around 0.1 mmol/g min near 700°C, followed by a quick drop in H_2 after 700°C. The gas profile from this wood pellet pyrolysis study closely aligns with other studies where waste wood was subjected to pyrolysis in a nitrogen environment between 350°C and 700°C at a heating rate of 10°C/min (Phan et al., 2008). Initial stages of the process primarily produced CO and CO_2, followed by CH_4 and H_2 at temperatures exceeding 500°C.

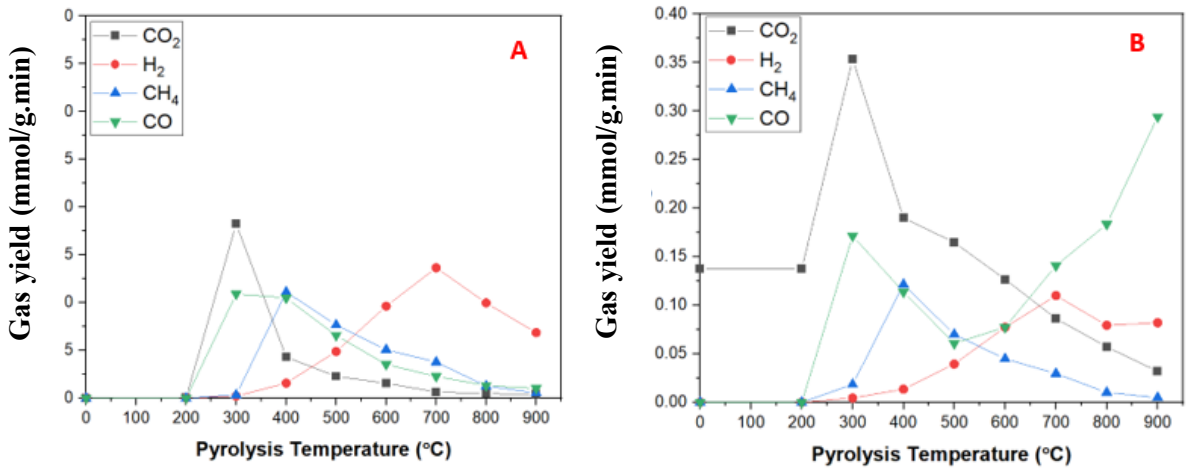

Figure 4.2 The gas evolution during the pyrolysis of wood pellets in (A.) nitrogen atmosphere and (B.) a carbon dioxide atmosphere (with an error margin of ±0.013 mmol/g.min)

When CO_2 was utilized as a carrier gas at a flow rate of 0.1 mmol/g (Figure 4.2(B)), the total quantity of CO_2 in the gas stream was equal to the sum of the input CO_2 and that resulting from decarboxylation (matching the amount acquired in an inert environment, Figure 4.2(A)). This suggests that CO_2 is inactive (behaving as an inert environment) at temperatures $\leq$ 500°C. However, at temperatures above 500°C, the CO and H_2 gas profiles were distinct from those found in the N_2 environment (Figure 4.2(A)). A sudden rise in CO concentration (Figure 4.2(B)) was noted, while CO_2 rapidly declined, even below the input flow rate. Additionally, the phenol content in the CO_2 pyrolysis oil was lowered by approximately 52wt% compared to the N_2 pyrolysis oil (as seen in Table 4.1). This can be attributed to dry reforming between CO_2 and volatiles at temperatures >500°C (Shah and Gardner, 2014) and the Boudouard reaction at temperatures above 700°C (Wiberg et al., 2001).

The gas yield from CO_2 pyrolysis (39.5%wt) was significantly higher than that from N_2 pyrolysis (28.1%wt) at 900°C, albeit at the expense of liquid oil and pyrolysis char (Table 4.1). The primary gas products from both N_2 and CO_2 environments were CO_2 and CO. This was due to the dry reforming of hydrocarbons (resulting in a substantial reduction of methane and C_2-C_5 as indicated in Table 4.1), and oxygenated compounds (leading to a decrease in phenol derivatives as shown in Table 4.1) at high temperatures (>600°C) to produce CO and H_2 (Shah and Gardner, 2014). Pyrolysis in the CO_2 environment lowered the phenol derivatives from 18.7wt% to 9.1wt%. A greater content of water and CO was discovered in CO_2 pyrolysis (Table 4.1). This can be explained by the consumption of H_2 by the abundant CO_2 in the gas stream

via the reverse water-gas shift reaction at temperatures above 500°C, leading to the production of CO and water (Rostrupnielsen and Hansen, 1993).

The liquid resulting from pyrolysis in the presence of CO_2 had a slightly higher water content, but significantly fewer phenol derivatives compared to the 100vol% N_2 environment (Table 4.1). The water content in the liquid fraction was over triple the moisture content in the feedstock, due to secondary reactions such as dehydration condensation, tar degradation, and the reverse water-gas shift reaction, among others (Solar et al., 2018). This water content aligns with other studies (Tanoh et al., 2020), typically ranging from 18-25wt% at pyrolysis temperatures between 700°C and 900°C. CO_2 pyrolysis also led to a higher presence of esters, ketones, alcohols, and aldehydes compared to N_2 pyrolysis (Table 4.1). This outcome mirrors that of pyrolysis oil, where these contents increase at higher temperatures due to the decomposition of lignin and anhydrous sugar (Yang et al., 2014, Chen et al., 2018).

Table 4.1: The comparison of yields and characteristics of the products derived from the pyrolysis of wood pellets at 900°C, with a constant heating rate of 20°C/min under different carrier gas.

Environment	**100%N_2**	**1:1 (vol/vol) CO_2/N_2**	**100%CO_2**
Product yield (wt% based on feedstock)			
Gas yield ±1.6	28.0	32.4	39.5
Pyrolysis oil ±2.4	51.8	49.3	43.3
Pyrolysis char ±0.8	20.2	18.2	17.2
Gas Composition (mol%)			
H_2	3.5	1.8	1.0
CO	36.3	43.4	46.2
CO_2	43.5	46.1	48.4
CH_4	15.3	7.4	4.4
C_2-C_5	1.4	1.3	0.3
Pyrolysis oil chemicals (wt% based on feedstock)			
Acids	0.7	0.6	0.5

Esters	0.6	0.6	0.7
Ketones	1.0	1.3	1.5
Alcohols	0.7	0.8	0.9
Aldehydes	0.6	0.6	0.7
Furans	3.8	3.4	2.9
Sugars	0.0	0.0	0.0
Phenols	18.7	13.4	9.1
Water	24.4	25.4	26.8
Others	1.3	3.2	0.2
Pyrolysis char			
Proximate Analysis (wt% based on pyrolysis char as received)			
Moisture ±0.2%	5.4	3.0	1.8
Fixed Carbon ±2.7%, by difference	86.6	92.5	95.4
Volatile Matters ±0.4%	6.8	3.2	1.3
Ash ±0.2%	1.2	1.3	1.5
Element Analysis (wt% based on pyrolysis char as moisture and ash free) ±0.3%			
C	90.3	91.8	92.7
H	1.6	1.4	1.1
O (by difference)	7.5	6.1	5.5
N	0.6	0.7	0.7
Ash constitutes (µg/g wood pellet)			
Mg	79	74	75
P	7	6	5
K	226	230	230
Ca	485	495	496
Mn	80	88	90

The structure of pyrolysis char obtained from N_2, and CO_2 pyrolysis is depicted in Figure 4.3. The pore size of the pyrolysis char produced from 100vol% CO_2 pyrolysis was smaller (3.9±1.1 μm, Figure 4.3(E)) compared to that from the N_2 atmosphere (7.0±1.8 μm, Figure 4.3(B)). This is attributed to CO_2 reacting with the pyrolysis char, increasing the pore size, and thus facilitating the release of volatiles trapped within the pyrolysis char (Brewer et al., 2009). This theory is further corroborated by the reduced volatile content in the CO_2 pyrolysis char relative to the N_2 pyrolysis char (Table 4.1). A previous study (Ouyang, 2020) stated that the pyrolysis char surface from CO_2 pyrolysis exhibits a more pronounced macropore structure than that from N_2 pyrolysis.

Additionally, our study found that the bulk density of the pyrolysis char (0.9±0.1 g/cm^3) was lower in the CO_2 environment than in the N_2 environment (1.0±0.1 g/cm^3). This suggests that the pyrolysis char produced in the CO_2 environment is more porous than that from the N_2 environment, thereby reducing diffusion limitations and improving the reactions between pyrolysis char and gas in the gasification stage (Lenis et al., 2013).

The goal of using pyrolysis char in the second stage of our study is to augment the production of gas products by enhancing the heterogeneous reactions between the volatiles released from the feedstock in the initial stage (e.g. CH_4, CO_2, CO, C_2-C_5, H_2, acids, esters, ketones, phenols, etc.) and the solid pyrolysis char. The key heterogeneous reactions taking place in the second stage are detailed in R4, R5, R8, R9, and R10 in Table 2.1.

Experiments were conducted both with and without pyrolysis char present in the second stage of the two-stage gasification process, in order to compare the efficacy of the proposed method. Results indicated that the gas yield was substantially increased by around 20 wt% (from 78.5wt% to 97.7wt%), when pyrolysis char was introduced at the second stage of the gasification process. This enhancement is attributed to pyrolysis char's catalytic role in the second gasification stage, which stimulates the heterogeneous reactions between the volatile constituents liberated from the feedstock in the initial stage and the solid char. Pyrolysis char's high surface area and porous structure offer numerous active sites for gas-solid interactions, thus leading to a surge in the generation of gas products such as CO, H_2, and CH_4. In addition, pyrolysis char aids in the reduction of tar and other impurities in the syngas by absorbing them onto its surface, which further ameliorates the quality of the gas output. In summary, the incorporation of pyrolysis char in the second gasification stage can enhance the efficiency and

yield of the process, rendering it a more sustainable and cost-effective alternative for synthesizing syngas from biomass waste feedstocks.

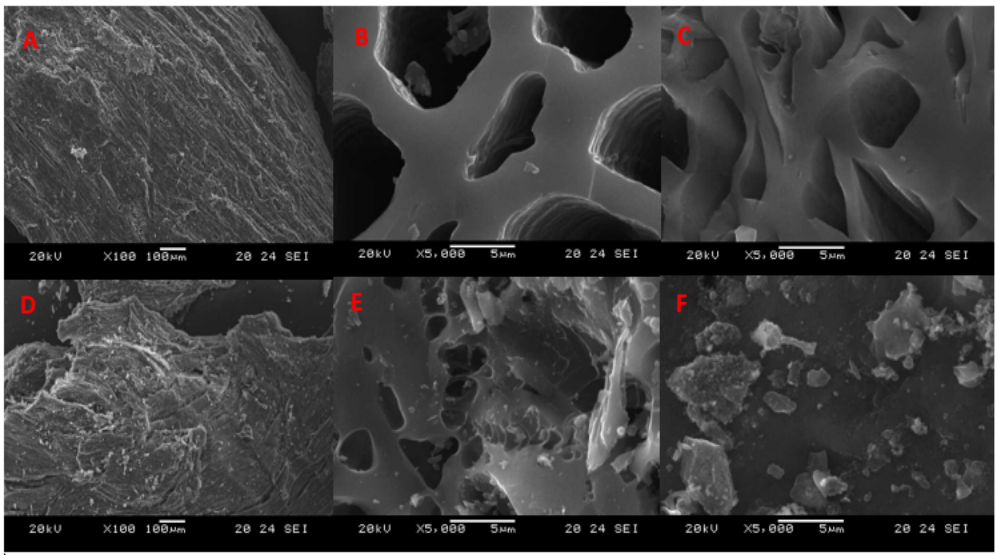

Figure 4.3: Scanning Electron Microscopy (SEM) examination of pyrolysis char derived from A.) N_2 at 100x magnification, B.) and C.) N_2 at 5000x magnification, D.) CO_2 at 100x magnification, E.) and F.) CO_2 at 5000x magnification

The composition of inorganic elements in the pyrolysis char obtained from both N_2 and CO_2 environments was comparable to that in the initial feedstock. The calcium (Ca) was found in the range of 417-496 µg/g feed, followed by potassium (K) with 226-230 µg/g feed, manganese (Mn) in the range of 80-103 µg/g feed, magnesium (Mg) at 70-79 µg/g feed, and phosphorus (P) measured between 5-7 µg/g feed. This can be attributed to the lower operational temperature utilized in this study (900°C), which is below the boiling points of these inorganic compounds (like Mg, Ca, Mn). As a result, these elements accumulate in the ash content as calcium silicates, oxides, hydroxides, phosphates, or carbonates (Dahou, 2021). Elements like Ca, P, and Mg tend to raise the ash melting temperature, resulting in enhancing ash stability and leading to higher ash recovery. On the other hand, potassium (K) at a high temperature (1100°C) can release 10-15% more and enhances the probability of corrosion when it reacts with silicon (Si) or sulfur (S), especially in comparison to a lower temperature (900°C) (Strandberg, 2017).

Figure 4.4 displays the correlation between the content of volatiles released and the residence time during an isothermal process at 700°C. The peak volume of volatiles emitted from both CO_2 and N_2 environments was akin after 90s of operation, though the emission rate from CO_2 pyrolysis was marginally slower than that in the N_2 environment during the initial 0-90s. This

could be due to the partial pressure from CO_2 inhibiting the production of CO and CO_2 via decarboxylation and decarbonylation from wood pellet pyrolysis. However, this effect diminished after the temperature reached 700°C due to the significant decrease in CO_2, which can be seen in Figure 4.2(B), as a consequence of the Boudouard reaction (Tang et al., 2017). This is consistent with the internal temperature profile observed during the pyrolysis of wood pellets. As illustrated by the dashed line in Figure 4.4, the recorded temperature inside a wood pellet during N_2 pyrolysis was slightly elevated compared to that in CO_2 pyrolysis at the onset (0-90s). Thus, to maximize the benefits derived from CO_2 pyrolysis, a retention time exceeding 90s is advised for the process at 700°C.

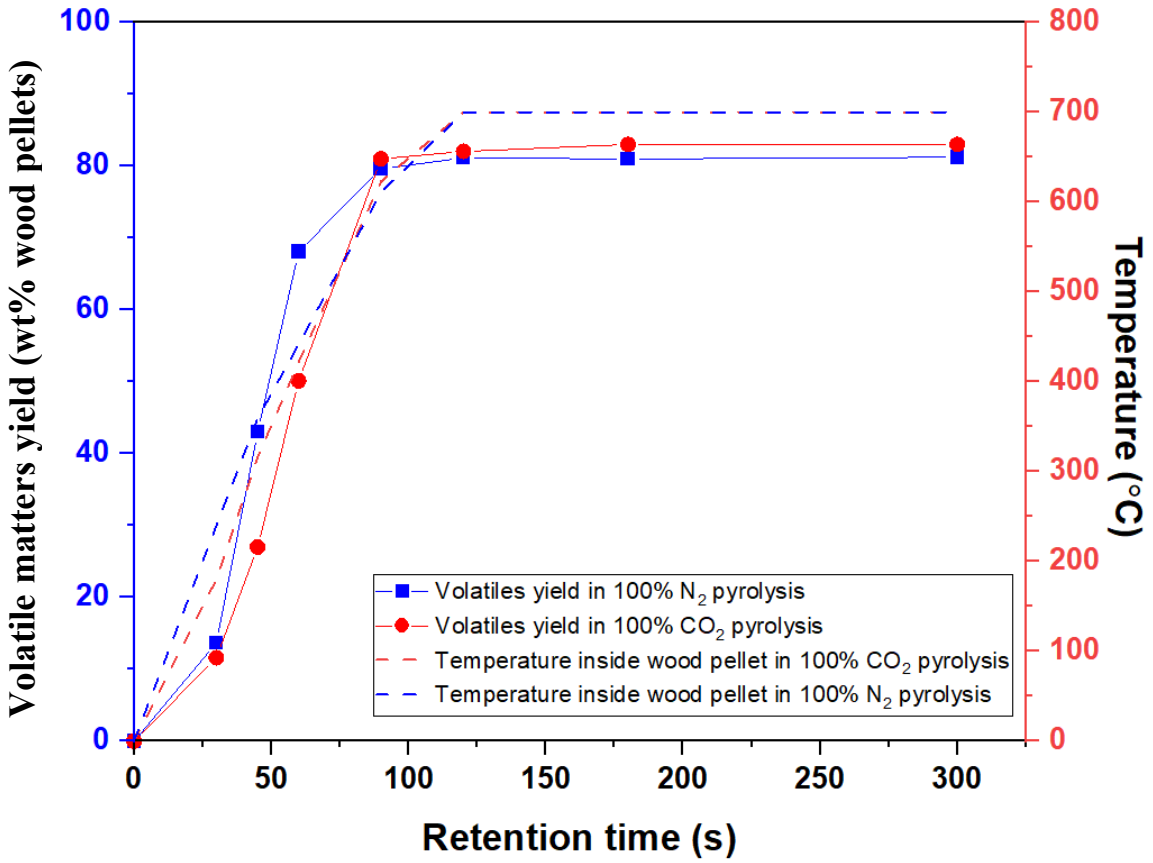

Figure 4.4: Evolution of volatile compounds during the pyrolysis of wood pellets in (100vol%) N_2 and (100vol%) CO_2 atmospheres at 700°C (isothermal process) and corresponding temperature trajectories within an individual wood pellet.

The environment in which pyrolysis is executed plays a significant role in influencing the outcome of the process. Utilizing CO_2 as a reaction medium in pyrolysis procedures has proven to enhance the efficiency of carbon conversion, evidenced by the rise in gas yield from 28.0wt% during N_2 pyrolysis to 39.5wt% in CO_2 pyrolysis (as illustrated in Table 4.1). Pyrolysis facilitated by CO_2 leads to more effective decomposition of the feedstock and yields lower

amounts of liquid (diminished by 8.5wt%) and solid by-products (diminished by 3.0wt%) compared to pyrolysis performed in N_2. The introduction of CO_2 can also amplify the production of CO during the pyrolysis of a majority of waste feedstocks (increased by 9.86 mol%). This might be attributed to CO_2's ability to impede the formation of secondary char, thereby fostering the cracking of tar and the polymerization of volatile species. Furthermore, pyrolysis assisted by CO_2 proves effective in waste treatment by inhibiting the generation of harmful chemicals such as phenols, which saw a reduction of 9.6 wt% compared to N_2 pyrolysis.

4.2 Two-stage Gasification with CO_2 and steam

In the first stage, fixed at 700°C for pyrolysis/devolatilization, the hydrogen content demonstrated an increase with the rising temperature in the second stage (gasification step). For instance, it went from 72 mg/g feed (wood pellets) at 700°C to 87.6 mg/g feed at 900°C (Figure 4.5) and maintained between 85.4-87.6 mg/g feed as the temperature in the second stage increased from 900 to 1000°C. This was observed for both steam and CO_2-steam gasification scenarios at a steam to carbon molar ratio of 5.7. The highest hydrogen content reached was 87mg/g wood pellets, nearly twice the H_2 yield from fluidized bed gasifiers performing steam gasification of wood pellets within a temperature range of 830°C to 900°C (32-49mg/g feed) (Umeki et al., 2010, Koppatz et al., 2011, Michel et al., 2011, Rapagnà et al., 2011). Elevating the second-stage temperature further to 1100°C caused a slight decrease in H_2 content to 70.4-75.6 mg/g wood pellets. This pattern has also been noted in other studies (Chojnacki et al., 2020, Tian et al., 2017, Robinson et al., 2016, Li, 2014) that recorded a decline in the hydrogen yield from biomass waste steam gasification at temperatures exceeding 917°C to 1000°C. It is inferred that 1000°C in steam gasification and 900°C in CO_2-steam gasification are optimal temperatures for steam reforming, dry reforming, and water-gas shift reactions, considering the thermal stability, CCE, H_2, and tar content. Based on the mass balance analysis, about 34.1wt%-55.4wt% of the hydrogen in the gas stream from steam gasification and 30.5-51.0wt% from CO_2-steam gasification were supplied from steam. These experimental findings align well with

simulation work (Demol et al., 2021) where H_2 produced from the water-gas shift reaction accounted for 44.2wt% of the total H_2 from the gasification process.

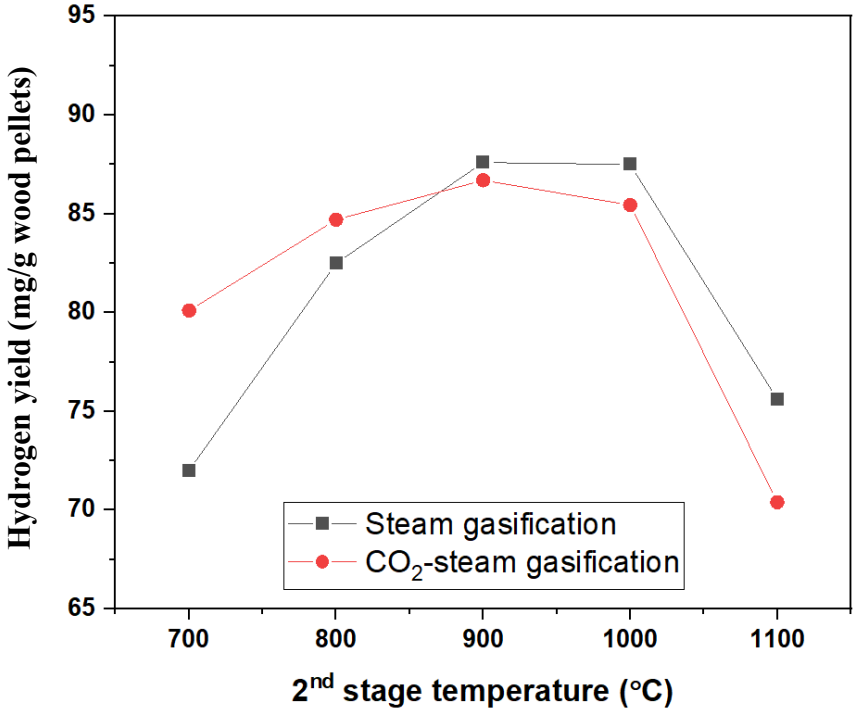

Figure 4.5: Hydrogen yield under different circumstances with a set temperature of 700°C in the first stage and a steam-to-carbon molar ratio of 5.7 (error ± 3.3 mg/g of wood pellets).

Even though the hydrogen production was equivalent, the H_2/CO ratio in CO_2-steam gasification (1.6-2.3), which is favourable for Fischer-Tropsch synthesis (dos Santos and Alencar, 2020), was lower compared to steam gasification (3.2-3.8). This is a result of CO_2 reacting with char to create CO via the Boudouard reaction. The lower heating value (LHV) of the gas yielded from steam gasification (9.6-11.6 MJ/kg) was inferior to that from CO_2-steam gasification (11.2-12.6 MJ/kg), due to the CO composition in the resultant gas. We achieved around 96.7%-99.5% carbon conversion efficiency, defined as the ratio of carbon in the producer gas to the carbon in wood pellets (Table 4.2).

An increase in methane yield could be partly due to the reduction in tar and hydrocarbons in the ash, which decompose more efficiently at elevated temperatures (Saleem et al., 2019). However, incorporating CO_2 into the gasification process can influence the methane yield differently. In the presence of CO_2, the methane yield doesn't increase with temperature, as CO_2 reacts with hydrocarbons and tar to form carbon monoxide (CO) rather than methane. This reaction, known as the Boudouard reaction (R8) (Wiberg et al., 2001).

The CO generated from this reaction can further engage with steam or other gases, leading to the production of additional H_2 and CO_2. The dry reforming reaction ($CH_4 + CO_2 \rightarrow 2CO + 2H_2$) also contributes to this behaviour, as it enhances the probability of CH_4 reacting with CO_2, thereby increasing CO and H_2 quantities, a mechanism mirrored in steam gasification (Gao et al., 2018). Our manuscript's Table 4.2 likewise illustrates that the CO content in the gas product is greater for CO_2 gasification than for steam gasification.

To summarize, the substantial increase in methane yield when using steam at 1100 °C can be ascribed to a reduction in tar and hydrocarbons in the ash. Introducing CO_2 into the gasification process can catalyse a different set of reactions yielding different products, such as the creation of CO in place of methane. These outcomes underscore the importance of selecting the proper gasifying agent to reach the desired products and yields in the gasification process.

Tar content in the gas stream affects process efficiency (Assima et al., 2019) and can lead to downstream complications such as clogging and fouling. Depending on the application pathways, there are limits on the acceptable level of tar in syngas, e.g., 50 mg/Nm^3 for internal combustion engines or <0.1 mg/Nm^3 for fuel cell and liquid fuel synthesis. Our study detected tar levels between 493.6-748.7 mg/Nm^3 and 31.3-222.2 mg/Nm^3 in steam gasification and CO_2-steam gasification, respectively (Table 4.2), which are considerably lower than those from fluidized bed gasifiers (20,000-38,000 mg/Nm^3) (Schmid et al., 2018) and updrafts (50-100 g/Nm^3) (James R et al., 2016). The amount of tar reduced with an increase in the operating temperature in the 2nd stage (gasification stage) and the concentration of CO_2 in the carrier gas. The main chemical constituents in tar were light poly aromatic hydrocarbons (PAHs) (42-45wt%), heavy PAHs (19-29wt%), naphthalene (22-25wt%), and heterocyclic aromatic (6-10wt%). Table 4.2 indicates that the gas yield significantly increased, while tar content decreased, when using CO_2-steam compared to steam at 900°C. This is because CO_2 reacts with volatiles via dry reforming.

Table 4.2: Performance and product yields from two-stage gasification of wood pellets at a constant first-stage temperature of 700°C and a steady steam to carbon (S/C) molar ratio of 5.7 across various second-stage temperatures

	Steam gasification			**CO_2 -steam gasification**		
2nd stage temperature, °C	900	1000	1100	900	1000	1100
Gas yield, wt%feed ±0.8	91.3	97.7	98.6	97.4	98.2	98.7
Water, wt%feed ±0.0	3.7	2.0	1.2	1.3	1.3	1.2
Tar yield, wt% feed ±0.5	0.1	0.1	0.1	0.1	0.0	0.0
Gasification char, wt%feed ±0.3	4.9	0.2	0.1	1.2	0.5	0.1
H_2, mg/g feedstock ±3.4	87.6	87.5	75.6	86.7	85.4	70.4
CO, mg/g feedstock ±29.4	380.3	325.8	289.3	529.2	584.4	613.9
CO_2 mg/g feedstock ±67.4	760.8	865.3	932.8	669.1	716.1	786.1
CH_4, mg/g feedstock ±2.6	43.6	40.0	107.6	66.1	59.4	50.5
Tar, mg/Nm^3 ±28.4	748.7	571.4	493.3	222.2	103.4	31.2
Heterocyclic aromatic (µg/g)	133.7	101.8	94.4	84.3	9.7	5.1
Light PAHs (µg/g)	557.2	428.6	39.8	188.0	99.1	33.5
Heavy PAHs (µg/g)	237.9	181.1	16.9	87.7	55.1	23.1
Naphthalene (µg/g)	319.3	243.1	222.6	118.5	47.8	18.0
Unknown (µg/g)	152.0	245.3	216.5	121.4	88.3	20.2
Solid residue						
Proximate analysis (based on pyrolysis char, as received)						

Moisture, wt% ±0.2	1.0	0.9	0.8	0.8	0.7	0.7
Fixed carbon, wt% ±2.7	85.2	63.5	54.4	66.0	58.7	55.2
VM, wt% ±0.4	5.9	3.2	2.6	1.2	0.6	0.6
Ash, wt% ±0.2	7.9	32.4	42.2	32.0	40.0	43.5
Element analysis (wt%, as received)						
C	90.5	65.6	55.4	66.3	58.0	54.1
H	0.9	0.6	0.4	0.5	0.5	0.3
O*	0.1	0.9	1.5	0.6	1.7	1.6
N	0.5	0.5	0.5	0.6	0.5	0.4
Efficiency						
CCE, %	87.0	96.7	99.1	99.2	99.5	100.0
CGE, %	57.7	55.0	61.6	63.0	61.8	59.3
PE, %	52.4	49.7	55.4	57.3	55.8	53.3
H_2/CO	3.2	3.8	3.7	2.3	2.0	1.6

*By difference

In both steam and CO_2-steam two-stage gasification processes, the hydrogen content in the gas stream was approximately 55-60mol%. A wood chip downdraft gasifier utilizing steam and air at 900°C generated only 19-23 mol% H_2 (Ngamchompoo and Triratanasirichai, 2017). Similarly, a steam/air fluidised bed gasifier produced 40 mol% H_2 at temperatures ranging between 820°C and 950°C (Schmid et al., 2018, Schweitzer et al., 2018). Using only steam (with an S/C molar ratio of 2) in a fluidised bed gasifier at 800°C-900°C resulted in up to 50mol% H_2 (Cortazar et al., 2018). These findings suggest that the highest amount of hydrogen in the synthetic gas product was obtained through a two-stage gasifier. In this process, the volatiles and char produced in the pyrolysis/devolatilization stage at a controlled temperature range (500°C -900°C) are transferred to the adjacent second stage set at a specific temperature (700°C-1100°C). Here, steam is injected, allowing ample time for interactions and reactions to occur.

The Sankey diagram in Figure 4.6 presents the total carbon balance for wood pellets CO_2-steam in a two-stage gasification at 700°C (1st stage or pyrolytic stage) and 900°C (2nd stage or gasification stage) with an S/C ratio of 5.7. The diagram aids in determining the quantity of

carbon recycled from CO_2. 'C in feed' and 'C in CO_2 agent', on the left side, represent the carbon inputs in this two-stage gasification system. 'C in CO', 'C in CO_2', 'C in CH_4', and 'C in tar and residue (gasification char)', on the right side, depict the outputs.

The primary source of carbon in this process was from the wood pellets, contributing to 86wt% (463.2 mg/g wood pellets), while the remaining 14wt% was from the CO_2 agent (73.9 mg/g wood pellet), shown in blue on the left. Following gasification, the carbon distributed into products such as CO, CO_2, CH_4, and tar and residue (gasification char). A negligible 0.80wt% (4.3 mg/g wood pellets) of carbon inputs were transformed into tar and residue (gasification char), thus yielding a 3%-12% higher CCE for the CO_2-steam gasification than the steam gasification. About 9.23wt% of carbon inputs turned into CH_4, with the CO_2-steam gasification producing 32wt%-34wt% higher CH_4 content than the steam gasification at temperatures between 900°C and 1000°C. This is likely due to CO_2 methanation that either converts CO_2 into CO followed by methanation or directly hydrogenates CO_2 into methane (Wei and Jinlong, 2011, Ren et al., 2020).

Approximately 42wt% of the total carbon inputs (or 226.8 mg/g wood pellets) were converted into CO. At high temperatures (above 500°C), CO reacts with hydrocarbons and oxygenated compounds to form H_2 and CO, resulting in a 39wt%-112wt% higher CO content from CO_2-steam gasification than steam gasification and subsequently increasing the CGE up to 60%-63%. Around 48wt% of the total carbon inputs (256.4 mg C/g wood pellets) were converted into CO_2, with 81wt% originating from the wood pellets. Past research (Mauerhofer et al., 2019) on softwood pellet gasification in a single-stage CO_2-steam fluidized bed gasifier suggested that higher levels of CO_2 and H_2 production can be attributed to the two-stage gasification system, which provides sufficient interaction time between CO from wood pellets and steam. This research quantified the carbon content in CO_2, amounting to 207.5 mg C, produced during the wood pellet steam gasification tests.

To isolate the carbon content in CO_2 that originated from steam reforming and the CO_2 gasifying agent, the carbon content in CO_2 derived from the wood pellet was deducted from the total carbon in CO_2 generated throughout the experiments. It was found that the carbon in CO_2 coming from the CO_2 gasifying agent was 48.9 mg C. The use of CO_2 as a gasifying agent led to less overall CO_2 production compared to tests that only used water, and the CO_2 introduced as the gasifying agent could be repurposed in the process, thereby decreasing the total CO_2 output.

Moreover, the CO_2 introduced as the gasifying agent can react with hydrocarbons in char and tar to generate CO, further limiting CO_2 production. As depicted in Table 4.2, the tests involving $CO_2 + H_2O$ yielded less CO_2 than those using only water, underscoring the potential advantages of using CO_2 as a gasifying agent. This research demonstrates that CO_2-steam gasification not only yields high H_2 content (86-87 mg/g feed), but also results in reduced CO_2 production (a decrease of 13-18wt% from steam gasification). Steam gasification was conducted at 700°C for the first stage and 900°C-1100°C for the second stage, with a S/C ratio of 5.7.

Under the same conditions, CO_2-steam gasification produced about 256.4-288.3 mg C in CO_2 per gram of wood pellets. However, since the CO_2 can be recycled (at 73.9mg C in CO_2/g feed), the total CO_2 generated decreased to 182.5-214.4 mg C in CO_2/g feed. This is less than half the carbon content in CO_2 produced from burning wood pellets (450mg/g feed) (Wei et al., 2012). This underlines the advantage of employing CO_2 as a gasifying agent in conjunction with steam gasification, facilitating carbon recycling in CO_2 and subsequently generating green hydrogen. This contributes significantly to the sustainability of the process and provides an alternative method for carbon capture and utilization.

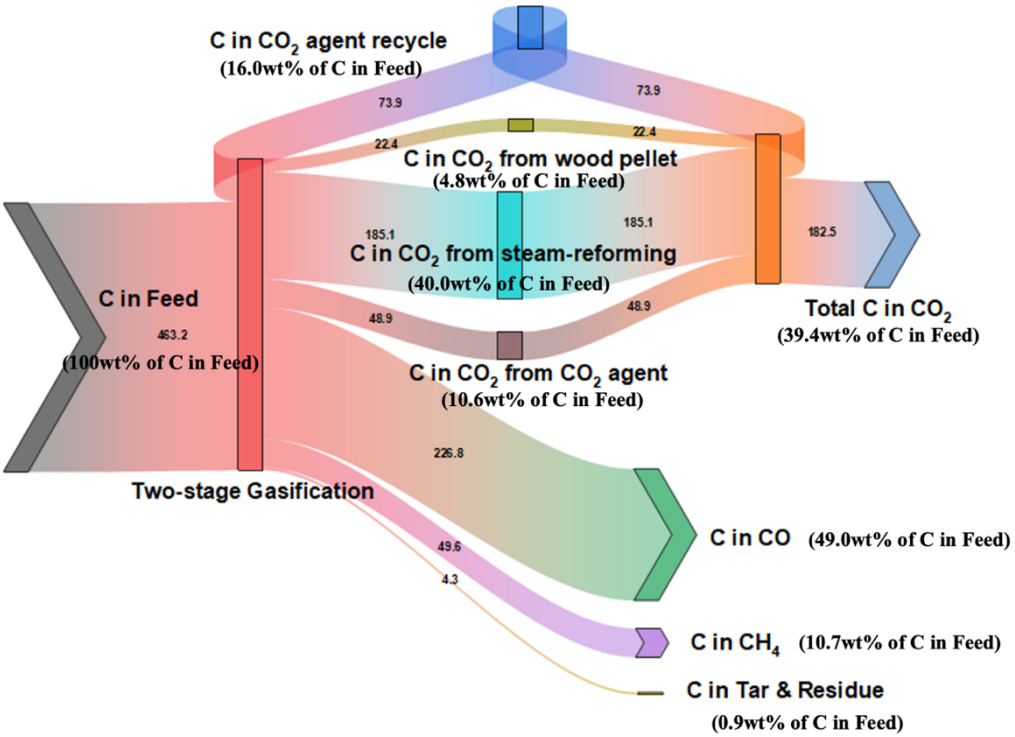

Figure 4.6: Illustration of carbon distribution in CO_2-steam gasification of wood pellets at a first-stage temperature of 700°C, second-stage temperature of 900°C, and a steam to carbon molar ratio of 5.7, with data represented in mg of carbon per g of wood pellets.

4.3 Summary

This research highlights the enhancement of biomass waste gasification and the use of CO_2 to significantly elevate hydrogen production. By independently managing the conditions in each phase (pyrolysis/devolatilization "1st stage" and gasification "2nd stage"), the process of CO_2-steam gasification produced a high gas yield of up to 97.4±0.8wt% with a significant hydrogen yield (86.7±3.3 mg H_2/g wood pellet) and a low tar content (0.2±0.0 g/Nm^3) at 700°C and 900°C in the 1st and 2nd stages. The hydrogen production exceeded the theoretical hydrogen content in wood pellets by 1.3 times. The tar content from this investigation was 47-79wt% and 95-99wt% less than that of a downdraft gasifier (152-414 mg/Nm^3) and a fluidised bed gasifier (6-14 g/Nm^3), respectively. The main constituents of tar were light PAHs (42-45 wt% of tar), naphthalene (22.6-25.2 wt% of tar), heavy PAHs (19.1-29 wt% of tar), and heterocyclic aromatics (6.4-10.7 wt% of tar).

The amalgamation of CO_2 and steam in gasification presented numerous advantages: it decreased the CO_2 in the gas stream by 13wt%-18wt% and augmented the CGE by 5.0%-6.8% in comparison to steam gasification due to steam reforming, dry reforming, and Boudouard reactions. Carbon conversion efficiency exceeded 99% at temperatures between 900°C -1000°C for CO_2-steam gasification or at 1100°C for steam gasification. It was determined that temperatures in the 1st stage (pyrolytic stage) above 700°C had a negligible impact on the gas characteristics (hydrogen content) and gasification performance (CCE). The H_2/CO ratio for steam and CO_2-steam gasification was 3.2-3.8 and 1.6-2.3, respectively. As a result, producer gas from steam gasification is appropriate for ammonia synthesis, fuel cell usage, methanol reactions, and Fischer-Tropsch liquid fuel production.

Chapter 5 Evaluate the effect of operational factors on hydrogen yield production in RDF CO_2-steam two-stage gasification

This chapter investigates the operational factors that influence the efficiency and production rates in two-stage gasification of refuse-derived fuel (RDF), focusing on variables such as first and second-stage temperatures, steam-to-carbon (S/C) ratios, and the role of CO_2 in the carrier gas. The study finds that optimizing these variables can significantly impact cold gas efficiency (CGE), process efficiency (PE), carbon conversion efficiency (CCE), and hydrogen yields. Higher first-stage temperatures in range of 600°C to 900°C increase overall gas yield and reduce solid and condensate yields, while second-stage temperatures between 870°C and 1100°C maximize hydrogen production. Optimal S/C ratios were identified for achieving the highest levels of PE and hydrogen production. Incorporating CO_2 as a carrier gas led to increased gas yield and environmental benefits, although it altered the H_2/CO ratio in specific applications. Importantly, the study establishes that different combinations of these operational parameters can be tailored for various end-use applications, such as ammonia production or fuel cells. The study also concludes that using RDF in an optimal CO_2-steam gasification setup could potentially contribute to approximately 11% of the UK's 2030 green hydrogen target. Future research is recommended for optimizing energy output, understanding scalability, and exploring additional environmental benefits, such as CO_2 reduction through catalysis.

5.1 Modelling of two-stage gasification using response surface methodology (RSM)

Response surface methodology (RSM) was applied to study the interactions of operating parameters on the two-stage gasification process (CCE, CGE, and PE) and properties of gas products such H_2 and CO_2 content and H_2/CO. The RSM coupled with a detailed 5-level analysis facilitates meaningful insights and provides comprehensive understanding with a reduced experimental test.

5.1.1 Statistical evaluation

In order to produce H_2-rich syngas, a total of 27 experiments were conducted, with additional runs (3 repetition at centre points, runs 25-27 shown in Table 5.1) executed to ensure

reproducibility. The experimental conditions and corresponding responses are presented in Table 5.1. Various models, including linear, two-factor interaction (2FI), cubic, and quadratic, were applied to fit the experimental data and establish the relationship between H_2 yield and the operational parameters of the two-stage gasification, such as 1st stage (pyrolytic stage) and 2nd stage (gasification stage) temperature, S/C, and CO_2 concentration in the carrier gas. Using the fitted data, a regression equation was derived to achieve the desired outcomes (Montgomery, 2017). Additionally, the model was assessed by comparing the seven (7) responses including H_2 (vol%), H_2 (mg/g RDF), CO_2 (mg/g RDF), H_2/CO, CCE, CGE, and PE with the experimental results.

Table 5.1 presents the sequential model sum of squares and corresponding model summary statistics. The selection of a model can be based on important parameters such as the p-value and F-value for the sequential model sum of squares. The p-value is a common and widely used statistical measure used to validate hypotheses against experimental data and is typically expected to be less than 0.05 for a significant model (Montgomery, 2017). A lower p-value indicates higher data significance toward the model.

Similarly, the F-value illustrates the impact of each controllable variable on the evaluated model and is calculated as the ratio of mean squares treatment to mean squares error. A larger F-value indicates greater variation across sample means in comparison to the variation within the samples. Furthermore, the lack of fit results indicates the significance of the model, and the lack of fit needs to be non-significant to properly fit the model with the response. Based on the results presented in Table 5.2, the quadratic model exhibited the highest lack of fit value. The model with the best fit for the response variables was determined based on the p-value of the lack of fit test.

Table 5.1: Experimental runs two-stage gasification of RDF pellets

where A: 1st stage (pyrolytic stage) temperature (°C), B: 2nd stage (gasification stage) temperature (°C), C: S/C (mol/mol), and D: CO_2 concentration in the carrier gas (vol%)

Run	**A**	**B**	**C**	**D**	**H_2**	**CO_2**	**H_2**	**H_2/CO**	**CCE**	**CGE**	**PE**
	°C	**°C**	**mol/mol**	**vol%**	**vol%**	**mg/g RDF**	**mg/g RDF**	**mol/mol**	**%**	**%**	**%**
1	500	700	2.8	50	40.0	807.6	44.2	1.8	90.0	63.5	63.1
2	700	700	2.8	50	40.2	829.6	45.7	1.7	90.5	63.5	57.6
3	500	1000	2.8	50	50.4	1073.1	83.0	2.1	96.1	69.2	83.4
4	700	1000	2.8	50	51.1	1060.4	88.5	2.1	97.0	72.2	78.9
5	600	850	0.0	0	32.0	379.1	22.0	0.9	84.3	79.3	61.1
6	600	850	5.7	0	51.2	1333.4	88.6	2.5	95.9	53.4	63.7
7	600	850	0.0	100	33.2	183.4	25.8	0.8	88.1	82.2	63.9
8	600	850	5.7	100	51.2	913.0	88.0	2.0	97.1	53.9	62.9
9	500	850	2.8	0	50.5	1213.5	81.1	2.4	93.7	68.7	79.0
10	700	850	2.8	0	50.5	1216.8	83.0	2.4	93.8	69.8	72.8
11	500	850	2.8	100	50.7	943.7	85.4	2.0	96.2	70.9	81.0
12	700	850	2.8	100	50.6	983.9	86.0	2.0	96.9	71.5	74.2
13	600	700	0.0	50	26.8	439.5	13.8	1.1	81.6	62.2	46.6
14	600	1000	0.0	50	28.3	162.0	20.3	0.7	85.0	87.0	66.0

Run	A	B	C	D	H_2	CO_2	H_2	H_2/CO	CCE	CGE	PE
	°C	°C	mol/mol	vol%	vol%	mg/g RDF	mg/g RDF	mol/mol	%	%	%
15	600	700	5.7	50	38.5	778.5	42.6	1.5	89.1	49.1	49.4
16	600	1000	5.7	50	51.2	1111.9	88.0	2.2	97.4	53.3	66.2
17	500	850	0.0	50	30.8	346.5	21.6	1.0	87.1	81.3	66.6
18	700	850	0.0	50	32.1	277.6	24.0	1.0	87.3	85.9	61.8
19	500	850	5.7	50	51.2	1136.1	83.4	2.4	96.7	50.0	62.0
20	700	850	5.7	50	50.6	1075.3	87.4	2.0	97.0	54.4	61.3
21	600	700	2.8	0	41.7	854.8	49.5	1.5	89.3	62.3	59.9
22	600	1000	2.8	0	52.6	1245.0	90.5	2.5	94.9	68.4	80.5
23	600	700	2.8	100	42.0	720.8	49.7	1.6	90.1	62.2	59.8
24	600	1000	2.8	100	52.0	760.1	95.8	1.7	97.0	77.6	86.8
25	600	850	2.8	50	52.2	1006.4	90.7	2.1	96.1	71.7	78.2
26	600	850	2.8	50	51.7	1053.9	88.4	2.2	96.2	71.1	77.6
27	600	850	2.8	50	51.9	1015.2	91.0	2.1	95.7	73.2	79.4

Table 5.2: The analysis of variance (ANOVA) of seven (7) responses versus operational factors; 1 = H_2 (vol%), 2 = H_2 (mg/g RDF), 3 = CO_2 (mg/g RDF), 4 = H_2/CO (mol/mol), 5 = CCE (%), 6 = CGE (%), 7 = PE (%)

Analysis of Variance (P value)

Source	**1**	**2**	**3**	**4**	**5**	**6**	**7**
Model	0.000	0.000	0.000	0.000	0.000	0.000	0.000
Linear	0.000	0.000	0.000	0.000	0.000	0.000	0.000
1st stage (pyrolytic stage) Temp (°C)	0.688	0.415	0.775	0.224	0.199	0.151	0.001
2nd stage (gasification stage) Temp (°C)	0.000	0.000	0.003	0.001	0.000	0.000	0.000
S/C (mo/moll)	0.000	0.000	0.000	0.000	0.000	0.000	0.933
CO_2 conc. (vol% of CO_2 in carrier)	0.746	0.417	0.000	0.001	0.000	0.089	0.082
Square	0.000	0.000	0.000	0.000	0.000	0.005	0.000
1st stage Temp (°C)*1st stage Temp (°C)	0.031	0.044	0.363	0.439	0.649	0.636	0.213
2nd stage Temp (°C)*2nd stage Temp (°C)	0.000	0.000	0.006	0.001	0.000	0.002	0.000
S/C (mol/moll)*S/C (mol/mol)	0.000	0.000	0.000	0.000	0.000	0.003	0.000
CO_2 conc.(vol% of CO_2 in carrier)*CO_2 conc.(vol% of CO_2 in carrier)	0.864	0.581	0.907	0.882	0.064	0.584	0.496
2-Way Interaction	0.009	0.119	0.020	0.007	0.016	0.037	0.456
1st stage Temp (°C)*2nd stage Temp (°C)	0.795	0.717	0.823	0.863	0.732	0.575	0.784
1st stage Temp (°C)*S/C (mol/mol)	0.370	0.888	0.959	0.203	0.952	0.971	0.272
1st stage Temp (°C)*CO_2 conc.(vol% of CO2 in carrier)	0.933	0.914	0.812	0.687	0.597	0.918	0.871

2nd stage Temp (C)*S/C (mol/mol)	0.000	0.004	0.002	0.002	0.001	0.002	0.496
2nd stage Temp (C)*CO2 conc.(vol% of CO_2 in carrier)	0.653	0.650	0.039	0.009	0.274	0.094	0.099
S/C (mol/mol)*CO_2 conc.(vol% of CO_2 in carrier)	0.591	0.697	0.164	0.093	0.038	0.637	0.333
Error							
Lack-of-Fit	0.056	0.055	0.089	0.071	0.149	0.137	0.214
Pure Error							

Table 5.3: Model summary statistics from RSM analysis

Model summary	**1**	**2**	**3**	**4**	**5**	**6**	**7**
Standard deviation	1.05168	5.5050	75.8465	0.1627	0.5711	2.5713	1.7813
R-sq	0.9934	0.9832	0.9770	0.9730	0.9933	0.9736	0.9866
R-sq(adj)	0.9858	0.9635	0.9501	0.9415	0.9854	0.9428	0.9710
R-sq(pred)	0.9624	0.9037	0.8688	0.8459	0.9619	0.8506	0.9251

Table 5.4: Standardize effect on 7 responses from 4 operational factors

	H_2 (vol%)	H_2 (mg/g RDF)	CO_2 (mg/g RDF)	H_2/CO (mol/mol)	CCE (%)	CGE (%)	PE (%)
1st stage (pyrolytic stage) temp. (°C)		2.25			1.12		4.62
2nd stage (gasification stage) temp. (°C)	15.49	11.57	3.74	4.43	18.68	7.25	20.31
S/C (mol/mol)	30.40	18.37	17.36	15.42	30.14	18.40	
CO_2 concentration (vol% in carrier gas)			6.61	4.62	6.84		
1st stage temp.*1st stage temp.	2.43						
2nd stage temp.*2nd stage temp.	11.73	7.59	3.32	4.28	11.75	3.90	8.38
S/C*S/C	22.07	13.15	9.82	9.40	17.54	3.72	19.15
CO_2*CO_2							
1st stage temp.* 2nd stage temp.							
1st stage temp.* S/C							
1st stage temp.* CO_2							
2nd stage temp.* S/C	5.29	3.53	4.03	4.08	4.25	4.00	
2nd stage temp.* CO_2			2.31	3.08			
S/C* CO_2					2.32		

According to the ANOVA table in Table 5.2, the overall model p-value (0.00), the liner p-value (0.00), the square p-vale (0.00), and the p-value of the two-way interaction (0.009) are lower than the level of significant (0.05) resulted in the rejection the null hypothesis of no relationship between the dependent and independent variables. Therefore, the full quadratic model, the linear terms, and the quadric terms of independent variables (1st stage temperature, 2nd stage (gasification stage) temperature, S/C, and CO_2 concentration) significantly affect the response percentage of responses (the dependant variable).
In term of prediction, the lack of fit (0.056) is higher than the level of significance (0.05) meaning that the quadratic model with the predictor variables significantly predict the percentage of seven (7) responses.

This Table 5.4 displays the standardized effects of various interactions between the four operational factors and their squared terms as well as interactions between the factors on seven (7) different responses. Interactions between factors are denoted by two letters (e.g., AB for the interaction between factors A and B). The table is organized as each row corresponds to a specific factor or interaction and each column corresponds to a different response (1 through 7).

The values in the Table 5.4 represent the standardized effects for each factor or interaction on the corresponding response which using the threshold of 2.18 for significance (alpha = 0.05), it can determine which factors and interactions have a significant effect on each response.
In the case of H_2 concentration (vol%), the effects of factors B, C, AA, BB, and CC are 15.49, 30.40, 2.43, 11.73, and 22.07, respectively, for instance. The detailed analysis of the effects of each operational factor on the seven distinct responses will be presented in the 5.2-5.5 section.

The method adopted in this research, utilizing RSM, offers several distinct advantages over traditional factorial designs. Primarily, RSM has been employed to succinctly evaluate the impact of operational variables on significant outcomes, including H_2 and CO_2 content, H_2/CO, CCE, CGE, and PE.

The RSM approach necessitates a mere 24 principal experiments, augmented by the additional three (3) repetitions to assess experimental variability. Such a structure allows for a preliminary understanding of the individual and combined effects of each operational variable. Though it's recognized that factorial design provides a comprehensive analysis of every factor, the exhaustive nature of such a design often proves to be resource intensive.

When combining the RSM methodology with this 5-level analysis, a total of 47 experiments suffices. Contrastingly, an equivalent exploration using a factorial design would necessitate as many as 625 experiments.

In light of these considerations, it becomes evident that while factorial design possesses merit in offering thorough insights, the combined RSM and 5-level approach proposed herein provides a more efficient and resource-conservative experimental strategy.

5.2 Effect of the 1st stage (pyrolytic stage) temperature

Gasification is a thermochemical process that converts carbonaceous materials into producer gas – a mixture of CO, H_2, and CO_2 and other impurities, which can be furthered purified and cleaned to produce syngas. A prominent method employed in this domain is two-stage gasification, where the initial stage, pyrolysis, revolves around thermal decomposition. The subsequent stage tackles the interaction of the pyrolyzed material with a gasifying agent to yield syngas. The pyrolysis temperature in the first stage is pivotal in this procedure. It affects the distribution of pyrolysis products, notably pyrolysis char, tar, and gases. Higher temperatures generally result in reduced tar and increased gas yields. Additionally, this temperature influences char reactivity, which is crucial for the second-stage gasification kinetics. Ultimately, optimizing the pyrolysis temperature is imperative to maximize process efficiency, enhance syngas quality, and minimize undesired by-products (see Table 5.5).

Table 5.5: Yield and properties of products derived RDF two-stage gasification over various temperature for the 1st stage (pyrolytic stage) temperature at a fixed the 2nd stage (gasification stage) temperature of 900°C, S/C of 3.5, CO_2 of 50vol%.

1st stage (pyrolytic stage) temperature (°C)	**500**	**600**	**700**	**800**	**900**
Gas yield (wt% RDF) ±1.2	85.7	87.3	87.0	87.9	88.0
Gasification char (wt% RDF) ±0.8	12.1	11.3	12.0	11.6	11.7
Condensate yields (wt% RDF) ±0.0	2.2	1.4	1.0	0.5	0.3
Wax (wt% RDF)	1.0	0.4	0.3	0.3	0.3
Tar (wt% RDF)	1.2	1.0	0.7	0.2	0.0
Gas (mol%)					
H_2 ±0.2	48.5	50.6	51.4	51.2	50.0

1st stage (pyrolytic stage) temperature (°C)	**500**	**600**	**700**	**800**	**900**
CO ±0.2	16.2	18.0	17.5	17.4	16.6
CO_2 ±0.1	28.9	28.9	29.9	30.1	32.1
CH_4 ±0.3	3.0	1.1	0.0	0.0	0.0
C_2-C_4 ±0.1	3.4	1.4	1.2	1.3	1.3
Gasification char (wt% gasification char**, as received)**					
C ±0.0	16.4	8.3	8.0	7.8	7.5
H ±0.0	0.2	0.2	0.2	0.2	0.2
N ±0.0	0.6	0.4	0.4	0.2	0.1
Wax (wt% wax as received)					
C ±0.0	70.3	62.1	60.1	58.3	54.7
H ±0.0	7.3	4.3	2.2	2.8	2.3
N ±0.0	0.1	0.1	0.2	0.3	0.4
Tar (g/Nm^3) ±0.7	8.1	6.6	4.2	1.1	0.1
Performances					
H_2/CO (mol/mol) ±0.0	3.0	2.8	2.9	2.9	3.0
CCE (%) ±0.2	93.3	96.3	96.8	97.8	98.2
CGE (%) ±0.9	63.5	62.8	62.4	62.2	60.4
PE (%) ±0.8	78.0	76.6	74.4	73.1	72.2

Table 5.5 showed a small increase in gas yield from 85.7% at 500°C to 88.0% at 900°C. This enhancement is attributed to the elevation in the first stage temperature, which augments the gas yield from both the pyrolysis and dry reforming reactions (Yazdani et al., 2019). The influence of temperature on the pyrolysis process, acting as the first stage in this experiment, is a well-documented phenomenon. For instance, an increment in the pyrolysis temperature from 300°C to 600°C has been found to escalate the gas yield by approximately 15.2-18.7% (He et al., 2018). However, the gas yield in this study did not exhibit a drastic increase, due to the fact that it is already approaching the maximum potential (89.6%) as dictated by the proximate analysis. This maximum yield is determined by the sum of volatile matter, moisture, and fixed carbon present in the refuse-derived fuel (RDF).

A distinctive advantage of a two-stage reactor, as employed in this study, is the extended retention time that it affords for the volatile matter from the RDF to be exposed to high heat zones. Evidence from past studies such as Kan et al. (2016) supports this, where increasing the

retention time from 0.2s to 1.7s corresponded to a reduction in condensate yield and an increase in gas yield by 7-18%.

Furthermore, in this two-stage gasification system, the retention time is observed to be around 2.5s-3.5s at 900°C. This contrasts with a single-stage system where the retention time ranges only between 0.4s-1.2s, thus highlighting the benefits of a two-stage system in enhancing gas yield.

Along with the rise in gas yield, the study also reveals a reduction in the gasification char (from 12.1wt% to 11.7wt%) and condensate yield (from 2.2wt% to 0.3wt%) as the first stage temperature increases (from 500°C to 900°C). This outcome suggests that the escalation in gas yield comes at the expense of the solid residue (gasification char) and condensate derived from the RDF. This phenomenon can be attributed to the influence of the higher first stage temperature on the overall system temperature, which consequently amplifies the thermal decomposition of RDF pellets into the gaseous phase.

This study also provides insights into the effect of increasing first-stage temperature on the carbon content in the solid residue (gasification char) and wax portion, as well as the tar yield. The carbon content in the solid residue (gasification char) saw a substantial decline from 16.4% to 8.3%. Even as the first stage temperature was further increased, the carbon content continued to decrease, albeit at a lower rate, from 8.3% at 600°C to 7.5% at 900°C. A similar trend was observed in the wax yield, where the carbon content reduced from 70.3% at 500°C to 54.7% at 900°C as the first-stage temperature was increased. These reductions in carbon content suggest that higher temperatures facilitate more efficient carbon conversion, leading to lower residual carbon content in both the solid and wax portions. Furthermore, the tar yield was also found to decrease significantly with higher first-stage temperature, plummeting from 8.1 g/Nm³ to a minuscule 0.1 g/Nm³. This further underscores the efficacy of higher in pyrolytic zone temperatures in reducing undesirable by-products like tar in the RDF gasification process.

It is observed in other chemicals such as methanol, formic acid, benzene, toluene, and the C_5-C_{13} hydrocarbon range that reduced as a function of 1st stage (pyrolytic stage) temperature (see Figure 5.1). However, an interesting anomaly occurs with Phenanthrene (C_{14}). Its concentration increases at 700°C but subsequently declines as the temperature escalates to 900°C. This transient increase in C_{14} is attributed to the tertiary tar formation involving precursor chemicals like toluene and indene. During this temperature window of 700°C to 900°C, these lighter

molecules evolve to form heavier molecules, specifically in the C_{13}-C_{26} range (Basu, 2018, Milne et al., 1998). Moreover, a thermal-induced shift in molecular sizes is also observed. Smaller molecules within the C_8-C_{13} range are reformed into larger molecules, such as C_{26}, as the temperature moves from 500°C to 900°C (Hwang et al., 2014).

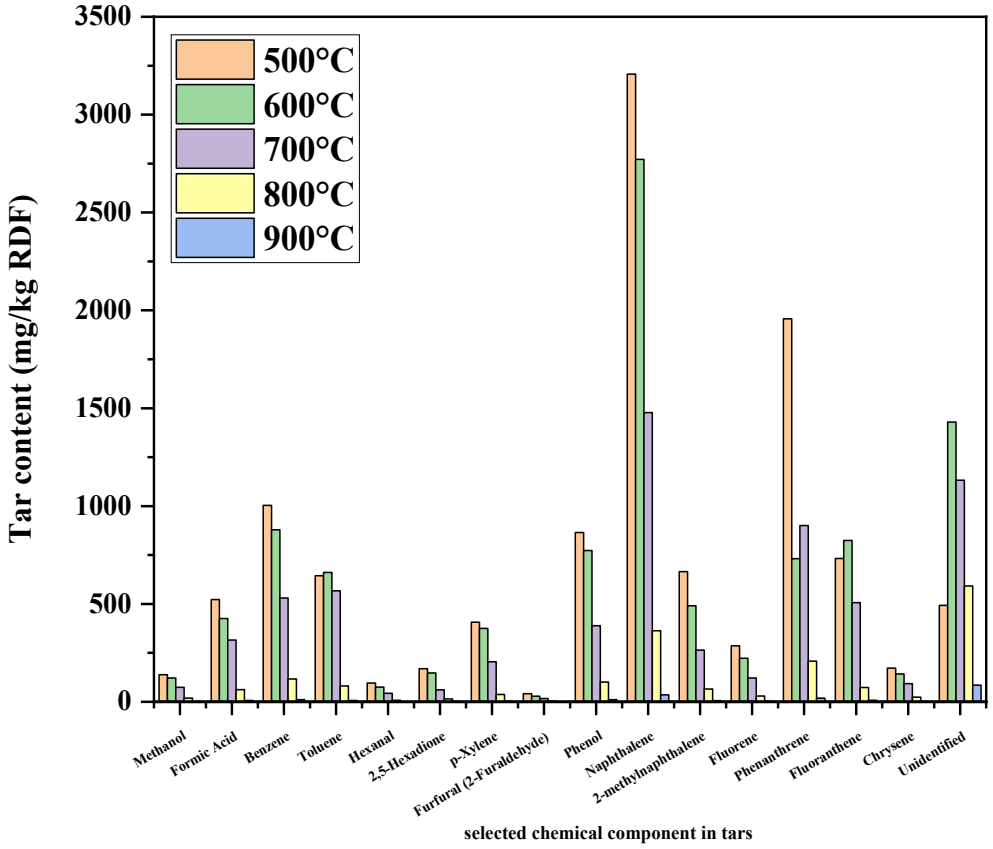

Figure 5.1: The composition of tar from RDF two-stage gasification with variation of the 1st stage (pyrolytic stage) temperature and fixed the 2nd stage (gasification stage) temperature (900°C, S/C = 3.5, CO_2 = 50vol%, based on 3 replicates).

Operating the first stage (pyrolytic stage) at temperatures lower than 400°C led to an interesting observation: wax accumulation at the junction between the steam and the second stage reactor. This is attributed to the significant generation of wax at such lower temperatures. Upon encountering the steam, which operates at 170°C, the wax causes a temperature drop and subsequent condensation. To tackle this technical challenge, researchers have proposed blending RDF with biomass waste (making up less than 25% of the total weight) to reduce blockages caused by wax formation, especially at temperatures above 550°C (Chavando et al., 2022). This blend is believed to facilitate secondary cracking reactions, thus reducing wax yield

and preventing the aforementioned issues. Considering of this, it is recommended that the operation be conducted at temperatures above 500°C to ensure the system runs smoothly, while also considering energy efficiency and gas yield.

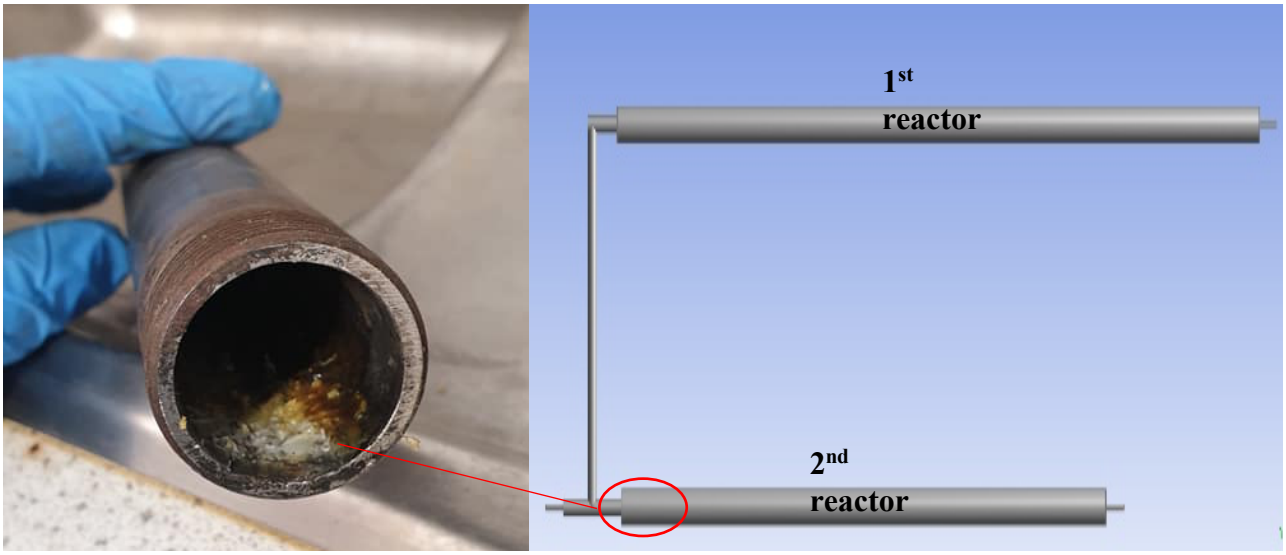

Figure 5.2: The waxy part that accumulated in the inlet of the 2nd reactor.

An elevation in the first stage temperature was also observed to increase CCE, experiencing an approximate increase of 5% when the temperature was raised from 500°C to 900°C. This confirms that a higher pyrolytic stage temperature promotes both dry reforming and pyrolysis reactions, as evidenced by the reduction in carbon content in the wax, tar, and solid residue (gasification char) in correlation with the first stage temperature. However, it is crucial to consider the energy consumption associated with this process. The benefits of a higher CCE resulting from an increase in the first stage temperature may be counterbalanced by the higher energy expenditure required to increase the temperature from 500°C to 900°C. Therefore, while the increase in temperature facilitates better carbon conversion and gas efficiency, it also necessitates a greater input of energy, which can impact the overall efficiency of the gasification process.

As the temperature is increased from room temperature to 600°C, the content of hydrogen (H_2) escalates to approximately 50 mmol/g RDF and remains fairly stable, ranging from 50.0-51.4 vol% beyond 600°C up to 900°C. The production mechanism of H_2, which primarily relies on steam and dry reforming reactions, benefits from high temperatures. Moreover, the water gas shift reaction, which typically favours a temperature around 400°C, is satisfied within this

temperature range. This demonstrates that a temperature of 600°C or higher is sufficient for optimizing hydrogen production in the RDF gasification process, as it effectively supports all the key reactions responsible for hydrogen generation.

In this study, it's found that the ratio of hydrogen to carbon monoxide (H_2/CO) remains fairly constant, ranging from 2.8-3.0, irrespective of changes in the first stage temperature. As the temperature increases, both H_2 and CO volumes rise, thus the ratio between these two gases does not show a significant shift. While CO holds utility for heat production, Fischer-Tropsch synthesis, and alcohol synthesis, it is less desirable in this context, particularly for ammonia syngas production. It's important to note that CO can temporarily deactivate ammonia synthesis catalysts (Zheng et al., 2022). Thus, in the process of ammonia production, it's necessary to reduce the CO content of the producer gas to below 1% before initiating ammonia synthesis (Pattabathula and Richardson, 2016). According to Yang et al. (2021), a H_2/CO ratio above 2.5 is deemed suitable for ammonia production. Considering the observed range of 2.8-3.0 in this study, it suggests that the resultant gas from the RDF gasification process can be potentially suitable for ammonia production, once the CO concentration is sufficiently reduced.

Cold gas efficiency (CGE) demonstrates an upward trend from 68.2% at 500°C to 70.6% at 800°C. However, a decrease is observed when the temperature is further increased to 900°C, dropping to 66.4%. The rise in CGE between 500°C and 800°C can be attributed to the concurrent increase in gas yield, which results in enhanced cold energy from the H_2 and CO-rich syngas. Conversely, the decline in CGE at 900°C can be linked to the composition of the producer gas at this temperature. At 900°C, the producer gas contains a higher proportion of CO_2 - up to 32.1 vol%. Given that CO_2 does not contribute to energy production, its increased presence results in a lower CGE.

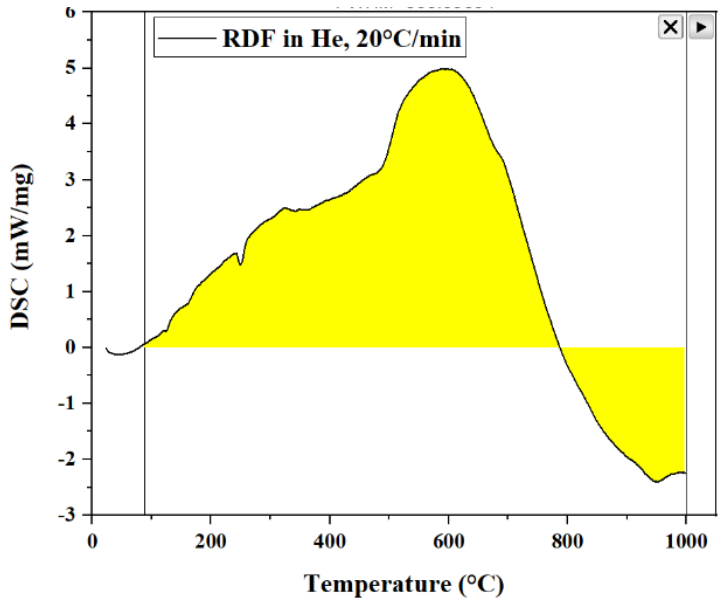

Figure 5.3: The Differential Scanning Calorimetry (DSC) of Refuse-Derived Fuel (RDF) at 20K/min in He atmosphere showing the energy used during pyrolysis.

Operating at 900°C requires an additional 2.6 MJ/kg RDF compared to operating at 500°C. Consequently, this higher energy demand results in a reduction in process efficiency (PE) to 16%. This is because the reactions occurring at the first stage (pyrolytic stage) temperature are primarily endothermic, necessitating more external energy.

For comparison, RDF gasification using air as a gasifying agent records a PE in the range of 65.8-68.5% (Dong et al., 2016). It is suggested that elevating the temperature beyond 750°C would significantly impair PE.

While air gasification has the advantage of self-heating from combustion reactions, the lower heating value (LHV) of its producer gas, 2-6 MJ/Nm³ (Dong et al., 2016), is less than that derived from CO_2-steam gasification (12.8-13.4 MJ/Nm³). This aligns with our findings that while gas yield marginally increases with higher first-stage temperature, it is not sufficient to offset the energy input, causing PE to decrease from 80.4% at 500°C to 64.3% at 900°C.

Therefore, the energy in air gasification predominantly derives from the lower heating energy required for the pyrolysis reaction. In contrast, the energy in steam gasification is sourced from the high LHV syngas, which is rich in H_2 and CO. Hence, while air gasification may seem more efficient due to self-heating, steam gasification provides a higher quality energy output.

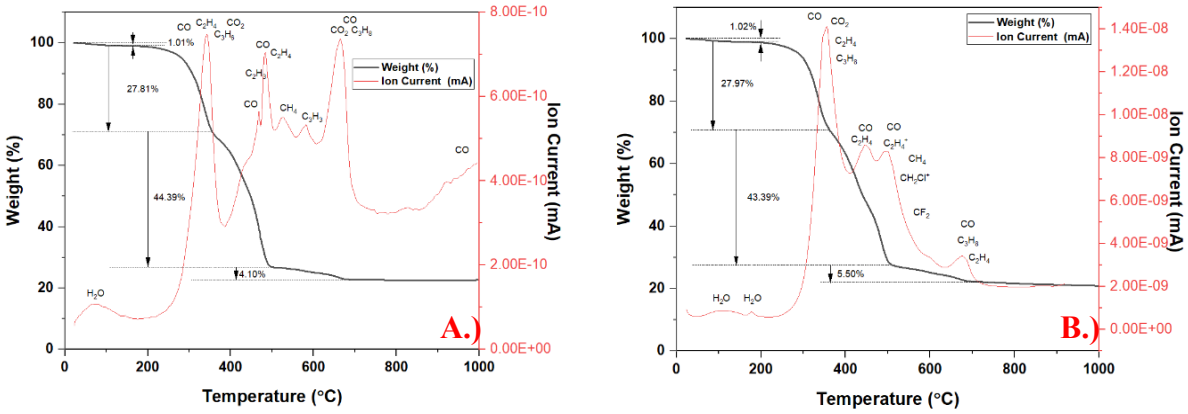

Figure 5.4: Comparison of weight loss and species detected by mass spectrometry (TGA-MS) of RDF in the pyrolysis (simulated the condition in the 1st stage rector) at A) 10°C/min and B) 20°C/min.

The Refuse-Derived Fuel (RDF) in this study already exhibits a low moisture content (1.0wt%), which is conducive to thermochemical reactions. The energy required for drying during the first stage reactor is approximately 0.8 MJ/kg RDF, as determined by Differential Scanning Calorimetry (DSC). This drying process occurs within the temperature range of 15°C to 130°C. It's important to note that high moisture content (above 30wt%) can prevent ignition and negatively affect the heating value of the syngas (Kirsanovs et al., 2014).

One way to overcome this issue is to transform RDF shreds into pellets, which helps maintain a more homogeneous moisture content and prevents the typically high moisture content in RDF shreds (15-20wt%). However, the conversion of RDF shreds into pellets does require additional energy (336-340 MJ/t (Caputo and Pelagagge, 2002)). The specifics of this energy input, and its impact on the overall energy efficiency of the process, will be discussed in the next chapter of the thesis. This discussion is essential to accurately assess the overall energy and environmental implications of using pelletized RDF for gasification.

The first major decomposition of the RDF in inert atmosphere (He) (see Figure 5.4) during the initial stage occurs between temperatures of 204°C and 361°C. This decomposition accounts for approximately 27.8-28.0wt% of RDF, with an energy consumption of 1.5 MJ/kg RDF during this period.

During this phase, gases such as CO, CO_2, C_2H_4, and C_3H_8 are generated. The compounds that typically undergo decomposition under these pyrolytic conditions include materials like

polystyrene (PS), which mainly produces C_2H_4, C_3H_6, CH_4, and H_2. Conversely, the production of CO and CO_2 in this temperature range is primarily associated with the biomass waste content of RDF (Aluri, 2018a). These findings underscore the heterogeneous nature of the materials that make up the RDF, reflecting the diverse origins of the waste that composes the fuel.

The third stage of the process (Figure 5.4A) involves a significant mass reduction occurring between 354°C and 498°C, accounting for 44.4wt% of RDF at a heating rate of 10°C/min. This stage also occurs between 361°C and 509°C, representing 43.4wt% of RDF.

This phase is typified by the presence of various gases, including CO, CH_4, CH_2Cl, C_2H_4, and C_3H_8. During this temperature range, the majority of plastic materials within the RDF, such as Low-Density Polyethylene (LDPE), High-Density Polyethylene (HDPE), Polypropylene (PP), and Polyethylene Terephthalate (PET), generally undergo volatilization (Aluri et al., 2018).

The final, fourth stage of the process in Figure 5.4A, involves a mass loss occurring between 498°C and 680°C, accounting for 4.1wt% of the RDF at a heating rate of 10°C/min. Similarly, this stage takes place between 509°C and 725°C, representing 5.5wt% of RDF.

During this phase, the primary substances detected are CO, C_2H_4, and C_3H_8. The remaining RDF mass stands at 22.8wt% at a heating rate of 10°C/min and 22.1wt% at a heating rate of 20°C/min. This remainder represents the yield of RDF-pyrolysis char. Due to the heterogeneous nature of RDF, the char yield resulting from pyrolysis can exhibit considerable variability, ranging between 16.9 wt% and 56.7 wt% of the original RDF (Ulusoy et al., 2019).

Table 5.6: The proximate analysis of RDF-pyrolysis char, products from 1st stage (pyrolytic stage) reactor, was varied with the 1st stage (pyrolytic stage) temperature between 500°C and 900°C with the atmosphere of CO_2 (50% balanced with N_2).

Proximate Analysis (% RDF as received)	**1st stage (pyrolytic stage) temperature (°C)**				
	500	**600**	**700**	**800**	**900**
VM, ±0.0	4.5	2.0	2.1	1.7	1.4
FC, ±0.1	2.0	0.9	1.0	0.9	0.9
Ash, ±0.1	12.0	11.3	11.7	11.4	11.5

Upon introducing a 50vol% CO_2 atmosphere during pyrolysis, it was observed that elevating the first-stage temperature from 500°C to 600°C resulted in a decrease in pyrolysis char yield from 18.5% RDF to 14.2%, as illustrated in Table 5.6. Throughout this temperature increase, the ash content remained stable, ranging between 11.4wt% and 12.0wt% RDF. However, the fixed carbon content saw a notable decline, plummeting from 2.0% RDF at 500°C to 0.9% RDF at 600°C, and then marginally decreasing further to 0.9% RDF at 900°C. Concurrently, the volatile matter (VM) significantly dropped from 4.5% RDF (which equates to 24.5% of pyrolysis char) at 500°C to 2.0% RDF (14.3% of pyrolysis char) at 600°C, with a subsequent moderate reduction to 1.4% RDF (or 10.3% of pyrolysis char) at 900°C. These findings align with previous research (Phan et al., 2008), which emphasized a substantial reduction in the fractions of VM and fixed carbon in various materials, such as waste wood, cardboard, and textiles, as the pyrolysis temperature increased. Notably, the research mentioned that the VM fraction was less than 10% of the pyrolysis char beyond a pyrolysis temperature of 600°C.

Thermogravimetric analysis (TGA) results reveal that during the pyrolysis of Refuse Derived Fuel (RDF), the process of energy adsorption spans from 15°C to 1000°C, with a range of 2.4 to 5.4 MJ/kg. This phase corresponds to the heating-induced physical and chemical transformations within the material, where the absorbed energy facilitates the breakdown of complex organic structures present in the RDF, such as lignin, cellulose, plastics, and more, into simpler compounds (Stępień et al., 2019).

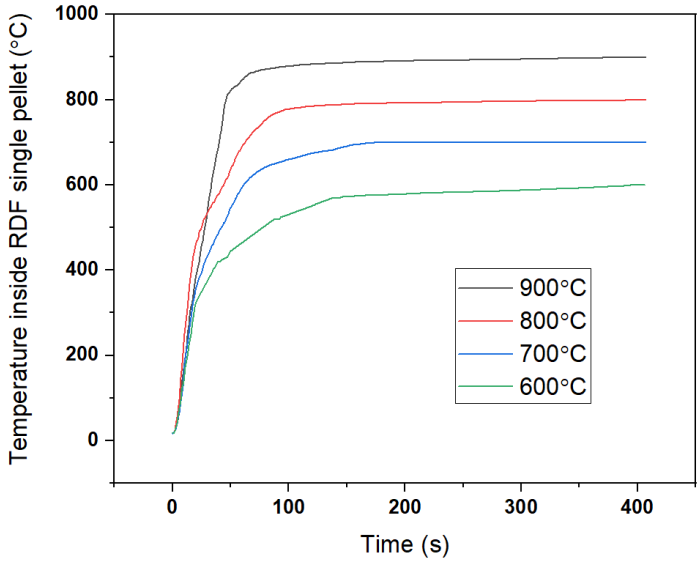

Figure 5.5: The temperature profile inside single RDF pellet during isothermal pyrolysis in N_2 atmosphere at different temperature.

Specifically, processes occurring during this phase include moisture evaporation, volatile compound release, and chemical bond breaking. These transformations contribute to the energy adsorption characteristics observed in the pyrolysis process. Comparatively, the enthalpy for woody biomass waste pyrolysis typically falls within 1.0 to 1.8 MJ/kg (Daugaard, 2003). This disparity is likely because conventional pyrolysis is commonly conducted at temperatures around 400°C-500°C (Yogalakshmi et al., 2022).

However, beyond the 788°C threshold, the DSC curve indicates that energy is being released, indicative of exothermic reactions occurring at higher temperatures, such as water-gas shift, methanation, or hydrogenation. As the RDF continues to decompose, these new chemical reactions start to dominate, releasing energy as heat.

Raising the first stage temperature may indeed lead to a reduction in process efficiency (PE), but it significantly increases the retention time inside RDF pellets. As depicted in the Figure 5.5, during the isothermal process in the first reactor at 900°C, the duration required for the temperature inside the RDF pellet to reach 600°C is only 33s. In contrast, when the same process is conducted at 600°C, it takes approximately 400s to reach the same temperature.

In other words, the higher the first stage temperature, the faster the pellet's internal temperature rises, which drastically reduces the time it takes for the pellet to reach optimal gasification temperature. This means that increasing the first stage temperature can significantly boost the production rate of the process, despite the associated decrease in PE.

Therefore, while high first-stage (pyrolysis stage) temperatures can result in lower PE, they can also increase the hydrogen production rate, which may benefit the operation of the plant overall. It must consider and strike a balance between PE and production rate according to their specific requirements and constraints. This trade-off is a critical consideration in optimizing the overall efficiency and throughput of the gasification process.

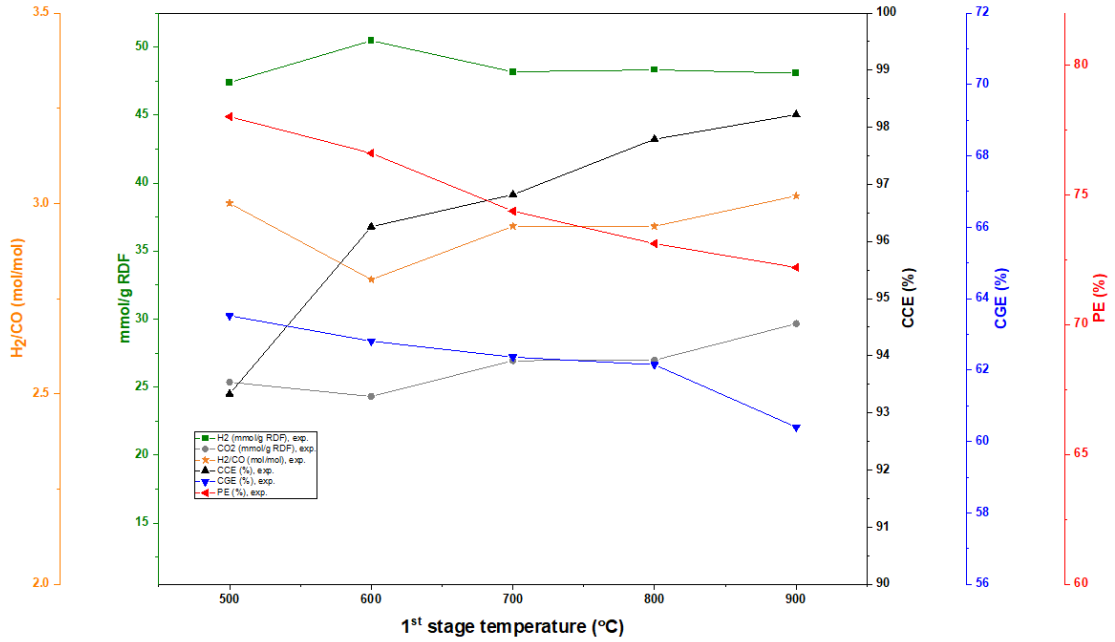

Figure 5.6: The summary performances of RDF two-stage gasification with the variation of 1st stage (pyrolytic stage) temperature and fixed the 2nd stage (gasification stage) temperature (900°C, S/C 3.5, and CO_2=50vol% balanced with N_2)

In summary, the investigation into the influence of first stage (pyrolysis) temperature in two-stage gasification of RDF demonstrates an intricate balance between process efficiency (PE) and hydrogen production rates. An increase in the first stage temperature not only augments the overall gas yield, as depicted by the rise from 85.7% at 500°C to 88% at 900°C, but it also reduces solid, and condensate yields due to enhanced thermal decomposition of the RDF. Additionally, it contributes to significant reduction in carbon content in both solid residues (gasification char) and wax fractions.

Moreover, the higher first stage temperatures have been found to increase Cold Gas Efficiency (CGE) up to 800°C, after which it starts declining due to increased CO_2 content in the producer gas. Process Efficiency (PE), however, sees an overall reduction with increased first stage (pyrolysis) temperatures.

Interestingly, despite the potential reduction in PE, the raised temperatures at the first stage have shown to remarkably increase the production rate by drastically reducing the time taken

for RDF pellets to reach optimal gasification temperatures. Therefore, while low PE may be a drawback, the increased production rate might be beneficial to plant operations. To that end, the operator must establish a delicate balance between PE and production rate, considering the specific needs and constraints of their limitations.

5.3 Effect of the 2nd stage (gasification stage) temperature

The second stage temperature in this study define as the gasification temperature, is a crucial determinant of the overall performance and efficiency of the gasification process. Any variation in this temperature can manifest in multiple aspects of the process, such as gas yield, solid residue (gasification char) formation, wax and tar reduction, the composition of producer gas, and various performance metrics like the hydrogen to carbon monoxide ratio (H_2/CO), cold gas efficiency (CGE), carbon conversion efficiency (CCE), and process efficiency (PE). Each of these parameters has a significant bearing on the practicality and effectiveness of the overall gasification, making it essential to understand their interplay with temperature. Drawing from both the experimental observations and literature comparisons, the following analysis seeks to elucidate the multifaceted impacts of changes in the second stage temperature on these parameters illustrated in the Table 5.7.

Table 5.7: Yields and product characteristic of RDF two-stage gasification with variation of the 2nd stage (gasification stage) temperature and fixed the 1st stage (pyrolytic stage) temperature (600°C, S/C = 3.5, CO_2 = 50vol%)

2nd stage (gasification stage) temperature (°C)	**700**	**800**	**900**	**1000**	**1100**
Gas yield (wt% RDF) ±1.2	83.3	85.3	87.3	87.9	87.8
Gasification char (wt% RDF) ±0.8	12.2	12.1	11.3	10.3	10.5
Condensate yields (wt% RDF) ±0.0	4.5	2.6	1.4	1.8	1.7
Wax (wt% RDF)	2.0	0.9	0.4	0.1	0.1
Tar (wt% RDF)	2.5	1.7	1.0	1.7	1.6
Gas (mol%)					
H_2 ±0.2	38.4	49.3	50.5	49.0	48.4
CO ±0.2	18.9	19.0	18.1	19.6	21.7
CO_2 ±0.1	37.4	27.5	28.9	29.7	28.4
CH_4 ±0.3	3.6	2.8	1.1	0.5	0.5
C_2-C_4 ±0.1	1.7	1.4	1.4	1.2	1.0

Gasification char (wt% gasification char, as received)					
C ±0.0	14.6	10.2	8.3	8.0	8.0
H ±0.0	0.5	0.3	0.2	0.2	0.2
N ±0.0	0.4	0.4	0.4	0.4	0.2
Wax (wt% wax as received)					
C ±0.0	71.3	66.8	62.1	59.3	56.7
H ±0.0	8.2	6.3	4.3	2.0	2.0
N ±0.0	0.2	0.1	0.1	0.1	0.1
Tar (g/Nm^3) ±0.7	17.7	11.5	6.6	11.1	10.0
Performances					
H_2/CO (mol/mol) ±0.0	2.0	2.6	2.8	2.5	2.2
CCE (%) ±0.2	90.9	94.3	96.5	95.8	96.1
CGE (%) ±0.9	55.3	63.9	62.8	61.0	62.4
PE (%) ±0.8	64.9	76.9	76.6	73.5	73.3

When the temperature of the second stage (gasification stage) was elevated from 700°C to 900°C, there was a 4% rise in gas yield. The yield stabilized at approximately 87.3%-87.9% in the temperature range of 900°C to 1100°C. These findings align with the results from a study on RDF steam gasification by Hwang et al. (2014). In their research, the gas yield increased from 0.7 Nm³/kg at 700°C to 1.1 Nm³/kg at 900°C, marking an increase of 36%. One possible explanation for this variance is that the RDF possesses a high volatile matter (VM), accounting for almost 81% of the RDF. In contrast, the RDF in the study by Hwang et al. (2014) had a higher fixed carbon content, which is more challenging to gasify due to its robust structure when compared to VM.

Nevertheless, both studies observed an escalation in gas yield with increased gasification temperature. The observations closely mirror those from an RDF gasification study in Italy by Galvagno et al. (2006). They reported a 3.4% increase in gas yield when the gasification temperature rose from 850°C to 950°C. Their peak gas yield, approximately 89% RDF, was achieved at 1050°C. These variations underscore the notion that RDF properties and behaviour during gasification can differ based on its source.

Increasing the second stage temperature leads to a reduction in both the solid residue (gasification char) and the condensate components. Notably, the waxy constituents are significantly affected by this temperature change, decreasing from 2wt% to a nearly undetectable level of 0.1wt% of RDF. The minimal change in solid residue (gasification char) yield, approximately 2wt%, can be attributed to its close alignment with the ideal ash content found in the proximate analysis, accounting for roughly 10.4wt% of the RDF. Moreover, carbon analysis indicates that after gasification at temperatures above 900°C, only about 8wt% of the solid residue (gasification char) remains as carbon, suggesting that most of the residue (gasification char) consists of inorganic elements.

The carbon content in both the waxy and solid residue (gasification char) components experienced a decline with increasing temperature. Specifically, for the waxy part, the carbon content decreased from 71.3wt% at 700°C to 56.7wt% at 1100°C, marking a 15wt% reduction. For the solid residue (gasification char), the carbon content decreased from 14.6wt% at 700°C to 8.0wt% at 1100°C, reflecting a 6.6wt% reduction.

In the study by Hwang et al. (2014), after gasification at 700°C, the carbon remaining in the solid residue (gasification char) amounted to about 25-30% of the solid residue (gasification char). In comparison, the work exhibited a lower carbon content, potentially due to the CO_2 in the carrier gas. This CO_2 might have actively reacted with the pyrolysis char during gasification, resulting in a carbon content approximately 10% lower than the RDF gasification reported by Hwang et al. (2014). However, as the temperature reached 900°C, the residual carbon content in the solid residue (gasification char) aligned closely with Hwang et al. (2014)'s findings, ranging between 5-8wt%. Furthermore, according to Galvagno et al. (2006), the carbon in the solid residue (gasification char) diminished to 4.2% when gasified at 1050°C. It is evident that increasing the gasification temperature leads to a reduction in the carbon content of both the solid residue (gasification char) and condensates.

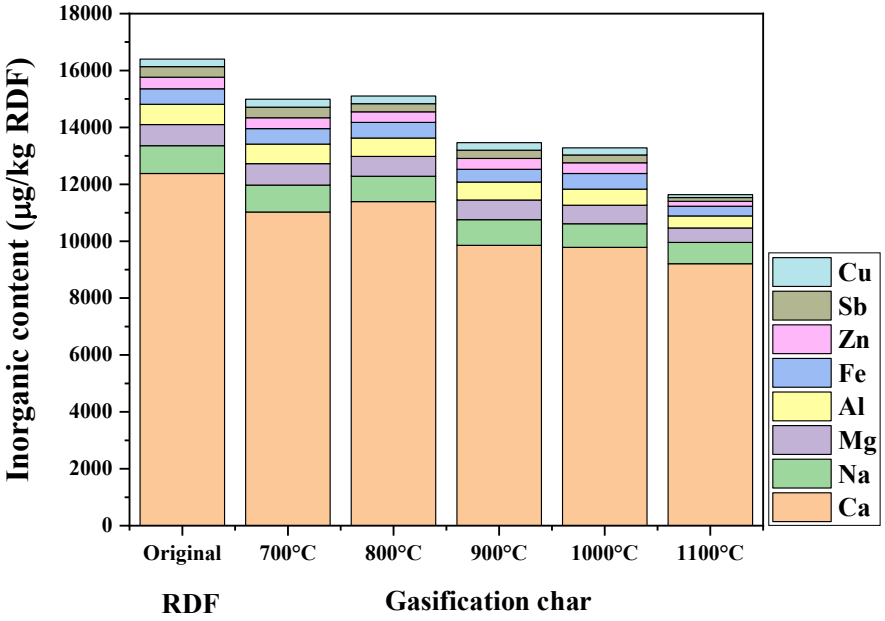

Figure 5.7: The inorganic content detected by ICP-MS methods from solid residue (gasification char) of RDF two-stage gasification with variation of the 2nd stage (gasification stage) temperature and fixed the 1st stage (pyrolytic stage) temperature (600°C, S/C = 3.5, CO_2 = 50vol%)

Raising the temperature notably increased the CCE. Specifically, when the 2nd stage (gasification stage) temperature was elevated from 700°C to 900°C, the CCE rose from 90.9% to 96.5%. However, beyond 900°C, a slight decline in CCE was observed, potentially due to the reformation of tar during gasification. The tar content exhibited an increase from 1.0% of RDF at 900°C to 1.7% of RDF at 1000°C. This rise can be attributed to the re-agglomeration of lighter tar molecules after their initial breakdown into lower molecule weight.

In a manner akin to the first stage (pyrolysis stage), the second stage (gasification stage) temperature also has a profound impact on tar levels. Specifically, as the temperature in the second stage rises from 700°C to 900°C, tar concentration decreases from 24.6 mg/kg RDF to 10.1 mg/kg RDF. However, a surprising increase in tar occurs when the temperature reaches 1000°C, elevating the levels to 17.2 mg/kg RDF, before slightly declining to 15.5 mg/kg RDF at 1100°C.

This complex behaviour can be elucidated by the mechanism of tertiary tar formation (Basu, 2018), as discussed earlier. At elevated temperatures, smaller tar molecules in the C_5-C_{10} range, including benzene, hexanol, phenols, and naphthalene, undergo decomposition. Interestingly, they recombine at even higher temperatures, as seen at 1000°C in this study. Here, an increase in the concentrations of specific heavier molecules, such as C_{11}, C_{14} (phenanthrene), C_{16} (fluoranthene), and C_{18} (chrysene), is observed (Figure 5.9).

These observations are consistent with previous work on RDF steam gasification conducted in a two-stage, pyrolysis/gasification setup. In this earlier study, it was found that tar consisting of naphthalene (C_{10}), acenaphthene (C_{12}), fluorene (C_{13}), and phenanthrene (C_{14}) are present at high temperatures (Blanco et al., 2012).

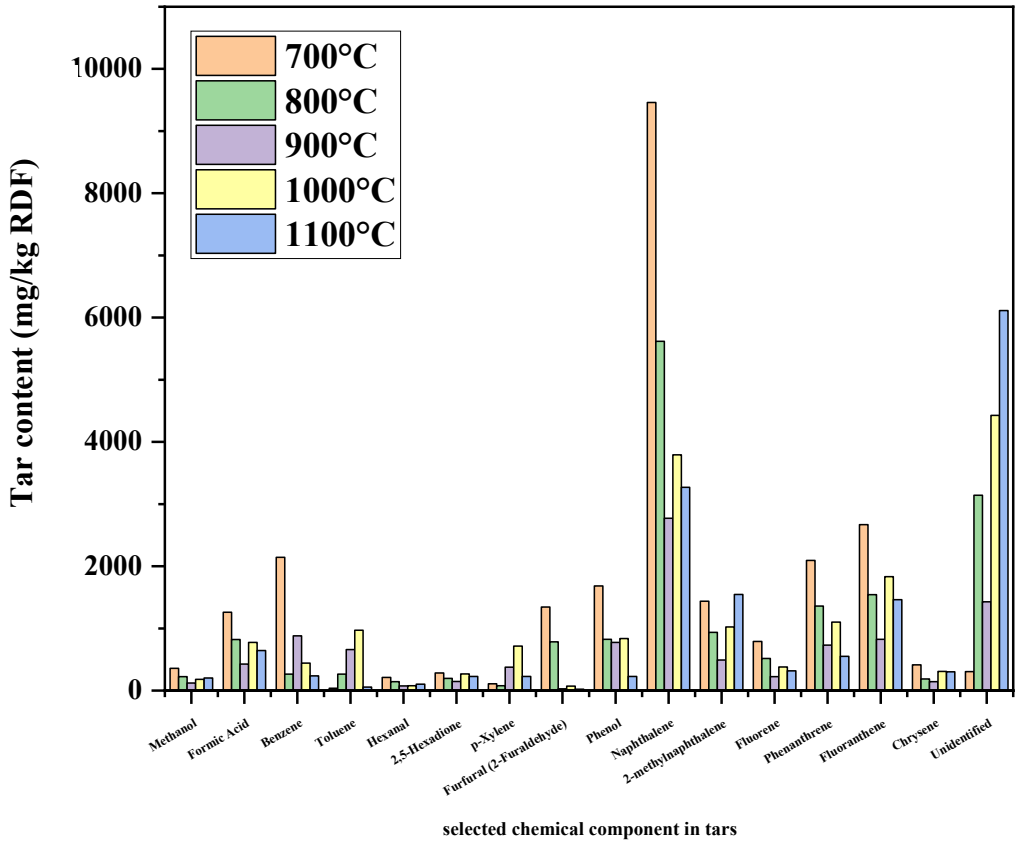

Figure 5.8: Selected chemicals compound in tar from RDF two-stage gasification with variation of the 2nd stage (gasification stage) temperature and fixed the 1st stage (pyrolytic stage) temperature (600°C, S/C = 3.5, CO_2 = 50 vol%, based on 3 replicates).

In a related study, gasification was conducted in steam at temperatures between 800°C and 900°C. The findings indicated that reaction rates accelerated with rising temperatures. For instance, at 900°C, a CCE of 80% was achieved in just 10 seconds, whereas at 800°C, the same efficiency took 20 seconds (Le and Kolaczkowski, 2015).

As the 2nd stage (gasification stage) temperature increased from 700°C to 1100°C, there was a discernible shift in the CO and H_2 content. Specifically, CO content rose from 18.9vol% at 700°C to 21.7vol% at 1100°C. Meanwhile, H_2 experienced a more pronounced increase, moving from 38.4% at 700°C to 50.6vol% at 900°C. However, beyond 900°C, H_2 levels began to decline. The rise in CO and H_2 with increasing temperature can be attributed to the Boudouard reaction and dry reforming. These reactions facilitate the decomposition of CO_2, CH_4, and other hydrocarbons into CO and H_2 as temperature increases. The decline in H_2 after 900°C is likely due to the contrasting thermal equilibrium temperatures associated with steam reforming and the water-gas shift reaction. While the former benefits from higher temperatures, the latter prefers a range of 400°C to 500°C. Indeed, the optimal H_2 yield is typically observed at temperatures between 750°C and 900°C in steam gasification, as noted by Vamvuka et al. (2022) and Dalai et al. (2009).

This temperature-dependent behaviour of H_2 is further supported by Wang et al. (2022), who reported a modest reduction in H_2 content from 60 vol% at 900°C to 58 vol% at 1200°C. Such variations also impact the H_2/CO ratio. At 700°C, this ratio was 2.0, but it increased to 2.8 at 900°C due to the more significant rise in H_2 compared to CO. However, as the temperature climbed from 900°C to 1100°C, the H_2/CO ratio decreased, settling at 2.5 at 1000°C and further dropping to 2.2 at 1100°C, reflecting the combined effects of increasing CO and decreasing H_2.

The CO_2 content decreased from 37.4 vol% at 700°C to 28.9 vol% at 900°C. It then saw a slight increase to 29.7 vol% at 1000°C before declining again at 1100°C. This trend mirrors that of H_2, stemming from the products of the water-gas shift reaction. As the temperature was raised, more CO reacted with H_2O to produce additional CO_2 and H_2. The observed reduction in CO_2 can be attributed to the Boudouard reaction where more carbon reacts with CO_2 (at high temperature > 700°C), producing increased amounts of CO.

With an increase in the 2nd stage (gasification stage) temperature, both $CH_4$and C_2-C_4 exhibited significant reductions. Specifically, methane levels dropped from 3.6 vol% at 700°C to 0.5 vol% at 1100°C, while C_2-C_4 hydrocarbons decreased from 1.7 vol% at 700°C to 1.0 vol% at

1100°C. This reduction is attributable to the prominence of dry reforming and steam reforming at elevated temperatures, leading to a decrease in small molecule hydrocarbons and an increase in permanent gases. This observation of reduced CH_4 and C_2-C_4 concentrations with increased temperature is supported by Galvagno et al. (2006) which reported CH_4 levels diminishing from 15.8 vol% at 850°C to 10.0 vol% at 1050°C, and C_2-C_3 hydrocarbons plunging from 6.0 vol% at 850°C to a mere 0.0vol% at 1050°C. Similarly, Luo et al. (2012) documented methane reduction from 10.3 vol% at 700°C to 1.3 vol% at 900°C, and ethylene (C_2H_4) from 3.3 vol% at 700°C to 0.1 vol% at 900°C.

Increasing the temperature can enhance the Carbon Conversion Efficiency (CCE) and hydrogen (H_2) production. However, it also demands a greater energy input to the process. Process efficiency (PE) sees an improvement from 64.9% at 700°C to 76.87% at 800°C, driven by the energy content of the producer gas, which stands at 13.5 MJ/Nm^3. Yet, as the 2nd stage (gasification stage) temperature is elevated to 900°C, there is a dip in PE to 76.6%. Further increases in temperature result in further reductions — 73.5% at 1000°C and 73.3% at 1100°C. This decline in PE stems from the energy needed to fuel the process surpassing the energy it produces, both in terms of chemical and sensible energy. Given that this gasification process is allothermal, it demands an additional 0.4 MJ/kg of RDF for every 100°C rise in the 2nd stage (gasification stage) temperature.

Additionally, research by Di Blasi (2009) indicates that raising the temperature to 1000°C doesn't significantly enhance the diffusion rate in the char nor does it boost the overall gasification reaction rate. Therefore, elevating the 2nd stage (gasification stage) temperature beyond 900°C might decrease PE. This presents a dilemma, as the primary objective of gasification is to maximize CCE. Hence, finding a balance between these two parameters becomes imperative.

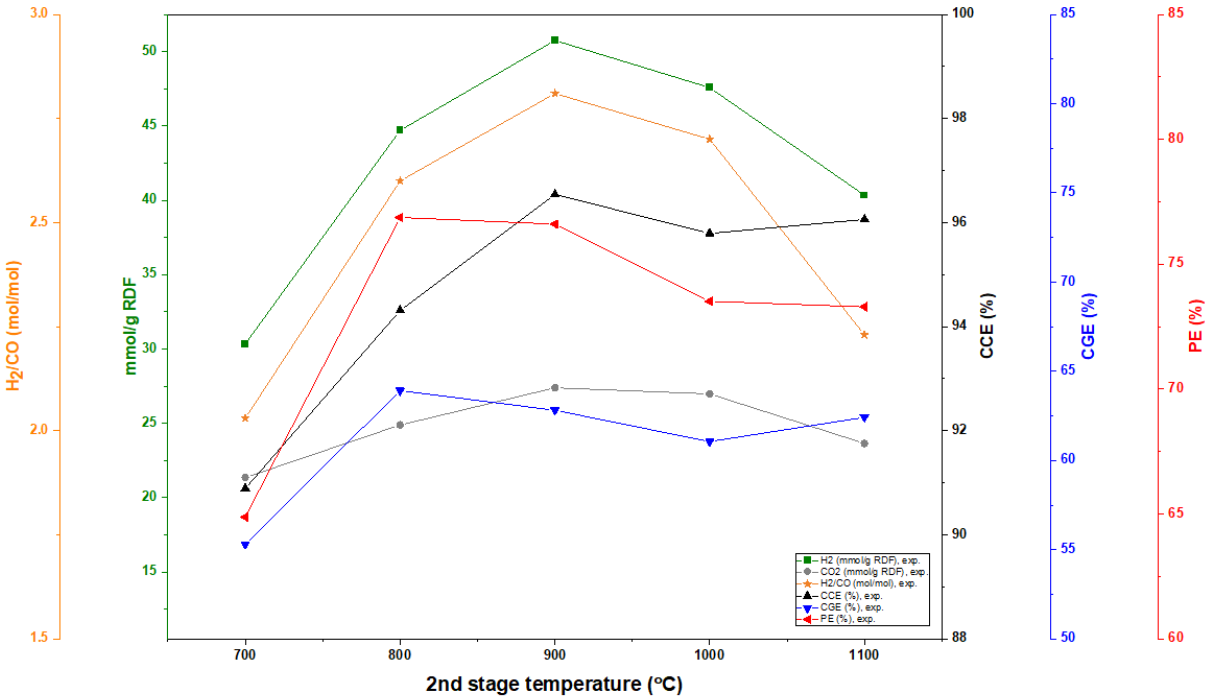

Figure 5.9: The summary performances of RDF two-stage gasification with the variation of 2nd stage temperature and fixed the 1st stage (pyrolytic stage) temperature (600°C, S/C 3.5, and CO_2=50 vol% balanced with N_2)

In summary, gasification efficiency is notably influenced by the 2nd stage (gasification stage) temperature. A trend of increased gas yield with temperature is observed until a stabilization point around 900°C to 1100°C, consistent with related studies. As temperature rises, reductions are seen in solid residues (gasification char), condensate components, and their respective carbon contents. Carbon conversion efficiency (CCE) improves with increased temperatures but faces challenges beyond 900°C due to complexities like tar re-agglomeration. Gaseous outputs, including CO, H_2, and CO_2, demonstrate varied behaviours with temperature changes, illustrating the intricate interplay of different thermal reactions. Process efficiency (PE) initially increases with temperature but declines post-900°C, emphasizing the energy trade-offs involved. Ultimately, while higher temperatures can enhance certain outputs, there's a critical need to define optimal operational limits for balanced energy efficiency and output quality.

5.4 Effect of the steam to carbon ratio (S/C, mol/mol)

Gasification is a thermochemical process that transforms carbonaceous materials into valuable gaseous products. The nuances of this transformation are governed by several key parameters, and among them, the steam to carbon ratio (S/C) stands out as particularly influential. This ratio

doesn't solely dictate the yield but affects an array of gasification outcomes, including the quality, composition, calorific value, tar content, and other vital properties of the produced syngas. It's essential to strike the right balance between steam and carbon feed, as deviations in this ratio can lead to diverse implications for both the process efficiency and the characteristics of the resulting gas. This sub-chapter delves into the multifaceted effects of varying S/C ratios on gasification (see Table 5.8), aiming to provide a comprehensive understanding and offer guidance for achieving optimal results.

Table 5.8: The yield and product characteristic of RDF two-stage gasification with variation of the S/C and fixed the 1st stage (pyrolytic stage) temperature at 600°C, 2nd stage (gasification stage) temperature at 900°C, CO_2 = 50vol%.

S/C (mol/mol)	**1**	**2**	**3**	**4**	**5**
Gas yield (wt% RDF) ±1.2	82.3	84.6	87.3	88.0	88.9
Gasification char **(wt% RDF) ±0.8**	13.5	12.6	11.3	10.9	10.0
Condensate yields (wt% RDF) ±0.0	4.2	2.8	2.4	2.1	2.1
Wax (wt% RDF)	2.4	1.0	0.6	0.3	0.3
Tar (wt% RDF)	1.8	1.8	0.8	0.8	0.8
Gas (mol%)					
H_2 ±0.2	40.5	48.2	49.4	51.4	50.5
CO ±0.2	22.6	21.0	18.6	18.1	17.6
CO_2 ±0.1	27.3	27.6	28.9	28.6	29.8
CH_4 ±0.3	5.4	1.2	1.4	0.5	0.5
C_2-C_4 ±0.1	4.2	2.0	1.7	1.4	1.6
Gasification char **(wt% gasification char , as received)**					
C ±0.0	12.3	10.8	9.3	7.5	7.1
H ±0.0	0.3	0.3	0.2	0.2	0.2
N ±0.0	0.4	0.4	0.4	0.4	0.3
Wax (wt% wax as received)					
C ±0.0	70.2	68.4	66.6	65.0	64.2
H ±0.0	6.5	5.9	5.0	5.0	5.0
N ±0.0	0.3	0.2	0.1	0.1	0.1
Tar (g/Nm^3) ±0.7	13.9	12.8	5.0	5.1	5.4
Performances					
H_2/CO (mol/mol) ±0.0	1.8	2.3	2.6	2.8	2.9

CCE (%) ±0.2	91.7	93.8	96.5	97.1	97.2
CGE (%) ±0.9	92.5	71.6	67.6	58.7	52.8
PE (%) ±0.8	92.3	81.4	80.3	73.2	67.0

The gas yield exhibited an increase of approximately 6.6wt% when the steam to carbon molar ratio (S/C) was raised from 1 to 5 mol/mol. Nevertheless, after the introduction of steam, there was no significant difference in the gas yield for S/C values between 4 and 5, with the yield stabilizing in the range of 88.0-88.9 wt%. It is noteworthy to mention that steam introduction plays a pivotal role in influencing gas yield. In comparative terms, incorporating steam into the system augments the gas yield by 12%, elevating it from 70% to 82% in comparison to processes devoid of steam.

There's a discernible decrease in both solid residue (gasification char) and condensate (tar and wax) yields with an increasing S/C ratio. Specifically, the solid residue yield decreases from 13.5 wt% at an S/C of 1 to 10.0 wt% at an S/C of 5. Concurrently, the condensate yield sees a reduction from 4.2 wt% at an S/C of 1 to 1.1wt% at S/C 5. This trend mirrors findings from a study on RDF steam gasification in a rotary kiln plant in Italy where there, an increase in S/C from 1 to 5.1 led to a decrease in solid residue (gasification char) yield, dropping from 22% to approximately 16% at a temperature of 850°C (Molino et al., 2013). Upon examining the carbon content within both the solid residue (gasification char) and wax, there was a notable decrease observed. The carbon in the solid residue (gasification char) diminished by 5.2wt%, while the carbon content in the waxy component dropped by nearly 6%. This decrease in both solid and waxy carbon content corroborates that an increase in steam—from S/C 1 to S/C 5—amplifies the reaction between water and carbon, leading to enhanced gas production. Consequently, the CCE also experienced an upturn, rising from 91.7% at an S/C of 1 to 97.2% at an S/C of 5.
Regarding tar content, a decline was observed from 13.9 g/Nm³ to 5.0 g/Nm³ as steam was increased from S/C 1 to 3.

However, this trend ceased upon further increase of steam to S/C 4 and 5, where tar content saw a slight increase, nearing between 5.1-5.4 g/Nm³. The initial reduction of tar between S/C 1 to 3 can be attributed to the surge in steam, which augmented the presence of OH radicals, thereby promoting further oxidation of Polycyclic Aromatic Hydrocarbons (PAHs) and enhancing gas yield. Notably, excessive steam diminishes the overall temperature within the second-stage reactor. This results in increased tar production when the S/C ratio exceeds 4. This observation is consistent with a study by Luo et al. (2012), wherein steam gasification that varied the S/C from 0 to 2.4 decreased tar content from 3.4wt% of Municipal Solid Waste (MSW) to none. Conversely, studies highlighted the potential pitfalls of an overabundance of steam: excessive steam led to increased tar yields, escalating from roughly 0.8 g/Nm³ to nearly 3 g/Nm³ (Ma et al., 2020, Hernández et al., 2013).

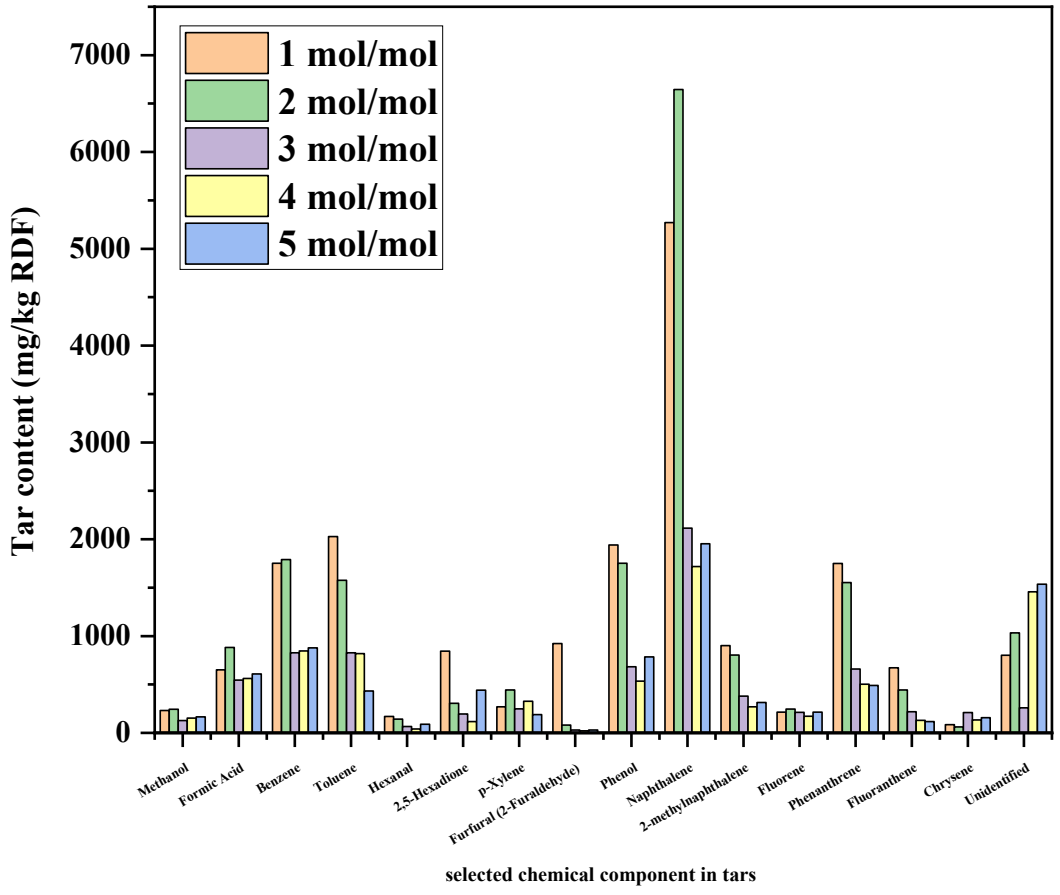

Figure 5.10: The selected chemicals compound in tar from RDF two-stage gasification with variation of the S/C (1-5) and fixed the 1st stage (pyrolytic stage) temperature at 600°C, 2nd stage (gasification stage) temperature (900°C, CO_2 = 50 vol%, based on 3 replicates).

With an increase in steam input, it has been observed that lighter aromatic compounds like toluene, benzene, and phenol, as well as polycyclic aromatic hydrocarbons (PAHs) like naphthalene, 2-methylnapthalene, phenanthrene and fluoranthene, undergo significant reductions in yields (Figure 5.10). In contrast, methanol, formic acid, hexanol and p-Xylene and Fluorene exhibit marginal reductions or remain relatively unchanged. This selectivity is attributed to steam's greater reactivity with heavy aromatic ring systems (Song et al., 2015). However, the application of steam in conjunction with volatile-char has been noted to diminish the production of light aromatic compounds (Song et al., 2015). This suggests that steam plays a crucial role with the pyrolysis char as a catalyst to be highly effective at both reducing light aromatics and heavier PAHs.

Increasing the steam to carbon ratio (S/C) from 1 to 4 led to a pronounced rise in both H_2 and CO_2 content, from 40.5 vol% to 51.4 vol% and 27.3 vol% to 28.6 vol%, respectively. In contrast, levels of CO diminished from 22.6 vol% to 18.1 vol%, CH_4 plummeted from 5.4 vol% to a mere 0.5 vol%, and C_2-C_4 hydrocarbons decreased from 4.2 vol% to 1.4 vol%. This alteration in gas composition is primarily due to the water gas shift and steam reforming reactions. As hydrocarbons interact with steam, there's a favoured production of H_2 and CO_2, leading to the concurrent consumption of CO, CH_4, and C_2-C_4 hydrocarbons.
Drawing from the literature, Waheed (2013) highlighted an H_2 yield increase from 2 mmol/g feed in pyrolysis to around 25 mmol/g feed during steam gasification. Similarly, typical steam gasification processes, with S/C ratios ranging between 0.5 to 7.5, have been reported to yield H_2 in the range of 26.1-42.1 mmol/g feed (Siwal et al., 2020).

In the context of this research, the H_2 yield was observed to increase from 30.0 mmol/g RDF at an S/C of 1 to 51.1 mmol/g RDF at an S/C of 4. CO_2 simultaneously showed an upward trend, moving from 14.2 mmol/g RDF to 26.4 mmol/g RDF as the S/C shifted from 1 to 4. Thus, identifying the optimal S/C ratio to maximize H_2 production while minimizing CO_2 emissions is crucial. In systems operating within an S/C range of 1 to 5, CO_2 emissions hovered around 10.4-11.4 kg CO_2/kg H_2.

However, a plateau in H_2 production was observed once the S/C reached 5, accompanied by a marginal increase in the concentrations of CH_4 and C_2-C_4. This phenomenon can be attributed to the introduction of a significantly higher amount of steam in the second stage, approximately 120°C. Such an influx of steam could potentially lower the overall temperature inside the second reactor, given the substantial mass of the introduced steam relative to the system.

Notably, the H_2 yield did not show any marked difference between S/C ratios of 4 and 5, registering a slight decrease to 50.4 mmol/g RDF. This underscores the importance of pinpointing an optimal S/C ratio. As the S/C ratio increases, so does the energy requirement for steam production. Specifically, generating steam at an S/C of 5 demands 11.6 MJ/kg RDF, leading to a reduction in process efficiency (PE) by 6.2% compared with the S/C of 4.

In terms of the H_2/CO ratio, there is a noticeable rise as the S/C increases from 1 to 5, with the ratio expanding from 1.8 to 2.9. As previously discussed, the introduction of more steam amplifies the H_2 concentration while simultaneously diminishing CO levels. This interplay results in a heightened H_2/CO ratio when the S/C is increased from 1 to 5. Interestingly, these values are marginally superior to those observed during steam gasification at around S/C 5.5 using RDF-landfill at a temperature of 800°C, which produced an H_2/CO ratio of 2.5 (Zaini et al., 2020). Such an enhancement can be ascribed to the elevated temperature in the gasification zone, which inherently supports a higher H_2/CO ratio.

Processes operating at an S/C of 1 yield an H_2/CO ratio below 1.8, making them ideal for DME and acetic acid production. The lower steam requirement in such processes not only maximizes process efficiency (PE), with values reaching up to 92.3%, but also results in a carbon conversion efficiency (CCE) that's nearly 5% less than processes operating at an S/C of 5. Processes with S/C ratios between 2 and 3 are optimal for methanol and Fischer-Tropsch synthesis, whereas those with S/C values exceeding 2.5 are best suited for ammonia production or H_2 purification.

An increase in the S/C ratio leads to a decrease in the lower heating value (LHV) of the producer gas, which drops from 14.2 MJ/Nm³ at an S/C of 1 to 13.0 MJ/Nm³ at an S/C of 5. This decline can be attributed to several factors. As previously discussed, introducing more steam raises the CO_2 content, which, despite an increase in H_2, diminishes the chemical energy of the producer gas. The reduced presence of methane and C_2-C_4 species, which contribute significantly to the energy content in the gaseous phase, further compounds this effect.

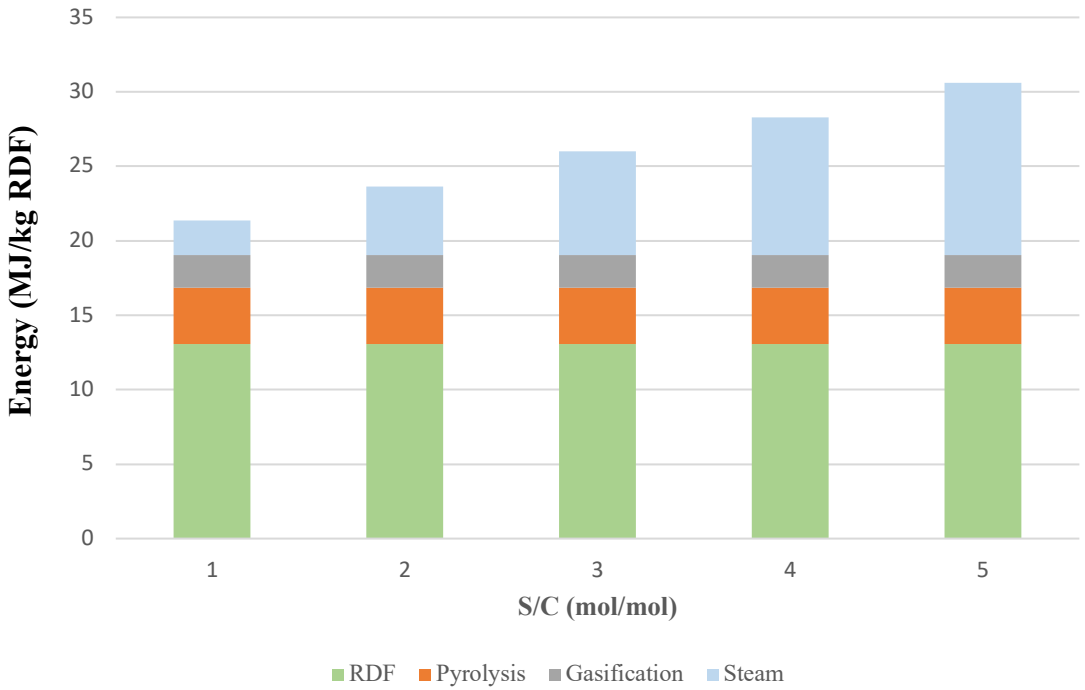

Figure 5.11: The energy input of RDF two-stage gasification with variation of the S/C and fixed the 1st stage (pyrolytic stage) temperature at 600°C, 2nd stage (gasification stage) temperature (900°C, CO_2 = 50 vol%)

For perspective, the LHV of producer gas from air gasification is typically between 6-8 MJ/Nm³, whereas steam gasification yields approximately 15MJ/Nm³ (Lopez et al., 2018). Consequently, the rise in S/C ratio has a marked impact on the Cold Gas Efficiency (CGE), which drastically drops from 92.5% to 52.8% and the LHV of the producer gas reduced from 14.2 MJ/kg RDF to 13.0 MJ/kg RDF. This decline isn't solely due to the augmented CO2 production; it also encompasses the energy necessary for steam generation (see energy input in the Figure 5.11), a factor integral to the efficiency calculation. For instance, the energy requirement for an S/C of 1 stands at 2.3 MJ/kg RDF, but this value escalates to about 11.6 MJ/kg RDF for an S/C of 5. Thus, while increasing steam offers several benefits, it also demands a significant energy input, highlighting the importance of system optimization.

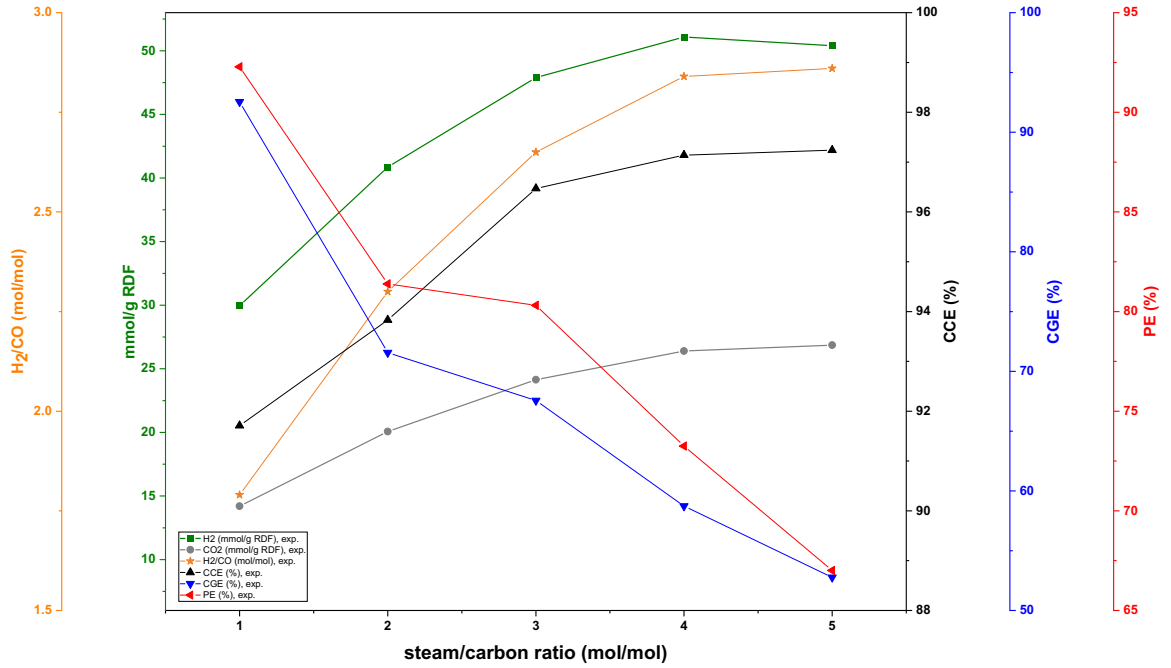

Figure 5.12: The summary performances of RDF two-stage gasification with the variation of the S/C and fixed the 1st stage (pyrolytic stage) temperature at 600°C, 2nd stage (gasification stage) temperature at 900°C, CO_2 = 50 vol% balanced with N_2.

Considering adjustments like elevating the temperature of the second stage or integrating CO_2 into the carrier gas might yield better efficiencies. Limiting steam to below an S/C of 3 could ensure a Process Efficiency (PE) greater than 80%. If PE drops below 70%, especially when linked with applications like integrated gasification combined cycle (IGCC), it could fall even below 55%. At such low efficiencies, alternative methods, such as combustion (Basu, 2018), might surpass the gasification process in terms of overall process efficiency.

The steam to carbon ratio (S/C) plays a pivotal role in gasification process. As the S/C ratio rises from 1 to 4, there's a notable increase in H_2 and CO_2 contents, with a simultaneous reduction in CO, CH_4, and C_2-C_4 components. However, an S/C ratio above 4 seems to stabilize H_2 production, while CH_4 and C_2-C_4 see a slight increment. This is likely due to excessive steam reducing temperatures in the second-stage reactor. Furthermore, an increased S/C ratio reduces solid residue (gasification char) and condensate yields, with accompanying decreases in carbon content in both components. This suggests that steam promotes reactions between water and

carbon. Yet, there's a nuanced relationship between steam and tar production. Tar content decreases with increased steam up to S/C 3 but rises again after S/C 4 due to temperature drops in the second-stage reactor. The H_2/CO ratio also increases with a rise in S/C, influencing the suitability of the gas for various applications, such as DME and acetic acid production, or Fischer-Tropsch synthesis. Producer gas's lower heating value (LHV) decreases with increasing S/C, affecting the CGE due to factors like rising CO_2 content and steam generation energy requirements.

5.5 Effect of CO_2 concentration (vol%) in the carrier gas

Gasification, a thermochemical process used for the conversion of organic materials into valuable gaseous products, hinges critically on several operational parameters. Among these, the composition of the carrier gas stands out as a paramount influence, governing not only the kinetics and thermodynamics of the process but also the quality and quantity of the end products. One key component of the carrier gas, carbon dioxide (CO_2), is particularly notable in this regard. Its concentration (vol%) has far-reaching implications on the entire gasification process. This section delves into the multifaceted effects of varying CO_2 concentrations in the carrier gas and elucidates how these concentrations influence the outcomes of gasification (see Table 5.9). Through a thorough analysis, the chapter 5.5 aims to bridge the understanding of theoretical principles with practical implications, paving the way for optimizing gasification processes in real-world scenarios.

Table 5.9: The yield and product characteristic of RDF two-stage gasification with variation of the CO_2 concentration (vol% balanced with N_2) in the carrier gas and fixed the 1st stage (pyrolytic stage) temperature at 600°C, 2nd stage (gasification stage) temperature at 900°C, S/C of 3.5.

CO_2 (vol% balanced with N_2) in carrier gas	**0**	**25**	**50**	**75**	**100**
Gas yield (wt% RDF) ±1.2	85.8	86.5	87.4	87.9	88.0
Gasification char (wt% RDF) ±0.8	12.6	12.1	11.3	10.9	10.9
Condensate yields (wt% RDF) ±0.0	1.6	1.4	1.3	1.2	1.1
Wax (wt% RDF)	0.6	0.4	0.3	0.3	0.3
Tar (wt% RDF)	1.0	1.0	1.0	0.9	0.8
Gas (mol%)					
H_2 ±0.2	50.4	50.4	50.5	50.4	50.6

CO ±0.2	16.7	17.4	18.1	19.0	23.5
CO_2 ±0.1	27.5	28.0	28.9	28.8	25.1
CH_4 ±0.3	3.5	2.8	1.1	1.0	0.4
C_2-C_4 ±0.1	1.9	1.4	1.4	0.8	0.4
Gasification char (wt% gasification char, as received)					
C ±0.0	12.5	9.3	8.3	7.9	7.4
H ±0.0	0.2	0.3	0.3	0.2	0.1
N ±0.0	0.4	0.4	0.4	0.3	0.3
Wax (wt% wax as received)					
C ±0.0	75.1	68.4	62.1	60.5	58.3
H ±0.0	5.2	4.8	4.3	4.2	4.2
N ±0.0	0.8	0.4	0.1	0.1	0.1
Tar (g/Nm^3) ±0.7	5.9	6.6	6.6	5.9	5.4
Performances					
H_2/CO (mol/mol) ±0.0	3.0	3.0	2.8	2.6	2.1
CCE (%) ±0.2	94.9	95.9	96.5	97.0	97.3
CGE (%) ±0.9	68.4	66.0	62.8	62.3	64.0
PE (%) ±0.8	80.9	78.9	76.6	76.3	77.7

When CO_2 was incorporated into the two-stage gasification process, there was some increase in gas yield by 2.2 wt%. This enhancement was attributed to the consumption of condensates and solid residue (gasification char). The uptick in yield can be understood in light of the additional reactions prompted by CO_2 from the carrier gas. Specifically, the presence of CO_2 augments the dry reforming and Boudouard reactions, especially when temperatures exceed 700°C. These reactions are thermodynamically favoured at higher temperatures, hence the efficiency of using CO_2 in steam gasification amplifies particularly in the temperature range of 700°C to 900°C (Śpiewak et al., 2021).

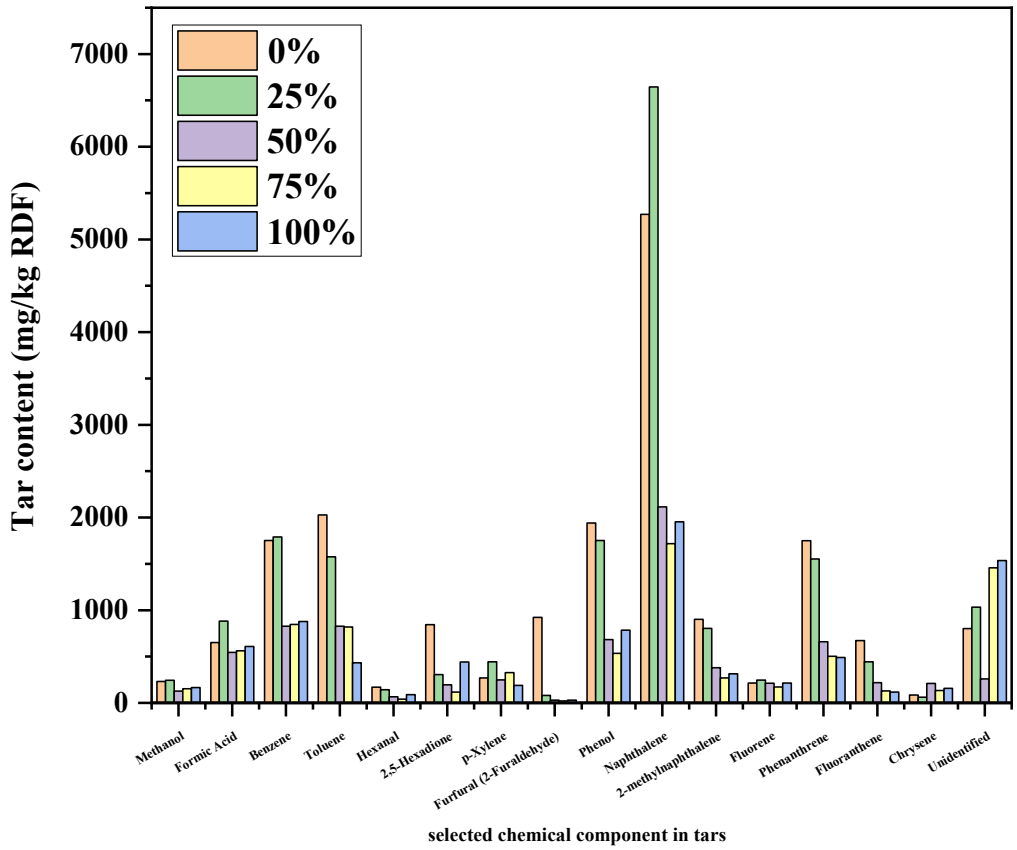

Figure 5.13: The selected chemicals compound in tar from RDF two-stage gasification with variation of the CO_2 concentration (0-100 vol% balanced with N_2) in the carrier gas and fixed the 1st stage (pyrolytic stage) temperature at 600°C, 2nd stage (gasification stage) temperature (900°C, S/C of 3.5, based on 3 replicates).

Interestingly, the influence of increased CO_2 concentrations varies across different components. It exhibits a more pronounced effect on waxy components than on tar. For instance, increasing the CO_2 concentration from 0 to 100% led to a reduction in wax yield from 0.7% to 0.3%. Conversely, tar yields remained relatively stable, fluctuating within a narrow band of 0.8% to 1.0%. An increase in the CO_2 concentration of the carrier gas, from 0 to 100%, results in an enhancement of the CCE, with values rising from 94.9% to 97.3%. This augmentation is further corroborated by the observed reduction in carbon content in the solid residue (gasification char) and waxy components, which decreased from 12.5% to 7.4% and 75.1% to 58.3%, respectively.

Notably, steam and CO_2 do not vie for specific binding sites on the char. Instead, they demonstrate a synergistic interaction, where their combined presence substantially amplifies the CCE (Shahabuddin and Bhattacharya, 2021). Contrary to the trends observed in wax and solid yields, the tar content exhibited an initial increase with rising CO_2 concentrations, moving from 5.9 g/Nm^3 at 0% CO_2 to 6.6 g/Nm^3 at 25% CO_2. However, as the CO_2 concentration continued to escalate from 50% to 100%, the tar content decreased, shifting from 6.6 g/Nm^3 to 5.4 g/Nm^3.

According to the data presented in the Figure 5.13, there is a generalized reduction in the concentration of chemical compounds present in tar as the CO_2 concentration in the carrier gas increases. This is attributed to CO_2's catalytic role in enhancing the gasification of char, which consequently leads to a reduction in tar content (Couto et al., 2016). This observation is further corroborated by an increase in the CCE as CO_2 concentration in the carrier gas increases, as noted in this study. This finding is in alignment with research conducted by Feng et al. (2018), where it was observed that the conversion rates of various compounds such as toluene, ethylbenzene, p-xylene, indene, naphthalene, and phenanthrene increased by 5% to 20% when the CO_2 concentration escalated from 0% to 29%. Thus, the increasing concentration of CO_2 in the carrier gas not only minimizes tar content but also improves the overall efficiency of the gasification process.

The impact of CO_2 in the carrier gas is notably evident in the carbon content of the pyrolysis char. As illustrated in Figure 5.15, the pyrolysis char obtained in an N_2 atmosphere at 700°C has a carbon content of 73.8 at%. In contrast, pyrolysis char produced in a CO_2 atmosphere at the same temperature has a reduced carbon content of 61.6 at%. This difference highlights the significant influence of CO_2 in the carrier gas. It not only affects the final products from the two-stage gasification process but also exerts its influence during the initial stage of the reactor. Specifically, introducing CO_2 into the carrier gas from 0% to 100% leads to a reduction in the carbon content of the RDF-pyrolysis char by 12.2 at%. This observation is in alignment with findings from Prasertcharoensuk (2019), which noted that increasing CO_2 in a wood cube pyrolysis reactor operating at 900°C decreased the carbon content in the pyrolysis char by nearly 6%.

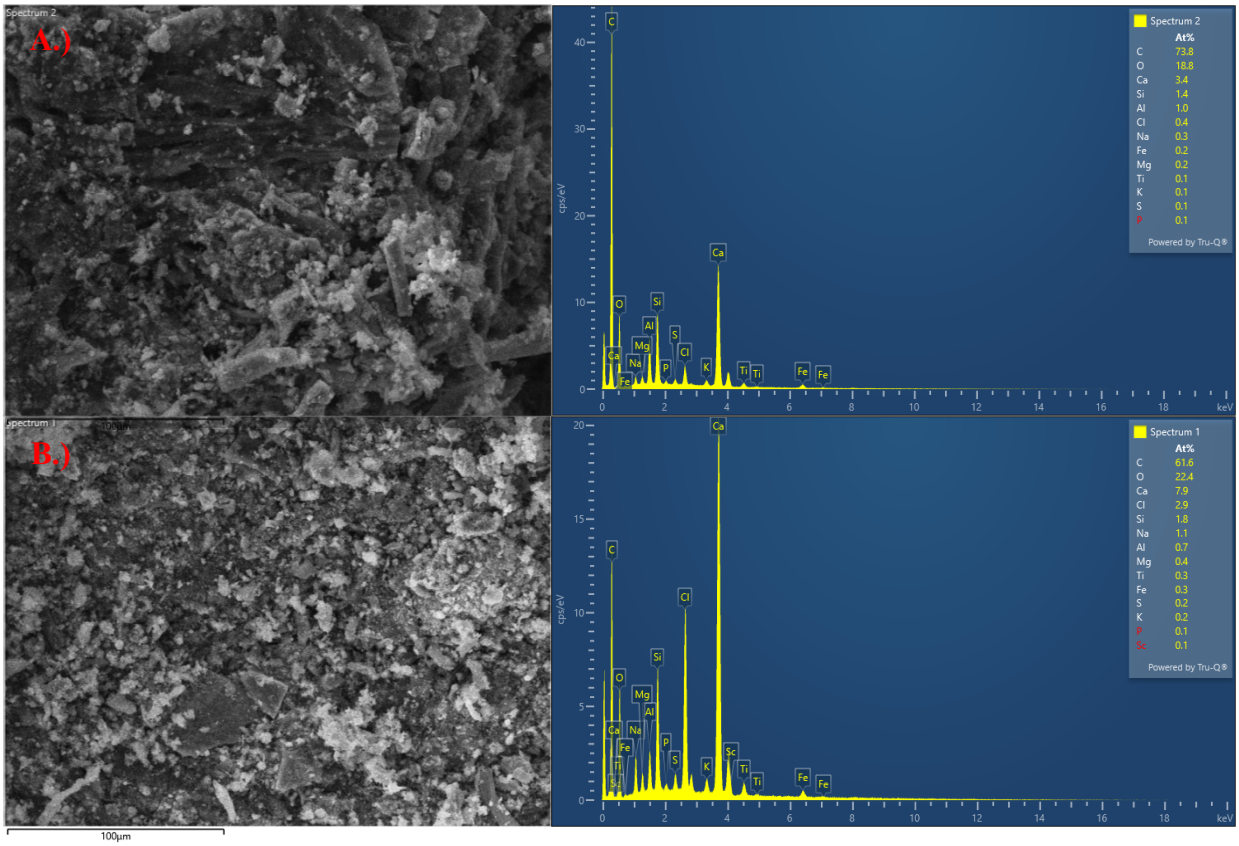

Figure 5.14: The SEM-edX images of RDF pyrolysis char (product from 1st stage reactor) A.) in N_2 atmosphere and B.) in 100% CO_2 atmosphere.

While an increase in CO_2 concentration enhances gas yield, the H_2 content remains relatively stable at 50 vol%. A significant observation is the pronounced elevation in the CO concentration, which increases from 16.7 vol% to 23.5 vol% as the CO_2 concentration in the carrier gas rises from 0% to 100%. This behaviour can be attributed to the transformation of CO_2 into CO upon reaching the high-temperature zone, specifically 900°C in this context. This observation aligns with data from RDF-steam CO_2 gasification studies (Śpiewak et al., 2021) conducted at 900°C, which reported producer gas with an H_2/CO ratio ranging between 2.1 and 3.6 and a LHV of 10.9-16.2 MJ/kg RDF. Consequently, this increase in CO concentration causes the H_2/CO ratio in the producer gas to decline from 3.01 to 2.15.

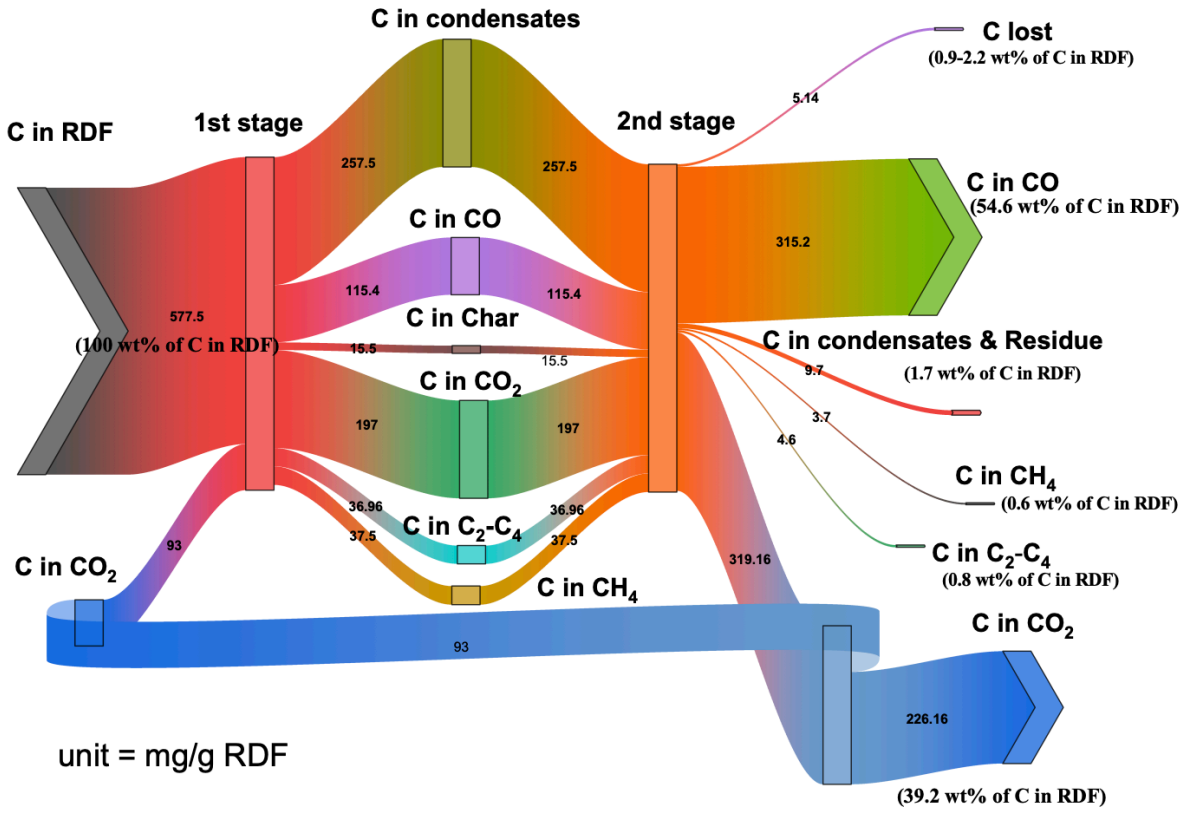

Figure 5.15: The carbon route in RDF CO_2-steam two-stage gasification (1st stage temperature at 600°C, 2nd stage (gasification stage) temperature (900°C, S/C3.5, CO_2 100% in the carrier gas)

While there is a noticeable increase in CO concentration, both CGE and PE see a minor decline, from 68.4% to 62.3%. This decrease can be attributed to the reduction in small hydrocarbon molecules, including methane (which dropped from 3.5% to 0.4%) and C_2-C_4 hydrocarbons (decreasing from 1.9% to 0.4%). These hydrocarbons, rich in energy content, contribute significantly to the LHV of the producer gas. However, an interesting trend emerges when the CO_2 concentration in the carrier gas exceeds 75%. At this threshold, both PE and CGE experience a surge, likely because the heating content of the CO-rich producer gas compensates for the energy lost from the diminution of small hydrocarbons. It's worth noting that future investigations might benefit from a greater concentration of CO_2 in the carrier gas. This study was confined to a CO_2 utilization of 3.4g CO_2/g RDF, a limit set by current technological constraints.

According to Figure 5.15, which outlines the carbon route in the RDF CO_2-steam two-stage gasification process, it was determined that 84% of the carbon source in this process is derived from RDF, with the remaining 16% coming from CO_2. The primary carbon outlet is CO, accounting for 54.6wt% of the carbon from RDF. Following this, CO_2 released from the process represents the second major carbon outlet, accounting for approximately 39.2% of the carbon from RDF. Of this percentage, 93 mg C is recycled as CO_2, serving as the carrier gas in the first stage. The remaining 3.1% of the carbon from RDF is retained in condensates, solid residue (gasification char), methane, and C_2-C_4.

While the H_2 content remained relatively consistent, ranging from 47.1 to 50.5 mmol/g RDF, increasing the CO_2 concentration in the carrier gas led to a discernible reduction in total CO_2 production. In the case of only steam gasification (0 vol% CO_2), the process yielded 13.5 kg CO_2/kg H_2. In contrast, CO_2-steam gasification (100 vol% CO_2 scenario) produced 8.5 kg CO_2/kg H_2. This decrement in CO_2 can be attributed to the dry reforming and Boudouard reactions, which facilitate the conversion of CO_2 into CO. The British Government stipulates that for H_2 to be considered "low emission", its production must release less than approximately 2.4 kg CO_2 per kg H_2 (Department for Business Energy & Industrial Strategy (BEIS), 2022).

If one tonne of RDF were discarded in an open dump or landfill and left for a duration spanning between 6 to 30 years, it could yield CO_2 emissions ranging from 17.2 to 91.4 kg CO_2 (Obersteiner et al., 2007). Taking this potential landfill CO_2 emission into account, utilizing RDF in CO_2-steam gasification could bring down its emissions to a level between 7.2 and 7.9 kg CO_2/kg H_2. Although this H_2 output doesn't align with the " low emission H_2" criteria set by British standards, the CO_2-steam gasification method still offers CO_2 emissions that are approximately 33%-39% lower than H_2 derived from methane reforming. The latter produces 11.7 kg CO_2/kg H_2 (Giaconia et al., 2021) and accounts for 90% of global H_2 generation through this method (Qian et al., 2020). Adopting RDF as feedstock for gasification serves multiple purposes. Beyond generating heat, power, and H_2, it crucially curtails CO_2 emissions that arise from both landfills and fossil fuel utilization. Additionally, it's worth mentioning that research focused on RDF CO_2-steam gasification remains scant and largely unexplored.

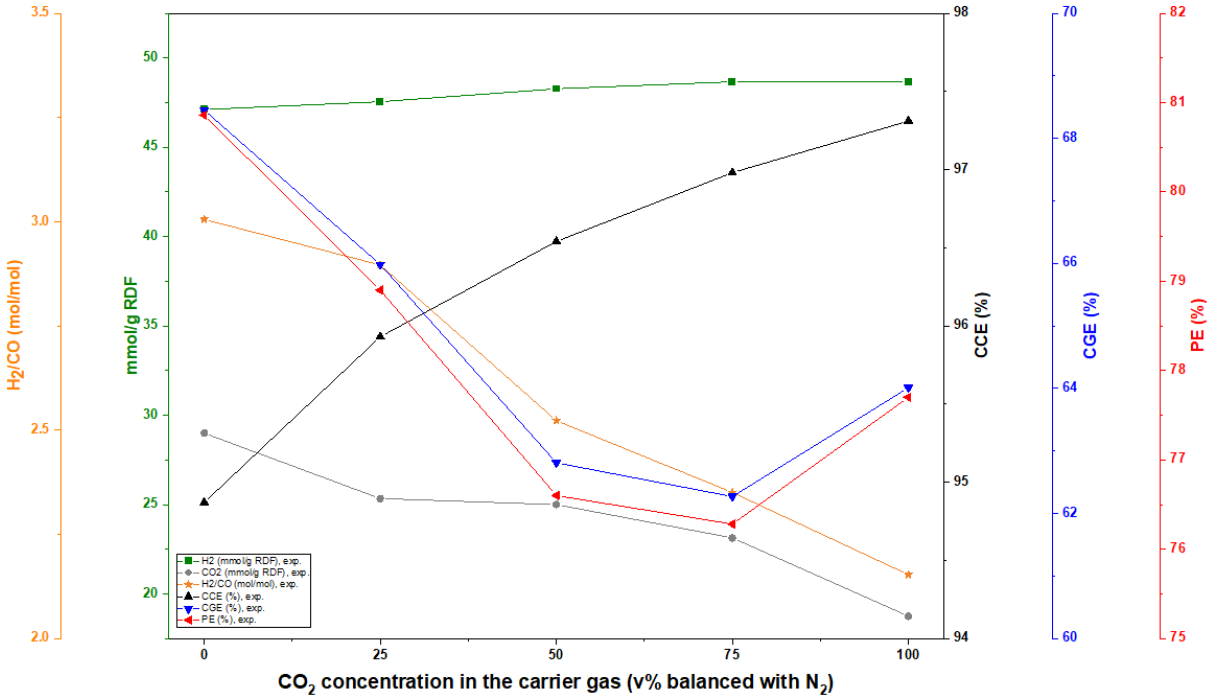

Figure 5.16: The summary performances of RDF two-stage gasification with the variation of the CO_2 concentration (vol% balanced with N_2) in the carrier gas and fixed the 1st stage (pyrolytic stage) temperature at 600°C, 2nd stage (gasification stage) temperature at 900°C, S/C of 3.5.

In the study of gasification processes, the role of CO_2 in the carrier gas proves to be pivotal in influencing several outcomes. By integrating CO_2 into the two-stage gasification process, there's an enhancement in gas yield by 2.2 wt%. This augmentation is attributed to the fostering of dry reforming and Boudouard reactions, especially when temperatures surpass 700°C. While the consistency of H_2 content remains around 50 vol%, the concentration of CO distinctly rises, moving from 16.7 vol% to 23.5 vol%, with the gradual increase of CO_2 concentrations from 0% to 100%. This shift is accompanied by a decrease in lighter hydrocarbons like methane and C_2-C_4. On the aspect of CO_2 production and the generation of 'low emission' H_2, elevating the CO_2 concentration in the carrier gas directly results in a significant cutback of total CO_2 production. It's noteworthy that CO_2-steam gasification, employing a complete 100% CO_2, yields markedly less CO_2 per kg of H_2 than its pure steam gasification counterpart. Despite such promising reductions, the resultant H_2 still falls short of the "low emission H_2" benchmark set by the British Government.

However, it's commendable that its CO_2 emissions are substantially lower than those observed in H_2 production via methane reforming. The environmental dimension of this study highlights the merits of using RDF as a gasification feedstock. If RDF were relegated to landfills, it would serve as a source of substantial CO_2 emissions over an extended period. In stark contrast, the practice of using RDF in CO_2-steam gasification slashes these potential emissions, emphasizing the environmental upsides of this method that extend beyond its inherent capabilities in generating heat, power, and H_2. Conclusively, the data underscores the tangible advantages of infusing CO_2 in the carrier gas during gasification, predominantly for curbing CO_2 emissions. However, these findings also flag the imperative for more in-depth research, especially in light of present-day technological constraints.

5.6 Synergy effects

In this exploration of synergy effects within the system, it has been discerned several intriguing interplays between distinct parameters. Three predominant synergistic relationships emerge: the interplay between the steam-to-carbon ratio (S/C) and the 2nd stage (gasification stage) temperature; the relationship between the 2nd stage (gasification stage) temperature and CO_2 concentration in the carrier gas; and the association between S/C and CO_2 concentration in the carrier gas. The synergy between the 2nd stage (gasification stage) temperature and S/C impacts nearly all aspects with the notable exception of the PE. Meanwhile, the link between the 2nd stage (gasification stage) temperature and CO_2 concentration distinctly influences CO_2 levels in the producer gas as well as the H_2/CO ratio. Furthermore, the relationship between steam and CO_2 concentration primarily affects the CCE. These nuanced interactions highlight the deeply interconnected nature of system parameters, offering promising pathways for further optimization.

5.6.1 2nd stage (gasification stage) temperature x S/C

The synergy effects between the second-stage temperature and the steam-to-carbon ratio (S/C) play a critical role in optimizing reaction kinetics and enhancing the efficiency of chemical processes. By adjusting these parameters, it is possible to manipulate the thermodynamic conditions to favour desired reaction pathways, reduce energy consumption, and improve overall system performance. This synergistic interaction can significantly influence the yield and quality of the end products, making it a vital area of study in process engineering.

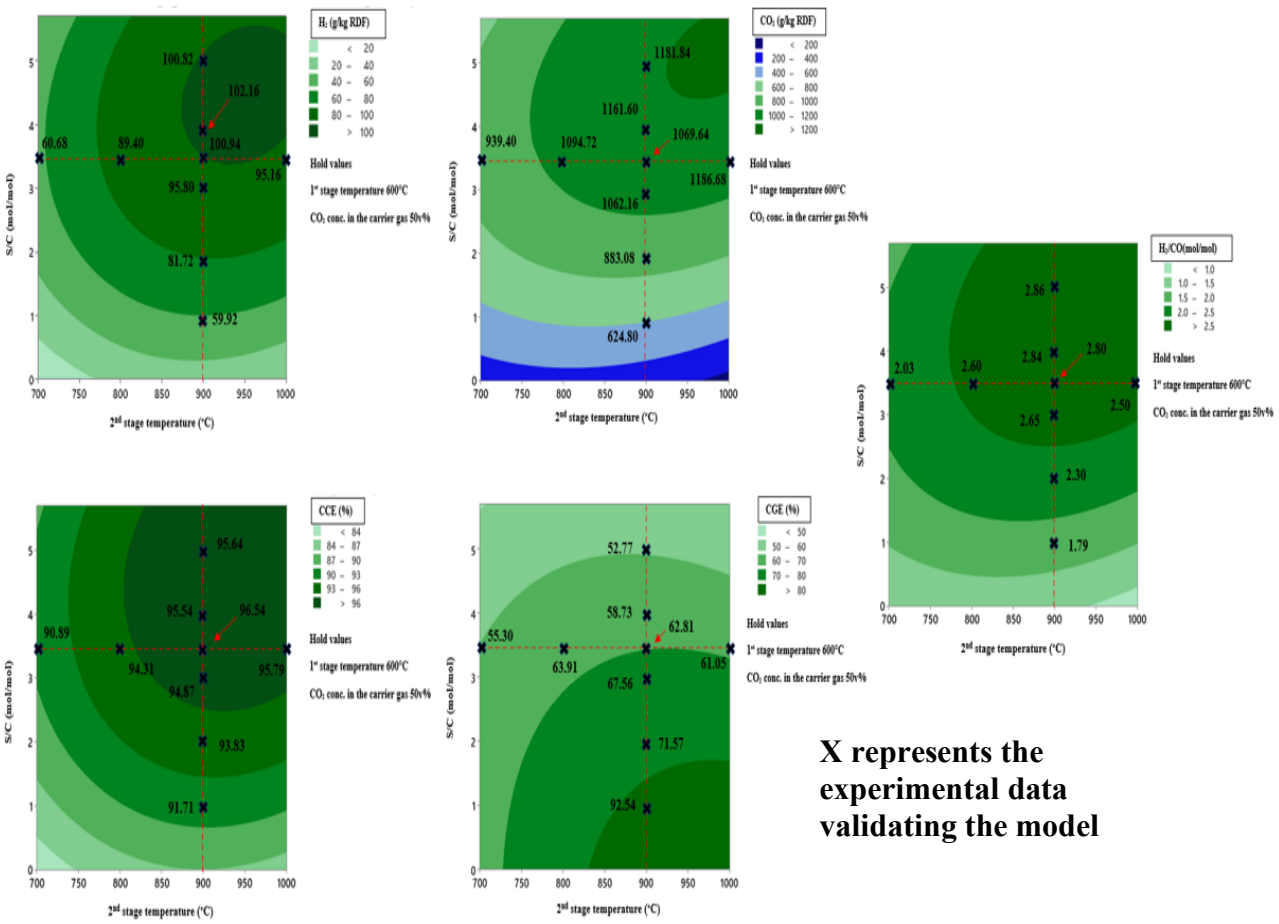

Figure 5.17: Contour plot illustrating the synergy of the 2nd stage (gasification stage) temperature and S/C ratio on various responses.

As highlighted in Figure 5.17, steam and the 2nd stage (gasification stage) temperature significantly influence H_2 production. Maximum H_2 levels are optimized when the S/C lies between 3.5 and 5.5, and the temperature ranges from 870°C to just under 1100°C. This model, derived from research in section 5.1, aligns closely with experimental results from sections 5.4 and 5.5. CO_2 production rises with an increase in both the 2nd stage (gasification stage) temperature and S/C due to the water-gas shift reaction. For tailoring specific H_2/CO ratios in gasification processes, peak CCE is achieved at a 2nd stage (gasification stage) temperature above 800°C with an S/C of about 4. Increasing the temperature to 900°C allows an optimal S/C reduction to 3.5. However, elevating the temperature can lead to a decrease in CGE due to reduced CH_4 and C_2-C_4 compounds, although the producer gas's LHV remains competitive.

5.6.2 2nd stage (gasification stage) temperature x CO_2 concentration in the carrier gas

In two-stage gasification processes, the synergy effects between the second-stage temperature and CO_2 concentration in the carrier gas are pivotal for optimizing gasification performance and product gas quality. The interaction between these parameters influences the thermochemical reactions, such as char gasification and tar reforming, enhancing the conversion efficiency and stability of the process. By carefully controlling the second-stage temperature and CO_2 concentration, it is possible to tailor the gasification environment to maximize the production of syngas with desired composition and minimize undesirable byproducts.

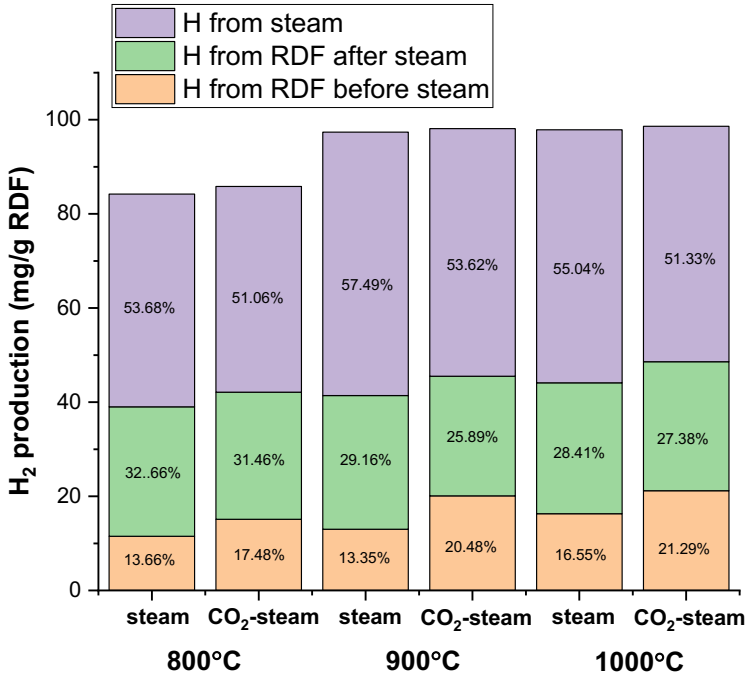

Figure 5.18: H source in both steam gasification and CO_2 (100 vol%)-steam gasification, with a fixed 1st stage (pyrolytic stage) temperature of 600°C and an S/C ratio of 3.5.

When examining the source of H_2, it's observed that CO_2-steam gasification yields a slightly higher amount of hydrogen from feedstock compared to steam gasification. Consequently, this reduces the amount of steam required to produce an equivalent volume of H_2.

In the graph presented, the H_2 yields from both steam gasification and CO_2 (100 vol%)-steam gasification was plotted against varying second-stage temperatures, ranging from 800°C to 1000°C. The first stage temperature was fixed at 600°C, with S/C of 3.5. This graph aimed to

delineate the origins of the hydrogen — either directly from the RDF or as a result of steam introduction.

In steam gasification, the hydrogen content derived from RDF stands at 39.0 mg/g RDF at 800°C. As the second-stage temperature increases, so does the hydrogen yield: 41.4 mg/g RDF at 900°C and 44.1 mg/g RDF at 1000°C. A parallel trend is observed in CO_2-steam gasification, with yields of 42.1 mg/g RDF at 800°C, 45.6 mg/g RDF at 900°C, and 48.6 mg/g RDF at 1000°C.

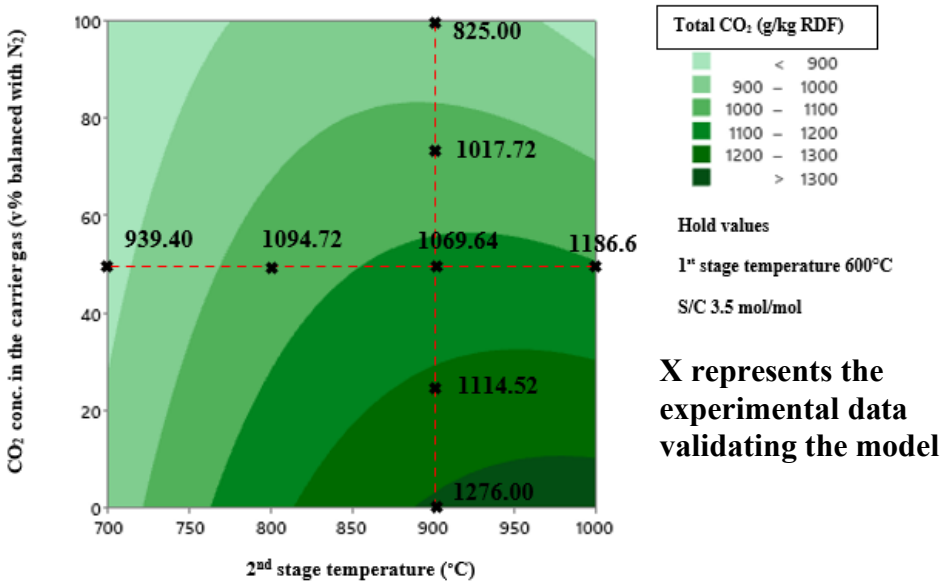

Figure 5.19: Contour representation of CO_2 production (g/kg RDF) with fixed parameters: 1st stage (pyrolytic stage) temperature at 600°C, S/C ratio of 3.5 and varies the 2nd stage (gasification stage) temperature and CO_2 concentration in the carrier gas. This contour is based on the modelling from Section 5.1 experiments. Data points from the 5-level test (section 5.2-5.5) for each parameter are marked with an "X" symbol to validate the model

It's evident that incorporating CO_2 as a carrier gas augments the hydrogen release from the RDF. This improvement in CCE during CO_2-steam gasification was previously discussed in Section 5.4. While the H_2 amounts from both gasification methods don't differ drastically, CO_2-steam gasification extracts a marginally greater quantity of hydrogen from RDF, thereby curbing steam consumption. This can be attributed to CO_2's interaction with both carbon and hydrogen in the RDF, resulting in the formation of gas-phase CH_4 or C_2-C_4 hydrocarbons.

Furthermore, the Figure 5.21 indicates that CO_2 gasification already has superior H_2 production before the steam introduction, hinting at the onset of the CO_2-RDF reaction. Yet, the addition of steam doesn't produce the anticipated rise in H_2 yield. This suggests that dry reforming and

steam reforming don't synergistically interact; they function separately, and H_2 production eventually plateaus upon reaching a saturation point in the reactor.

A closer examination reveals a nuanced distinction in the H_2 origin between the two methods. In steam gasification, 53.7-57.5% of H_2 originates from steam, and 46.3%-45.0% from RDF. In contrast, CO_2-steam gasification accounts for 51.1%-53.6% from steam and 48.9%-46.4% from RDF. There's a dearth of research focusing on discerning the source of H_2. Nonetheless, a study by dos Santos and Alencar (2020) estimated that approximately 44.2% of the total H_2 comes from the water gas shift reaction. Their findings can serve as a benchmark for future endeavours aiming to optimize the process, reduce steam derived H_2, and bolster hydrogen extraction from feedstock. This would not only promote efficient waste utilization but also curtail energy consumption for steam production.

5.6.3 CO_2 concentration in the carrier gas and S/C

The synergy between gasifying agents, specifically steam and CO_2, has a pronounced influence on the H_2/CO ratio, a pivotal factor in determining the end application of syngas. As such, the calibration of the S/C and the quantity of CO_2 used as a carrier gas is of paramount importance. When evaluated under fixed 1st and 2nd stage (gasification stage) temperatures of 600°C and 900°C respectively, distinct optimal ranges emerge based on desired applications.

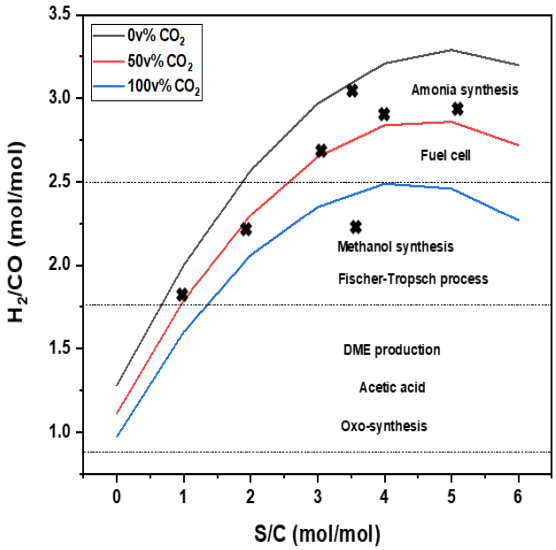

X represents the experimental data validating the model

Figure 5.20: The H_2/CO versus S/C with the variation of CO_2 concentration in the carrier gas 0, 50, and 100% modelled from the experiment section 5.1 and the "X" symbol represent the experimental data from the experiment section 5.4-5.5.

For a high H_2/CO ratio exceeding 2.5, the best results are achieved with a CO_2 concentration ranging from 0% to 50% and an S/C ratio between 2 and 6. Such a configuration is particularly conducive for ammonia production and fuel cells. Conversely, a moderate H_2/CO ratio, falling between 1.8 and 2.5, is realized under several conditions: 0% CO_2 with an S/C from 0.8 to 2, 50% CO_2 with an S/C from 1 to 2.5, and 100% CO_2 with an S/C from 1.5 to 6. This range is aptly suited for methanol production and Fisher-Tropsch fuel synthesis. Lastly, the lowest H_2/CO ratios are obtained by not exceeding an S/C of 1.5 for 100% CO_2, 1 for 50% CO_2, and 0.8 for 0% CO_2. Such low ratios are tailored for processes like Dimethyl Ether (DME) production, acetic acid synthesis, and oxo-synthesis.

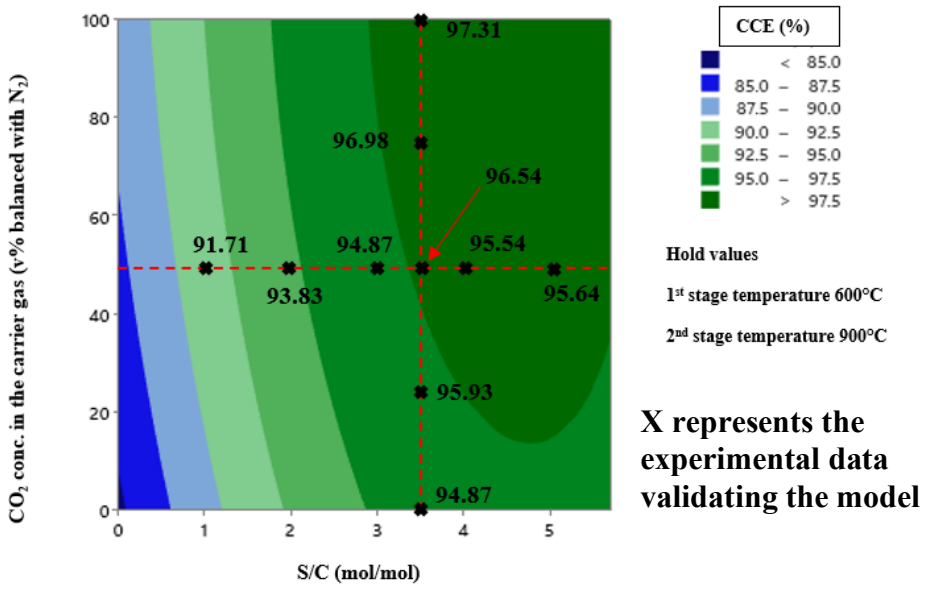

Figure 5.21: Contour representation of CCE with fixed parameters: 1st stage (pyrolytic stage) temperature at 600°C, 2nd stage (gasification stage) temperature at 900°C, S/C ratio of 3.5, and CO_2 concentration at 50vol%. This contour is based on the modelling from Section 5.1 experiments. Data points from the 5-level test (section 5.2-5.5) for each parameter are marked with an "X" symbol to validate the model

In the accompanying graphical representation, "X" symbols demarcate experimental data points, contrasting with a line based on the modelling elucidated in Section 5.1. It's noteworthy that while escalating CO_2 concentrations proffer advantages like heightened CCE and diminished overall CO_2 emissions, they also lead to a reduction in the H_2/CO ratio. This

decrement can be a determining factor, especially in applications such as ammonia production and fuel cells where a specific H_2/CO balance is integral.

5.6.4 PE

Process Efficiency (PE) is a crucial metric in engineering and operations management, quantifying the effectiveness with which a process converts inputs into outputs.

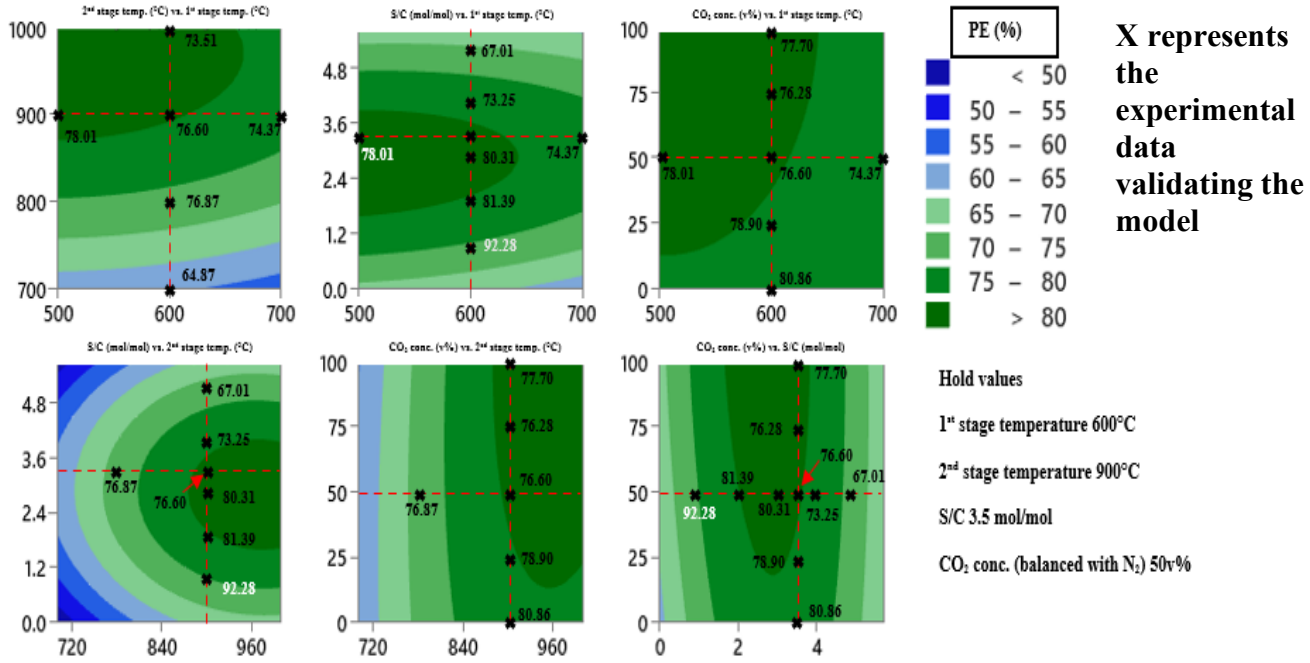

Figure 5.22: Contour representation of PE with fixed parameters: 1st stage (pyrolytic stage) temperature at 600°C, 2nd stage (gasification stage) temperature at 900°C, S/C ratio of 3.5, and CO_2 concentration at 50 vol%. This contour is based on the modelling from Section 5.1 experiments. Data points from the 5-level test (section 5.2-5.5) for each parameter are marked with an "X" symbol to validate the model.

Operational factors individually influence the PE without any synergy between them. To achieve the best PE results, ranging between 75% and 80%, several conditions are vital. The temperature in the 1st stage (pyrolytic stage) should be maintained below 650°C to 680°C. In the 2nd stage (gasification stage), the temperature should be set between 870°C and 990°C. Additionally, to obtain the highest PE, the S/C values must lie between 1.8 and 3.8, and the concentration of CO_2 in the carrier gas should surpass 12.5%. To provide a comprehensive perspective, a contour graph derived from the experiments in section 5.1 has been compared

with results from sections 5.2 to 5.5. This comparative analysis, illustrating the PE, is depicted in Figure 5.22.

5.7 Optimal condition prediction for two-stage gasification for applications in fuel cells, ammonia, FT fuel, methanol, acetic acid, DME, and iron reduction: validation included

Optimization is used to identify the best conditions or geometric parameters to maximize or minimize specific goals, subject to predefined constraints. Objectives can vary, from maximizing product yield or profit to minimizing production time or carbon emissions, all while meeting certain demands or criteria (Ahmad et al., 2016). The optimization process discussed in section 5.7 aims to fine-tune the H_2/CO ratio, maximize overall efficiency, and minimize CO_2 content in the producer gas. Recommendations for specific conditions tailored to various applications are detailed in Table 5.10. and the validation of the optimal condition is shown in the Table 5.11.

To create an effective and environmentally friendly combustion process, multiple factors must be taken into account. A PE of over 70% is required for competitive combustion applications (Basu, 2018). At the same time, reduced levels of CO_2, N_2, H_2O, NH_3, and CH_4 in syngas are favoured as they have a negative impact on flame dynamics and combustion temperature (Wang et al., 2012). Interestingly, the ratio of hydrogen to carbon monoxide (H_2/CO) in syngas serves as a useful metric to predict flame flow and ignition delay time (Lee et al., 2014). This ratio is generally operated between 0.25 and 2.33 in plants, with an optimal range of 1.8-2.3 for improved combustion performance (Slatter et al., 2022).

Catalysts in the Fischer-Tropsch (FT) process are particularly sensitive to impurities such as sulfur, nitrogen, chlorine, arsenic, and mercury, requiring syngas to be free from these elements for optimal catalyst life and effectiveness (Steynberg, 2004). Additionally, the FT process demonstrates higher selectivity when the syngas has low concentrations of CO_2, H_2O, and CH_4 (Steynberg, 2004). It's worth noting that in ammonia plants, these concentrations can be further optimized to below 1 vol% for CO, 0.2 vol% for CO_2, and 1 vol% for H_2S, enhancing the overall process efficiency (Amhamed et al., 2022, Abdin, 2020).

As the world shifts towards sustainable energy solutions, high H_2 yield and purity have become crucial, especially for fuel cell applications. Pressure swing adsorption (PSA) technology can recover up to 88.4% of total hydrogen, achieving near 100% purity, which is a requisite for fuel

cell applications (Shamsudin et al., 2019). However, fuel cells also demand syngas of the highest cleanliness, free from contaminants like tar, H_2S, COS, HCl, and NH_3, which cause degradation and corrosion (Li et al., 2021c). Emerging technologies are focusing on integrating gasification processes with fuel cells to produce cleaner energy, although these are still in nascent stages (Iaquaniello and Mangiapane, 2006, Behzadi et al., 2020).

The EU aims to replace fossil fuels by generating 100% hydrogen from renewable sources (IEA, 2023). Syngas derived from waste gasification shows promise in reducing CO_2 emissions, achieving iron pellet reduction efficiency levels comparable to coal or natural gas methods (Guo et al., 2016). This gasification process is typically operated at temperatures between 800°C and 1000°C, but new research shows that biomass pyrolysis products can actively react with iron oxide at temperatures below 800°C (Bagatini et al., 2021). This opens the door for using syngas with tar and other volatiles in iron ore reduction, offering a potentially more sustainable pathway. Overall, achieving optimal syngas composition and purity is crucial for various industrial applications, from fuel cells to iron ore reduction and chemical synthesis.

Table 5.10: Predictive conditions needed for chemical production, iron ore reduction, and fuel cell operations

Optimisation			Solution				Results						Suggested applications
PE, CGE, CCE, H_2 yield	**CO_2**	**H_2/CO**	**1st stage temp.**	**2nd stage temp.**	**S/C**	**CO_2 conc.**	**PE**	**CGE**	**CCE**	**H_2**	**CO_2/H_2**	**H_2/CO**	
			°C	**°C**	**mol/mol**	**vol%**	**%**	**%**	**%**	**g/kg RDF**	**kg/kg**	**mol/mol**	
Max	Min	Max	509	812	4.3	4	71.8	60.6	97.4	82.4	15.3	3.1	**Fuel cell**
Max	Min	3	510	817	3.9	6	74.1	63.0	95.2	92.4	13.6	3.0	**Ammonia**
Max	Min	2.5	697	883	3.5	93	77.1	71.1	98.5	95.2	10.5	2.5	**FT fuel, FC**
Max	Min	2.0	517	841	1.6	100	77.3	76.6	93.4	65.6	10.6	2.0	**Methanol**
Max	Min	1.5	607	1000	1.6	100	82.1	83.9	93.9	69.2	7.2	1.5	**Acetic acid**
Max	Min	1	575	1000	0.8	100	78.6	87.4	90.8	47.6	5.6	1.0	**DME**
Max	Min	Min	577	1000	0.5	100	76.5	88.8	89.6	39.0	4.3	0.8	**Iron ore reduction**

The optimization targets key performance indicators like hydrogen volume percentage (H_2 vol%), hydrogen yield (H_2 mg/g RDF), carbon dioxide yield (CO_2 mg/g RDF), hydrogen-to-carbon monoxide ratio (H_2/CO), cold gas efficiency (CGE), carbon conversion efficiency (CCE), and overall process efficiency (PE).

For most variables like H_2 vol%, H_2 mg/g RDF, H_2/CO, CGE, CCE, and PE, the aim is to maximize the values. For CO_2 mg/g RDF, the aim is to minimize the value. Following optimization, the results indicated that the target value for each response was closely approximated in Test3, as detailed in Table 5.11.

Table 5.11: Simultaneous multiple response surface optimization results with three repetitions for validation

	Test1	**Test 2**	**Test 3**	**Validation1**	**Validation2**	**Validation3**
Optimization				No data		
H_2(vol%)	Max	Max	Target= 52.2			
H_2 (mg/g RDF)	Max	Max	Target=93.5			
CO_2 (mg/g RDF)	Min	Min	Target=814.3			
H_2/CO	Max	Target = 2.2	Target=2.2			
CGE	Max	Max	Target=76.9			
CCE	Max	Max	Target=97.4			
PE	Max	Max	Target=83.7			
Independent variables						
1st stage temp	605.0	610.4	586.9	587	587	587
2nd stage temp	948.5	945.5	924.2	924	924	924
S/C	2.8	2.7	2.6	2.6	2.6	2.6
CO_2 conc. (vol%)	100	100	100	100	100	100
Responses						
H_2(vol%)	52.4	52.2	51.9	51.9	52.7	52.4
H_2 (mg/g RDF)	94.2	93.5	91.6	91.7	94.6	94.0

CO_2 (mg/g RDF)	820.2	814.3	813.4	793.9	793.8	790.1
H_2/CO	2.2	2.2	2.2	2.1	2.2	2.2
CGE	76.5	76.9	76.9	74.9	75.2	76.6
CCE	97.5	97.4	97.0	97.5	97.6	97.3
PE	83.9	83.7	83.5	83.9	84.5	85.5
Composite desirability	0.8	0.8	1.0			

Consequently, three additional experiments were conducted to validate the results obtained in Test 3. The table illustrates that various independent variables such as stage temperatures and S/C ratios are fine-tuned to achieve the optimization objectives. For example, the H_2 vol% and H_2 mg/g RDF are targeted to be maximized and closely approach or surpass their targets in the validation runs. Similarly, CO_2 values are minimized but still hover near the target. Efficiencies like CGE, CCE, and PE all have high values and reach near the optimization target during the validation phases.

The composite desirability values suggest that "Test 3" was the most successful in achieving the desired optimization, with a score of 1.0. Overall, the table shows that the 2-stage gasification process has been carefully optimized for performance, showing that it's not only efficient but also reliable when scaled or implemented under varying conditions.

The Figure 5.23 shows the energy balance of a two-stage gasification system that uses RDF pellets with a heating value of 15.0 MJ/kg. The gasification system operates at two different temperatures, with the first stage temperature maintained at 587°C and the second stage temperature at 924°C. The steam-to-carbon (S/C) ratio used was 2.6, and the CO_2 content was 93 g/kg RDF.

In the first stage, pyrolysis takes place, which is an endothermic reaction. To sustain this reaction, an external energy of 3.6 MJ/kg RDF is required, which is calculated from the DSC of RDF, as explained in pyrolysis stage. In the second stage, steam is used, requiring around 6.0 MJ/kg RDF with an S/C of 2.6. To maintain the temperature at 924°C, additional energy is required, which is estimated at 2.22 MJ/kg RDF based on prior research on gasification.

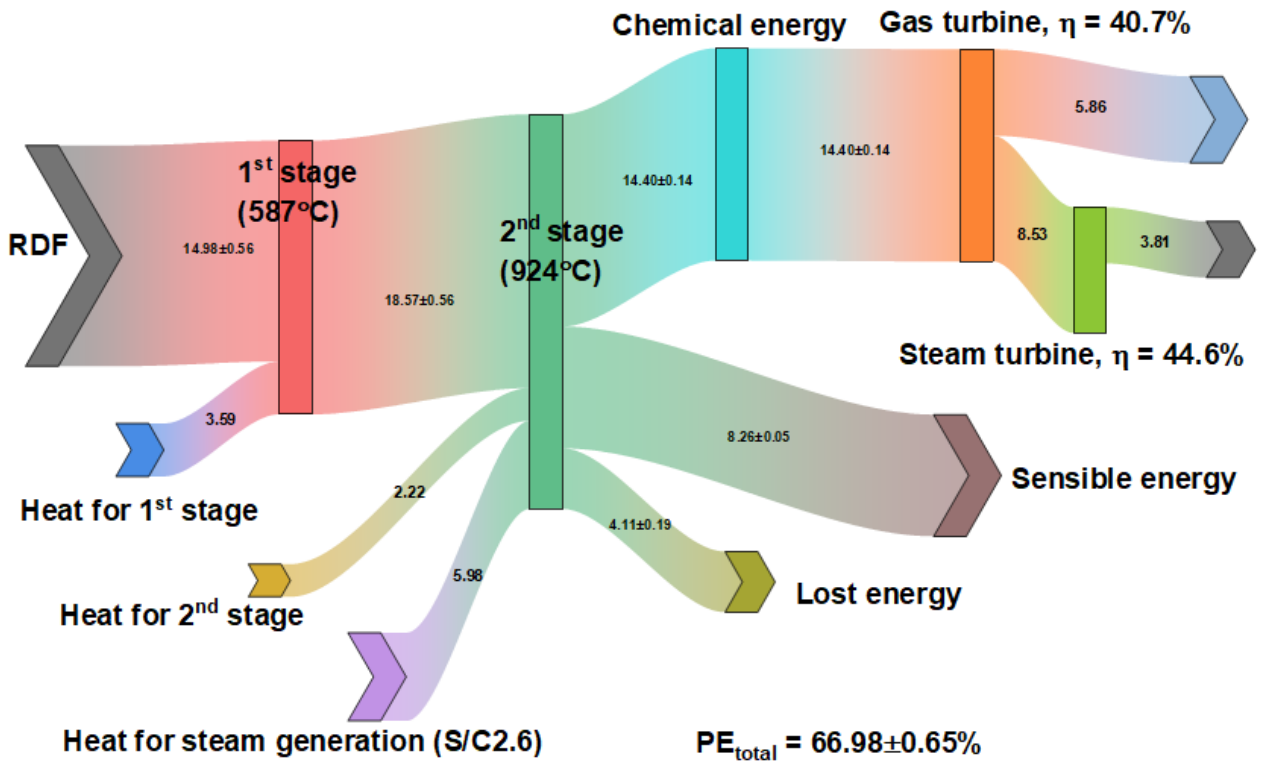

Figure 5.23: Energy flow in two-stage CO_2-steam gasification used in CHP system

After the two-stage gasification process, the resulting producer gas contains H_2 (52.4 mol%), CO (24.3 mol%), CO_2 (22.6 mol%), CH_4 (0.3 mol%), and C_2-C_4 (0.4 mol%). The gas yield was 1.6 Nm^3/kg RDF, resulting in 14.4 MJ/kg of cold gas energy. The sensible heat generated in this system is 8.3 MJ/kg. Therefore, the energy efficiency of this gasification process is 84.6%.

If this gasification system is connected to gas and steam turbines to produce heat and power, the resulting electricity and thermal efficiency would be 21.9% and 45.1%, respectively. The overall efficiency of the system in producing heat and power would be 67.0%. The turbine efficiency values used are based on Basu (2018).

Table 5.12: Performance and products from RDF pellets two-stage CO_2-steam gasification

	2-stage gasification
Performance	
PE $_{gasification}$ (%)	84.6±0.6
PE $_{over\ all\ (thermal\ +\ electricity)}$	67.0±0.6
CCE (%)	97.5±0.1
CGE (%)	75.6±0.7
H_2/CO	2.1±0.0
Gas (Nm^3/kg RDF)	1.6±0.0
Gasification char) (g/kg RDF)	107.3±3.8
Wax (g/kg RDF)	2.4±0.3
Tar (g/kg RDF)	3.1±0.2
Gas quality	
H_2 (vol%)	52.4±0.3
CO (vol%)	24.3±0.3
CO_2 (vol%)	22.6±0.2
CH_4 (vol%)	0.3±0.1
C_2-C_4 (vol%)	0.4±0.2
H_2 (mg/g RDF)	93.4±1.2
CO_2 (mg/g RDF)	792.6±1.8
LHV gas (MJ/kg RDF)	14.4±0.1
Gasification char) **(wt% as received)**	
C	7.8±0.0
H	0.0±0.0
N	0.4±0.0
Inorganic (mg/kg RDF)	
Ca	10 550
Na	468.5
Mg	580.1
Al	642.4
Fe	507.3

Zn	33.2
Sb	15.4
Cu	36.1
Wax (wt% as received)	
C	60.2
H	4.1
N	0.2
Tar (mg/kg RDF)	
Methanol	44.2
Formic acid	174.9
Benzene	31.7
Toluene	289.1
Hexanal	25.4
2,5-Hexadione	57.5
p-Xylene	91.3
Furfural	12.7
Phenol	286.3
Naphthalene	1029.5
Naphthalene, 2-methyl	141.5
Fluorene	76.3
Phenanthrene	267.3
Fluoranthene	78.9
Chrysene	26.5
Unidentified	466.7

RDF CO_2-steam gasification under optimal conditions produces around 90-93 mg H_2/g RDF, while wood pellet (WP) CO2-steam gasification yields 86-87 mg H_2/g WP. The UK RDF exportation peaked at 3.2 million tonnes of RDF/year which is transport to Europe for CHP plant (Langley, 2022). If this RDF is used to produce H_2 with this technology, it is calculated to be around 1096-1132 MW which is around 11.00-11.32% of the total green H_2 targeted (10GW) by the UK in 2030 (Department for Business, 2022a).

This demonstrates that the system can effectively recover energy from waste, converting it into valuable products such as hydrogen. However, an increase in CO_2 concentration in the

carrier gas leads to a reduction in the H_2/CO ratio. This occurs because higher CO production from reforming and Boudouard reactions results in a decreased H_2/CO ratio. Nevertheless, different H_2/CO ratios can be utilized for various applications.

5.8 Summary

By examining the operational factors affecting the efficiency and production rates in the two-stage gasification of refuse-derived fuel (RDF). The analysis encompassed the influence of the first and second-stage temperatures, steam-to-carbon (S/C) ratios, and the incorporation of CO_2 in the carrier gas on a range of outcomes including cold gas efficiency (CGE), process efficiency (PE), carbon conversion efficiency (CCE), and hydrogen yields.

- **Influence of first (pyrolysis) and second (gasification)-stage temperature**

The investigation revealed that elevating the first-stage temperature substantially augments the overall gas yield, diminishes the solid and condensate yields, and reduces the carbon content in solid residues (gasification char) and wax fractions. The second-stage temperature was pivotal in achieving maximum hydrogen levels, notably between 870°C and 1100°C. However, beyond 900°C, complexities such as tar re-agglomeration begin to surface.

- **Role of steam to carbon (S/C) ratio**

The S/C ratio was found to be a pivotal operational variable affecting the gas composition, with higher S/C ratios favouring the production of H_2 and CO_2 while reducing CO, CH_4, and C_2-C_4 components. Optimal hydrogen production is achieved when the S/C ratio lies between 3.5 and 5.5. S/C values between 1.8 and 3.8 were found to be optimal for achieving the highest PE, underlining the significance of this parameter.

- **Incorporation of CO_2 in carrier gas**

Integrating CO_2 as a carrier gas enhances the gas yield by fostering dry reforming and Boudouard reaction, although at the cost of reducing the H_2/CO ratio in certain applications. A significant reduction in total CO_2 production was also observed, underlining the environmental benefits of this operational modification. It suggests that CO_2 and steam do not synergistically affect hydrogen yields; they operate independently, reaching a saturation point in the reactor.

- **Optimal condition**

A striking outcome is that different combinations of these operational parameters can be tailored to suit various end applications, such as ammonia production, fuel cells, or Fischer-Tropsch synthesis. In terms of process efficiency, maintaining the 1st stage (pyrolytic stage) temperature between 650°C and 680°C and the 2nd stage (gasification stage) temperature between 870°C and 990°C, along with an S/C between 1.8 and 3.8 and CO_2 concentration above 12.5%, appeared most conducive for optimal results. The study shows that using RDF in an optimal condition of CO_2-steam gasification can produce 90-93 mg of H_2 per gram of RDF, compared to 86-87 mg H_2/g from wood pellets. If the UK's annual RDF export of 3.2 million tonnes were used for this technology, it could meet around 11% of the UK's 2030 green hydrogen target. However, increasing CO_2 concentration in the carrier gas reduces the H_2/CO ratio, which could be adjusted for specific applications.

- **Limitations and Future Work**

While the presented work significantly enhances the understanding of RDF two-stage gasification, further research is essential for multiple areas. These include a.) optimizing energy output from steam generation, gaining a more comprehensive understanding of the process's scalability for commercial application, and b.) examining heat transfer dynamics. Additionally, implementing CaO as a catalyst to potentially lower CO_2 emissions deserve further exploration and understanding the Life Cycle Assessment (LCA) of this process could also provide further invaluable insights.

Chapter 6 Life cycle assessment of hydrogen production processes

A comprehensive life cycle assessment (LCA) of various hydrogen production technologies, aiming to quantify their environmental, resource and health impacts. Utilizing the ReCiPe2016 (H) framework (Huijbregts et al., 2016), the study evaluates multiple hydrogen production scenarios including steam methane reforming (SMR), conventional gasification of coal, biomass waste, and MSW, partial oxidation of oil products (POX), and water electrolysis using different energy sources such as coal, wind, solar, and nuclear energy. Additionally, it explores innovative two-stage gasification (TSG) processes using waste wood and RDF pellets. Key findings reveal significant variances in global warming potential (GWP100), human toxicity potential, and other environmental impacts across these technologies. The study highlights the environmental challenges of traditional methods like SMR and coal gasification, which demonstrate high GWP100 and toxicity potentials. In contrast, electrolysis powered by renewable sources emerges as more environmentally favourable, though not without its challenges. The novel two-stage gasification methods, particularly using wood pellets, show promise for lower GWP100, yet face constraints like high land occupation and resource utilization. The chapter also investigates into the impact of transportation of raw materials and the potential benefits of incorporating alternative energy sources and carbon capture and storage (CCS) technology. The findings of this LCA provide critical insights into the environmental and health implications of different hydrogen production technologies, offering guidance for selecting more sustainable methods in the pursuit of a clean energy future.

6.1 Goal and scope definition

Goal and scope definition: The objective from this study is to compare different hydrogen production paths namely, steam methane reforming, traditional gasification, electrolysis from coal, wind, solar, and nuclear energy and two-stage gasification using waste wood and RDF pellets as feedstock.

Functional Unit: 1kg of H_2 at 3MPa, 99.9%purity according to UK government (Department for Business, 2022b)

Database for reference: Ecoinvent 3.9.1 cutoff with openLCA software (Appendix D)

Table 6.1: Keys assumptions of the Life Cycle Assessment (LCA) study of hydrogen production

Life cycle stage	**Assumption**
Pelletisation	Waste wood made of waste wood from agriculture, sawdust, shavings of hardwood and softwood and wood chip
	50% of RDF made from biomass waste
Transportation	The distance between pellet manufacture and gasification reactor is 50 km
	The transportation is used lorry under Euro standard 0-4
	The transportation by ship with 43,000 tonnes per container ship
WP and RDF-TSG	Energy and mass balance are from optimal condition discussed in the previous chapter
	50% of energy excess from TSG is recycled as electricity to the grid
Steam production	No heat loss during the heat recycled from TSG to steam production
	No energy required for recycle water in the TSG system
External energy	No heat loss from distance
Cleaning in two-stage gasification	Only acetone and isopropanol are used in this cleaning
	Energy required for cleaning is based on flue gas treatment unit
Screening	This data is based on PSA technology
Storage	No H_2 loss
	Based on natural gas storage since there is no data on H_2 storage equipment yet

The Table 6.1 outlines various scenarios for hydrogen production, each with its unique processes and considerations

Scenario A focuses on SMR, a process that combines methane with steam to produce hydrogen and carbon dioxide. This method involves several steps, including desulfurization, reforming, and water gas shift, and is characterized by its high energy consumption. SMR requires external heat and catalysts and generates excess steam and electricity, which can be utilized within the plant or sold.

Scenario B examines conventional gasification with sub-scenarios B1, B2, and B3, focusing on coal, biomass waste, and RDF, respectively. These options represent different feedstock choices for gasification.

Scenario C, Partial oxidation of oil products (POX), is detailed in a dataset from the European plastics industry, highlighting naphtha cracking.

Scenario D covers electrolysis with different energy sources: D1 uses energy from coal, representing global hard coal power plant production. D2 involves a 4.5MW wind turbine, designed for a 20-year operational span, while D3 describes a 50 MW solar thermal parabolic trough power plant in Upington, South Africa. D4 considers a grid-connected nuclear pressure water reactor (PWR), based on a Swiss model, focusing on fuel use and radioactive emissions.

Scenario E explores wood pellet two-stage gasification (WP-TSG), with sub-scenarios based on different energy sources and detailing the origins and import routes of wood pellets to the UK. These pellets are sourced from both local and international locations, including the USA, Canada, Portugal, Latvia, and the Netherlands.

Scenario F delves into RDF pellets two-stage gasification (RDF-TSG), with similar energy source sub-scenarios as Scenario E. The RDF pellets composition is designed to mimic the UK's RDF, combining biomass waste and food waste.

Table 6.2: Overview of hydrogen production technologies: scenario comparisons

Scenarios	**Definition**	**Sensitive analysis**	**Note**
A	Steam methane reforming (SMR)	None	Steam methane reforming (SMR) involves reacting methane with steam to produce hydrogen and carbon dioxide, using processes like desulfurization, reforming, and water gas shift. The process is energy-intensive, requiring external heat and catalysts, and generates excess steam and electricity, which are used within the plant or sold to the grid.
B	Traditional gasification	B1: Coal	The fluidized bed technologies are implemented with a steam-to-carbon (S/C) ratio of 2, employing energy derived from combustion processes utilizing various feedstocks
		B2: Biomass waste	
		B3: RDF	

			such as coal, biomass waste, and RDF.
C	Partial oxidation of oil products (POX)	None	This dataset from the European plastics industry focuses on naphtha cracking
D	Electrolysis (PEM)	D1: energy from coal	This dataset represents average global hard coal power plant electricity production in 2012, including emissions data and operational specifics. It merges data from ecoinvent versions 2 and 3, covering 14 countries plus additional ones in version 3. Key aspects include coal quality, plant efficiency, and emission control measures like desulfurization and denitrification.
		D2: Wind	4.5MW wind turbine with a

			rotor diameter of 113 meters. Its nacelle, weighing around 355,000 kg, is perched on a 120-meter reinforced concrete tower. Additionally, each turbine is equipped with a 1000-meter network connection cable and is designed to operate for 20 years.
		D3: Solar	This activity details a 50 MW solar thermal parabolic trough power plant in Upington, South Africa, with a 600,000 m^2 collector field and a 1100 MWh_{th} nitrate salt thermal storage system. It operates for 5379 hours/year, harnessing a steam mass flow rate of 105 kg/s and

			requiring co-firing diesel fuel.
		D4: Nuclear	A grid-connected nuclear pressure water reactor (PWR), based on a Swiss PWR dataset from 1995-2002. It assumes an average burnup of 53 MWd/kg heavy metal, with an average enrichment of 4.2% U235 for fresh uranium fuel, and 8% energy production from MOX fuel. The dataset includes the full upstream chain for fuel, lifetime electricity production estimates, and material requirements during operation. It accounts for diesel for emergency generators and averages

			radioactive emissions from specific Swiss plants. Waste streams include spent fuel for reprocessing and conditioning, low active waste, and waste from dismantling.
E	Wood pellet Two-stage gasification (WP-TSG)	E1: energy from WP incineration	This is based on lab scale TSG developed in Newcastle University (Mankasem et al., 2023).
		E2: Wind	
		E3: Solar	
		E4: Nuclear	
		Origin and distance imported the WP to the UK	The wood pellets' origins are diversified, encompassing local production within 50 km, national production within 500 km, and imports based on 2014 routes from the USA, Canada, Portugal, Latvia, and the Netherlands.

F	RDF pellets Two-stage gasification (RDF-TSG)	E1: energy from RDF incineration	Same as E
		E2: Wind	
		E3: Solar	
		E4: Nuclear	
		The composition of the RDF pellets (based on RDF in the UK)	The composition of the RDF (Refuse-Derived Fuel) pellets is designed to mimic the UK's RDF, consisting of 50% - 85% food waste, biomass waste and paper components.

6.2 Inventory

The inventory details for Scenarios A to D are included in the Appendix D, as they are not the primary focus of this work. These scenarios have been sourced from the Ecoinvent database to provide a basis for comparison with the novel elements introduced in Scenarios E and F.

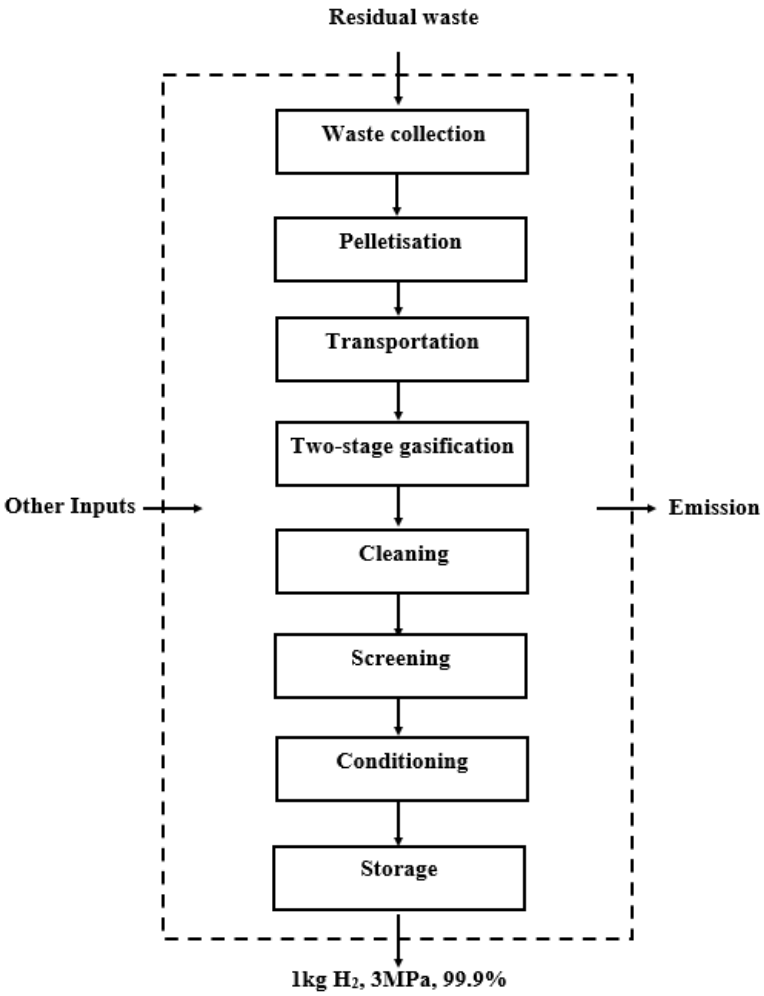

Figure 6.1: The process to produce hydrogen from waste pellets (E and F)

The process efficiently transforms residual waste into high-purity hydrogen, delineated in a diagram on Figure 6.1, detailing the production of 1kg of hydrogen at 3MPa with 99.9% purity. Initially, this collects residual waste, serving as the primary feedstock for two-stage gasification. This waste is pelletized to enhance manageability and facilitate efficient transport and processing. The pellets are conveyed to the primary facility, assumed to be within a range of 50-8000 km.

Table 6.3: Case E: Wood pellets two-stage gasification (WP-TSG)

Pelletisation			**Reference or sources**
Inputs	**Amount**	**Unit**	Derived from the optimized conditions outlined in Chapter 4, the input and output data for pelletisation have been sourced from the Ecoinvent 3.9.1 cut-off dataset "Production in a modern wood pellets factory in Switzerland (years 2011- 2012)"
Waste wood from agriculture	0.5	kg	
Sawdust	0.3	kg	
Shavings, hardwood	0.2	kg	
Shaving, softwood	0.2	kg	
Wood chips	0.4	kg	
Electricity, medium voltage	1.1	kWh	
Heat, central or small scale	1.3	MJ	
Lubricating oil	9.7e-4	kg	
Water, unspecified	3.5e-4	m^3	
Outputs			
Wood pellets	11.5	kg	
Water, emission to air	5.2e-5	m^3	
Water, emission to water	2.9e-4	m^3	
Transportation			Derived from the optimized conditions outlined in Chapter 4, the input and output data for transportation have been sourced from the Ecoinvent 3.9.1 cut-off dataset "transport, freight, lorry, all sizes, EURO4 to generic market for transport, freight, lorry, unspecified"
Inputs	**Amount**	**Unit**	
Wood pellets	11.5	kg	
Transportation, lorry Euro 0-4	11.5*50	kg*km	
Outputs			
Wood pellets, transported	11.5	kg	
WP-TSG			Derived from the optimized conditions outlined in Chapter 4. The input and output data
Wood pellet, transported	11.5	kg	

Recycled CO_2, from PSA	1.0	kg	for Two-stage gasification plant have been sourced from the Ecoinvent 3.9.1 cut-off dataset "chemical factory construction, organics"
Steam, from steam production	19.8	kg	
Heat, from external energy	74.4 (1st 45.5MJ, 2nd 28.8MJ)	MJ	
Waste incineration furnace facility	4.8e-7	unit	
Outputs			
Contaminated producer gas	21.9	m^3	
Gasification char, waste	0.1	kg	
C	0.1	kg	
H	7.2e-4	kg	
N	8.1e-4	kg	
Ca	5.1e-7	kg	
Mg	6.4e-8	kg	
K	2.2e-7	kg	
Unused water	14.4	kg	
Heat, to recycled in steam production	53.5	MJ	
Heat, to recycled in external energy	17.4	MJ	
Steam production			Derived from the optimized conditions outlined in Chapter 4, the input and output data for steam production have been sourced from the Ecoinvent 3.9.1 cut-off dataset "steam production, in chemical industry"
Inputs	**Amount**	**Unit**	
Water, unspecified	5.4	kg	
Unused water, from cleaning	14.4	kg	
Heat from recycled of TSG	53.5	MJ	
Outputs			
Steam	19.8	kg	

External energy			E1:“ heat production, wood chips from industry, at furnace 1000kW, state-of-the-art 2014” E2: “electricity production, wind, >3MW turbine, offshore” E3: “electricity production, solar thermal parabolic trough, 50 MW” E4: “electricity production, nuclear, pressure water reactor”
Inputs	**Amount**	**Unit**	
Electricity from heat surplus from TSG (50%)	8.7	MJ	
WP incineration (E1)	(74.4-8.7) 65.7	MJ	
Wind (E2)	(74.4-8.7)	MJ	
Solar (E3)	(74.4-8.7)	MJ	
Nuclear (E4)	(74.4-8.7)	MJ	
Outputs			
Heat	74.4	MJ	
Cleaning			Derived from the optimized conditions outlined in Chapter 4, the input and output data for plant unit have been sourced from the Ecoinvent 3.9.1 cut-off dataset “Gas Power Plant, 100MW Electrical”
Inputs	**Amount**	**Unit**	
Contaminated producer gas	22.7	m^3	
Isopropanol/acetone	3.3e-5	kg	
Energy	1.1e-1	MJ	
Unit gas power plant, cleaning unit 100MW	6.0e-10	unit	
Water, unspecified	1.5e-4	m^3	
Outputs			
Producer gas	22.7	m^3	
Heterocyclic aromatics	9.7e-7	kg	
Light PAHs	2.2e-6	kg	
Heavy PAHs	1.0e-6	kg	
Naphthalene	1.4e-6	kg	
Unidentified	1.4e-6	kg	
Screening (PSA)			Derived from the optimized conditions outlined in Chapter 4, the input and output data for PSA unit have been sourced
Inputs	**Amount**	**Unit**	
Producer gas	22.7	m^3	
Charcoal	3.1e-3	kg	

Chemical factory, organics	8.0e-10	unit	from the Ecoinvent 3.9.1 cut-off dataset "biogas purification to biomethane by pressure swing adsorption"
Electricity, low voltage	2.7	kWh	
Lubricating oil	2.2e-3	kg	
Potassium hydroxide	5.9e-5	kg	
Outputs			
Carbon dioxide, non-fossil	3.7	m^3	
Recycled carbon dioxide	0.5	m^3	
Carbon monoxide, non-fossil	5.2	m^3	
Methane, non-fossil	1.2	m^3	
Hydrogen, 99.9%	12.0	m^3	
Hydrocarbons (C_2-C_4)	0	m^3	
Heat, waste	18.8	MJ	
Storage			Derived from the optimized conditions outlined in Chapter 4, the input and output data for PSA unit have been sourced from the Ecoinvent 3.9.1 cut-off dataset "compressed air production, 1000 kPa gauge, <30kW, optimised generation"
Inputs	**Amount**	**Unit**	
H_2 (0.5MPa), 99.9%	1	kg	
Compressor, screw-type compressor, 4kW	8.3e-5	unit	
Aluminium, cast alloy	1.0e-5	kg	
aluminium, wrought alloy	2.2e-05	kg	
electricity, low voltage	0.2	kWh	
lubricating oil	1.0e-05	kg	
section bar extrusion, aluminium	3.2e-05	kg	
Outputs			
H_2 (3MPa), 99.9%	1	kg	
Mineral oil, waste	1.0e-5	kg	

At the heart of the operation is the two-stage gasification (see details in Figure 6.2), thermally converting pellets into syngas. Following this, a cleaning phase removes impurities and unwanted elements from the gas such as sulfur compounds, particulates, and tar. The gas then undergoes a screening process to ensure consistent quality and eliminate residual particulates. During conditioning, the gas is further treated to obtain the desired properties, readying it for hydrogen conversion.

Conditioned gas is stored before the final conversion. While additional inputs are introduced to drive specific reactions and achieve outcomes, we're mindful of emissions—striving for minimal environmental impact. The input and output are detailed in the Table 6.3 for case E and Table 6.4 for case F.

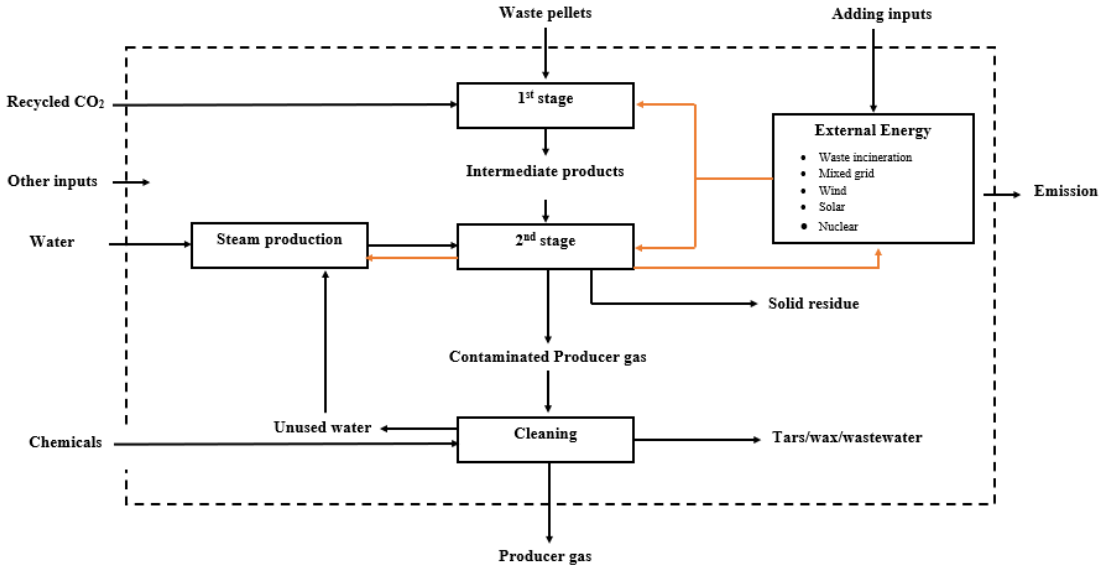

Figure 6.2: The detailed process in the two-stage gasification

Table 6.4: Case F: RDF pellets two-stage gasification (RDF-TSG)

Pelletisation			**Reference or sources**
Inputs	**Amount**	**Unit**	Derived from the optimized conditions outlined in Chapter 5, the input and output data for pelletisation have been sourced from the Ecoinvent 3.9.1 cut-off dataset
RDF	9.6	kg	
Electricity, medium voltage	1.0	kWh	
Heat, central or small scale	1.2	MJ	

Lubricating oil	9.0E-4	kg	"Production in a modern wood pellets factory in Switzerland (years 2011- 2012)"
$CaCO_3$	1.1	kg	
Water, unspecified	3.2e-4	m^3	
Outputs			
RDF pellets	10.7	kg	
Water, emission to air	4.8e-5	m^3	
Water, emission to water	2.7e-4	m^3	
Transportation			Derived from the optimized conditions outlined in Chapter 5, the input and output data for transportation have been sourced from the Ecoinvent 3.9.1 cut-off dataset "transport, freight, lorry, all sizes, EURO4 to generic market for transport, freight, lorry, unspecified"
Inputs	**Amount**	**Unit**	
RDF pellets	10.7	kg	
Transportation, lorry Euro 0-4	10.7*50	kg*km	
Outputs			
RDF pellets, transported	10.7	kg	
Steam production			Derived from the optimized conditions outlined in Chapter 5, the input and output data for steam production have been sourced from the Ecoinvent 3.9.1 cut-off dataset "steam production, in chemical industry"
Inputs	**Amount**	**Unit**	
Water, unspecified	(23.9-17.5) 6.5	kg	
Unused water, from cleaning	17.5	kg	
Heat from recycled of TSG	64.0	MJ	
Outputs			
Steam	23.9	kg	
External energy			F1:" heat, from municipal waste incineration to generic market for heat district or industrial, other than natural gas"
Inputs	**Amount**	**Unit**	
Electricity from heat surplus from TSG (50%)	12.2	MJ	
Waste incineration (F1)	(62.2-12.2)	MJ	

Wind (F2)	(62.2-12.2)	MJ	F2: “electricity production, wind, >3MW turbine, offshore” F3: “electricity production, solar thermal parabolic trough, 50 MW” F4: “electricity production, nuclear, pressure water reactor”
Solar (F3)	(62.2-12.2)	MJ	
Nuclear (F4)	(62.2-12.2)	MJ	
Outputs			
Heat, to TSG	62.2	MJ	
Two-stage gasification			Derived from the optimized conditions outlined in Chapter 5. The input and output data for Two-stage gasification plant have been sourced from the Ecoinvent 3.9.1 cut-off dataset “chemical factory construction, organics”
Inputs	**Amount**	**Unit**	
RDF pellet, transported	10.7	kg	
Recycled CO_2, from PSA	1.0	kg	
Steam, from steam production	23.9	kg	
Heat, from external energy	62.2	MJ	
Waste incineration furnace facility	4.8e-7	unit	
Outputs			
Contaminated producer gas	23.0	m^3	
Gasification char, waste	1.2	kg	
C	9.0e-2	kg	
H	2.3e-4	kg	
N	4.4e-3	kg	
Ca	1.1e-4	kg	
Na	5.0e-6	kg	
Mg	6.2e-6	kg	
Al	6.9e-6	kg	
Fe	5.4e-6	kg	
Zn	3.6e-7	kg	

Sb	1.6e-7	kg	
Cu	3.9e-7	kg	
Unused water	17.5	kg	
Heat, to recycled in steam production	64.0	MJ	
Heat, to recycled in external energy	24.4	MJ	
Cleaning unit			Derived from the optimized conditions outlined in Chapter 5, the input and output data for plant unit have been sourced from the Ecoinvent 3.9.1 cut-off dataset "Gas Power Plant, 100MW Electrical"
Inputs	**Amount**	**Unit**	
Contaminated producer gas	23.0	m^3	
Isopropanol/acetone	3.3E-05	kg	
Energy	1.1e-1	MJ	
Unit gas power plant, cleaning unit 100MW	6.1e-10	unit	
Water, unspecified	1.5e-4	m^3	
Outputs			
Producer gas	23.0	m^3	
N, waste to water, unspecified	1.8e-2	kg	
Methanol	4.5E-07	kg	
Formic acid	1.8E-06	kg	
Benzene	3.2E-07	kg	
Toluene	2.9E-06	kg	
Hexanal	2.6E-07	kg	
2,5-Hexadione	5.8E-07	kg	
p-Xylene	9.3E-07	kg	
Furfural	1.3E-07	kg	
Phenol	2.9E-06	kg	
Naphthalene	1.0E-05	kg	
Naphthalene, 2-methyl	1.4E-06	kg	
Fluorene	7.8E-07	kg	
Phenanthrene	2.7E-06	kg	
Fluoranthene	8.0E-07	kg	

Chrysene	2.7E-07	kg	
Unidentified	4.8E-06	kg	
Screening (PSA unit)			Derived from the optimized conditions outlined in Chapter 5, the input and output data for PSA unit have been sourced from the Ecoinvent 3.9.1 cut-off dataset "biogas purification to biomethane by pressure swing adsorption"
Inputs	**Amount**	**Unit**	
Producer gas	23.0	m^3	
Charcoal	3.1e-3	kg	
Chemical factory, organics	8.1e-10	unit	
Electricity, low voltage	2.8	kWh	
Lubricating oil	2.2e-4	kg	
Potassium hydroxide	6.0e-5	kg	
Outputs			
Carbon dioxide, non-fossil	4.7	m^3	
Recycled carbon dioxide	0.5	m^3	
Carbon monoxide, non-fossil	5.6	m^3	
Methane, non-fossil	0.1	m^3	
Hydrogen, 99.9%	12.0	m^3	
Hydrocarbons (C_2-C_4)	0.1	m^3	
Heat, waste	19.1	MJ	
Hydrogen sulfide	1.0e-4	kg	
Storage			Derived from the optimized conditions outlined in Chapter 5, the input and output data for PSA unit have been sourced from the Ecoinvent 3.9.1 cut-off dataset "compressed air production, 1000 kPa gauge, <30kW, optimised generation"
Inputs	**Amount**	**Unit**	
H_2 (0.5MPa), 99.9%	1	kg	
Compressor, screw-type compressor, 4kW	8.3e-5	unit	
Aluminium, cast alloy	1.0e-5	kg	
aluminium, wrought alloy	2.2e-05	kg	
electricity, low voltage	0.2	kWh	
lubricating oil	1.0e-05	kg	

section bar extrusion, aluminium	3.2e-05	kg	
Outputs			
H_2 (3MPa), 99.9%	1.0	kg	
Mineral oil, waste	1.0e-5	kg	

6.3 Impact assessment methods

Drawing upon the Recipe2016 (H) framework, the primary objective of this study is the comprehensive evaluation of environmental consequences, tracing them from their origins as raw emissions to discerning potential long-term consequences. It is noted that the ReCiPe method is an advanced life cycle impact assessment (LCIA) framework, originally developed in 2008 through collaboration among RIVM, Radboud University Nijmegen, Leiden University, and PRé Sustainability (Huijbregts et al., 2016).

At the foundation of the LCA lies empirical data carefully gathered within the laboratory scale. As an illustrative example (see Figure 6.3), the RDF two-stage gasification process reveals that the production of 1 kg of H_2 yields emissions totalling 1.0e-5 kg of naphthalene.

While this raw data serves as a crucial foundation, it inherently lacks the capacity to provide a direct environmental perspective. To bridge this gap, the Recipe method was employed, which facilitates the translation of emissions into quantifiable environmental impacts (Huijbregts et al., 2016). In this specific case, the naphthalene emissions are translated into an equivalent of 2.3 kg of 1,4-DCB for every kilogram of H_2 produced, with respect to Freshwater Eutrophication Potential (FETP).

These conversions termed to 'midpoint impacts,' which are standardized environmental scores. These scores offer insights into various environmental categories (see Table 6.5 for full list of midpoint impacts). Additionally, these are intermediate indicators or scores that provide insight into specific environmental categories during a Life Cycle Assessment (LCA). They occur after the initial emissions or releases but before the ultimate environmental outcomes. For example, midpoint impacts could include indicators like greenhouse gas emissions, acidification potential, or eutrophication potential. They serve as a way to quantify and understand the environmental stressors or pressures created by a product or process.

Taking a step further, the study extends the analysis beyond midpoints, delving into the potential long-term consequences across three essential domains: Human health, ecosystems, and resource impacts or called endpoint impacts.

This methodological approach facilitates a transparent pathway, systematically connecting raw emissions to their potential implications on both the environment and human health. This framework is designed to furnish stakeholders with a comprehensive understanding of the multifaceted implications associated with distinct hydrogen (H_2) production.

Table 6.5: ReCiPe 2016 Midpoint (H)

	Impact category	**Indicator**	**Reference Unit**
Ecosystem impacts	particulate matter formation	particulate matter formation potential (PMFP)	kg PM2.5 eq
	ecotoxicity: freshwater	freshwater ecotoxicity potential (FETP)	kg 1,4-DCB eq
	eutrophication: freshwater	freshwater eutrophication potential (FEP)	kg Peq
	climate change	global warming potential (GWP100)	kg CO_2 eq
	ionising radiation	ionising radiation potential (IRP)	kBq Co-60 eq
	ecotoxicity: marine	marine ecotoxicity potential (METP)	kg 1,4-DCB eq
	eutrophication: marine	marine eutrophication potential (MEP)	kg N eq
	photochemical oxidant formation: terrestrial ecosystems	photochemical oxidant formation potential: ecosystems (EOFP)	kg NOx eq
	ozone depletion	ozone depletion potential (ODPinfinite)	kg CFC11 eq

	acidification: terrestrial	terrestrial acidification potential (TAP)	kg SO_2 eq
	ecotoxicity: terrestrial	terrestrial ecotoxicity potential (TETP)	kg 1,4-DCB eq
Human health impacts	photochemical oxidant formation: human health	photochemical oxidant formation potential: humans (HOFP)	kg NOx eq
	human toxicity: carcinogenic	human toxicity potential (HTPc)	kg 1,4-DCB eq
	human toxicity: non-carcinogenic	human toxicity potential (HTPnc)	kg 1,4-DCB eq
Resource impacts	energy resources: non-renewable, fossil	fossil fuel potential (FFP)	kg oil eq
	land use	agricultural land occupation (LOP)	m^2a crop eq
	material resources: metals/minerals	surplus ore potential (SOP)	kg Cu eq
	water use	water consumption potential (WCP)	m^3

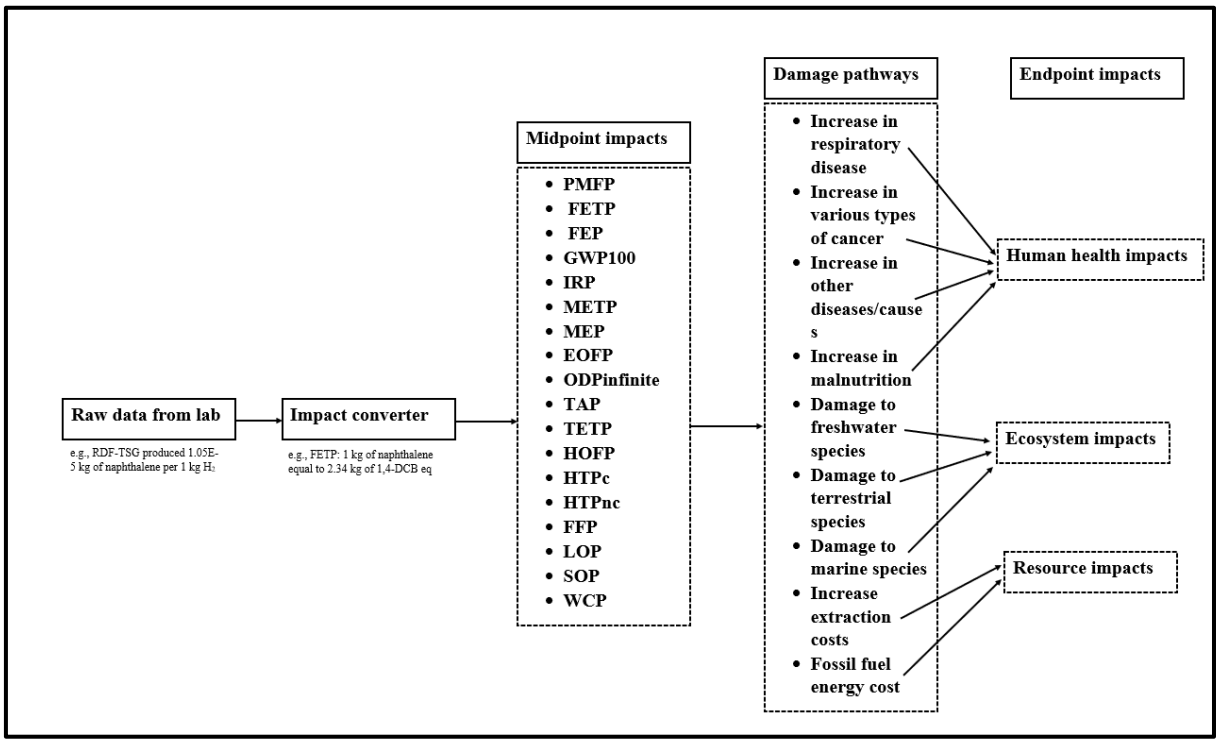

Figure 6.3: Impacts method translated from raw data in the lab to midpoint and endpoint impacts using ReCiPe 2016 (Huijbregts et al., 2016).

6.4 Assessment and Interpretation

6.4.1 Environmental, Resource and Human Health impacts with diverse H_2 production technologies

Hydrogen, as a clean fuel, holds immense promise in the transition towards a sustainable energy future. The environmental impacts associated with various hydrogen production pathways can be quantified using the ReCiPe 2016 (H) method in Figure 6.3. This provides a comprehensive framework to evaluate and compare different technologies on the basis of their environmental repercussions.

Steam methane reforming (SMR) for hydrogen production

The SMR process stands as a primary method for producing hydrogen from natural gas (A) (Zhang et al., 2021a). The SMR process has a significant GWP100, largely due to the direct carbon dioxide emissions from the methane-steam reaction and potential methane leakage. Methane, with its higher GWP compared to CO_2, is particularly concerning. The total GWP100 for SMR is measured at 14.4 kg CO_2 eq/kg H_2. Though not the most alarming GWP100, it's certainly far from the best. Alarmingly, methane leakage during mining contributes to around 13% of this figure, and in some instances, leakages have been found to be 60% higher than earlier estimates (Andrews, 2020).

Furthermore, the International Energy Agency (IEA, 2023b) highlighted that curbing atmospheric methane could prevent nearly a million premature deaths and significant crop losses linked to ozone exposure and climate change. In this study's context, 74.5% of the GWP100 arises from the SMR process and methane leakage, with another 24.4% due to hydrogen pressurization. Infrastructure like reforming factories and storage tanks contribute a mere 1%. The SMR process results in a TETP risk of 8.6 kg 1,4-DCBeq/kg H_2. The major contributors include the construction of the reforming factory and natural gas extraction, accounting for 51.7% of the TETP, which poses potential groundwater contamination risks. Energy used in pressurizing natural gas and its extraction results in 25.4% of the TETP.

Catalyst mining, involving materials like copper oxide, nickel, and zeolite, constitutes approximately 21.9%. A salient feature of the SMR process is its heavy reliance on natural gas, emphasizing its FFP and consumption of this finite resource. However, a recent study by Cho

et al. (2022) suggests that replacing natural gas with landfill gas could cut environmental impacts by 68%, thus offering a potential reduction in both FFP and GWP100. The SMR process necessitates specific metal-based catalysts and infrastructure materials, leading to an increased SOP of 8.1e-2 kg Cu eq/kg H_2. Notably, producing 4.8L of methane/h requires around 1.0e-3 kg of a Ni-based catalyst and 4.0e-3 kg of quartz sand (Ou et al., 2021).

Coal gasification for hydrogen production

Coal gasification, which transforms coal into a hydrogen-rich syngas (B1), has numerous environmental and health repercussions. A prominent concern is the Human Toxicity Potential, both non-cancerous (HTPnc) and cancerous (HTPc), measured at 2.9e+1 kg 1,4-DCBeq/kg H_2 and 1.3 kg 1,4-DCBeq/kg H_2 respectively. This stems from toxic by-products such as BTEX, PAHs, and phenol compounds, with concentrations around 1900-2100 mg/Nm^3 (Wiatowski and Kapusta, 2020). When these compounds are released into the environment, they pose risks, potentially contaminating groundwater or becoming airborne, thereby threatening human health upon ingestion, inhalation, or absorption. For instance, a link has been suggested between Balkan endemic nephropathy (BEN), a kidney disease, and toxins from Pliocene lignite deposits entering groundwater (Finkelman et al., 2002).

Furthermore, concerning findings from northwest China revealed that levels of elements like Arsenic, Selenium, and Thallium, resultant from coal gasification, exceeded both Chinese and U.S. water safety standards (Wang et al., 2021b). The coal extraction process poses its own set of health challenges. Workers and nearby inhabitants face risks from coal dust, leading to ailments like coal worker's Pneumoconiosis, commonly referred to as "black lung disease" (Finkelman et al., 2002).

Additionally, they show substantial contamination potential: 3.9e-2 kg PM2.5 eq/kg H_2 from respiratory concerns and 9.2e-3 kg P eq/kg H_2 and 3.2e-3 kg N eq/kg H_2 from potential water pollution. Coal gasification is intrinsically water-demanding, especially for functions like syngas cleaning and cooling. A prime example is the fluidized bed technology, where coal, after being finely ground, is combined with water to produce a slurry. This slurry typically contains 62-69% water by weight (Yao et al., 2022), accounting for a significant WCP of 2.4e-1 m^3/kg H_2. While coal gasification is more efficient than standard coal combustion (Basu, 2018), it's not without its carbon footprint. The GWP100 stands at a significant 2.7e+1 kg CO_2 eq/kg H_2.

Biomass waste gasification for hydrogen production

Biomass waste gasification (B2), often promised as a renewable energy solution, brings with it specific environmental challenges, particularly in terms of agricultural land occupation (LOP) and water consumption potential (WCP). The production of dedicated energy crops, such as switchgrass or miscanthus, can require expansive agricultural lands. This often comes at the harm of food crops or natural ecosystems, resulting in an LOP of 5.2e-1 m^2 a crop eq/kg H_2, the highest in this study.

Although these crops can enrich the soil, detoxify it, and even support biodiversity (Sa et al., 2021), the repurposing of land can lead to biodiversity losses, disruptions to ecosystem services, and potentially higher carbon emissions, especially if forests are felled for this purpose (Fernando et al., 2010). In fact, research indicates that relying solely on agricultural residues is not sustainable for biomass waste gasification; tree farming is essential (Abe et al., 2007). This shift has already resulted in a global forest reduction from 4.6 billion hectares in 1950 to 4.0 billion hectares in 2018 (Ritchie and Roser, 2021). Water usage is another critical aspect. Certain energy crops can be highly water-intensive, potentially worsening water scarcity in already strained regions. For instance, while wheat's water consumption ranges between 1.0-1.2 m^3/kg and barley's is around 1.0-1.1 m^3/kg, crops like poplar demand between 1.2-1.5 m^3/kg (Núñez et al., 2013). Additionally, the gasification process itself has high water requirements, similar to coal gasification, needing water for stages from syngas purification to residue handling, resulting in a water consumption potential (WCP) of 1.3e-1 m^3/kg H_2

Table 6.6: Midpoint impacts evaluations for different hydrogen production technologies

	Impact scores																	Unit
Index	**A**	**B1**	**B2**	**B3**	**C**	**D1**	**D2**	**D3**	**D4**	**E1**	**E2**	**E3**	**E4**	**F1**	**F2**	**F3**	**F4**	
PMFP	2.4E-3	3.9E-2	2.1E-2	3.7E-2	8.9E-3	9.4E-2	4.0E-3	2.1E-3	9.4E-4	1.7E-2	1.4E-2	1.3E-2	1.2E-2	1.8E-2	1.4E-2	1.3E-2	1.2E-2	kg PM 2.5 eq
FETP	9.8E-2	7.4E-1	4.0E-1	6.9E-1	3.5E-2	5.6E-1	2.5E+0	1.0E-1	3.8E-2	5.3E-1	1.8E+0	5.3E-1	4.9E-1	5.8E-1	2.5E+0	1.5E+0	5.9E-1	kg 1,4-DCB eq
FEP	3.1E-4	9.2E-3	5.0E-3	8.7E-3	1.1E-4	1.6E-2	1.1E-3	2.6E-4	1.4E-4	2.8E-3	3.0E-3	2.5E-3	2.4E-3	3.4E-3	3.8E-3	3.5E-3	3.4E-3	kg P eq
GWP100	1.4E+1	2.7E+1	3.5E+0	1.8E+1	1.8E+1	3.7E+1	1.2E+0	1.8E+0	2.3E-1	2.0E+0	1.4E+0	1.7E+0	8.8E-1	1.1E+1	8.7E+0	8.9E+0	8.3E+0	kg CO_2 eq
IRP	4.7E-2	1.5E+0	8.0E-1	1.4E+0	6.4E-4	5.8E-2	4.9E-2	2.7E-2	2.3E+1	4.6E-1	4.1E-1	4.0E-1	1.3E+1	3.9E-1	4.1E-1	4.0E-1	1.0E+1	kBq Co-60 eq

METP	1.3E-1	1.1E+0	6.0E-1	3.5E-1	4.8E-2	7.8E-1	3.1E+0	1.3E-1	5.5E-2	7.0E-1	2.3E+0	6.9E-1	6.5E-1	7.3E-1	2.9E+0	7.7E-1	7.4E-1	kg 1,4-DCB eq
MEP	3.1E-5	3.2E-3	1.7E-3	3.0E-3	3.0E-5	1.0E-3	8.4E-5	6.9E-5	4.2E-4	2.9E-4	2.8E-4	2.7E-4	4.7E-4	6.1E-4	6.2E-4	6.2E-4	6.3E-4	kg N eq
EOFP	1.1E-2	6.4E-2	3.5E-2	6.1E-2	2.6E-2	1.2E-1	4.4E-3	5.1E-3	1.2E-3	4.0E-2	1.8E-2	1.8E-2	1.6E-2	2.6E-2	1.8E-2	1.8E-2	1.6E-2	kg NOx eq
ODPinfinite	1.1E-6	3.4E-6	1.9E-6	3.2E-6	1.4E-8	6.1E-6	4.4E-7	7.1E-7	1.4E-7	5.7E-6	3.3E-6	3.4E-6	3.1E-6	3.3E-6	3.2E-6	3.4E-6	3.1E-6	kg CFC11 eq
TAP	6.0E-3	1.4E-1	7.7E-2	1.4E-1	2.7E-2	2.7E-1	1.0E-2	4.7E-3	1.2E-3	3.5E-2	2.9E-2	2.6E-2	2.4E-2	5.4E-2	5.8E-2	5.6E-2	5.5E-2	kg SO_2 eq
TETP	8.6E+0	9.3E-1	5.0E-1	5.8E-1	2.6E-1	2.3E+1	6.2E+1	4.9E+0	1.1E+1	5.6E+1	7.9E-1	4.8E-1	5.1E-1	5.7E-1	8.2E-1	5.9E-1	6.1E-1	kg 1,4-DC

																	B eq
HOFP	9.2E-3	4.4E-2	2.4E-2	4.2E-2	2.4E-2	1.2E-1	4.2E-3	4.9E-3	1.2E-3	3.9E-2	1.7E-2	1.7E-2	1.5E-2	2.5E-2	1.7E-2	1.7E-2	1.6E-2	kg NOx eq
HTPc	2.6E-1	1.3E+0	7.1E-1	1.2E+0	1.9E-1	1.5E+0	6.2E-1	2.7E-1	10.0E-2	5.4E-1	7.6E-1	5.7E-1	4.8E-1	5.4E-1	7.9E-1	6.4E-1	5.7E-1	kg 1,4-DCB eq
HTPnc	1.6E+0	2.9E+1	1.5E+1	2.7E+1	6.2E-1	2.5E+1	1.1E+1	9.3E-1	3.0E+0	1.1E+1	1.4E+1	8.8E+0	9.9E+0	1.2E+1	1.6E+1	1.2E+1	1.3E+1	kg 1,4-DCB eq
FFP	5.3E+00	5.1E+00	8.2E-01	2.5E+00	1.5E+01	8.2E+00	2.9E-01	5.4E-01	6.2E-02	2.0E+00	1.8E+00	2.0E+00	1.7E+00	1.8E+00	1.9E+00	2.0E+00	1.8E+00	kg oil eq
LOP	2.4E-02	2.4E-01	5.2E-01	2.3E-01	7.1E-04	3.8E-01	6.1E-02	2.1E-01	8.6E-03	5.8E+00	3.8E-01	3.9E-01	3.8E-01	2.8E-01	3.8E-01	3.9E-01	3.8E-01	m^2a crop eq

SOP	8.1E-02	2.1E-02	1.1E-02	1.9E-02	1.6E-03	5.6E-02	1.8E-01	1.6E-01	3.7E-02	9.0E-02	3.4E-02	3.2E-02	1.8E-02	1.5E-02	3.0E-02	2.8E-02	1.8E-02	kg Cu eq
WCP	9.3E-03	2.4E-01	1.3E-01	2.2E-01	2.7E-01	6.0E-02	1.2E-02	8.4E-03	1.0E-01	1.9E+00	1.9E-02	1.9E-02	2.0E-02	3.4E-02	3.8E-02	3.7E-02	7.5E-02	m^3

Note:
Scenario A.) steam methane reforming B1.) coal gasification B2.) Biomass waste gasification B3.) municipal solid waste (MSW) gasification C.) partial oxidation of oil products D1.) water electrolysis with coal combustion D2.) water electrolysis with wind energy D3.) water electrolysis with solar energy D4.) water electrolysis with nuclear energy E1.) wood pellets two-stage gasification with wood pellet combustion E2.) wood pellets two-stage gasification with wind energy E3.) wood pellets two-stage gasification with solar energy E4.) wood pellets two-stage gasification with nuclear energy F1.) RDF pellets two-stage gasification with MSW combustion F2.) RDF pellets two-stage gasification with wind energy F3.) RDF pellets two-stage gasification with solar energy F4.) RDF pellets two-stage gasification with nuclear energy.

Particulate matter formation potential (PMFP), freshwater ecotoxicity potential (FETP), freshwater eutrophication potential (FEP), global warming potential (GWP100), ionising radiation potential (IRP), marine ecotoxicity potential (METP), marine eutrophication potential (MEP), photochemical oxidant formation potential: ecosystem (EOFP), ozone, depletion potential (ODPinfinite), terrestrial acidification potential (TAP), terrestrial ecotoxicity potential (TETP), photochemical oxidant formation potential: humans (HOFP), human toxicity potential: carcinogenic (HTPc), human toxicity potential: non-carcinogenic (HTPnc), fossil fuel potential (FFP), agricultural land occupation (LOP), surplus ore potential (SOP), and water consumption potential (WCP).

RDF gasification for hydrogen production

Gasification of RDF (B3), a process that converts municipal waste into gas, brings with it several environmental and health challenges. RDF typically consists of 52% organic materials, 26% recyclables, and the rest being inorganic substances (Sajid et al., 2022). This diversity results in the release of hazardous compounds during gasification: 0.06-0.1 kg of tar and wax/kg RDF, 1.95 g of fine particles/kg RDF, and 170-190 g of heavy metals/kg RDF (Haydary, 2021, Haydary et al., 2023). Certain RDFs produce detrimental gases like H_2S (2240 mg/kg RDF) and HCl (7880 mg/kg RDF) (Yasar et al., 2021, Haydary et al., 2023). After gasification, the resultant ash is mainly calcium-based, a product of RDF pre-treatment (Chen et al., 2007, September).

However, the specific composition varies, with elements like Mg, Na, K, Si, and others depending on the RDF source (Fazil et al., 2023). These contaminants possess both carcinogenic (1.2 kg 1,4-DCBeq/kg H_2) and non-carcinogenic risks (2.7e+1 kg 1,4-DCBeq/kg H_2). The wet scrubber is the primary wastewater source post-gasification (Bridgwater, 1995, Sharma et al., 2008), and treating it to meet environmental standards can be costly (Vaish et al., 2019). The gasification process itself, including steam gasification (0.5-2 kg steam/kg RDF, Ren, 2022) and syngas cooling and cleaning, consumes significant water. The latter, particularly the scrubber unit, generates wastewater as it primarily uses oil-based tar solvents (Göransson et al., 2011). This can strain water resources, especially in already water-scarce areas. While RDF gasification reduces methane emissions from decomposing waste – with roughly equal parts of methane and CO_2 in carbon emissions from Quebec landfills (Moreau et al., 2023) – it still emits considerable CO_2. This contributes to its GWP100 of 1.8e+1 kg CO_2eq/kg H_2.

Other environmental challenges include the release of phosphorus (8.7e-3 kg P eq/kg H_2) and nitrogen compounds (3.0e-3 kg N eq/kg H_2) potentially leading to eutrophication. The variability in RDF waste can also produce fine particulate matter (3.7e-2 kg PM2.5 eq/kg H_2), linked to respiratory and cardiovascular issues (Combes and Franchineau, 2019).

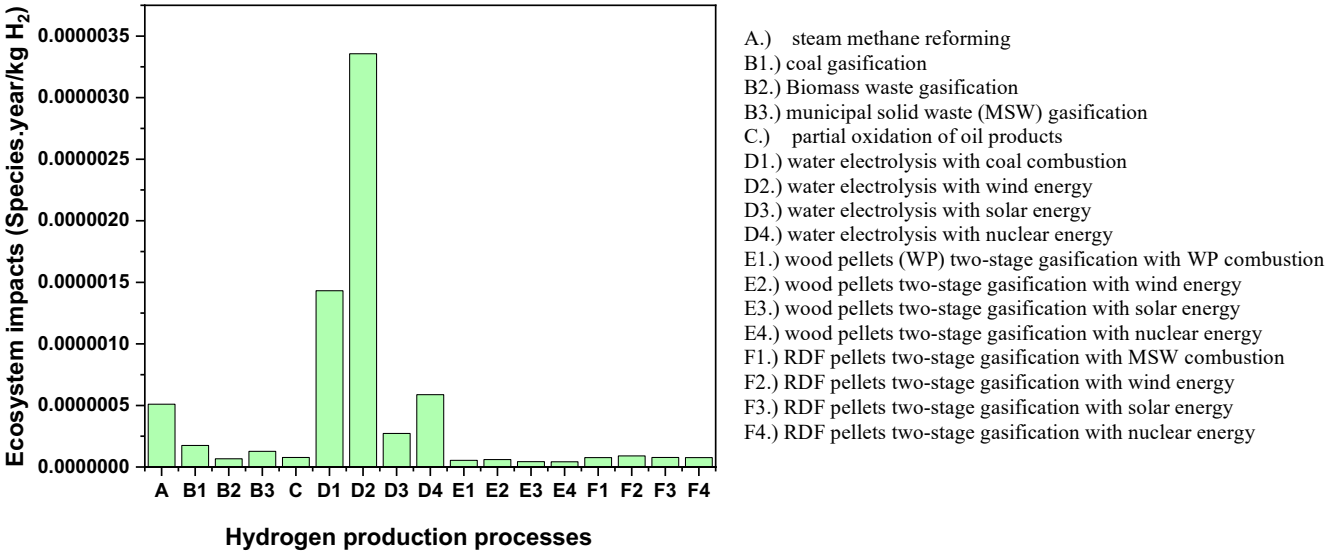

Figure 6.4: Ecosystem impacts (Endpoint) from different hydrogen production technologies

Partial Oxidation of oil products (POX) for hydrogen production

The POX method, a prevalent approach for deriving hydrogen from oil products (C), carries notable environmental implications. At the heart of POX lies the reaction of oil products, primarily consisting of hydrocarbons like n-hexane, with steam under high temperatures ranging from 750°C to 1000°C (Haribal et al., 2018). Inherent to this process is the emission of carbon dioxide (CO_2) as carbon in the feedstock undergoes oxidation. This CO_2 release is a significant greenhouse gas contributor, amplifying global warming effects to the tune of 1.8e+1 kg CO_2 eq/kg H_2.

Notably, employing hydrogen combustion for steam cracking using tail gas can reduce these CO_2 emissions by about 20% per kg olefin when contrasted with facilities that rely on natural gas for heating while exporting hydrogen (Young et al., 2022). Given its dependence on oil-derived feedstocks, the POX method exacerbates the consumption of non-renewable fossil fuels, measured at 1.5e+1 kg oil eq/kg H_2.

Furthermore, hydrogen constitutes a mere 0.9-6.2% of the feedstocks in oil product cracking (Young et al., 2022). Water resource management is another significant challenge with POX. To augment hydrogen yield, the method often incorporates the water-gas shift reaction, which

requires considerable water volumes, quantified at 2.7e-1 m^3/kg H_2. On top of this, industrial cooling mechanisms linked to processes such as POX further pressurize water resources.

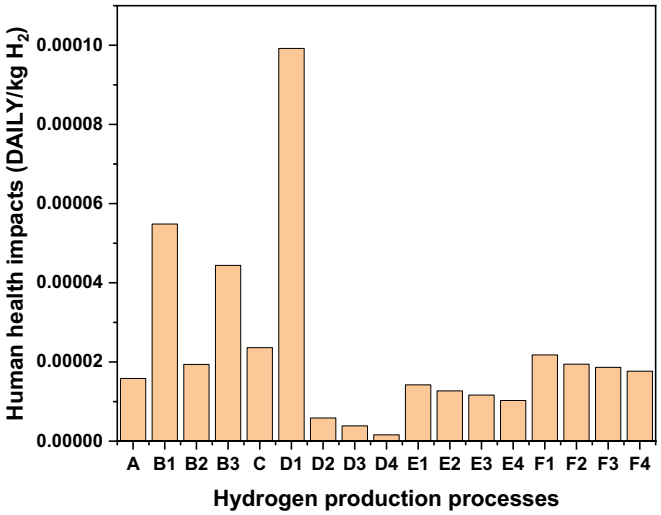

A.) steam methane reforming
B1.) coal gasification
B2.) Biomass waste gasification
B3.) municipal solid waste (MSW) gasification
D.) partial oxidation of oil products
D1.) water electrolysis with coal combustion
D2.) water electrolysis with wind energy
D3.) water electrolysis with solar energy
D4.) water electrolysis with nuclear energy
E1.) wood pellets (WP) two-stage gasification with WP combustion
E2.) wood pellets two-stage gasification with wind energy
E3.) wood pellets two-stage gasification with solar energy
E4.) wood pellets two-stage gasification with nuclear energy
F1.) RDF pellets two-stage gasification with MSW combustion
F2.) RDF pellets two-stage gasification with wind energy
F3.) RDF pellets two-stage gasification with solar energy
F4.) RDF pellets two-stage gasification with nuclear energy

Figure 6.5: Human health impacts (Endpoint) from different hydrogen production technologies

Water electrolysis supplied energy from coal combustion for hydrogen production

Water electrolysis represents a compelling approach for H_2 production. On paper, the production of 1 kg of H_2 demands roughly 33.3 kWh. Yet, real-world laboratory conditions, due to inevitable energy losses, tend to require between 37.5 and 38.8 kWh (Milewski et al., 2021). Utilizing energy from coal combustion for this process (D1), however, brings with it a slew of environmental and health challenges. The combustion of coal releases particulate matter (9.4e-2 kg PM2.5 eq/kg H_2), deteriorating air quality and posing serious respiratory health risks.

Additionally, emissions of volatile organic compounds and nitrogen oxides (1.2e-1 kg NOx/kg H_2) from coal can result in the formation of ground-level ozone, harmful to both humans and vegetation. Nitrogen (1.0e-3 kg N eq/kg H_2) and other by-products (1.6e-2 kg P eq/kg H_2) of coal combustion, when introduced to water bodies, contribute to nutrient surges. These can instigate harmful algal blooms, underlining coal's role in freshwater eutrophication. Being carbon-rich, coal's combustion naturally increases CO_2 atmospheric concentrations, thereby exacerbating global warming (3.7e+1 kg CO_2eq/kg H_2). Toxins from Pliocene lignite deposits, linked to coal, may contaminate groundwater, potentially correlating with Balkan endemic nephropathy (BEN) – a specific kidney condition (Finkelman et al., 2002). Furthermore, trace

metals in coal, when combusted, introduce risks not only to the environment but also possess both carcinogenic and non-carcinogenic hazards to humans. The emission of sulfur dioxide (2.7e-1 kg SO_2eq/kg H_2) alongside NOx (1.2e-1 kg NO_x/kg H_2) can lead to acid rain formation, posing threats to terrestrial soil and aquatic habitats.

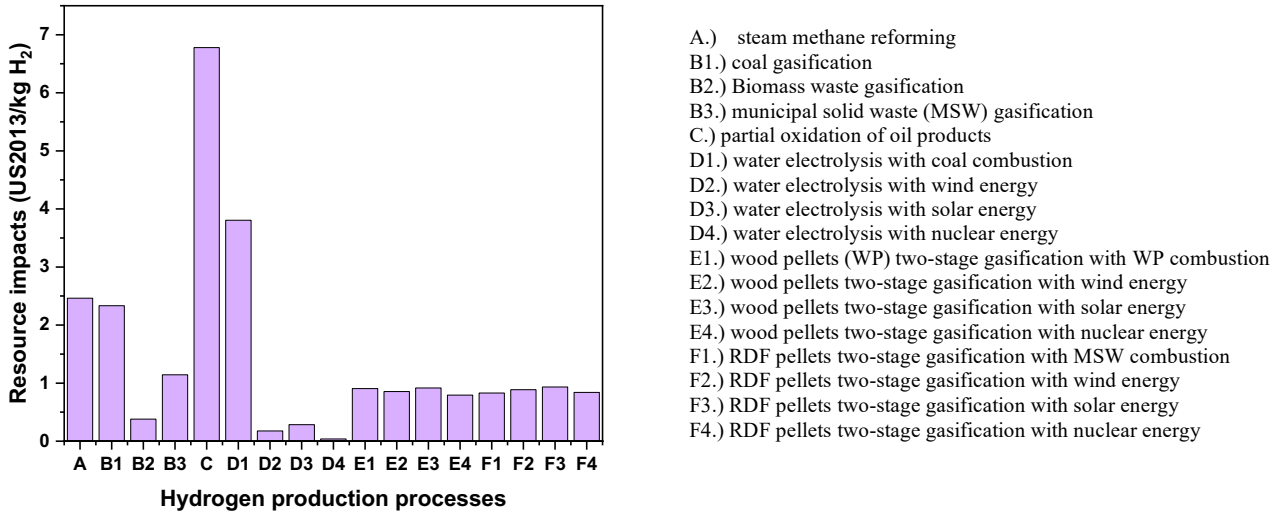

Figure 6.6: Resource impacts (Endpoint) from different hydrogen production technologies

Water electrolysis supplied energy from wind energy for hydrogen production

Harnessing wind energy for hydrogen production via water electrolysis (D2) is a promising venture, but it's essential to consider the associated environmental repercussions. The life cycle of wind turbines, from raw material extraction to disposal, introduces potential contaminants. This leads to freshwater ecotoxicity, affecting aquatic ecosystems with an impact quantified at 2.5 kg 1,4-DCBeq/kg H_2. A substantial 70.1% of this freshwater ecotoxicity potential (FETP) is attributed to constructing wind turbine infrastructure. Within this framework, mining activities contribute 95.1%, but an encouraging 71.5% of the mined rare elements (Al, Fe, Cu) are anticipated for recycling. Reinforced steel foundations account for around 1.1% of the total FETP. Separately, the wind turbine network connection contributes 29.9% to the FETP, primarily due to copper-based cables, responsible for 92.5% of the network's FETP. Maintaining wind farms encompasses activities like cleaning, repairing, and replacing turbine parts including blades, gearboxes, generators, and lubricants (Yang et al., 2018). Some by-products from these activities risk seeping into marine environments, impacting marine life at 3.1 kg 1,4-DCBeq/kg H_2. Land ecosystems face threats too, with impacts quantified at 6.2e+1

kg 1,4-DCBeq/kg H_2. A significant 87.7% of this terrestrial ecotoxicity potential (TETP) arises from copper mining processes, including activities linked to chromium steel production.

Moreover, mining and waste disposal contaminate habitats, posing threats to local wildlife. For instance, between 140,000-328,000 birds meet their end annually due to collisions with monopole structures (Loss et al., 2013). Offshore turbines present concerns, including altering light penetration into the seawater, affecting fish distribution, and overall marine biodiversity (Reubens et al., 2011). Notably, species such as cod, herring, dab, and salmon are sensitive to turbine noises. Even though turbine operational noise becomes inaudible below 20m depth, species like harbour porpoises and seals remain affected (Ren et al., 2021). The appetite for specific metals, particularly neodymium and dysprosium for turbine magnets, intensifies ore mining, marked at 1.8e-1 kg Cu eq/kg H_2.

Water electrolysis supplied energy from solar energy for hydrogen production

Solar energy, particularly harnessed through photovoltaic (PV) panels, is emerging as a predominant method for hydrogen production via water electrolysis (D3). With a commendable efficiency, PV panels exhibit a hydrogen production rate of 153.3 ml/min (Amori et al., 2016). Creating these panels demands a variety of metals and minerals. Notably, modern thin-film PV panels employ metals such as cadmium telluride, amorphous silica, and copper indium gallium diselenide (Li et al., 2021b).

Despite their trace presence in panels, the extraction processes for these metals are resource-intensive, with large ore volumes processed. Cutting-edge solar solutions also incorporate rare earth elements, pushing the surplus ore potential (SOP) to 1.6e-1 kg Cu eq/kg H_2. PV panels carry an associated terrestrial ecotoxicity potential (TETP) of 4.9 kg 1,4-DCB eq/kg H_2. This arises from several reasons: the manufacturing process involves chemicals, like silver paste, that have potential environmental repercussions (Chen et al., 2016b). Moreover, resource extraction, such as quartz mining for silicon-based panels, disrupts habitats and elevates risks like silicosis from silica dust exposure (de Carvalho et al., 2021).

After approximately 25 years of service, solar panels face disposal and recycling challenges. Their composition, enriched with specialized metals, emphasizes the need for advanced waste management and potential resource conservation (Chowdhury et al., 2020). Solar installations, especially expansive solar farms, exhibit a pronounced agricultural land occupation (LOP) of

2.1e-1 m^2 a crop eq/kg H_2, comparatively more than other renewables like wind and nuclear energy. The infrastructure for such farms, encompassing substations and roads, often converts fertile lands, amplifying their footprint (Hosseini, 2019). Projections indicate that by 2050, solar infrastructure may occupy between 0.5-5% of total land, indirectly resulting in emissions ranging from 0-50 g CO_2/kWh (Van de Ven et al., 2021).

Water electrolysis supplied energy from solar energy for hydrogen production

Utilizing nuclear energy for hydrogen production through water electrolysis (D4) introduces specific concerns, particularly related to ionizing radiation potential (IRP) and water consumption potential (WCP). The comprehensive nuclear fuel cycle, from uranium extraction to fuel preparation, emits ionizing radiation at a level of 2.3e+1 kg Bq Co-60 eq for each kilogram of H_2 produced using pressurized water reactor technology. Despite rigorous safety measures, the risk of radiation exposure remains.

Immediate, severe exposure can result in symptoms such as nausea and hair loss. Chronic exposure, as evidenced by studies on atomic bomb survivors, is linked to increased cancer risk, and radiation-induced DNA damage could potentially impact subsequent generations (Kamiya et al., 2015).

Post-use, spent nuclear fuel retains a high level of radioactivity, amounting to 25-30m^3 of used fuel annually per 1000MWe reactor (Kurniawan et al., 2022). This necessitates prolonged, secure storage until radioactivity diminishes to safe levels. Multi-faceted disposal techniques combine natural geological barriers with engineered systems to effectively confine nuclear waste (Ojovan and Steinmetz, 2022). While contemporary nuclear reactors incorporate state-of-the-art materials, like cast nanostructured alloys, enhancing their high-temperature resilience (Was et al., 2019), the total elimination of risks related to radioactive material releases remains elusive.

In addition, water's role in nuclear power is undeniable. Beyond general operational needs, water is vital for emergency decontamination and extensive cooling processes, both post-turbine and for core cooling directly (Zakrzewska-Kołtuniewicz, 2017).

Although a significant portion of this water returns to its original source, a substantial amount (63%) undergoes evaporation, resulting in considerable consumption (Giusti and Meyer, 1977).

This extensive water involvement throughout the nuclear fuel cycle culminates in a consumption value of 1.0e-1 m^3/kg H_2. Yet, in light of the IPCC's Net Zero objectives, prominent investors assert that nuclear energy might be the key to meeting these ambitious energy demands (Sadekin et al., 2019). This is attributed to nuclear's lower land (8.6e-3 m^2 a crop eq/kg H_2) and resource requirements (3.7e-2 kg Cu eq/kg H_2) when compared with other energy alternatives. Nuclear-powered hydrogen production offers a potentially low-carbon solution (only 2.3e-1 kg CO_2 eq/kg H_2), they mostly comes from uranium enrichment (Karaca et al., 2020), but its implications for radiation and water resource management are undeniable.

Wood pellet two-stage gasification for hydrogen production

Utilizing the two-stage gasification method with self-energy supplied from wood pellet combustion (E1) to produce hydrogen from wood pellets offers a unique balance of environmental benefits and challenges. A primary concern centres on the considerable agricultural land occupation (LOP) that this method demands, registering at 4.8e-1 m^2 a crop eq/kg H_2. The major contributors to this LOP are the wood pellets utilized in two-stage gasification (67.3%) and those for self-energy supply (31.3%). Derived from timber, these wood pellets necessitate expansive tracts of land for cultivation, growth, and harvesting.

Even with sustainable forestry management, there remains a consistent need for large tree plantations. In some regions, this can rival essential food crop production, potentially raising concerns about food security and the balance of ecosystems. However, the method stands out in its low global warming potential, at 1.8 kg CO_2 eq/kg H_2 (GWP100). This favourable attribute can be attributed to the carbon cycle of trees. As they grow, trees absorb CO_2 — to the tune of approximately 1 kg CO_2 per kg of wood pellet (45-49% C in tree) (Duangsathaporn et al., 2023). When these trees are transformed into wood pellets and undergo gasification, that absorbed CO_2 is released back into the environment. Augmenting this balance, the optimal process proposed recycles CO_2 post the PSA unit, recycling roughly 1 kg of CO_2 for every kg H_2 produced. This cyclical process ensures the net addition of CO_2 to the atmosphere remains minimal.

Moreover, embracing wood pellets as a hydrogen production medium reduces dependency on high GWP100 fossil fuels. The intrinsic efficiencies of the two-stage gasification process, combined with its superior syngas purification, yield diminished greenhouse gas emissions when compared with alternative methods. Comparative ecosystem (Figure 6.4) and human

health impacts (Figure 6.5) also show that biomass waste single stage gasification (B2) exhibits greater negative effects than WP-TSG (E1). The additional gasification steps in TSG allow for cleaner syngas products, with substantially reduced tar outputs (0.03 g/Nm^3) (Mankasem et al., 2023). However, TSG presents higher resource impacts (Figure 6.6) because the distinct separation of pyrolysis and gasification zones necessitates additional reactors and, consequently, more construction materials.

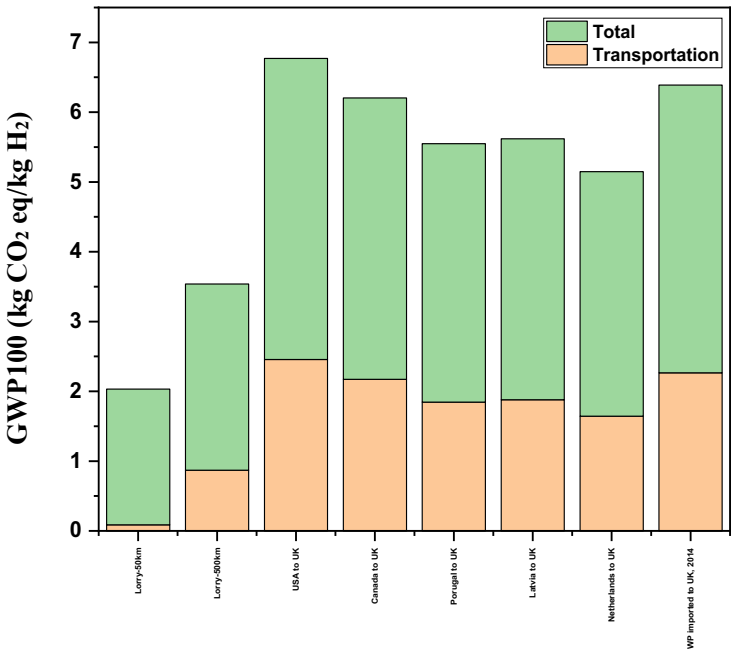

Figure 6.7: Global warming potential (GWP100) of wood pellets two-stage gasification: A sensitivity analysis of transportation distances from various origins to the UK

The transportation scenario presented in E1 posits that the wood pellets (WP) are produced within a local vicinity, specifically a 50 km radius from the pellet manufacturing facilities and the two-stage gasification (TSG) infrastructure.

The GWP100 for this transportation decision is depicted in the first bar of Figure 6.7, indicating an emission of approximately 0.1 kg CO_2 eq/kg H_2. This represents the option with the least GWP100 impact. Contrastingly, the reality often diverges from this local production model. Even in nations capable of producing their own WP, it is common practice to transport them over long distances, sometimes internationally or across oceans.

The second bar from the left in Figure 6.7 illustrates the emissions associated with national WP transportation, which is estimated at 0.9 kg CO_2 eq/kg H_2. Specifically, for the UK, WP imports are distributed as follows: 58% from the USA, 21% from Canada, 9% from Portugal, 9% from Latvia, and the remaining 3% from other countries (Zwolinski, 2015). The USA stands out as the predominant WP exporter, contributing 7.52 billion tonnes annually (Fernández, 2022). The distances between the ports of these exporting countries and the UK are as follows: 7,009.82 km from the USA (Port of New York to London), 4,634 km from Canada (Liverpool to Halifax), 1,886 km from Portugal (Lisbon to London), 2,182 km from Latvia (Riga to London), and 208 km from the Netherlands (Rotterdam to Felixstowe).

It is assumed that WP is conveyed by lorries from the pellet manufacturer to a port (covering 500 km), then shipped, and subsequently transported to the TSG infrastructure. The total emissions attributable to WP transportation increase from 2.0 kg CO_2 eq/kg H_2 for locally produced WP to 4.1 kg CO_2 eq/kg H_2 for WP imported into the UK, as shown in the far-right bar of Figure 6.7.

Wood pellet two-stage gasification with renewable energy for hydrogen production

Using wind (E2), solar (E3), or nuclear energy (E4) as a power source for the two-stage gasification of wood pellets, instead of relying on the combustion of the wood pellets themselves, introduces several potential benefits and challenges. On the upside, employing these cleaner energy sources can significantly diminish greenhouse gas emissions (lowest at 0.9 kg CO_2 eq/kg H_2 in E4) and alternative energy sources such as wind, solar, and nuclear (designated as E2, E3, and E4) have shown a reduction in several environmental impact indicators when compared with the baseline, E1. Specifically:

- Particulate matter formation potential (PMFP) decreased by 18.4-28.4%.
- Global warming potential over 100 years (GWP100) by 5.5-51.6%.
- Eutrophication in oceans formation potential (EOFP) by 53.7-59.1%.
- Terrestrial acidification potential (TAP) by 16.8-30.9%.
- Photochemical oxidant formation potential: humans (HOFP) by 54.6-59.8%.
- Land occupation potential (LOP) by 18.6-21.9%.

However, the adoption of these alternative energy sources also introduced increases in some environmental impacts: In freshwater ecotoxicity potential (FETP), E2 exhibited the most

significant impact, almost 3.5 times higher than E1. E3's impact was comparable to E1, while E4 demonstrated a reduction in impact by 6.3% from E1.

Freshwater Eutrophication Potential (FEP) followed a similar pattern to the freshwater ecotoxicity potential (FETP), with E3 showing a reduction of about 9.2% compared with E1. IRP was notably higher in E4, with an increase of 2,763% from E1. Both E2 and E3 showed a slight reduction (9.2-11.9%) in Ionization Radiation Potential (IRP) compared to E1.

Marine ecotoxicity potential (METP) mirrored the freshwater ecotoxicity potential (FETP) trends, with E2 increasing the impact by 230%. E3's impact was akin to E1, and E4 showed a modest reduction of 6.6% compared to E1. E4 posed the highest increase in marine eutrophication potential (MEP), at 169.0% over E1, primarily due to the requirement of a nearby water source for cooling, which is often discharged at elevated temperatures, exacerbating thermal pollution and hence eutrophication.

Pressure water reactors, a type of reactor used in E4, account for 92.7% of this increased impact. In the category of ozone depletion potential (ODPinfinite), E1 remained the preferable option, with increases in ODPinfinite seen in E2 (74%), E3 (82%), and E4 (65.4%). Notably, while solar energy (E3) does not directly contribute to ODP during energy production, the manufacturing process involves chemicals like Diphenyl ether, a heat transfer fluid that can have ODP-associated concerns.

Terrestrial ecotoxicity potential (TETP) saw a 42% increase in E2 compared to E1. E3 and E4 showed reductions of 8-14%. The rise in E2 is attributed to wind turbine infrastructure, which accounts for 71.1% of this impact, and network connections, accounting for the remaining 28.9%.

For both human toxicity potential: carcinogenic (HTPc) and non-carcinogenic (HTPnc) effects, E4 and E3 emerged as the better options, respectively. Surprisingly, E2 experienced the most significant impact increase by 44% in HTPc and 28% in HTPnc over E1, with wind turbine manufacturing contributing to 68.8-92.0% of these impacts and network connections to 8.0-31.1%.

Regarding resource impact, E3 recorded the highest fossil fuel potential (FFP), due to the indirectly use of natural gas during installation and manufacturing. For agricultural land

occupation (LOP), E1 exhibited the highest impact, necessitating additional land for afforestation. In the case of surplus ore potential (SOP), E2 was the most affected, as it requires rare elements for key components of wind turbines. Finally, water consumption potential (WCP) was highest in E4; although recycling efforts are in place, losses through evaporation remain a concern.

In summary, transitioning to wind, solar, or nuclear energy for powering the two-stage gasification of wood pellets seems environmentally in term of particulate matter formation potential (PMFP), global warming potential (GWP100), photochemical oxidant formation potential: ecosystems (EOFP), terrestrial acidification potential (TAP), photochemical oxidant formation potential: humans (HOFP) and agricultural land occupation (LOP). Yet, it necessitates careful planning and consideration of other challenges like freshwater ecotoxicity potential (FETP), freshwater eutrophication potential (FEP), ionising radiation potential (IRP), marine ecotoxicity potential (METP), marine eutrophication potential (MEP), ozone depletion potential (ODPinfinite), terrestrial ecotoxicity potential (TETP), human toxicity potential: carcinogenic (HTPc), human toxicity potential: non-carcinogenic (HTPnc) and resource impacts. Making such a move requires a comprehensive approach that weighs these environmental impacts.

RDF two-stage gasification for hydrogen production

Hydrogen production through the two-stage gasification of RDF pellets introduces marginally higher environmental (as shown in Figure 6.4) and health (detailed in 6.5) risks compared to the use of wood pellets. The composition of RDF is more complex, being sourced from mixed municipal waste that typically includes a variety of materials such as plastics, metals, and composites. During the gasification process, this diverse matter can yield a spectrum of pollutants and potent greenhouse gases.

For instance, the gasification of plastics within RDF can significantly boost levels of carbon dioxide and methane, thus amplifying the global warming potential (GWP100). Assuming a 50% biomass waste content in RDF, the production emits approximately 9.2 kg CO_2 eq/kg H_2. If the biomass waste content increases, the GWP100 can decline, benefiting from the carbon sequestration ability of biomass waste over a century. Data from the RDF TGA in Chapter 7 indicates a biomass waste presence of 76.7%, correlating to lower GWP100 emissions at 6.3 kg CO_2 eq/kg H_2. Despite RDF pellets through two-stage gasification (TSG) yielding GWP100

values roughly fourfold those of wood pellets (WP-TSG), this method is preferable over landfilling, where RDF-open dumping can emit more than 8.36 kg CO_2 eq/kg MSW (Anasstasia et al., 2020, April). RDF-TSG (F1 and F1-UK), in contrast, results in only 0.8-1.0 kg CO_2 eq/kg RDF, while also mitigating additional problems associated with landfills such as soil acidification and methane leakage.

Additionally, toxic emissions from RDF gasification, including dioxins, furans, and heavy metals, pose substantial environmental threats, disrupting aquatic and terrestrial ecosystems and leading to the accumulation of toxins in the food chain. This is reflected in modest increases in particulate matter formation potential (PMFP), freshwater ecotoxicity potential (FETP), freshwater eutrophication potential (FEP), marine ecotoxicity potential (METP), marine eutrophication potential (MEP), ozone depletion potential (ODPinfinite), terrestrial acidification potential (TAP), and terrestrial ecotoxicity potential (TETP) indicators. The human health implications are also significant, with RDF exhibiting a 1.3-19.5% higher human toxicity potential: carcinogenic (HTPc) and a 6.4-27.3% higher human toxicity potential: non-carcinogenic (HTPnc) compared to wood pellets.

Conversely, transitioning to wood pellets (WP or E) does raise certain impact indicators like the ionising radiation potential (IRP), photochemical oxidant formation potential: ecosystems (EOFP), and photochemical oxidant formation potential: humans (HOFP). Wood pellets, due to their higher oxygen content, contribute to the formation of more NOx during gasification, intensifying these environmental impacts. The IRP is particularly affected because wood pellet production involves intensive processes such as wood cultivation and processing, which demand more materials and energy, resulting in a greater release of radioisotopes like Cobalt-60.

From a resource utilization perspective (illustrated in Figure 6.6), RDF (F1) consumes less fossil fuel in transportation compared to wood pellets (E1). This is because the RDF has higher yield of H_2 production than wood pellets and resulted in lower carried weight in transportation. However, the lower moisture content in RDF pellets, ranging from 1-2%, versus 10-13% for WP, necessitates additional steam in gasification. Consequently, RDF has a markedly higher water consumption potential (WCP), between 77.5-286.7% more than WP. Furthermore, the additional processing and transportation in the E series incrementally increase the surplus ore potential (SOP) over the F series.

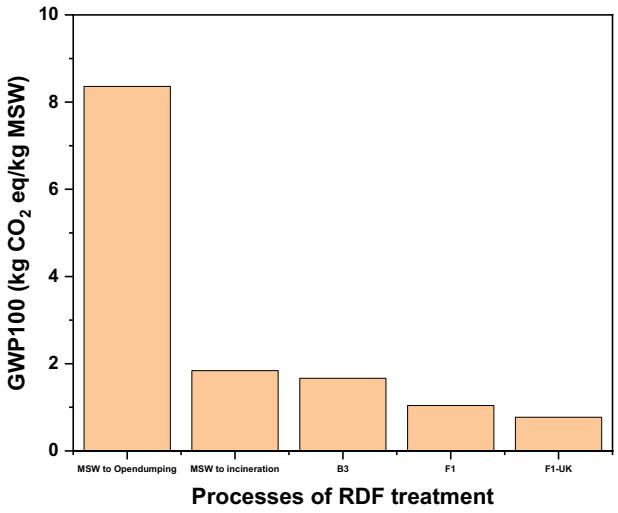

Figure 6.8: GWP100 Profiles for MSW treatment options: Open dump to RDF-TSG with UK composition

The global production of municipal solid waste (MSW) stands at a significant 2.02 billion tons per year, with projections indicating a rise to 3.4 billion tons by 2050 (Tiseo, 2018). Alarmingly, only about 25% of these wastes are effectively managed. In developing countries, open dumping remains the predominant disposal method, as highlighted by Nanda and Berruti (2021). A study conducted by Anasstasia et al. (2020, April) revealed that transporting MSW to open dumping sites—approximately 2 km to collection points and further 25 km to dumping areas—results in an emission of 8.4 kg CO_2 eq/kg MSW. Another disposal method discussed is incineration of MSW, which generates around 1.8 kg CO_2 eq/kg MSW. In contrast, this research found that conventional RDF gasification, referred to as B3, emits approximately 1.7 kg CO_2 eq/kg MSW. This amount is nearly 80% lower than open dumping and 10% lower than RDF incineration. Further advancements in the two-stage gasification process, detailed in

Chapter 7, demonstrate that the RDF-TSG (F1) method produces only 1.0 kg CO_2 eq/kg MSW. This reduction is even more significant when considering the decomposition of RDF containing biomass waste, food waste, and paper, which constitute about 76.7%-85% of MSW. Using the RDF-TSG method with a composition mimicking that of the UK's RDF, the emissions reduce further to 0.8 kg CO_2 eq/kg MSW. Comparative analysis of these RDF treatments in terms of global warming potential (GWP100) per kilogram of MSW is illustrated in Figure 6.8. While the RDF-TSG (F) methods generate higher GWP100 than the WP-TSG method (E), as seen in Figure 6.9, the novel RDF-TSG technique presents a significantly improved alternative over current MSW treatments, such as open dumping, incineration, and traditional gasification.

RDF two-stage gasification with renewable energy for hydrogen production

When contemplating the use of wind, solar, or nuclear energy to power the RDF two-stage gasification process instead of energy derived from RDF combustion, several implications arise. The foremost advantage is the potential substantial reduction in greenhouse gas emissions (reduced from 9.2 (F1) to 8.3 (F4) kg CO_2 eq/kg H_2). Wind, solar, and nuclear energy are inherently cleaner, with diminished carbon footprints compared to RDF combustion. Furthermore, switching energy sources can improve air quality by lowering emissions of particulate matter (from 1.8e-2 (F1) to 1.2e-2 (F4) kg PM2.5 eq/kg H_2), nitrogen oxides (from 2.5 (F1) to 1.6 (F4) kg NO_x eq/kg H_2), and other pollutants.

However, challenges persist. The initial financial burden of establishing infrastructure for wind, solar, or nuclear power might be substantial. Additionally, the intermittent nature of wind and solar energy might necessitate advanced energy storage or grid integration systems. If the choice leans towards nuclear energy, then safety, waste management, and public acceptance become prime concerns. Also, the land or marine area requirements for wind (3.8e-1 m^2 a crop eq/kg H_2 in F2) and solar farms (3.9e-1 m^2 a crop eq/kg H_2 in F3) could lead to environmental and social issues stemming from land-use changes.

6.4.2 Evaluating GWP100 emissions in hydrogen production: From Black to Green hydrogen

The global warming potential (GWP100) is a critical factor in assessing environmental impact. A unanimous global consensus has emerged, aiming to achieve net-zero CO_2 emissions by 2050 (Fankhauser et al., 2022). This study focuses on the GWP100 emissions associated with various hydrogen (H_2) production technologies, using a color-coded system to categorize their environmental impact.

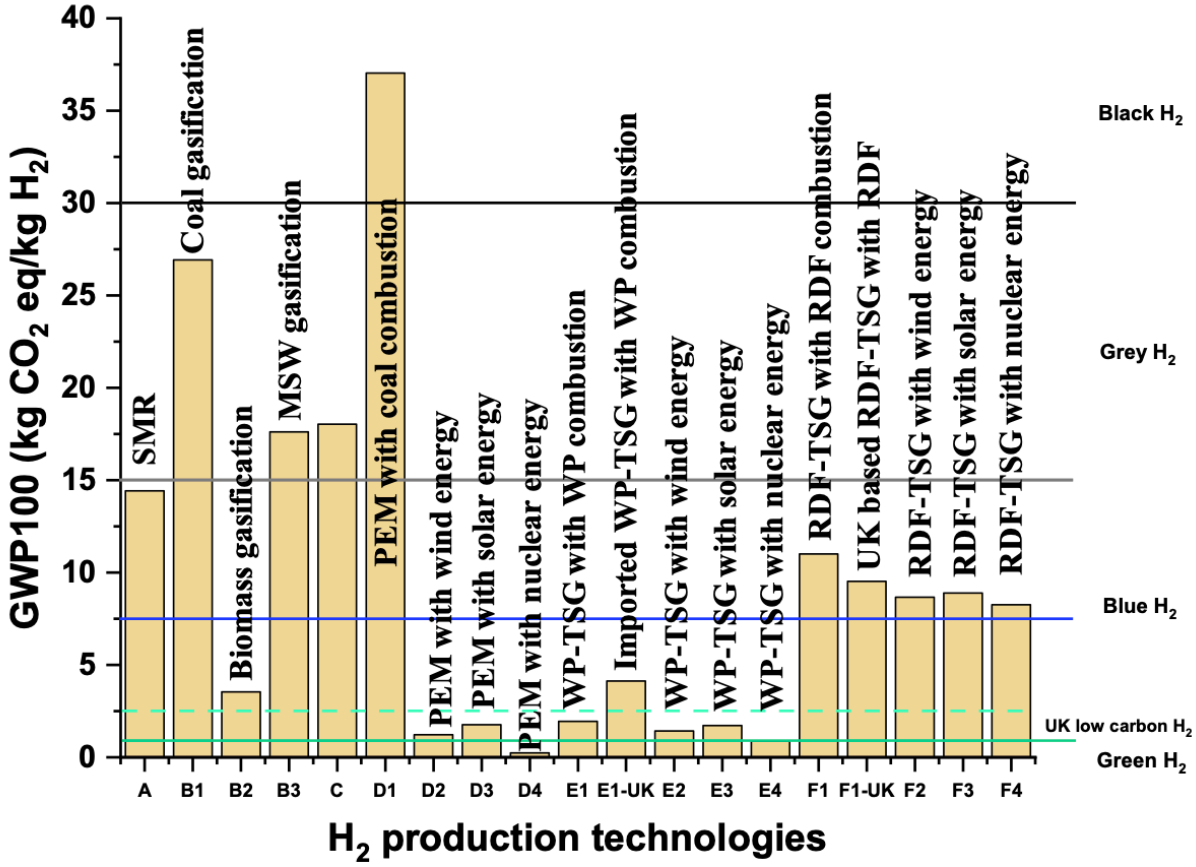

Figure 6.9: GWP100 comparisons for hydrogen production technologies categorized by emission levels: Black to Green.

Black H_2, typically derived from fossil fuels (Hosseini, 2022), is the most polluting form, producing over 30 kg of CO_2 equivalent per kilogram of H_2. In particular, the study found that using coal combustion for electricity, which then powers water electrolysis, results in the highest GWP100 impact, generating around 38 kg CO_2 eq/kg H_2.

Grey H_2 includes processes such as gasification of coal and municipal solid waste, along with the partial oxidation of oil products. These methods are known for being the most cost-effective (Ajanovic et al., 2022). These methods generate approximately 27 (B1), 17 (B3), and 18 (C) kg CO_2 eq/kg H_2, respectively, contributing to emissions within the range of 15-30 kg CO_2 eq/kg H_2.

Blue H_2, essentially black and grey hydrogen with carbon capture and storage (CCS) technology (Dawood et al., 2020), emits about 7-15 kg CO_2 eq/kg H_2. Although carbon capture and storage (CCS) can reduce up to 70-90% of CO_2 emissions from power plants, it is energy-intensive and costly (Wilberforce et al., 2019). Significant research, notably by Wilberforce et al. (2019), (Wilberforce et al., 2021), focuses on reducing these costs. Technologies like steam methane reforming (A) and RDF-Two-stage gasification (F) fall under blue hydrogen, emitting around 14, and 8-12 kg CO_2 eq/kg H_2, respectively.

The study notes the crucial role of Refuse-Derived Fuel (RDF) composition in emission levels. For instance, if RDF consists predominantly (80%-85%) of biomass waste, food waste, and paper—a common scenario in the UK (Ng et al., 2021, Amaya-Santos et al., 2021)—the GWP100 of certain technologies can drop to 4-7 g CO_2 eq/kg H_2. This shift potentially reclassifies these technologies from blue H_2 to **near-low carbon H_2** by UK standards.

In 2022, the UK proposed a low carbon H_2 standard, defining it as hydrogen that produces less than 20 g CO_2 per MJ_{LHV} (BEIS, 2022), equivalent to about 2.5 kg CO_2 eq/kg H_2. In this study, technologies D2, D3, E1, E2, and E3 meet this criterion. However, factors like the origin and transportation of wood pellets (WP) significantly affect these figures. For instance, WP sourced from the USA, Canada, Latvia, and the Netherlands could raise GWP100 emissions to nearly 5 kg CO_2 eq/kg H_2, disqualifying E1 from low carbon H_2 status.

6.4.3 Hotspot analysis in two-stage gasification for hydrogen production

The hotspot analysis for E and F technologies, as shown in Figure 6.10, reveals critical insights into their global warming potential (GWP100) emissions. A significant finding is that the PSA unit in both E and F technologies is the primary source of emissions, contributing approximately 8-10 kg CO_2 equivalent per kilogram of H_2. This is largely due to the two-stage gasification process, which produces CO_2, CH_4, and smaller hydrocarbon molecules like C_2-C_4. Notably, F

technology emits slightly more GWP100 than E, mainly because it generates a higher quantity of CH_4 and C_2-C_4, as detailed in chapters 6 and 7. Furthermore, the dense CO_2 emissions produced during manufacturing in these technologies make them ideal candidates for existing carbon capture and storage (CCS) methods. There's potential for further exploration into carbon capture technology and its implications.

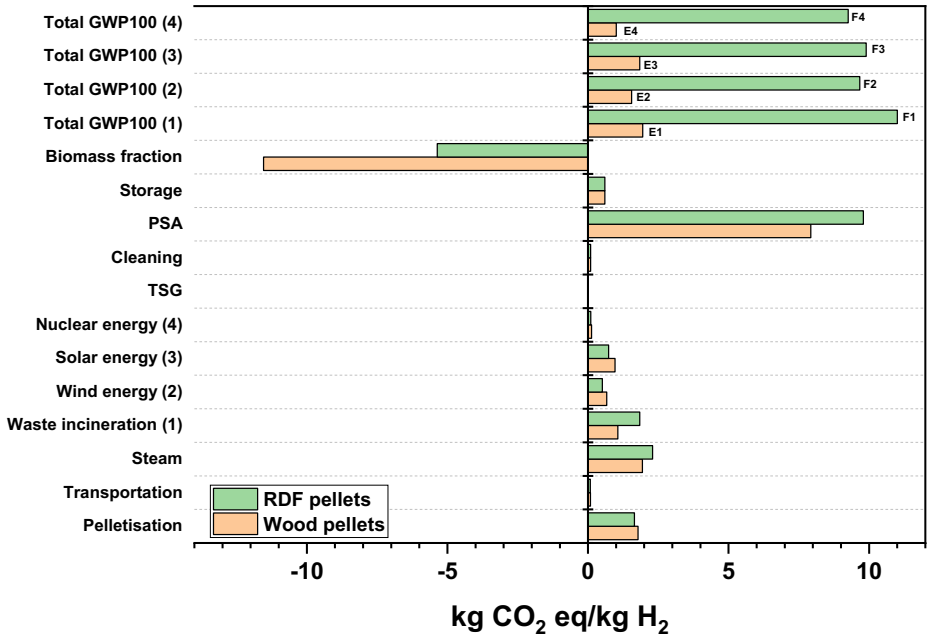

Figure 6.10: Hotspot analysis of Global Warming Potential 100 (GWP100) for hydrogen production via two-stage gasification from pelletization to clean hydrogen using waste wood and RDF pellets.

The second largest GWP100 impact is found in steam generation units, accounting for about 2-3 kg CO_2 eq/kg H_2. RDF, in particular, contributes more to GWP100 in this unit due to its higher steam requirements during operation. Interestingly, the third largest GWP100 impacts differ between E and F technologies. In E, the pelletisation unit is a significant contributor, while for F, it's the external energy supply from waste incineration. Waste incineration produces a substantial amount of CO_2 and methane, and while waste wood combustion also emits CO_2, it's discounted since it's considered non-fossil fuel.

In the pelletisation unit, wood pellets (WP) generate a slightly higher GWP100 emission. This is attributed to the need for more collection and the lower hydrogen yield compared to RDF-two-stage gasification (TSG), necessitating more WP to produce an equivalent amount of H_2.

The GWP100 emissions from renewable energy sources like wind, solar, and nuclear are comparable to those from the H_2 storage unit, where hydrogen is compressed from 0.1 MPa to 3MPa. Notably, WP-TSG generates significantly lower GWP100 emissions than RDF pellets-TSG, as wood pellets are classified as a neutral carbon resource.

In the context of carbon absorption, using WP for H_2 production results in the absorption of around 11.5 kg CO_2 eq/kg H_2. In comparison, RDF, assuming a composition of 50% food waste, paper, and biomass waste, absorbs about 5.5 kg CO_2 eq/kg H_2. This highlights the efficiency and environmental benefits of using WP in hydrogen production.

6.4.4 Carbon dioxide reduction with Carbon capture and storage (CCS)

Interestingly, incorporating carbon capture and storage (CCS) technology into these processes could result in negative global warming potential (GWP100) emissions. As can be seen in the Figure 6.11, where the E-UK and F-UK with CCS technology (70% of CO_2 captured at PSA unit) reduced the GWP100 emission to around -1.3 and 0.4 kg CO_2 eq/kg H_2. Green hydrogen (Abad and Dodds, 2020), characterized by emissions less than 1 kg CO_2 eq/kg H_2, is best exemplified by technologies D4 and E4 without CCS technology. However, their reliance on nuclear energy, which is not yet commercially viable due to security concerns, limits their current application.

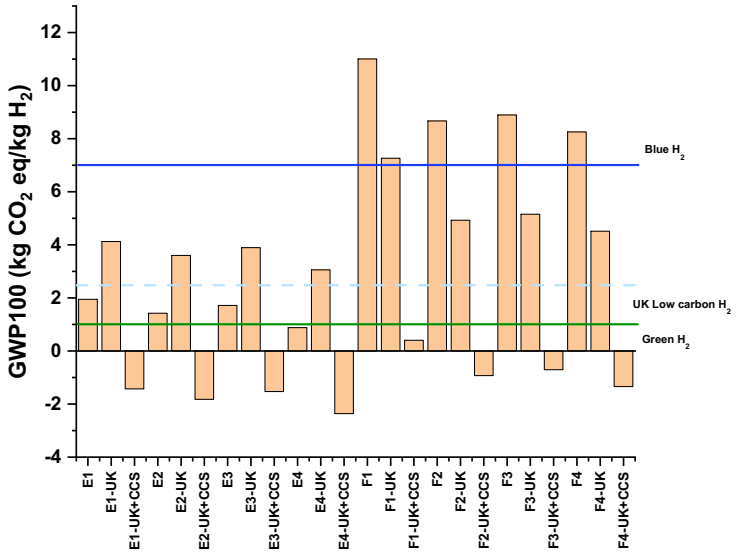

Figure 6.11: Comparative GWP100 analysis for two-stage gasification with imported wood pellets (E, E-UK) and local RDF pellets (F, F-UK), incorporating external energy from feedstock (1), wind (2), solar (3), and nuclear Sources (4).

In conclusion, the market predominantly features black, grey, and blue hydrogen. Utilizing WP and RDF with two-stage gasification (TSG) can facilitate the production of low, near-low, or even negative carbon H_2 with carbon capture and storage technology. Although this study does not investigate the economic feasibility of two-stage gasification (TSG), it references research indicating that TSG becomes economically viable with feedstock costs under $50 per ton or when scaled up to a capacity of 1000 tons per day resulted in the price of $1.6/kg H_2 (Kargbo et al., 2022).

6.5 Summary

The concluding chapter of this thesis on the Life Cycle Assessment of hydrogen production processes provides a comprehensive evaluation of various hydrogen production technologies, considering their environmental and health impacts. The study systematically analyses multiple scenarios, each representing different hydrogen production methods, including steam methane reforming (SMR), conventional gasification of coal, biomass waste, and refuse-derived fuel (RDF), partial oxidation of oil products (POX), Electrolysis using coal, wind, solar, and nuclear energy, and two-stage gasification using waste wood and RDF pellets.
Key findings include:

1. **Environmental impacts**: Each hydrogen (H_2) production exhibits distinct environmental impacts. Steam methane reforming (SMR), although common, raises concerns due to high global warming potential (GWP100) and methane leakage. Traditional gasification processes, especially coal gasification, are associated with high human toxicity potential (HTP) and water consumption potential (WCP). Electrolysis powered by renewable sources like wind, solar and nuclear is more favourable in terms of reduced GWP100 but faces challenges like higher freshwater ecotoxicity potential (FETP), terrestrial ecotoxicity potential (TETP), ionising radiation potential (IRP), and surplus ore potential (SOP).
2. **Health and resource impacts**: The study delves into the human health and resource impacts of hydrogen production. Processes like coal gasification have significant health impacts due to the release of harmful compounds. On the resource front, methods like Wood pellet two-stage gasification (WP-TSG) require extensive land for wood pellet production.

3. **Two-stage gasification**: Wood pellet two-stage gasification (WP-TSG) and RDF pellet two-stage gasification (RDF-TSG) are novel methods assessed for their lower global warming potential (GWP100) compared to traditional methods. However, they face challenges like high land occupation for WP-TSG and increased toxicity emissions in RDF-TSG. Additionally, the impact of transporting raw materials like wood pellets over varying distances is also considered, revealing higher emissions for longer transportation routes.
4. **Alternative energy sources**: The use of alternative energy sources such as wind, solar, and nuclear for hydrogen production is explored. Each source has its benefits and drawbacks, with solar and wind showing lower GWP100 but higher impacts in other categories like FETP and TETP.
5. **Hydrogen colour spectrum**: The study categorizes hydrogen based on its environmental impact using a color-coded system (Black, Grey, Blue, and Green H_2). It is found that cleaner production methods like waste wood and RDF pellets via two-stage gasification can produce UK-low or near-low carbon hydrogen.
6. **Potential improvements**: The thesis suggests potential improvements, such as the use of landfill gas in SMR to reduce environmental impacts and incorporating carbon capture and storage (CCS) technology to achieve negative GWP100 emissions in some scenarios.

In summary, this chapter offers a detailed and systematic assessment of various hydrogen production technologies, highlighting their environmental and health impacts. It underscores the need for a balanced approach in choosing hydrogen production methods, considering both their benefits and drawbacks, to move towards a more sustainable energy future.

Chapter 7 Conclusions

Motivation and global energy challenge: Hydrogen is emerging as a crucial energy carrier for the 21st century, prized for its high calorific value (120-142 MJ/kg) and the fact that it emits no pollutants upon combustion (Rasul et al., 2022). It is a vital component in various industries, including ammonia and methanol production, liquid fuel generation, and even in traditionally unabated sectors like iron production. However, a significant challenge lies in its current production methods. Over 98% of hydrogen is derived from fossil fuels (Ji and Wang, 2021), contributing to around 900 million tonnes of CO_2 equivalent emissions annually, accounting for 2-3% of global CO_2 emissions (Liu et al., 2022).

Gasification as an alternative: Gasification, a well-established technology since World War II, offers an alternative route for hydrogen-rich gas production (Basu, 2018). This process can convert carbonaceous materials into a mix primarily consisting of hydrogen, carbon monoxide, with traces of carbon dioxide, methane, and small hydrocarbons. Historically operated with fossil fuels, gasification needs to adapt to contemporary environmental challenges.

Adaptation to biomass waste and RDF waste gasification: In line with the directives of COP28, which emphasize ceasing new fossil fuel-based plants to limit global temperature rise to 1.5°C above pre-industrial levels, there's a growing interest in using biomass waste and RDF waste in the energy sector (Birol, 2023). However, conventional gasifiers struggle with these materials due to their heterogeneous nature and composition. Pelletisation of waste, growing at a rate of over 2-14% annually (Fernandez, 2023), addresses this by reducing heterogeneity and ensuring consistent quality, thus easing operational challenges in gasifiers.

Challenges and innovations in multi-stage gasification: Despite the high calorific potential of biomass waste and RDF waste, they present challenges, notably in terms of high ash and tar content post-gasification. To adapt waste for gasification, pre-treatment processes like pyrolysis are essential. This multi-stage gasification approach reduces moisture and volatile matter, increasing the fixed carbon content to resemble that of fossil fuels (Gøbel et al., 2002). This results in a syngas with lower tar content compared to traditional gasification methods. However, multi-stage gasification can reduce energy efficiency due to the need for external energy inputs.

Towards renewable energy integration: Fortunately, the global shift towards renewable energy, with its surplus production, offers a solution. This surplus energy can be harnessed to power the multi-stage gasification process, facilitating the production of purer and cleaner gas. This approach aligns with global efforts to reduce reliance on fossil fuels and mitigate climate change, making it a promising avenue for sustainable hydrogen production.

This thesis has successfully explored the potential of a two-stage steam gasification process in optimizing hydrogen and syngas production from waste wood and refuse-derived fuel (RDF). The implementation of multi-stage gasification, incorporating a preliminary pyrolysis stage, has been identified as a crucial step in enhancing the suitability of heterogeneous waste materials for gasification. This approach effectively reduces moisture and volatile matter content, increasing the fixed carbon proportion, thereby rendering the waste characteristics more akin to those of conventional fossil fuels. This alignment enables the utilization of existing gasification technologies while also yielding a syngas with significantly lower tar content.

However, a notable consideration in this process is the trade-off between enhanced gas quality and energy efficiency. The segmentation of the gasification process into multiple stages inherently requires additional external energy inputs, potentially lowering the overall energy efficiency. This challenge has been addressed in the context of the global shift towards renewable energy sources. The surplus energy generated from renewable sources presents a viable solution to power these multi-stage gasifiers, thereby aligning the process with environmental sustainability goals. Here are some significant conclusions drawn from chapters 4 to 6.

Enhancing Wood Pellet Gasification for Increased Hydrogen Yield

1. **Enhanced hydrogen production:** Waste wood pellets can produce up to 88 mg of hydrogen per gram in a two-stage gasification process, significantly higher than the theoretical yield. This is achieved by recycling CO_2 (up to 271 mg CO_2/g wood pellet), which not only increases carbon conversion efficiency by 3-12% and reduces tar content by up to 93%, but also does not interfere with the steam and hydrocarbon reaction, thereby producing a high yield of hydrogen.
2. **Improved gasification process with CO_2:** The two-stage gasification process (WP-TSG) utilizes CO_2 effectively, resulting in increased carbon conversion efficiency and significantly lower tar levels compared to steam gasification. This process also demonstrates the potential for recycling CO_2 within the system, underlining the sustainability benefits.

3. **Impact of CO_2 on pyrolysis and gasification:** The use of CO_2 as a carrier gas in pyrolysis leads to different gas profiles and yields compared to nitrogen. CO_2 actively participates in reactions above 500°C, affecting the composition of liquid by-products and the characteristics of pyrolysis char. The choice of CO_2 as a reaction medium enhances carbon conversion, increases gas yield, and reduces harmful chemicals like phenols compared to an N_2 environment.

Optimization of RDF CO_2/steam two-stage gasification

1. **Optimization using Response Surface Methodology (RSM):** RSM is employed to model the two-stage gasification process of RDF pellets, focusing on how operational variables impact key outcomes like hydrogen and carbon dioxide content, H_2/CO ratio, and various efficiencies (carbon conversion efficiency, carbon gasification efficiency, process efficiency). This method offers a comprehensive understanding of the gasification dynamics with efficient resource use.
2. **Outcomes of RDF gasification under specific conditions:** The study finds that RDF gasification is most efficient at a first-stage temperature of 587°C and a second-stage temperature of 924°C, with a steam-to-carbon ratio of 2.6 and CO_2 flow of 100 cm^3/min. This setup yields the highest hydrogen production (93.4±1.2 mg H_2/g RDF) and process efficiency (67.0±0.6%). However, challenges like the formation of sticky residues during the first stage, potential blockages in the screw feeder, and wax accumulation at lower temperatures are noted.
3. **Temperature and material impact on gasification:** Increasing the first-stage temperature enhances gas yield and reduces solid and condensate yields due to more efficient RDF decomposition. The study also suggests blending RDF with biomass waste to mitigate wax accumulation and blockages. Additionally, the study observes stable hydrogen content and a consistent H_2/CO ratio across varying temperatures, emphasizing the importance of temperature control in optimizing gasification outcomes.

Life Cycle Assessment (LCA) of hydrogen production processes

1. **Comparative analysis of hydrogen production methods:** The chapter compares various hydrogen production methods, including traditional ones like steam methane reforming (SMR) and partial oxidation of oil products (POX), as well as innovative approaches like two-stage gasification using wood pellets and RDF. The assessment is

based on the Ecoinvent database and considers different energy sources, including coal, wind, solar, and nuclear energy. The life cycle assessment adheres to ISO 14040 standards and incorporates novel data from laboratory experiments.

2. **Environmental impact of different hydrogen production systems:** The study finds that hydrogen production from nuclear energy has the lowest CO_2 emissions but the highest radiation impact. It also reveals that while wood pellets TSG hydrogen production can be considered low emission when produced locally, importing wood pellets increases CO_2 emissions, thus impacting its classification. RDF-TSG hydrogen is classified as low blue hydrogen and could be closer to UK low-carbon hydrogen standards if the RDF contains less than 15% plastic. This suggests a potential policy direction for reducing emissions from RDF.
3. **Potential of carbon capture and storage (CCS) in TSG plants:** The chapter explores the assumption of incorporating CCS technology in two-stage gasification plants. It finds that using CCS in wood pellets and RDF-TSG processes can potentially lead to negative carbon emissions. This opens avenues for future studies to explore the integration of CCS in TSG plants, especially given the high concentration of CO_2, which might make it easier to capture.

Recommendations and future work:

1. **Enhanced CO_2 capture with CaO sorbents:** Investigate the use of calcium oxide (CaO) as a sorbent in the gasification process. This study should focus on the efficiency of CO_2 capture by CaO, its impact on the overall process efficiency, and the potential for regeneration and reuse of the sorbent. Understanding the reaction mechanisms between CaO and other gasification by-products will also be critical.
2. **Feedstock diversification in co-gasification:** Explore the co-gasification of mixed feedstocks, such as combining wood pellets with RDF pellets, or incorporating other types of waste like sewage sludge. This research should assess the synergistic effects on gas yield, energy efficiency, and emissions. Particular attention should be given to the impact of different feedstock compositions and ratios on the operational stability and product gas quality.
3. **Scaling up process through computational fluid dynamics (CFD):** Utilize CFD modelling to simulate the upscaling of the two-stage gasification process. This should include assessments of flow dynamics, heat and mass transfer, and reaction kinetics at

a larger scale. The goal is to identify potential scale-up challenges and design optimization strategies for large-scale hydrogen production.

4. **Optimization of CO_2 in carrier gas:** Investigate the effects of increasing CO_2 concentration in the carrier gas on the gasification process. This research should evaluate how varying CO_2 levels influence gas composition, process efficiency, and emissions. The study could also explore the potential for enhanced carbon capture within the gasification system due to increased CO_2 levels.
5. **Public and policy advocacy for plastic waste reduction:** Promote public awareness and policy initiatives aimed at reducing single-use plastic waste. Emphasize the environmental and operational benefits of reducing plastic content in RDF, particularly in terms of lower emissions and improved gasification performance. Collaborations with waste management agencies and policy makers could be essential.
6. **Advanced research on carbon capture and storage (CCS):** Conduct in-depth studies on the integration of CCS technologies in the downstream process of two-stage gasification. This should include the development of cost-effective and efficient CCS systems, understanding the interactions between syngas and capture technologies, and assessing the overall carbon footprint of the process.
7. **Direct utilization of high-hydrogen syngas in Fuel Cells:** Explore the direct use of high-hydrogen syngas produced from gasification in fuel cell technologies. This research should focus on the compatibility of syngas with different types of fuel cells, the purification requirements to meet fuel cell standards, and the overall system efficiency and sustainability.
8. **Techno-economic analysis of full-scale operations:** Conduct a techno-economic analysis of the scaled-up two-stage gasification process. This should include capital and operational cost assessments, potential revenue streams from hydrogen and other by-products, and a comparison with other hydrogen production methods.
9. **Collaboration with industry partners:** Foster collaborations with industry partners for pilot-scale testing and real-world application of the developed gasification technologies. This could help in validating the research findings and accelerating the commercialization of the technology.

References

ABAD, A. V. & DODDS, P. E. 2020. Green hydrogen characterisation initiatives: Definitions, standards, guarantees of origin, and challenges. *Energy Policy,* 138**,** 111300.

ABDIN, Z., ZAFARANLOO, A., RAFIEE, A., MÉRIDA, W., LIPIŃSKI, W. AND KHALILPOUR, K.R. 2020. Hydrogen as an energy vector. *Renewable and Sustainable Energy Reviews,* 120**,** 109620.

ABE, H., KATAYAMA, A., SAH, B. P., TORIU, T., SAMY, S., PHEACH, P., ADAMS, M. A. & GRIERSON, P. F. 2007. Potential for rural electrification based on biomass gasification in Cambodia. *Biomass and Bioenergy,* 31**,** 656-664.

AHMAD, A. A., ZAWAWI, N. A., KASIM, F. H., INAYAT, A. & KHASRI, A. 2016. Assessing the gasification performance of biomass: A review on biomass gasification process conditions, optimization and economic evaluation. *Renewable and Sustainable Energy Reviews,* 53**,** 1333-1347.

AJANOVIC, A., SAYER, M. & HAAS, R. 2022. The economics and the environmental benignity of different colors of hydrogen. *International Journal of Hydrogen Energy,* 47**,** 24136-24154.

ALFÈ, M., GARGIULO, V., PORTO, M., MIGLIACCIO, R., LE PERA, A., SELLARO, M., PELLEGRINO, C., ABE, A. A., URCIUOLO, M., CAPUTO, P. & CALANDRA, P. 2022. Pyrolysis and Gasification of a Real Refuse-Derived Fuel (RDF): The Potential Use of the Products under a Circular Economy Vision. *Molecules,* 27**,** 8114.

ALURI, S. 2018a. *Gasification Studies of Model Refuse Derived Fuel (RDF).* Doctor of Philosophy, Georgia Institute of Technology.

ALURI, S., SYED, A., FLICK, D. W., MUZZY, J. D., SIEVERS, C. & AGRAWAL, P. K. 2018. Pyrolysis and gasification studies of model refuse derived fuel (RDF) using thermogravimetric analysis. *Fuel processing technology,* 179**,** 154-166.

ALURI, S., SYED, A., FLICK, D.W., MUZZY, J.D., SIEVERS, C. AND AGRAWAL, P.K. 2018b. Pyrolysis and gasification studies of model refuse derived fuel (RDF) using thermogravimetric analysis. *Fuel processing technology,* 179**,** 154-166.

AMAYA-SANTOS, G., CHARI, S., SEBASTIANI, A., GRIMALDI, F., LETTIERI, P. & MATERAZZI, M. 2021. Biohydrogen: A life cycle assessment and comparison with alternative low-carbon production routes in UK. *Journal of Cleaner Production,* 319**,** 128886.

AMHAMED, A. I., SHUIBUL QARNAIN, S., HEWLETT, S., SODIQ, A., ABDELLATIF, Y., ISAIFAN, R. J. & ALREBEI, O. F. 2022. Ammonia production plants—A review. *Fuels,* 3**,** 408-435.

AMORI, K. E., SALMAN, S. M. & KAREEM, Z. H. 2016. Hydrogen Production by Water Electrolysis Via Photovoltaic Panel. *Journal of Engineering,* 22**,** 72-91.

ANASSTASIA, T. T., LESTIANINGRUM, E., CAHYONO, R. B. & AZIS, M. M. Life cycle assessment of refuse derived fuel (RDF) for municipal solid waste (MSW) management: case study area around cement industry, Cirebon, Indonesia. IOP Conference Series: Materials Science and Engineering, 2020, April. IOP Publishing, 012146.

ANDREWS, J. W. 2020. Hydrogen production and carbon sequestration by steam methane reforming and fracking with carbon dioxide. *International Journal of Hydrogen Energy,* 45**,** 9279-9284.

ANTOLINI, D., AIL, S. S., PATUZZI, F., GRIGIANTE, M. & BARATIERI, M. 2019. Experimental investigations of air-CO2 biomass gasification in reversed downdraft gasifier. *Fuel,* 253**,** 1473-1481.

ANTONINI, C., TREYER, K., STREB, A., VAN DER SPEK, M., BAUER, C. & MAZZOTTI, M. 2020. Hydrogen production from natural gas and biomethane with carbon capture and storage–A techno-environmental analysis. *Sustainable Energy & Fuels,* 4**,** 2967-2986.

ANWAR, S., KHAN, F., ZHANG, Y. & DJIRE, A. 2021. Recent development in electrocatalysts for hydrogen production through water electrolysis. *International Journal of Hydrogen Energy,* 46**,** 32284-32317.

ARENA, ZACCARIELLO & MASTELLONE. 2010. Fluidized bed gasification of waste-derived fuels. *Waste Management,* 30**,** 1212-1219.

ASADULLAH, M. 2014. Biomass gasification gas cleaning for downstream applications: A comparative critical review. *Renewable & Sustainable Energy Reviews,* 40**,** 118-132.

ASHOK, J., PATI, S., HONGMANOROM, P., TIANXI, Z., JUNMEI, C. & KAWI, S. 2020. A review of recent catalyst advances in CO2 methanation processes. *Catalysis Today,* 356.

ASSIMA, G. P., MARIE-ROSE, S. & LAVOIE, J. M. 2018. Role of fixed carbon and metal oxides in char during the catalytic conversion of tar from RDF gasification. *Fuel,* 218**,** 406-416.

ASSIMA, G. P., PAQUET, A. & LAVOIE, J. 2019. Utilization of MSW-Derived Char for Catalytic Reforming of Tars and Light Hydrocarbons in the Primary Syngas Produced During Wood Chips and MSW-RDF Air Gasification. *Waste and Biomass Valorization,* 10**,** 1203-1222.

AYERS, K. 2019. The potential of proton exchange membrane–based electrolysis technology. *Current Opinion in Electrochemistry,* 18**,** 9-15.

AYERS, K. 2021. High efficiency PEM water electrolysis: Enabled by advanced catalysts, membranes, and processes. *Current Opinion in Chemical Engineering,* 33**,** 100719.

BABATABAR, M. A. & SAIDI, M. 2021. Hydrogen production via integrated configuration of steam gasification process of biomass and water-gas shift reaction: Process simulation and optimization. *International Journal of Energy Research,* 45**,** 19378-19394.

BAGATINI, M. C., KAN, T., EVANS, T. J. & STREZOV, V. 2021. Iron ore reduction by biomass volatiles. *Journal of Sustainable Metallurgy,* 7**,** 215-226.

BAREIS, K., DE LA RUA, C., MÖCKL, M. & HAMACHER, T. 2019. Life cycle assessment of hydrogen from proton exchange membrane water electrolysis in future energy systems. *Applied Energy,* 237**,** 862-872.

BASU, P. 2018. *Biomass gasification, pyrolysis and torrefaction: practical design and theory*, Academic press.

BEHZADI, A., ARABKOOHSAR, A. & GHOLAMIAN, E. 2020. Multi-criteria optimization of a biomass-fired proton exchange membrane fuel cell integrated with organic rankine cycle/thermoelectric generator using different gasification agents. *Energy,* 201**,** 117640.

BELGACEM, M. N. & PIZZI, A. 2016. *Lignocellulosic Fibers and Wood Handbook: Renewable Materials for Today's Environment*, John Wiley & Sons.

BEOHAR, H., GUPTA, B., SETHI, V. K. & PANDEY, M. 2012. Parametric study of fixed bed biomass gasifier: a review. *International Journal of Thermal Technologies,* 2(1)**,** 134-140.

BILLAUD, J., VALIN, S., PEYROT, M. & SALVADOR, S. 2016. Influence of H2O, CO2 and O2 addition on biomass gasification in entrained flow reactor conditions: Experiments and modelling. *Fuel,* 166**,** 166-178.

BIROL, F. 2023. What does COP28 need to do to keep 1.5 °C within reach? These are the IEA's five criteria for success. IEA.

BLANCO, P. H., WU, C., ONWUDILI, J. A. & WILLIAMS, P. T. 2012. Characterization of tar from the pyrolysis/gasification of refuse derived fuel: influence of process parameters and catalysis. *Energy & Fuels,* 26**,** 2107-2115.

BRAND, M. A., RODRIGUES, T. M., DA SILVA, J. P. & DE OLIVEIRA, J. 2021. Recovery of agricultural and wood wastes: the effect of biomass blends on the quality of pellets. *Fuel,* 284**,** 118881.

BRANDT, P., LARSEN, E. & HENRIKSEN, U. 2000. High tar reduction in a two-stage gasifier. *Energy & Fuels,* 14(4)**,** 816-819.

BREAULT, R. W. 2010. Gasification processes old and new: a basic review of the major technologies. *Energies,* 3**,** 216-240.

BREWER, C. E., SCHMIDT-ROHR, K., SATRIO, J. A. & BROWN, R. C. 2009. Characterization of biochar from fast pyrolysis and gasification systems. *Environmental Progress & Sustainable Energy,* 28**,** 386-396.

BRIDGWATER, A. V. 1995. The technical and economic feasibility of biomass gasification for power generation. *Fuel,* 74**,** 631-653.

BRITISH STANDARDS 1973. Methods for the analysis and testing of coal and coke. *Proximate analysis of coal.*

BRITISH STANDARDS 2005. Solid biofuels Determination of total content of carbon, hydrogen and nitrogen Instrumental methods. Brussels.

BRITISH STANDARDS 2006. Solid biofuels — Determination of total content of sulphur and chlorine. Brussels.

BRITISH STANDARDS 2009. Solid biofuels Determination of moisture content Oven dry method. *Moisture in general analysis sample.* Brussels.
BRITISH STANDARDS 2011. Solid biofuels — Sampling. Brussels: BSI Standards Publication.
BUI, T., LOOF, R. & BHATTACHARYA, S. C. 1994. Multi-stage reactor for thermal gasification of wood. *Energy,* 19**,** 397-404.
BURHENNE, L., MESSMER, J., AICHER, T. & LABORIE, M. P. 2013. The effect of the biomass components lignin, cellulose and hemicellulose on TGA and fixed bed pyrolysis. *Journal of Analytical and Applied Pyrolysis,* 101**,** 177-184.
CAI, J., ZENG, R., ZHENG, W., WANG, S., HAN, J., LI, K., LUO, M. & TANG, X. 2021. Synergistic effects of co-gasification of municipal solid waste and biomass in fixed-bed gasifier. *Process Safety and Environmental Protection,* 148**,** 1-12.
CĂLIN, C., ION, I. V., RUSU, E. & FRĂTIŢA, M. 2021. Performance analysis of a RDF gasification and solar thermal energy based CCHP system. *Energy Reports,* 7**,** 186-192.
CANO, D. J. F. 2013. *Studies on tar formation and conversion for the development of a three-stage gasifier* Doctor of Philosophy, University of Seville.
CAO, L., IRIS, K. M., XIONG, X., TSANG, D. C., ZHANG, S., CLARK, J. H., HU, C., NG, Y. H., SHANG, J. & OK, Y. S. 2020. Biorenewable hydrogen production through biomass gasification: A review and future prospects. *Environmental research,* 186**,** 109547.
CAPUTO, A. C. & PELAGAGGE, P. M. 2002. RDF production plants: I Design and costs. *Applied Thermal Engineering,* 22**,** 423-437.
CERONE, N., ZIMBARDI, F., VILLONE, A., STRJIUGAS, N. & KIYIKCI, E. G. 2016. Gasification of wood and torrefied wood with air, oxygen, and steam in a fixed-bed pilot plant. *Energy & Fuels,* 30(5)**,** 4034-4043.
CHAN, Y. H., RAHMAN, S. N. F. S. A., LAHURI, H. M. & KHALID, A. 2021. Recent progress on CO-rich syngas production via CO2 gasification of various wastes: A critical review on efficiency, challenges and outlook. *Environmental Pollution,* 278**,** 116843.
CHAVANDO, J. A. M., DE MATOS, E. C. J., SILVA, V. B., TARELHO, L. A. & CARDOSO, J. S. 2022. Pyrolysis characteristics of RDF and HPDE blends with biomass. *International Journal of Hydrogen Energy,* 47**,** 19901-19915.
CHEN, D., LI, Y., CEN, K., LUO, M., LI, H. & LU, B. 2016a. Pyrolysis polygeneration of poplar wood: Effect of heating rate and pyrolysis temperature. *Bioresource Technology,* 218**,** 780-788.
CHEN, D., ZHAI, X. & ZHOU, G. Life cycle assessment of RDF production from aged MSW and its utilization system. the international conference on sustainable solid waste management, 2007, September Chennai, India 5-7.
CHEN, W., HONG, J., YUAN, X. & LIU, J. 2016b. Environmental impact assessment of monocrystalline silicon solar photovoltaic cell production: a case study in China. *Journal of Cleaner Production,* 112**,** 1025-1032.
CHEN, Z., WANG, M., JIANG, E., WANG, D., ZHANG, K., REN, Y. & JIANG, Y. 2018. Pyrolysis of torrefied biomass. *Trends in Biotechnology,* 36**,** 1287-1298.
CHI, J. & YU, H. 2018. Water electrolysis based on renewable energy for hydrogen production. *Chinese Journal of Catalysis,* 39**,** 390-394.
CHO, H. H., STREZOV, V. & EVANS, T. J. 2022. Environmental impact assessment of hydrogen production via steam methane reforming based on emissions data. *Energy Reports,* 8**,** 13585-13595.
CHOJNACKI, J., NAJSER, J., ROKOSZ, K., PEER, V., KIELAR, J. & BERNER, B. 2020. Syngas composition: gasification of wood pellet with water steam through a reactor with continuous biomass feed system. *Energies,* 13**,** 4376.
CHOWDHURY, M. S., RAHMAN, K. S., CHOWDHURY, T., NUTHAMMACHOT, N., TECHATO, K., AKHTARUZZAMAN, M., TIONG, S. K., SOPIAN, K. & AMIN, N. 2020. An overview of solar photovoltaic panels' end-of-life material recycling. *Energy Strategy Reviews,* 27**,** 100431.
CHRISTENSEN, E., FERRELL, J., OLARTE, M. V. & PADMAPERUMA, A. B. 2016. Quantification of Semi-Volatile Oxygenated Components of Pyrolysis Bio-Oil by Gas Chromatography/Mass Spectrometry (GC/MS). United States: National Renewable Energy Lab (NREL).

COMBES, A. & FRANCHINEAU, G. 2019. Fine particle environmental pollution and cardiovascular diseases. *Metabolism,* 100**,** 153944.
CORTAZAR, M., ALVAREZ, J., LOPEZ, G., AMUTIO, M., SANTAMARIA, L., BILBAO, J. & OLAZAR, M. 2018. Role of temperature on gasification performance and tar composition in a fountain enhanced conical spouted bed reactor. *Energy Conversion and Management,* 171**,** 1589-1597.
CUI, X., SONG, G., YAO, A., WANG, H., WANG, L. & XIAO, J. 2021. Technical and Economic Assessments of a novel biomass-to-synthetic natural gas (SNG) process integrating O2-enriched air gasification. *Process Safety and Environmental Protection,* 156**,** 417-428.
DAHOU, T., DEFOORT, F., KHIARI, B., LABAKI, M., DUPONT, C. AND JEGUIRIM, M. 2021. Role of inorganics on the biomass char gasification reactivity: A review involving reaction mechanisms and kinetics models. *Renewable and Sustainable Energy Reviews,* 135**,** 110136.
DAI, Z., GONG, X., GUO, X., LIU, H., WANG, F. & YU, Z. 2008. Pilot-trial and modeling of a new type of pressurized entrained-flow pulverized coal gasification technology. *Fuel,* 87**,** 2304-2313.
DALAI, A. K., BATTA, N., ESWARAMOORTHI, I. & SCHOENAU, G. J. 2009. Gasification of refuse derived fuel in a fixed bed reactor for syngas production. *Waste Management,* 29**,** 252-258.
DAWOOD, F., ANDA, M. & SHAFIULLAH, G. M. 2020. Hydrogen production for energy: An overview. *International Journal of Hydrogen Energy,* 45**,** 3847-3869.
DE ALMEIDA, S. G., TARELHO, L. A., HAUSCHILD, T., COSTA, M. A. M. & DUSSAN, K. J. 2022. Biochar production from sugarcane biomass using slow pyrolysis: Characterization of the solid fraction. *Chemical Engineering and Processing-Process Intensification,* 179.
DE CARVALHO, F. A., NOBRE, J. N., CAMBRAIA, R. P., SILVA, A. C., FABRIS, J. D., DOS REIS, A. B. & PRAT, B. V. 2021. Quartz mining waste for concrete production: environment and public health. *Sustainability,* 14**,** 389.
DEFRA 2020. Recycling rate of household waste collected by local authorities in England from 2000/01 to 2018/19. *In:* DEPARTMENT FOR ENVIRONMENT, F. R. A. (ed.).
DEFRA 2024. Refuse derived fuel market in England Call for evidence. *In:* AFFAIRS, D. F. E. F. R. (ed.).
DEMOL, R., DUFOUR, A., ROGAUME, Y. & MAUVIEL, G. 2021. Production of Purified H2, Heat, and Biochar from Wood: Comparison between Gasification and Autothermal Pyrolysis Based on Advanced Process Modeling. *Energy & Fuels,* 36**,** 488-501.
DEPARTMENT FOR BUSINESS, E. I. S. 2022a. Hydrogen Strategy update to the market: December 2022 The UK Goverment.
DEPARTMENT FOR BUSINESS, E. I. S. 2022b. UK Low Carbon Hydrogen Standard: Guidance on the greenhouse gas emissions and sustainability criteria.
DEPARTMENT FOR BUSINESS ENERGY & INDUSTRIAL STRATEGY (BEIS) 2022. UK Low Carbon Hydrogen Standard: emissions reporting and sustainability criteria. *In:* DEPARTMENT FOR BUSINESS, E. I. S., (BEIS) (ed.). UK.
DERRIEN, M. L. 1986. Selective hydrogenation applied to the refining of petrochemical raw materials produced by steam cracking. *Studies in surface science and catalysis.* Elsevier.
DI BLASI, C. 2009. Combustion and gasification rates of lignocellulosic chars. *Progress in energy and combustion science,* 35**,** 121-140.
DING, L., YOSHIKAWA, K., FUKUHARA, M., KOWATA, Y., NAKAMURA, S., XIN, D. & MUHAN, L. 2018. . Development of an ultra-small biomass gasification and power generation system: Part 2. Gasification characteristics of carbonized pellets/briquettes in a pilot-scale updraft fixed bed gasifier. *Fuel,* 220**,** 210-219.
DONG, J., CHI, Y., TANG, Y., NI, M., NZIHOU, A., WEISS-HORTALA, E. & HUANG, Q. 2016. Effect of operating parameters and moisture content on municipal solid waste pyrolysis and gasification. *Energy & Fuels,* 30**,** 3994-4001.
DOS SANTOS, R. G. & ALENCAR, A. C. 2020. Biomass-derived syngas production via gasification process and its catalytic conversion into fuels by Fischer Tropsch synthesis: A review. *International Journal of Hydrogen Energy,* 45**,** 18114-18132.

DUANGSATHAPORN, K., SANGRAM, N., OMULE, Y., PRASOMSIN, P., PALAKIT, K. & LUMYAI, P. 2023. Formulating Equations for Estimating Forest Stand Carbon Stock for Various Tree Species Groups in Northern Thailand. *Forests,* 14**,** 1584.

EFIKA, C. E., ONWUDILI, J. A. & WILLIAMS, P. T. 2018. Influence of heating rates on the products of high-temperature pyrolysis of waste wood pellets and biomass model compounds. *Waste Management,* 76**,** 497-506.

EFIKA, E. C., ONWUDILI, J. A. & WILLIAMS, P. T. 2015. Products from the high temperature pyrolysis of RDF at slow and rapid heating rates. *Journal of analytical and applied pyrolysis,* 112**,** 14-22.

ELLIOTT, J. R. & LIRA, C. T. 2012. *Introductory chemical engineering thermodynamics* Upper Saddle River, NJ, Prentice Hall.

FAHEEM, H. H., TANVEER, H. U., ABBAS, S. Z. & MAQBOOL, F. 2021. Comparative study of conventional steam-methane-reforming (SMR) and auto-thermal-reforming (ATR) with their hybrid sorption enhanced (SE-SMR & SE-ATR) and environmentally benign process models for the hydrogen production. *Fuel,* 297**,** 120769.

FANG, Y., PAUL, M. C., VARJANI, S., LI, X., PARK, Y. K. & YOU, S. 2021. Concentrated solar thermochemical gasification of biomass: Principles, applications, and development. *Renewable and Sustainable Energy Reviews,* 150**,** 111484.

FANKHAUSER, S., SMITH, S. M., ALLEN, M., AXELSSON, K., HALE, T., HEPBURN, C., KENDALL, J. M., KHOSLA, R., LEZAUN, J., MITCHELL-LARSON, E. & OBERSTEINER, M. 2022. The meaning of net zero and how to get it right. *Nature Climate Change,* 12**,** 15-21.

FAZIL, A., KUMAR, S. & MAHAJANI, S. M. 2023. Gasification and Co-gasification of paper-rich, high-ash refuse-derived fuel in downdraft gasifier. *Energy,* 263**,** 125659.

FENG, D., ZHANG, Y., ZHAO, Y., SUN, S. & GAO, J. 2018. Improvement and maintenance of biochar catalytic activity for in-situ biomass tar reforming during pyrolysis and H2O/CO2 gasification. *Fuel Processing Technology,* 172**,** 106-114.

FERNANDEZ, L. 2023. Global wood pellets production 2000-2018. Statista.

FERNÁNDEZ, L. 2022. Export volume of wood pellets worldwide in 2021, by major country (in 1,000 metric tons). Statista.

FERNANDO, A. L., DUARTE, M. P., ALMEIDA, J., BOLÉO, S. & MENDES, B. 2010. Environmental impact assessment of energy crops cultivation in Europe. *Biofuels, Bioproducts and Biorefining,* 4**,** 594-604.

FINKELMAN, R. B., OREM, W., CASTRANOVA, V., TATU, C. A., BELKIN, H. E., ZHENG, B., LERCH, H. E., MAHARAJ, S. V. & BATES, A. L. 2002. Health impacts of coal and coal use: possible solutions. *International Journal of Coal Geology,* 50**,** 425-443.

FORTIN, P., KHOZA, T., CAO, X., MARTINSEN, S. Y., BARNETT, A. O. & HOLDCROFT, S. 2020. High-performance alkaline water electrolysis using Aemion™ anion exchange membranes. *Journal of Power Sources,* 451**,** 227814.

FRANCO, C., PINTO, F., GULYURTLU, I. & CABRITA, I. 2003. The study of reactions influencing the biomass steam gasification process. *Fuel,* 82**,** 835-842.

FU, B., HOWER, J. C., ZHANG, W., LUO, G., HU, H. & YAO, H. 2022. A review of rare earth elements and yttrium in coal ash: Content, modes of occurrences, combustion behavior, and extraction methods. *Progress in Energy and Combustion Science,* 88**,** 100954.

GADSBØLL, R. Ø., SÁROSSY, Z., JØRGENSEN, L., AHRENFELDT, J. & HENRIKSEN, U. B. 2018. Oxygen-blown operation of the TwoStage Viking gasifier. *Energy,* 158**,** 495-503.

GALVAGNO, S., CASU, S., CASCIARO, G., MARTINO, M., RUSSO, A. & PORTOFINO, S. 2006. Steam gasification of refuse-derived fuel (RDF): influence of process temperature on yield and product composition. *Energy & fuels,* 20**,** 2284-2288.

GAO, Y., JIANG, J., MENG, Y., YAN, F. & AIHEMAITI, A. 2018. A review of recent developments in hydrogen production via biogas dry reforming. *Energy Conversion and Management,* 171**,** 133-155.

GARCÍA, R., GONZÁLEZ-VÁZQUEZ, M. D. P., RUBIERA, F., PEVIDA, C. & GIL, M. V. 2021. Co-pelletization of pine sawdust and refused derived fuel (RDF) to high-quality waste-derived pellets. *Journal of Cleaner Production,* 328**,** 129635.

GAUTHIER, G., JOSSART, J. & CALDERÓN, C. 2017. AEBIOM STATISTICAL REPORT: PELLET MARKET OVERVIEW. Brussels: European Biomass Association.
GEZICI-KOÇ, Ö., ERICH, S. J., HUININK, H. P., VAN DER VEN, L. G. & ADAN, O. C. 2017. Bound and free water distribution in wood during water uptake and drying as measured by 1D magnetic resonance imaging. *Cellulose,* 24(2)**,** 535-553.
GIACONIA, A., IAQUANIELLO, G., MORICO, B., SALLADINI, A. & PALO, E. 2021. Techno-economic assessment of solar steam reforming of methane in a membrane reactor using molten salts as heat transfer fluid. *International Journal of Hydrogen Energy,* 46**,** 35172-35188.
GIUSTI, E. V. & MEYER, E. Water consumption by nuclear powerplants and some hydrological implications. 1977.
GLASSMAN, I., YETTER, R. A. & GLUMAC, N. G. 2014. *Combustion*, Academic press.
GØBEL, B., HINDSGAUL, C., HENRIKSEN, U. B., AHRENFELDT, J., FOCK, F., HOUBAK, N. & QVALE, E. B. High Performance Gasification with the Two-Stage Gasifier. 2002.
GOH, C. S., JUNGINGER, M., COCCHI, M., MARCHAL, D., THRÄN, D., HENNIG, C., HEINIMÖ, J., NIKOLAISEN, L., SCHOUWENBERG, P. P., BRADLEY, D. & HESS, R. 2013. Wood pellet market and trade: a global perspective. *Biofuels, Bioproducts and Biorefining,* 7**,** 24-42.
GÖRANSSON, K., SÖDERLIND, U., HE, J. & ZHANG, W. 2011. Review of syngas production via biomass DFBGs. *Renewable and Sustainable Energy Reviews,* 15**,** 482-492.
GUNARATHNE, D. S., MELLIN, P., YANG, W., PETTERSSON, M. & LJUNGGREN, R. 2016. Performance of an effectively integrated biomass multi-stage gasification system and a steel industry heat treatment furnace. *Applied energy,* 170**,** 353-361.
GUO, D., ZHU, L., GUO, S., CUI, B., LUO, S., LAGHARI, M., CHEN, Z., MA, C., ZHOU, Y., CHEN, J. & XIAO, B. 2016. Direct reduction of oxidized iron ore pellets using biomass syngas as the reducer. *Fuel Processing Technology,* 148**,** 276-281.
GUO, Y., LI, G., ZHOU, J. & LIU, Y. 2019. Comparison between hydrogen production by alkaline water electrolysis and hydrogen production by PEM electrolysis. *IOP Conference Series: Earth and Environmental Science.* IOP Publishing.
HARIBAL, V. P., CHEN, Y., NEAL, L. & LI, F. 2018. Intensification of ethylene production from naphtha via a redox oxy-cracking scheme: Process simulations and analysis. *Engineering,* 4**,** 714-721.
HASSELRIIS, F. & LICATA, A. 1996. Analysis of heavy metal emission data from municipal waste combustion. *Journal of hazardous materials,* 47**,** 77-102.
HAYDARY, J., RAPČANOVÁ, E. & ŠKULEC, M. 2023. Purification of syngas from Refuse-Derived Fuel (RDF) gasification: Techno-economic analysis. *Thermal Science and Engineering Progress,* 44**,** 102024.
HAYDARY, J., ŠUHAJ, P. AND ŠORAL, M. 2021. Semi-batch gasification of refuse-derived fuel (RDF). *Processes,* 9**,** 343.
HE, X., LIU, Y., REHMAN, A. & WANG, L. 2021. A novel air separation unit with energy storage and generation and its energy efficiency and economy analysis. *Applied Energy,* 281**,** 115976.
HE, X., LIU, Z., NIU, W., YANG, L., ZHOU, T., QIN, D., NIU, Z. & YUAN, Q. 2018. Effects of pyrolysis temperature on the physicochemical properties of gas and biochar obtained from pyrolysis of crop residues. *Energy,* 143**,** 746-756.
HEIDENREICH, S. & FOSCOLO, P. U. 2015. New concepts in biomass gasification. *Progress in energy and combustion science,* 46**,** 72-95.
HERNÁNDEZ, J. J., BALLESTEROS, R. & ARANDA, G. 2013. Characterisation of tars from biomass gasification: Effect of the operating conditions. *Energy,* 50**,** 333-342.
HIGMAN, C. 2008. Gasification. *Combustion engineering issues for solid fuel systems.* Academic Press.
HONGRAPIPAT, J., RAUCH, R., PANG, S., LIPLAP, P., ARJHARN, W., MESSNER, M., HENRICH, C., KOCH, M. & HOFBAUER, H. 2022. Co-Gasification of Refuse Derived Fuel and Wood Chips in the Nong Bua Dual Fluidised Bed Gasification Power Plant in Thailand. *Energies,* 15**,** 7363.
HOSSEINI, S. E. 2019. Development of solar energy towards solar city Utopia. *Energy Sources, Part A: Recovery, Utilization, and Environmental Effects,* 41**,** 2868-2881.
HOSSEINI, S. E. 2022. Hydrogen has found its way to become the fuel of the future. *Future Energy,* 1**,** 11-12.

HRBEK, J., PFEIFER, C., BARISANO, D., VREUGDENHIL, B., LUNDGREN, J., RAUCH, R., KOROVESHI, X. & CATIZZONE, E. 2021. Gasification applications in existing infrastructures for production of sustainable value-added products. IEA Bioenergy Task 33 report.

HU, Q., CHENG, W., MAO, Q., HU, J., YANG, H. & CHEN, H. 2022. Study on the physicochemical structure and gasification reactivity of chars from pyrolysis of biomass pellets under different heating rates. *Fuel,* 314**,** 122789.

HU, Y., CHENG, Q., WANG, Y., GUO, P., WANG, Z., LIU, H. & AKBARI, A. 2019. Investigation of biomass gasification potential in syngas production: characteristics of dried biomass gasification using steam as the gasification agent. *Energy & Fuels,* 34**,** 1033-1040.

HUANG, Q., CHEN, G., WANG, Y., CHEN, S., XU, L. & WANG, R. 2020. Modelling the global impact of China's ban on plastic waste imports. *Resources, Conservation and Recycling,* 154**,** 104607.

HUIJBREGTS, M. A., STEINMANN, Z. J., ELSHOUT, P. M., STAM, G., VERONES, F., VIEIRA, M. D., HOLLANDER, A., ZIJP, M. & VAN ZELM, R. 2016. ReCiPe 2016: a harmonized life cycle impact assessment method at midpoint and endpoint level report I: characterization. National Institute for Public Health and the Environment, Netherlands.

HUNT, R. G. 1974. *Resource and environmental profile analysis of nine beverage container alternatives*, Environmental Protection Agency.

HWANG, I. H., KOBAYASHI, J. & KAWAMOTO, K. 2014. Characterization of products obtained from pyrolysis and steam gasification of wood waste, RDF, and RPF. *Waste management,* 34**,** 402-410.

IAQUANIELLO, G. & MANGIAPANE, A. 2006. Integration of biomass gasification with MCFC. *International Journal of Hydrogen Energy,* 31**,** 399-404.

IEA 2023. Task 33 Database. International Energy Agency (IEA).

INSTITUTION, B. S. 2014. Solid biofuels — Fuel specifications and classes *Part 2: Graded wood pellets.* Brussels: BSI Standards Limited 2014.

INTERNATIONAL ENERGY AGENCY, I. 2023a. Global Hydrogen Review 2023. International Energy Agency, IEA.

INTERNATIONAL ENERGY AGENCY, I. 2023b. The Imperative of Cutting Methane from Fossil Fuels: An assessment of the benefits for the climate and health.

INTHARATHIRAT, R. & ABDUL SALAM, P. 2015. Valorization of MSW-to-Energy in Thailand: Status, Challenges and Prospects. *Waste and Biomass Valorization.* Springer Science+Business Media Dordrecht.

ISO 2006a. Environmental management - Life cycle assessment - Principles and framework. International Standard Organisation.

ISO 2006b. Environmental management - Life cycle assessment - Requirements and guidelines. International Standard Organisation.

JAMES R, A. M., YUAN, W. & BOYETTE, M. D. 2016. The effect of biomass physical properties on top-lit updraft gasification of woodchips. *Energies,* 9**,** 283.

JI, M. & WANG, J. 2021. Review and comparison of various hydrogen production methods based on costs and life cycle impact assessment indicators. *International Journal of Hydrogen Energy,* 46**,** 38612-38635.

KALINCI, Y., HEPBASLI, A. & DINCER, I. 2012. Life cycle assessment of hydrogen production from biomass gasification systems. *International journal of hydrogen energy,* 37**,** 14026-14039.

KAMIYA, K., OZASA, K., AKIBA, S., NIWA, O., KODAMA, K., TAKAMURA, N., ZAHARIEVA, E. K., KIMURA, Y. & WAKEFORD, R. 2015. Long-term effects of radiation exposure on health. *The lancet,* 386**,** 469-478.

KAN, T., STREZOV, V. & EVANS, T. J. 2016. Lignocellulosic biomass pyrolysis: A review of product properties and effects of pyrolysis parameters. *Renewable and sustainable energy reviews,* 57**,** 1126-1140.

KARACA, A. E., DINCER, I. & GU, J. 2020. Life cycle assessment study on nuclear based sustainable hydrogen production options. *International Journal of Hydrogen Energy,* 45**,** 22148-22159.

KARGBO, H. O., NG, K. S. & PHAN, A. N. 2022. Evaluation of the economic feasibility of a two-stage gasification system for hydrogen, liquid fuels and energy production from residues. *Energy Conversion and Management,* 253**,** 115126.

KARUPPIAH, P. S., GANESAN, P. & TAMILMANI, T. 2022. Experimental and simulation results of gasification of biomedical waste and Indian palm kernel shell in a fluidized bed gasifier under steam atmosphere. *Proceedings of the Institution of Mechanical Engineers, Part A: Journal of Power and Energy,* 236**,** 1433-1445.

KATEBAH, M. & LINKE, P. 2022. Analysis of hydrogen production costs in Steam-Methane Reforming considering integration with electrolysis and CO2 capture. *Cleaner Engineering and Technology,* 10**,** 100552.

KAUPP, A. & GOSS, J. R. 1984. History of Small Gas Producer Engine Systems. *Small Scale Gas Producer-Engine Systems.* Wiesbaden: Vieweg+ Teubner Verlag.

KAZA, S., YAO, L. C., BHADA-TATA, P. & VAN WOERDEN, F. 2018. What a Waste 2.0: A Global Snapshot of Solid Waste Management to 2050. Washington, DC: World Bank.

KIRSANOVS, V., ŽANDECKIS, A., BLUMBERGA, D. & VEIDENBERGS, I. The influence of process temperature, equivalence ratio and fuel moisture content on gasification process: A review. In Proceedings of the 27th International Conference on Efficiency, Cost, Optimization, Simulation and Environmental Impact of Energy Systems—ECOS, 2014 Turku, Finland.

KLUSKA, J., TURZYŃSKI, T., OCHNIO, M. & KARDAŚ, D. 2020. Characteristics of ash formation in the process of combustion of pelletised leather tannery waste and hardwood pellets. *Renewable energy,* 149**,** 1246-1253.

KNOEF, H. 2005. *Handbook biomass gasification,* Netherlands, BTG biomass technology group.

KONG, L., BAI, J. & LI, W. 2021. Viscosity-temperature property of coal ash slag at the condition of entrained flow gasification: A review. *Fuel Processing Technology,* 215**,** 106751.

KOPPATZ, S., PFEIFER, C. & HOFBAUER, H. 2011. Comparison of the performance behaviour of silica sand and olivine in a dual fluidised bed reactor system for steam gasification of biomass at pilot plant scale. *Chemical Engineering Journal,* 175**,** 468-483.

KOPPATZ, S., PFEIFER, C., RAUCH, R., HOFBAUER, H., MARQUARD-MOELLENSTEDT, T. & SPECHT, M. 2009. H2 rich product gas by steam gasification of biomass with in situ CO2 absorption in a dual fluidized bed system of 8 MW fuel input. *Fuel Processing Technology,* 90**,** 914-921.

KORONEOS, C., DOMPROS, A., ROUMBAS, G. & MOUSSIOPOULOS, N. 2004. Life cycle assessment of hydrogen fuel production processes. *International journal of hydrogen energy,* 29**,** 1443-1450.

KUMAR, A., JONES, D. D. & HANNA, M. A. 2009. THERMOCHEMICAL BIOMASS GASIFICATION—A REVIEW OF THE CURRENT STATUS OF THE TECHNOLOGY. *Energies,* 2**,** 556-581.

KURNIAWAN, T. A., OTHMAN, M. H. D., SINGH, D., AVTAR, R., HWANG, G. H., SETIADI, T. & LO, W. H. 2022. Technological solutions for long-term storage of partially used nuclear waste: A critical review. *Annals of Nuclear Energy,* 166**,** 108736.

LAHIJANI, P., ZAINAL, Z. A., MOHAMMADI, M. & MOHAMED, A. R. 2015. Conversion of the greenhouse gas CO2 to the fuel gas CO via the Boudouard reaction: A review. *Renewable and Sustainable Energy Reviews,* 41**,** 615-632.

LAM, C. H., IP, A. W., BARFORD, J. P. & MCKAY, G. 2010. Use of incineration MSW ash: a review. *Sustainability,* 2**,** 1943-1968.

LANGLEY, J. 2022. Decline in English RDF exports slowing, data shows. *Letsrecycle*.

LAOSENA, R., PALAMANIT, A., LUENGCHAVANON, M., KITTIJARUWATTANA, J., NAKASON, C., LEE, S. H. & CHOTIKHUN, A. 2022. Characterization of mixed pellets made from rubberwood (hevea brasiliensis) and refuse-derived fuel (RDF) waste as pellet fuel. *Materials,* 15**,** 3093.

LE, C. D. & KOLACZKOWSKI, S. T. 2015. Steam gasification of a refuse derived char: Reactivity and kinetics. *Chemical Engineering Research and Design,* 102**,** 389-398.

LEBROUHI, B. E., DJOUPO, J. J., LAMRANI, B., BENABDELAZIZ, K. & KOUSKSOU, T. 2022. Global hydrogen development-A technological and geopolitical overview. *International Journal of Hydrogen Energy,* 47**,** 7016-7048.

LEE, D. Y. & ELGOWAINY, A. 2018. By-product hydrogen from steam cracking of natural gas liquids (NGLs): Potential for large-scale hydrogen fuel production, life-cycle air emissions reduction, and economic benefit. *International Journal of Hydrogen Energy,* 43**,** 20143-20160.

LEE, H. C., JIANG, L. Y. & MOHAMAD, A. A. 2014. A review on the laminar flame speed and ignition delay time of Syngas mixtures. *International Journal of Hydrogen Energy,* 39**,** 1105-1121.

LEE, J. H. & TRIMM, D. L. 1995. Catalytic combustion of methane. *Fuel processing technology,* 42**,** 339-359.

LENG, L., XIONG, Q., YANG, L., LI, H., ZHOU, Y., ZHANG, W., JIANG, S., LI, H. & HUANG, H. 2021. An overview on engineering the surface area and porosity of biochar. *Science of the total Environment,* 763**,** 144204.

LENIS, Y. A., OSORIO, L. F. & PÉREZ, J. F. 2013. Fixed bed gasification of wood species with potential as energy crops in Colombia: The Effect of the physicochemical properties. *Energy Sources, Part A: Recovery, Utilization, and Environmental Effects,* 35**,** 1608-1617.

LI, J., XU, K., YAO, X. & CHEN, S. 2021a. Prediction and optimization of syngas production from steam gasification: Numerical study of operating conditions and biomass composition. *Energy Conversion and Management,* 236**,** 114077.

LI, W., LI, Q., CHEN, R., WU, Y. AND ZHANG, Y. 2014. Investigation of hydrogen production using wood pellets gasification with steam at high temperature over 800 C to 1435 C. *International journal of hydrogen energy,* 39**,** 5580-5588.

LI, X., LI, P., WU, Z., LUO, D., YU, H. Y. & LU, Z. H. 2021b. Review and perspective of materials for flexible solar cells. *Materials Reports: Energy,* 1**,** 100001.

LI, X. T., GRACE, J. R., LIM, C. J., WATKINSON, A. P., CHEN, H. P. & KIM, J. R. 2004. Biomass gasification in a circulating fluidized bed. *Biomass and bioenergy,* 26**,** 171-193.

LI, Y., PANG, Y., TU, H., TORRIGINO, F., BIOLLAZ, S. M., LI, Z., HUANG, Y., YIN, X., GRIMM, F. & KARL, J. 2021c. Impact of syngas from biomass gasification on solid oxide fuel cells: A review study for the energy transition. *Energy Conversion and Management,* 250**,** 114894.

LI, Y., WEI, C., LIU, X., ZHANG, Z., WAN, J. & HE, X. 2023. Application of gasification slag in construction materials and high value-added materials: a review. *Construction and Building Materials,* 402**,** 133013.

LIPIÄINEN, S., SERMYAGINA, E., KUPARINEN, K. & VAKKILAINEN, E. 2022. Future of forest industry in carbon-neutral reality: Finnish and Swedish visions. *Energy Reports,* 8**,** 2588-2600.

LIU, Z., DENG, Z., DAVIS, S. J., GIRON, C. & CIAIS, P. 2022. Monitoring global carbon emissions in 2021. *Nature Reviews Earth & Environment,* 3**,** 217-219.

LOSS, S. R., WILL, T. & MARRA, P. P. 2013. Estimates of bird collision mortality at wind facilities in the contiguous United States. *Biological Conservation,* 168**,** 201-209.

LUO, S., ZHOU, Y. & YI, C. 2012. Syngas production by catalytic steam gasification of municipal solid waste in fixed-bed reactor. *Energy,* 44**,** 391-395.

LUQUE, R. & CLARK, J. 2010. *Handbook of biofuels production: Processes and technologies*, Elsevier.

MA, W., CHU, C., WANG, P., GUO, Z., LIU, B. & CHEN, G. 2020. Characterization of tar evolution during DC thermal plasma steam gasification from biomass and plastic mixtures: Parametric optimization via response surface methodology. *Energy Conversion and Management,* 225**,** 113407.

MAGELLI, F., BOUCHER, K., BI, H. T., MELIN, S. & BONOLI, A. 2009. An environmental impact assessment of exported wood pellets from Canada to Europe. *Biomass and Bioenergy,* 33**,** 434-441.

MAHINPEY, N. & GOMEZ, A. 2016. Review of gasification fundamentals and new findings: Reactors, feedstock, and kinetic studies. *Chemical Engineering Science,* 148**,** 14-31.

MAKARYAN, I. A., SALGANSKY, E. A., ARUTYUNOV, V. S. & SEDOV, I. V. 2023. Non-Catalytic Partial Oxidation of Hydrocarbon Gases to Syngas and Hydrogen: A Systematic Review. *Energies,* 16**,** 2916.

MANEERUNG, T., LI, X., LI, C., DAI, Y. & WANG, C. H. 2018. Integrated downdraft gasification with power generation system and gasification bottom ash reutilization for clean waste-to-energy and resource recovery system. *Journal of cleaner production,* 188**,** 69-79.

MANKASEM, J., PRASERTCHAROENSUK, P. & PHAN, A. N. 2023. Intensification of two-stage biomass gasification for hydrogen production. *International Journal of Hydrogen Energy*.
MARTIGNON, G. P. 2020. Trends in the use of solid recovered fuels. IEA Bioenergy.
MAUERHOFER, A. M., FUCHS, J., MÜLLER, S., BENEDIKT, F., SCHMID, J. C. & HOFBAUER, H. 2019. CO2 gasification in a dual fluidized bed reactor system: Impact on the product gas composition. *Fuel,* 253**,** 1605-1616.
MEDNIKOV, A. S. 2018. A review of technologies for multistage wood biomass gasification. *Thermal Engineering,* 65**,** 531-546.
MEHMETI, A., ANGELIS-DIMAKIS, A., ARAMPATZIS, G., MCPHAIL, S. J. & ULGIATI, S. 2018. Life cycle assessment and water footprint of hydrogen production methods: from conventional to emerging technologies. *Environments,* 5**,** 24.
MICHEL, R., RAPAGNÀ, S., BURG, P., DI CELSO, G. M., COURSON, C., ZIMNY, T. & GRUBER, R. 2011. Steam gasification of Miscanthus X Giganteus with olivine as catalyst production of syngas and analysis of tars (IR, NMR and GC/MS). *biomass and bioenergy,* 35**,** 2650-2658.
MILEWSKI, J., KUPECKI, J., SZCZĘŚNIAK, A. & UZUNOW, N. 2021. Hydrogen production in solid oxide electrolyzers coupled with nuclear reactors. *International Journal of Hydrogen Energy,* 46**,** 35765-35776.
MILNE, T. A., EVANS, R. J. & ABATZAGLOU, N. 1998. Biomass gasifier''Tars'': their nature, formation, and conversion. Golden, US: National Renewable Energy Laboratory.
MINH, D. P., SIANG, T.J., VO, D.V.N., PHAN, T.S., RIDART, C., NZIHOU, A. AND GROUSET, D. 2018. *Hydrogen Supply Chains*, Academic Press.
MISHRA, S. & UPADHYAY, R. K. 2021. Review on biomass gasification: Gasifiers, gasifying mediums, and operational parameters. *Materials Science for Energy Technologies,* 4**,** 329-340.
MOLBURG, J. C. & DOCTOR, R. D. Hydrogen from steam-methane reforming with CO2 capture. 20th annual international Pittsburgh coal conference, September 2003. 1-21.
MOLINO, A., IOVANE, P., DONATELLI, A., BRACCIO, G., CHIANESE, S. & MUSMARRA, D. 2013. Steam gasification of refuse-derived fuel in a rotary kiln pilot plant: Experimental tests. . *Chem. Eng. Trans.,* 32**,** 337.
MONTGOMERY, D. C. 2017. *Design and analysis of experiments*, John wiley & sons.
MOREAU, L., THIFFAULT, E., KURZ, W. A. & BEAUREGARD, R. 2023. Under what circumstances can the forest sector contribute to 2050 climate change mitigation targets? A study from forest ecosystems to landfill methane emissions for the province of Quebec, Canada. *GCB Bioenergy,* 15**,** 1119-1139.
MSHEIK, M., RODAT, S. & ABANADES, S. 2021. Methane Cracking for Hydrogen Production: A Review of Catalytic and Molten Media Pyrolysis. *Energies,* 14**,** 3107.
MURADOV, N., RAMASAMY, K., LINKOUS, C., HUANG, C., ADEBIYI, I., SMITH, F., ALI, T. & STEVENS, J. 2010. Combined pre-reforming–desulfurization of high-sulfur fuels for distributed hydrogen applications. *Fuel,* 89**,** 1221-1229.
NANDA, S. & BERRUTI, F. 2021. Municipal solid waste management and landfilling technologies: a review. *Environmental Chemistry Letters,* 19**,** 1433-1456.
NECHACHE, A. & HODY, S. 2021. Alternative and innovative solid oxide electrolysis cell materials: A short review. *Renewable and Sustainable Energy Reviews,* 149**,** 111322.
NERL 2016. Gasification Plant Databases. U. S. Department of Energy, National Energy Technology Laboratory's Gasification Plant Databases.
NETL 2014. China Gasification Database. National Energy Technology Laboratory (NERL).
NG, K. S., PHAN, A. N., IACOVIDOU, E. & GHANI, W. A. W. A. K. 2021. Techno-economic assessment of a novel integrated system of mechanical-biological treatment and valorisation of residual municipal solid waste into hydrogen: A case study in the UK. *Journal of Cleaner Production,* 298**,** 126706.
NGAMCHOMPOO, W. & TRIRATANASIRICHAI, K. 2017. Experimental investigation of high temperature air and steam biomass gasification in a fixed-bed downdraft gasifier. *Energy Sources, Part A: Recovery, Utilization, and Environmental Effects,* 39(8)**,** 733-740.

NGO, T. N. L. T., CHIANG, K. Y., LIU, C. F., CHANG, Y. H. & WAN, H. P. 2021. Hydrogen production enhancement using hot gas cleaning system combined with prepared Ni-based catalyst in biomass gasification. *International Journal of Hydrogen Energy,* 46**,** 11269-11283.

NIEVA, M. A., VILLAVERDE, M. M., MONZÓN, A., GARETTO, T. F. & MARCHI, A. J. 2014. Steam-methane reforming at low temperature on nickel-based catalysts. *Chemical Engineering Journal,* 235**,** 158-166.

NILSSON, S., GÓMEZ-BAREA, A., FUENTES-CANO, D. & OLLERO, P. 2012. Gasification of biomass and waste in a staged fluidized bed gasifier: Modeling and comparison with one-stage units. *Fuel,* 97**,** 730-740.

NIU, M., HUANG, Y., JIN, B., SHAOHUA, L., DONG, Q., GU, H. & SUN, R. 2019. A novel two-stage enriched air biomass gasification for producing low-tar high heating value fuel gas: Pilot verification and performance analysis. *Energy*.

NIU, M., HUANG, Y., JIN, B. & WANG, X. 2014. Oxygen gasification of municipal solid waste in a fixed-bed gasifier. *Chinese Journal of Chemical Engineering,* 22**,** 1021-1026.

NOBRE, C., LONGO, A., VILARINHO, C. & GONÇALVES, M. 2020. Gasification of pellets produced from blends of biomass wastes and refuse derived fuel chars. *Renewable Energy,* 154**,** 1294-1303.

NÚÑEZ, M., PFISTER, S., ANTÓN, A., MUÑOZ, P., HELLWEG, S., KOEHLER, A. & RIERADEVALL, J. 2013. Assessing the environmental impact of water consumption by energy crops grown in Spain. *Journal of Industrial Ecology,* 17**,** 90-102.

OBERSTEINER, G., BINNER, E., MOSTBAUER, P. & SALHOFER, S. 2007. Landfill modelling in LCA–a contribution based on empirical data. *Waste management,* 27**,** 58-74.

OCAMPO, A., ARENAS, E., CHEJNE, F., ESPINEL, J., LONDONO, C., AGUIRRE, J. & PEREZ, J. D. 2003. An experimental study on gasification of Colombian coal in fluidised bed. *Fuel,* 82**,** 161-164.

OJOVAN, M. I. & STEINMETZ, H. J. 2022. Approaches to Disposal of Nuclear Waste. *Energies,* 15**,** 7804.

OSMAN, A. I., MEHTA, N., ELGARAHY, A. M., HEFNY, M., AL-HINAI, A., AL-MUHTASEB, A. A. H. & ROONEY, D. W. 2022. Hydrogen production, storage, utilisation and environmental impacts: a review. *Environmental Chemistry Letters***,** 1-36.

OU, Z., ZHANG, Z., QIN, C., XIA, H., DENG, T., NIU, J., RAN, J. & WU, C. 2021. Highly active and stable Ni/perovskite catalysts in steam methane reforming for hydrogen production. *Sustainable Energy & Fuels,* 5**,** 1845-1856.

OUYANG, J., HONG, D., JIANG, L., LI, Z., LIU, H., LUO, G. AND YAO, H. 2020. Effect of CO2 and H2O on char properties. Part 1: pyrolysis char structure and reactivity. *Energy & Fuels,* 34**,** 4243-4250.

PARIKH, J., CHANNIWALA, S.A. AND GHOSAL, G.K. 2005. A correlation for calculating HHV from proximate analysis of solid fuels. *Fuel,* 84(5)**,** 487-494.

PARTHASARATHY, P. & NARAYANAN, K. S. 2014. Hydrogen production from steam gasification of biomass: influence of process parameters on hydrogen yield–a review. *Renewable Energy,* 66**,** 570-579.

PASHCHENKO, D. 2018. First law energy analysis of thermochemical waste-heat recuperation by steam methane reforming. *Energy,* 143**,** 478-487.

PASHCHENKO, D. 2019. Numerical study of steam methane reforming over a pre-heated Ni-based catalyst with detailed fluid dynamics. *Fuel,* 236**,** 686-694.

PATTABATHULA, V. & RICHARDSON, J. 2016. Introduction to ammonia production. *Chem. Eng. Prog,* 112**,** 69-75.

PATUZZI, F., BASSO, D., VAKALIS, S., ANTOLINI, D., PIAZZI, S., BENEDETTI, V., CORDIOLI, E. & BARATIERI, M. 2021. State-of-the-art of small-scale biomass gasification systems: An extensive and unique monitoring review. *Energy,* 223**,** 120039.

PEI, H., WANG, X., DAI, X., JIN, B. & HUANG, Y. 2018. A novel two-stage biomass gasification concept: Design and operation of a 1.5 MWth demonstration plant. *Bioresource technology,* 267**,** 102-109.

PHAN, A. N., RYU, C., SHARIFI, V. N. & SWITHENBANK, J. 2008. Characterisation of slow pyrolysis products from segregated wastes for energy production. *Journal of Analytical and Applied Pyrolysis,* 81**,** 65-71.

PIO, D. T. & TARELHO, L. A. C. 2021. Industrial gasification systems (> 3 MWth) for bioenergy in Europe: Current status and future perspectives. *Renewable and Sustainable Energy Reviews,* 145**,** 111108.

PLACIDO, A., CHALLMAN, D., LIU, K., ANDREWS, R., JACOBS, G., DAVIS, B., MA, W. & DARKWAH, K. 2018. Small-scale pilot plant for gasification of coal and coal/biomass blends and conversion of derived syngas to liquid fuels via Fischer-Tropsch synthesis. University of Kentucky, United States: Reasearch Foundation.

POHOŘELÝ, M., VOSECKÝ, M., HEJDOVÁ, P., PUNČOCHÁŘ, M., SKOBLJA, S., STAF, M., VOŠTA, J., KOUTSKÝ, B. & SVOBODA, K. 2006. Gasification of coal and PET in fluidized bed reactor. *Fuel,* 85**,** 2458-2468.

PRASERTCHAROENSUK, P. 2019. *Gasification of waste for hydrogen production.* Doctor of Philosophy, Newcastle University.

PRASERTCHAROENSUK, P., BULL, S. J. & PHAN, A. N. 2019. Gasification of waste biomass for hydrogen production: Effects of pyrolysis parameters. *Renewable Energy,* 143**,** 112-120.

QIAN, J. X., CHEN, T. W., ENAKONDA, L. R., LIU, D. B., BASSET, J. M. & ZHOU, L. 2020. Methane decomposition to pure hydrogen and carbon nano materials: State-of-the-art and future perspectives. *International Journal of Hydrogen Energy,* 45**,** 15721-15743.

RANZI, E., CUOCI, A., FARAVELLI, T., FRASSOLDATI, A., MIGLIAVACCA, G., PIERUCCI, S. & SOMMARIVA, S. 2008. Chemical kinetics of biomass pyrolysis. *Energy & Fuels,* 22**,** 4292-4300.

RAPAGNÀ, S., VIRGINIE, M., GALLUCCI, K., COURSON, C., DI MARCELLO, M., KIENNEMANN, A. & FOSCOLO, P. U. 2011. Fe/olivine catalyst for biomass steam gasification: Preparation, characterization and testing at real process conditions. *Catalysis Today,* 176**,** 163-168.

RASUL, M. G., HAZRAT, M. A., SATTAR, M. A., JAHIRUL, M. I. & SHEARER, M. J. 2022. The future of hydrogen: Challenges on production, storage and applications. *Energy Conversion and Management,* 272**,** 116326.

READ, A. 2017. *What is the future of RDF?* [Online]. Recycling and Waste World. Available: http://www.recyclingwasteworld.co.uk/in-depth-article/what-is-the-future-for-rdf/157066/ [Accessed 04/11/2019].

REARDON, T. 2018. Opinion: It's time to reinvent the waste-to-energy industry. *Waste Today*.

REINMÖLLER, M., SCHREINER, M., GUHL, S., NEUROTH, M. & MEYER, B. 2019. Ash behavior of various fuels: The role of the intrinsic distribution of ash species. *Fuel,* 253**,** 930-940.

REN, J., LIU, Y. L., ZHAO, X. Y. & CAO, J. P. 2020. Methanation of syngas from biomass gasification: An overview. *International Journal of Hydrogen Energy,* 45**,** 4223-4243.

REN, R., WANG, H. & YOU, C. 2022. Steam Gasification of Refuse-Derived Fuel with CaO Modification for Hydrogen-Rich Syngas Production. *Energies,* 15**,** 8279.

REN, Z., VERMA, A. S., LI, Y., TEUWEN, J. J. & JIANG, Z. 2021. Offshore wind turbine operations and maintenance: A state-of-the-art review. *Renewable and Sustainable Energy Reviews,* 144**,** 110886.

REUBENS, J. T., DEGRAER, S. & VINCX, M. 2011. Aggregation and feeding behaviour of pouting (Trisopterus luscus) at wind turbines in the Belgian part of the North Sea. *Fisheries Research,* 108**,** 223-227.

RIBEIRO, A., VILARINHO, C., ARAÚJO, J. & CARVALHO, J. Refuse Derived Fuel (RDF) Gasification Using Different Gasifying Agents. ASME 2017 International Mechanical Engineering Congress and Exposition, 2017. V006T08A057.

RITCHIE, H. & ROSER, M. 2021. *Forests and deforestation* [Online]. Our world in data. Available: https://ourworldindata.org/deforestation?ref=planksip.org [Accessed].

RITTER, J. A. & EBNER, A. D. 2007. State-of-the-art adsorption and membrane separation processes for hydrogen production in the chemical and petrochemical industries. *Separation Science and Technology,* 42**,** 1123-1193.

ROBINSON, T., BRONSON, B., GOGOLEK, P. & MEHRANI, P. 2016. Comparison of the air-blown bubbling fluidized bed gasification of wood and wood–PET pellets. *Fuel,* 178**,** 263-271.

ROBINSON, T., BRONSON, B., GOGOLEK, P. & MEHRANI, P. 2017. Air-blown bubbling fluidized bed co-gasification of woody biomass and refuse derived fuel. *The Canadian journal of chemical engineering,* 95(1)**,** 55-61.
ROGOFF, M. J. & SCREVE, F. 2019. Waste-to-energy: technologies and project implementation. *Chapter 3 - Energy from Waste Technology.* Academic Press.
ROSTRUPNIELSEN, J. R. & HANSEN, J. B. 1993. CO2-reforming of methane over transition metals. *Journal of Catalysis,* 144**,** 38-49.
RUSSEL, B. 1977. Energy Tax Act of 1977. Washington, US: U.S. Government printing office.
SA, M., ZHANG, B. & ZHU, S. 2021. Miscanthus: Beyond its use as an energy crop. *BioResources,* 16**,** 5.
SADEKIN, S. M. S., ZAMAN, S., MAHFUZ, M. K. & SARKAR, R. 2019. Nuclear power as foundation of a clean energy future: A review. *Energy Procedia*.
SAFDARI, M. S., AMINI, E., WEISE, D. R. & FLETCHER, T. H. 2019. Heating rate and temperature effects on pyrolysis products from live wildland fuels. *Fuel,* 242**,** 295-304.
SAJID, M., RAHEEM, A., ULLAH, N., ASIM, M., REHMAN, M. S. U. & ALI, N. 2022. Gasification of municipal solid waste: Progress, challenges, and prospects. *Renewable and Sustainable Energy Reviews,* 168**,** 112815.
SALEEM, F., UMER, J., REHMAN, A., ZHANG, K. & HARVEY, A. 2019. Effect of Methane as an Additive in the Product Gas toward the Formation of Lower Hydrocarbons during the Decomposition of a Tar Analogue. *Energy & Fuels,* 34**,** 1744-1749.
SALMAN, C. A. & OMER, C. B. 2020. Process modelling and simulation of waste gasification-based flexible polygeneration facilities for power, heat and biofuels production. *Energies,* 13**,** 4264.
SAMBYAL, S. S. 2018. Government notifies new solid waste management rules. *DownToEarth*.
SARACENO, E., RUOCCO, C. & PALMA, V. 2023. A Review of Coal and Biomass Hydrogasification: Process Layouts, Hydrogasifiers, and Catalysts. *Catalysts,* 13**,** 417.
SCHMID, M., BEIROW, M., SCHWEITZER, D., WAIZMANN, G., SPÖRL, R. & SCHEFFKNECHT, G. 2018. Product gas composition for steam-oxygen fluidized bed gasification of dried sewage sludge, straw pellets and wood pellets and the influence of limestone as bed material. *Biomass and Bioenergy,* 117**,** 71-77.
SCHWEITZER, D., GREDINGER, A., SCHMID, M., WAIZMANN, G., BEIROW, M., SPÖRL, R. & SCHEFFKNECHT, G. 2018. Steam gasification of wood pellets, sewage sludge and manure: Gasification performance and concentration of impurities. *Biomass and Bioenergy,* 111**,** 308-319.
SELVARAJOO, A., WONG, Y.L., KHOO, K.S., CHEN, W.H. AND SHOW, P.L. 2022. Biochar production via pyrolysis of citrus peel fruit waste as a potential usage as solid biofuel. *Chemosphere,* 294**,** 133671.
SETTER, C., SILVA, F. T. M., ASSIS, M. R., ATAÍDE, C. H., TRUGILHO, P. F. & OLIVEIRA, T. J. P. 2020. Slow pyrolysis of coffee husk briquettes: Characterization of the solid and liquid fractions. *Fuel,* 261**,** 116420.
SHAH, Y. T. & GARDNER, T. H. 2014. Dry reforming of hydrocarbon feedstocks. *Catalysis Reviews,* 56**,** 476-536.
SHAHABUDDIN, M. & BHATTACHARYA, S. 2021. Effect of reactant types (steam, CO2 and steam+ CO2) on the gasification performance of coal using entrained flow gasifier. *International Journal of Energy Research,* 45**,** 9492-9501.
SHAHABUDDIN, M. A. A., T. 2022. Gasification of solid fuels (coal, biomass and MSW): overview, challenges and mitigation strategies. *Energies,* 15**,** 4444.
SHAMSUDIN, I. K., ABDULLAH, A., IDRIS, I., GOBI, S. & OTHMAN, M. R. 2019. Hydrogen purification from binary syngas by PSA with pressure equalization using microporous palm kernel shell activated carbon. *Fuel,* 253**,** 722-730.
SHARMA, P., SHETH, P. N. & MOHAPATRA, B. N. 2022a. Recent Progress in Refuse Derived Fuel (RDF) Co-processing in Cement Production: Direct Firing in Kiln/Calciner vs Process Integration of RDF Gasification *Waste and Biomass Valorization***,** 1-28.

SHARMA, P., SHETH, P. N. & MOHAPATRA, B. N. 2022b. Co-processing of petcoke and producer gas obtained from RDF gasification in a white cement plant: A echno-economic analysis. *Energy*, 126248.

SHARMA, S. D., DOLAN, M., PARK, D., MORPETH, L., ILYUSHECHKIN, A., MCLENNAN, K., HARRIS, D. J. & THAMBIMUTHU, K. V. 2008. A critical review of syngas cleaning technologies—fundamental limitations and practical problems. *Powder Technology,* 180**,** 115-121.

SHEN, M., YE, S., ZENG, G., ZHANG, Y., XING, L., TANG, W., WEN, X. & LIU, S. 2020. Can microplastics pose a threat to ocean carbon sequestration? *Marine pollution bulletin,* 150**,** 110712.

SIDEK, F. N., SAMAD, N. A. & SALEH, S. 2020. Review on effects of gasifying agents, temperature and equivalence ratio in biomass gasification process. *In IOP Conference Series: Materials Science and Engineering.* IOP Publishing.

SIEDLECKI, M., DE JONG, W. & VERKOOIJEN, A. H. 2011. Fluidized bed gasification as a mature and reliable technology for the production of bio-syngas and applied in the production of liquid transportation fuels—A review. *Energies,* 4(3)**,** 389-434.

SIMONE, M., BARONTINI, F., NICOLELLA, C. & TOGNOTTI, L. 2012. Gasification of pelletized biomass in a pilot scale downdraft gasifier. *Bioresource technology,* 116**,** 403-12.

SIMONS, A. & BAUER, C. 2011. Life cycle assessment of hydrogen production. *In:* WOKAUN, A. & WILHELM, E. (eds.) *Transition to Hydrogen: Pathways toward Clean Transportation.*

SIMPSON, A. P. & LUTZ, A. E. 2007. Exergy analysis of hydrogen production via steam methane reforming. *International journal of hydrogen energy,* 32**,** 4811-4820.

SITUMORANG, Y. A., ZHAO, Z., YOSHIDA, A., ABUDULA, A. & GUAN, G. 2020. Small-scale biomass gasification systems for power generation (< 200 kW class): A review. *Renewable and Sustainable Energy Reviews,* 117**,** 109486.

SIWAL, S. S., ZHANG, Q., SUN, C., THAKUR, S., GUPTA, V. K. & THAKUR, V. K. 2020. Energy production from steam gasification processes and parameters that contemplate in biomass gasifier–A review. *Bioresource technology,* 297**,** 122481.

SLATTER, N. L., VICHANPOL, B., NATAKARANAKUL, J., WATTANAVICHIEN, K., SUCHAMALAWONG, P., HASHIMOTO, K., TSUBAKI, N., VITIDSANT, T. & CHARUSIRI, W. 2022. Syngas Production for Fischer–Tropsch Synthesis from Rubber Wood Pellets and Eucalyptus Wood Chips in a Pilot Horizontal Gasifier with CaO as a Tar Removal Catalyst. *ACS omega,* 7**,** 44951-44961.

SLOW, E. 2019. RDF exports decline in 2018. LetsRecycle.

SMOOT, L. D. & BROWN, B. W. 1987. Controlling mechanisms in gasification of pulverized coal. *Fuel,* 66**,** 1249-1256.

SOLAR, J., CABALLERO, B. M., DE MARCO, I., LÓPEZ-URIONABARRENECHEA, A. & GASTELU, N. 2018. Optimization of charcoal production process from woody biomass waste: Effect of Ni-containing catalysts on pyrolysis vapors. *Catalyst,* 8**,** 191.

SONG, Y., WANG, Y., HU, X., XIANG, J., HU, S., MOURANT, D., LI, T., WU, L. & LI, C. Z. 2015. Effects of volatile–char interactions on in-situ destruction of nascent tar during the pyrolysis and gasification of biomass. Part II. Roles of steam. *Fuel,* 143**,** 555-562.

SPEIGHT, J. G. 2014. *Gasification of unconventional feedstocks*, Gulf Professional Publishing.

ŚPIEWAK, K., CZERSKI, G. & BIJAK, K. 2021. The Effect of Temperature-Pressure Conditions on the RDF Gasification in the Atmosphere of Steam and Carbon Dioxide. *Energies,* 14**,** 7502.

SPRENGER, C. J., TABIL, L. G., SOLEIMANI, M., AGNEW, J. & HARRISON, A. 2018. Pelletization of Refuse-Derived Fuel Fluff to Produce High Quality Feedstock. *Journal of Energy Resources Technology,* 140**,** 042003.

STAPF, D., CECERI, G., JOHANSSON, I. & WHITTY, K. 2019. Biomass pre-treatment for bioenergy: Case study 3 – Pretreatment of municipal solid waste (MSW) for gasification. IEA Bioenergy.

STĘPIEŃ, P., PULKA, J., SEROWIK, M. & BIAŁOWIEC, A. 2019. Thermogravimetric and calorimetric characteristics of alternative fuel in terms of its use in low-temperature pyrolysis. *Waste and Biomass Valorization,* 10**,** 1669-1677.

STEYNBERG, A. P. 2004. Introduction to fischer-tropsch technology. *Studies in surface science and catalysis.* Elsevier.

STRANDBERG, A., HOLMGREN, P., WAGNER, D.R., MOLINDER, R., WIINIKKA, H., UMEKI, K. AND BROSTRÖM, M. 2017. Effects of pyrolysis conditions and ash formation on gasification rates of biomass char. *Energy & Fuels,* 31**,** 6507-6514.

STRAUSS, W. 2023. *2023 wood pellet markets outlook* [Online]. Available: https://www.canadianbiomassmagazine.ca/2023-wood-pellet-markets-outlook/ [Accessed 05 December 2023].

ŠULC, J., ŠTOJDL, J., RICHTER, M., POPELKA, J., SVOBODA, K., SMETANA, J., VACEK, J., SKOBLJA, S. & BURYAN, P. 2012. Biomass waste gasification - can be the two stage process suitable for tar reduction and power generation? *Waste management,* 32 4**,** 692-700.

SURIAPPARAO, D. V. A. V., R. 2015. Bio-oil production via catalytic microwave pyrolysis of model municipal solid waste component mixtures

. *RSC Advances,* 5(71)**,** 57619-57631.

TANG, Y., MA, X., WANG, Z., WU, Z. & YU, Q. 2017. A study of the thermal degradation of six typical municipal waste components in CO2 and N2 atmospheres using TGA-FTIR. *Thermochimica Acta,* 657**,** 12-19.

TANOH, T. S., AIT OUMEZIANE, A., LEMONON, J., ESCUDERO SANZ, F. J. & SALVADOR, S. 2020. Green Waste/Wood Pellet Pyrolysis in a Pilot-Scale Rotary Kiln: Effect of Temperature on Product Distribution and Characteristics. *Energy & Fuels,* 34**,** 3336-3345.

THE INTERNATIONAL ENERGY AGENCY, I. 2023. Towards hydrogen definitions based on their emissions intensity. The International Energy agency.

THOMSEN, T. P., SÁROSSY, Z., GØBEL, B., STOHOLM, P., AHRENFELDT, J., FRANDSEN, F. J. & HENRIKSEN, U. B. 2017. Low temperature circulating fluidized bed gasification and co-gasification of municipal sewage sludge. Part 1: Process performance and gas product characterization. *Waste Management,* 66**,** 123-133.

THRÄN, D., PEETZ, D. & SCHAUBACH, K. 2017. Global Wood Pellet Industry and Trade Study 2017. IEA Bioenergy Task 40.

TIAN, T., LI, Q., HE, R., TAN, Z. & ZHANG, Y. 2017. Effects of biochemical composition on hydrogen production by biomass gasification. *International Journal of Hydrogen Energy,* 42**,** 19723-19732.

TISEO, I. 2018. Projected generation of municipal solid waste worldwide from 2016 to 2050 (in billion metric tons) [Grap]. *In:* BANK, W. (ed.). Statista.

TOSTI, S., SOUSA, M. A., BUCETI, G., MADEIRA, L. M. & POZIO, A. 2019. Process analysis of refuse derived fuel hydrogasification for producing SNG. *International Journal of Hydrogen Energy,* 44(39)**,** 21470-21480.

TURSUN, Y., XU, S., WANG, C., XIAO, Y. & WANG, G. 2016. Steam co-gasification of biomass and coal in decoupled reactors. *Fuel Processing Technology,* 141**,** 61-67.

ULUSOY, B., WU, H., LIN, W., KARLSTRÖM, O., LI, S., SONG, W., GLARBORG, P. & DAM-JOHANSEN, K. 2019. Reactivity of sewage sludge, RDF, and straw chars towards NO. *Fuel,* 236**,** 297-305.

UMEKI, K., YAMAMOTO, K., NAMIOKA, T. & YOSHIKAWA, K. 2010. High temperature steam-only gasification of woody biomass. *Applied energy,* 87**,** 791-798.

VAISH, B., SHARMA, B., SRIVASTAVA, V., SINGH, P., IBRAHIM, M. H. & SINGH, R. P. 2019. Energy recovery potential and environmental impact of gasification for municipal solid waste. *Biofuels,* 10**,** 87-100.

VALIZADEH, S., HAKIMIAN, H., FAROOQ, A., JEON, B. H., CHEN, W. H., LEE, S. H., JUNG, S. C., SEO, M. W. & PARK, Y. K. 2022. Valorization of biomass through gasification for green hydrogen generation: A comprehensive review. *Bioresource Technology***,** 128143.

VAMVUKA, D., AFTHENTOPOULOS, E. & SFAKIOTAKIS, S. 2022. H2-rich gas production from steam gasification of a winery waste and its blends with industrial wastes. Effect of operating parameters on gas quality and efficiency. *Renewable Energy* 197**,** 1224-1232.

VAN BEURDEN, P. 2004. On the catalytic aspects of steam-methane reforming. Energy Research Centre of the Netherlands (ECN).

VAN DE VEN, D. J., CAPELLAN-PERÉZ, I., ARTO, I., CAZCARRO, I., DE CASTRO, C., PATEL, P. & GONZALEZ-EGUINO, M. 2021. The potential land requirements and related land use change emissions of solar energy. *Scientific reports,* 11**,** 2907.

WAHEED, Q. M. K. 2013. *Ultra-high temperature steam gasification of biomass.* University of Leeds.

WALDHEIM, L. 2018. Gasification of waste for energy carriers: A review. IEA Bioenergy.

WALDHEIM, L., NILSSON, T. 2001. Heating value of gases from biomass gasification. IEA bioenergy agreement, Task, 20.

WANG, J., HUANG, Z., KOBAYASHI, H. & OGAMI, Y. 2012. Laminar burning velocities and flame characteristics of CO–H2–CO2–O2 mixtures. *international journal of hydrogen energy,* 37**,** 19158-19167.

WANG, J., LIU, J., ZHANG, L., DAI, S., LI, A. & CHEN, J. 2022. Synergistic effect of physico-chemical properties and reaction temperature on the gasification of coal-waste activated carbon-slurry coke for H2 production. *Fuel,* 327**,** 125076.

WANG, S., LU, A. & ZHONG, C. J. 2021a. Hydrogen production from water electrolysis: role of catalysts. *Nano Convergence,* 8**,** 1-23.

WANG, Y., TANG, Y., LI, R., GUO, X., HURLEY, J. P. & FINKELMAN, R. B. 2021b. Measurements of the leachability of potentially hazardous trace elements from solid coal gasification wastes in China. *Science of The Total Environment,* 759**,** 143463.

WANG, Y., WEN, C., TU, J., ZHAN, Z., ZHANG, B., LIU, Q., ZHANG, Z., HU, H. & LIU, T. 2023. The multi-scenario projection of cost reduction in hydrogen production by proton exchange membrane (PEM) water electrolysis in the near future (2020–2060) of China. *Fuel,* 354**,** 129409.

WANG, Z., BURRA, K. G., ZHANG, M., LI, X., HE, X., LEI, T. & GUPTA, A. K. 2020. Syngas evolution and energy efficiency in CO2-assisted gasification of pine bark. *Applied Energy,* 269**,** 114996.

WAS, G. S., PETTI, D., UKAI, S. & ZINKLE, S. 2019. Materials for future nuclear energy systems. *Journal of Nuclear Materials,* 527**,** 151837.

WEI, W. & JINLONG, G. 2011. Methanation of carbon dioxide: an overview. *Frontiers of Chemical Science and Engineering,* 5**,** 2-10.

WEI, W., ZHANG, W., HU, D., OU, L., TONG, Y., SHEN, G., SHEN, H. & WANG, X. 2012. Emissions of carbon monoxide and carbon dioxide from uncompressed and pelletized biomass fuel burning in typical household stoves in China. *Atmospheric environment,* 56**,** 136-142.

WIATOWSKI, M. & KAPUSTA, K. 2020. Evolution of tar compounds in raw gas from a pilot-scale underground coal gasification (UCG) trial at Wieczorek mine in Poland. *Fuel,* 276**,** 118070.

WIBERG, E., HOLLEMAN, A. F. & WIBERG, N. 2001. *Inorganic chemistry*, Academic press.

WIDJAYA, E. R., CHEN, G., BOWTELL, L. & HILLS, C. 2018. Gasification of non-woody biomass: A literature review. *Renewable and Sustainable Energy Reviews*.

WILBERFORCE, T., BAROUTAJI, A., SOUDAN, B., AL-ALAMI, A. H. & OLABI, A. G. 2019. Outlook of carbon capture technology and challenges. *Science of the total environment,* 657**,** 56-72.

WILBERFORCE, T., OLABI, A. G., SAYED, E. T., ELSAID, K. & ABDELKAREEM, M. A. 2021. Progress in carbon capture technologies. *Science of The Total Environment,* 761**,** 143203.

WIN, M. M., ASARI, M., HAYAKAWA, R., HOSODA, H., YANO, J. AND SAKAI, S.I., 2019. Characteristics of gas from the fluidized bed gasification of refuse paper and plastic fuel (RPF) and wood biomass. *Waste management,* 87**,** 173-182.

Y., L., Z., Z., W., T., T., Y. & R., L. 2016. Future Development of Waste Management in China According to the 13th Five-Year Plan. *Waste Management,* 6**,** 139-146.

YANG, J., CHANG, Y., ZHANG, L., HAO, Y., YAN, Q. & WANG, C. 2018. The life-cycle energy and environmental emissions of a typical offshore wind farm in China. *Journal of Cleaner Production,* 180**,** 316-324.

YANG, W., ZHANG, J. H., SI, R., CAO, L. M., ZHONG, D. C. & LU, T. B. 2021. Efficient and steady production of 1: 2 syngas (CO/H2) by simultaneous electrochemical reduction of CO2 and H2O. *Inorganic Chemistry Frontiers,* 8**,** 1695-1701.

YANG, Z., SARKAR, M., KUMAR, A., TUMULURU, J. S. & HUHNKE, R. L. 2014. Effects of torrefaction and densification on switchgrass pyrolysis products. *Bioresource technology,* 174**,** 266-273.

YAO, D., LI, H., DAI, Y. & WANG, C. H. 2021. Impact of temperature on the activity of Fe-Ni catalysts for pyrolysis and decomposition processing of plastic waste. *Chemical Engineering Journal,* 408**,** 127268.

YAO, D., ZHAO, H., CHEN, Z. & LIU, H. 2022. Preparation of high concentration coal water slurry with good fluidity based on preferentially modified ultrafine particle under three-peak grading. *International Journal of Coal Preparation and Utilization***,** 1-16.

YASAR, A., SADIQ, K., TABINDA, A. B., GHAFFAR, A., RASHEED, R. & IQBAL, A. 2021. Gasification of mixed waste at high temperature to enhance the syngas efficiency and reduce gaseous emissions and tar production. *Energy Sources***,** 1-10.

YAZDANI, E., HASHEMABADI, S. H. & TAGHIZADEH, A. 2019. Study of waste tire pyrolysis in a rotary kiln reactor in a wide range of pyrolysis temperature. *Waste Management,* 85**,** 195-201.

YOGALAKSHMI, K. N. S., P., KAVITHA, S., KANNAH, Y., VARJANI, S., ADISHKUMAR, S. & KUMAR, G. 2022. Lignocellulosic biomass-based pyrolysis: A comprehensive review. *Chemosphere,* 286**,** 131824.

YOUNG, B., HAWKINS, T. R., CHIQUELIN, C., SUN, P., GRACIDA-ALVAREZ, U. R. & ELGOWAINY, A. 2022. Environmental life cycle assessment of olefins and by-product hydrogen from steam cracking of natural gas liquids, naphtha, and gas oil. *Journal of Cleaner Production,* 359**,** 131884.

YU, S., PARK, J., KIM, M., KIM, H., RYU, C., LEE, Y., YANG, W. & JEONG, Y. G. 2019. Improving energy density and grindability of wood pellets by dry torrefaction. *Energy & Fuels,* 33**,** 8632-8639.

YUAN, T., TAHMASEBI, A. & YU, J. 2015. Comparative study on pyrolysis of lignocellulosic and algal biomass using a thermogravimetric and a fixed-bed reactor. *Bioresource technology,* 175**,** 333-341.

ZAINI, I. N., GARCÍA LÓPEZ, C., PRETZ, T., YANG, W. & JÖNSSON, P.G. 2019. Characterization of pyrolysis products of high-ash excavated-waste and its char gasification reactivity and kinetics under a steam atmosphere. *Waste Management,* 97**,** 149-163.

ZAINI, I. N., GOMEZ-RUEDA, Y., LÓPEZ, C. G., RATNASARI, D. K., HELSEN, L., PRETZ, T., JÖNSSON, P. G. & YANG, W. 2020. Production of H2-rich syngas from excavated landfill waste through steam co-gasification with biochar. *Energy,* 207**,** 118208.

ZAINI, I. N., LÓPEZ, C. G., PRETZ, T., YANG, W. & JÖNSSON, P. G. 2019. Characterization of pyrolysis products of high-ash excavated-waste and its char gasification reactivity and kinetics under a steam atmosphere. *Waste Management,* 97**,** 149-163.

ZAKRZEWSKA-KOŁTUNIEWICZ, G. 2017. Water management in nuclear power plant using advanced low temperature systems. *Eur. Wat,* 58**,** 345-350.

ZHANG, H., SUN, Z. & HU, Y. H. 2021a. Steam reforming of methane: Current states of catalyst design and process upgrading. *Renewable and Sustainable Energy Reviews,* 149**,** 111330.

ZHANG, S., HE, S., GAO, N., QUAN, C. & WU, C. 2022. Effect of steam addition for energy saving during CaCO3 calcination of auto thermal biomass gasification. *Biomass and Bioenergy,* 161**,** 106416.

ZHANG, Y., GHALY, A., MANSARAY, K. & LI, B. 2021b. Determination of the Energy and Exergy of the Syngas Produced from Gasification of Rice Husk at Different Fluidization Velocities and Equivalence Ratios. *Journal of Energy Resources and Conversion,* 1**,** 104.

ZHENG, J. L., ZHU, Y. H., SUN, G. T., DONG, Y. Y. & ZHU, M. Q. 2022. Bio-oil gasification for production of the raw gas as ammonia syngas. *Fuel,* 327**,** 125029.

ZWOLINSKI, D. 2015. UK and EU trade of wood pellets. UK Government.

Appendix A Proximate analysis

Moisture content (BS EN 14774-3: 2009)

Procedure:

1. Weighing the crucible (M_1): Begin by accurately weighing an empty crucible.
2. Sample preparation: Add at least 1 gram of the sample into the crucible, then weigh again to get M_2.
3. Drying: Place the crucible with the sample in an oven set at 105°C ±2. Dry for 2 hours.
4. Cooling: After drying, transfer the crucible to a desiccator to cool to room temperature.
5. Final weighing (M_3): Weigh the crucible with the dried sample.

Ash content (BS 1016-3: 1973)

Procedure:

1. Weighing the crucible (M_1): Weigh an empty crucible.
2. Sample preparation: Add at least 1 gram of the sample into the crucible, then weigh to get M_2.
3. Temperature increase: Gradually raise the temperature to 550°C to avoid thermal shock.
4. Incineration: Place the crucible with the sample in a muffle furnace. Note: Be cautious of any flames that might be generated during this step.
5. Duration: Leave in the furnace for at least 1 hour and 30 minutes, or until no black carbon remains.
6. Removal and cooling: Carefully remove the crucible from the furnace and allow it to cool on a thick metal plate for 10 minutes.
7. Final weighing (M_3): Weigh the crucible and the ash.
8. Residue removal (M_4): Brush out all the residue and reweigh the empty crucible.

Volatile matter content (BS 1016-3: 1973)

Procedure:

1. Weighing the crucible (M_1): Start with an empty crucible's weight.
2. Sample preparation: Add at least 1 gram of the sample, then weigh to get M_2.
3. Temperature preparation: Increase the temperature setting to 900°C.
4. Sample placement: Place the crucible and sample into a glass tube.
5. Nitrogen injection: Inject nitrogen at a rate of 100 ml/min for at least 7 minutes.
6. Heating: Place the glass tube with the sample in a 900°C furnace for exactly 7 minutes.
7. Removal and cooling: Remove the crucible and let it cool for 7 minutes in a nitrogen atmosphere.

8. Final weighing (M_3): Weigh the crucible and the sample.
9. Crucible preparation for next experiment: Burn off any residue from the empty crucible before using it in the next experiment.

Formula used in this analysis

$$\%Moisture = \frac{M_2 - M_3}{M_2 - M_1} x100$$

$$\%Ash = \frac{M_3 - M_4}{M_2 - M_1} x100$$

$$\%Volatile = \left(\frac{M_2 - M_3}{M_2 - M_1} x100\right) - \%Moisture$$

$$\%Fixed\ Carbon = 100 - \%Moisture - \%Ash - \%Volatile$$

Appendix B Standard chemicals

Standard chemicals employed for quantifying components in liquid products obtained from pyrolysis and gasification processes

No.	Chemicals	Purity (%)	Formula	Molecular weight
1	1,1'-Biphenyl, 3-methyl	97.9	$C_{13}H_{12}$	168.23
2	1,2-dimethoxybenzene	99.98	$C_8H_{10}O_2$	138.16
3	1,3-benzodioxole	99.9	$C_7H_6O_2$	122
4	11H-Benzo[b]fluorene	98.2	$C_{17}H_{12}$	216.28
5	1-methoxy-4-methylbenzene	99.8	$C_8H_{10}O$	122.16
6	2(5H)-Furanone	98.7	$C_4H_4O_2$	84.07
7	2,3-dihydrobenzofuran	99.9	C_8H_8O	120.15
8	2,4-dimethylphenol	99.99	$C_8H_{10}O$	122.16
9	2,4-xylenol	98	$C_8H_{10}O$	122.16
10	2,5-dimethylphenol	99.99	$C_8H_{10}O$	122.16
11	2,5-Hexadione	99.7	$C_6H_{10}O_2$	114.14
12	2,6-dimethoxyphenol	99.1	$C_8H_{10}O_3$	154.16
13	2,6-dimethylphenol	99.82	$C_8H_{10}O$	122.16
14	2′,4′-Dimethoxyacetophenone	97	$C_{10}H_{12}O_3$	180.2
15	2-cyclopenten-1-one	98.6	C_5H_6O	82.1
16	2-methoxy-4-vinylphenol	99.6	$C_9H_{10}O_2$	150.17
17	2-methoxy-5-methylphenol	98	$C_8H_{10}O_2$	138.16
18	2-methoxytoluene	98.99	$C_8H_{10}O$	122.16
19	3-hydroxy-2-butanone	95	$C_8H_{16}O_4$	176.22
20	4-ethylguaiacol	98	$C_9H_{12}O_2$	152.19
21	4H-Cyclopenta[def]phenanthrene	98.9	$C_{15}H_{10}$	190.24
22	4-methylcatechol	99.8	$C_7H_8O_2$	124.14
23	4-methylguaiacol	99.5	$C_8H_{10}O_2$	138.16
24	4-methylmethoxybenzene	99.4	$C_8H_{10}O$	122.16
25	5-hydroxymethylfurfural	99.9	$C_6H_6O_3$	126.11
26	5-methylfurfural	97.7	$C_6H_6O_2$	110.11
27	Acenaphthylene	91.7	$C_{12}H_8$	152.19

28	Acephenanthrylene	98	$C_{16}H_{10}$	202.25
29	Acetaldehyde	99.97	C_2H_4O	44.05
30	Acetic acid	99.79	$C_2H_4O_2$	60.05
31	Acetol	99	$C_3H_6O_2$	74.08
32	Acetosyringone	97	$C_{10}H_{12}O_4$	196.2
33	Anthracene	98.6	$C_{14}H_{10}$	178.23
34	Anthracene, 2-methyl	98.6	$C_{15}H_{12}$	192.26
35	Apocynin	97.7	$C_9H_{10}O_3$	166.17
36	Benz[a]anthracene	99.98	$C_{18}H_{12}$	228.29
37	Benzaldehyde	99.5	C_7H_6O	106.12
38	Benzene	99.99	C_6H_6	78.11
39	Benzo[a]pyrene	96	$C_{20}H_{12}$	252.31
40	Benzofuran	99.9	C_8H_6O	118.13
41	Biphenyl	99.99	$C_{12}H_{10}$	154.21
42	Butanoic acid	99.99	$C_4H_8O_2$	88.11
43	Catechol	99.8	$C_6H_6O_2$	110.11
44	Chrysene	97.4	$C_{18}H_{12}$	228.29
45	Cyclopenta[cd]pyrene	97.7	$C_{18}H_{10}$	226.27
46	Decahydronaphthalene	99	$C_{10}H_{18}$	138.25
47	Dibenzofuran	99.99	$C_{12}H_8O$	168.19
48	Dibenzofuran, 4-methyl	99.99	$C_{13}H_{10}O$	182.22
49	Ethylbenzene	99.9	C_8H_{10}	106.17
50	Eugenol	99	$C_{10}H_{12}O_2$	164.2
51	Fluoranthene	98.2	$C_{16}H_{10}$	202.25
52	Fluoranthene, 2-methyl	98.2	$C_{17}H_{12}$	216.28
53	Fluorene	98.2	$C_{13}H_{10}$	166.21
54	Formic acid	97.9	CH_2O_2	46.03
55	Furfural	99.6	$C_5H_4O_2$	96.08
56	Furfural alcohol	99.1	$C_5H_6O_2$	98.1
57	Glycolaldehyde	95	$C_2H_4O_2$	60.05
58	Glycolaldehyde dimer	99.1	$C_4H_8O_4$	120.1
59	Guaiacol	99.1	$C_7H_8O_2$	124.14
60	Hexanal	98	$C_6H_{12}O$	100.16
61	Hydroquinone	99.9	$C_6H_6O_2$	110.11

62	Indene	99.5	C_9H_8	116.16
63	Isoamyl ether	99	$C_{10}H_{22}O$	158.28
64	Levoglucosan	99.95	$C_6H_{10}O_5$	162.14
65	Maltol	99.9	$C_6H_6O_3$	126.11
66	Methanol	99.99	CH_4O	32.04
67	Methoxybenzene	99.9	C_7H_8O	108.14
68	Methyl laurate	99.5	$C_{13}H_{26}O_2$	214.34
69	Naphthalene	99.9	$C_{10}H_8$	128.17
70	Naphthalene, 1-methyl	99.9	$C_{11}H_{10}$	142.2
71	Naphthalene, 2-methyl	99.9	$C_{11}H_{10}$	142.2
72	o/m-cresol	99.99	C_7H_8O	108.14
73	o/m-xylene	99.98	C_8H_{10}	106.17
74	p-cresol	99.98	C_7H_8O	108.14
75	Phenanthrene	99.5	$C_{14}H_{10}$	178.23
76	Phenanthrene, 4-methyl	99.5	$C_{15}H_{12}$	192.26
77	Phenol	99.8	C_6H_6O	94.11
78	Propanol	99.6	C_3H_6O	58.08
79	Propanoic acid	99.5	$C_3H_6O_2$	74.08
80	p-xylene	99.7	C_8H_{10}	106.17
81	Pyrazine	99.99	$C_4H_4N_2$	80.09
82	Pyrene	98.2	$C_{16}H_{10}$	202.25
83	Pyrene, 1-methyl	98.2	$C_{17}H_{12}$	216.28
84	Syringylaldehyde	99.9	$C_9H_{10}O_4$	182.17
85	Toluene	99.5	C_7H_8	92.14
86	Vanillin	99.7	$C_8H_8O_3$	152.15

Analytical Method (Christensen et al., 2016)

Creating the standard solution

1. In a 1.0 mL graduated flask, accurately weigh about 1.2 mg of 1-octanol. Note the weights to the nearest 0.1 mg.
2. Top up the flask to its calibration line using acetonitrile. To ensure thorough mixing, invert the flask at least three times, then transfer the solution into a marked 250 mL container. Store this solution in a freezer when it is not being used.

Formulation of the Combined Standard Stock

1. In a pre-weighed 25 mL volumetric flask, accurately weigh each standard compound into the volumetric flask.
2. After adding all compounds, fill the flask to its marked line with acetonitrile and secure the stopper. Place the flask in an ultrasonic bath at 25 °C and sonicate for 5 minutes or until the dissolution of all compounds is complete.
3. Invert the flask at least three times to ensure proper mixing, then pour the solution into a marked 30 mL container. Store this solution in a freezer when not in use.

Creation of Calibration Standards

1. Employ gas-tight syringes to introduce specified volumes of the stock mixed standard, internal standard solution, and acetonitrile into clearly labelled GC autosampler vials.
2. Seal these vials promptly after adding the solutions and solvent to avert evaporation. It's important to maintain the relative proportions of each component, although the total volumes can be adjusted as needed

Curve point	1	2	3	4	5	6	7	8
Stock standard, µL	25	50	75	100	250	500	750	1000
Internal standard, µL	100	100	100	100	100	100	100	100
Acetonitrile, µL	975	950	925	900	750	500	250	0

3. Once each solution has been added and the vials are securely capped, ensure to thoroughly shake each vial for effective mixing.

Sample Preparation Process

1. Begin by weighing roughly 400 mg of the sample into a marked 8 mL vial. Using a gas-tight syringe, introduce 500 µL of the internal standard solution. Then, add 5 mL of acetonitrile with a Class A volumetric pipette. Vigorously shake the mixture to ensure complete dissolution of the bio-oil.
2. For assessing the consistency of sample preparation, prepare at least one sample in triplicate per set of samples, or one per every ten samples when dealing with larger batches.
3. Next, place the diluted samples in an ultrasonic bath. Sonicate them at 30 °C for 20 minutes to achieve complete dissolution. Be aware that the sample may develop a precipitate due to the presence of insoluble polymeric materials.
4. Finally, transfer the diluted sample into a labelled 1.5 mL GC autosampler vial and securely seal it. In cases where a precipitate is observed, first pass the sample through a

0.45 μm syringe filter using a 5 mL disposable syringe, then transfer the filtered sample into the autosampler vial.

Appendix C Regression equations

H_2 (vol%) = -190.6 + 0.1318 1st stage Temp (C) + 0.4124 2nd stage Temp (C)
+ 5.89 S/C (mol/mol) + 0.0375 CO_2 conc.(vol% of CO_2 in carrier)
- 0.000111 1st stage Temp (C)*1st stage Temp (C)
- 0.000237 2nd stage Temp (C)*2nd stage Temp (C) - 1.2374 S/C (mol/mol)*S/C (mol/mol)
+ 0.000032 CO_2 conc.
(vol% of CO_2 in carrier)*CO_2 conc.(vol% of CO_2 in carrier)
+ 0.000009 1st stage Temp (C)*2nd stage Temp (C)
- 0.00172 1st stage Temp (C)*S/C (mol/mol) - 0.000009 1st stage Temp (C)*CO_2 conc.
(vol% of CO_2 in carrier) + 0.00651 2nd stage Temp (C)*S/C (mol/mol)
- 0.000032 2nd stage Temp (C)*CO_2 conc.(vol% of CO_2 in carrier)
- 0.00204 S/C (mol/moll)*CO_2 conc.(vol% of CO_2 in carrier)

H_2 (mg/g RDF) = -763 + 0.598 1st stage Temp (C) + 1.375 2nd stage Temp (C)
+ 12.46 S/C (mol/mol) - 0.006 CO_2 conc.(vol% of CO2 in carrier)
- 0.000537 1st stage Temp (C)*1st stage Temp (C)
- 0.000804 2nd stage Temp (C)*2nd stage Temp (C) - 3.860 S/C (mol/moll)*S/C (mol/mol)
- 0.000540 CO_2 conc.
(vol% of CO_2 in carrier)*CO_2 conc.(vol% of CO_2 in carrier)
+ 0.000068 1st stage Temp (C)*2nd stage Temp (C)
+ 0.00139 1st stage Temp (C)*S/C (mol/mol)
- 0.000061 1st stage Temp (C)*CO_2 conc.(vol% of CO_2 in carrier)
+ 0.02274 2nd stage Temp (C)*S/C (mol/mol)
+ 0.000171 2nd stage Temp (C)*CO2 conc.(vol% of CO_2 in carrier)
- 0.0077 S/C (mol/moll)*CO_2 conc.(vol% of CO_2 in carrier)

CO_2 (mg/g RDF) = -2255 - 3.41 1st stage Temp (C) + 8.70 2nd stage Temp (C) + 71 S/C (mol/mol) + 6.91 CO_2 conc.(vol% of CO_2 in carrier) + 0.00310 1st stage Temp (C)*1st stage Temp (C) - 0.00485 2nd stage Temp (C)*2nd stage Temp (C) - 39.70 S/C (mol/moll)*S/C (mol/mol) + 0.0016 CO_2 conc.(vol% of CO2 in carrier)*CO_2 conc.(vol% of CO_2 in carrier) - 0.00058 1st stage Temp (C)*2nd stage Temp (C) + 0.007 1st stage Temp (C)*S/C (mol/mol) + 0.00185 1st stage Temp (C)*CO_2 conc. (vol% of CO_2 in carrier) + 0.3573 2nd stage Temp (C)*S/C (mol/mol) - 0.01170 2nd stage Temp (C)*CO_2 conc.(vol% of CO_2 in carrier) - 0.394 S/C (mol/mol)*CO_2 conc.(vol% of CO2 in carrier)

H_2/CO (mol/mol) = -6.71 - 0.00742 1st stage Temp (C) + 0.02304 2nd stage Temp (C)
+ 0.342 S/C (mol/mol) + 0.0226 CO2 conc.(vol% of CO_2 in carrier)
+ 0.000006 1st stage Temp (C)*1st stage Temp (C)
- 0.000013 2nd stage Temp (C)*2nd stage Temp (C) - 0.08154 S/C (mol/mol)*S/C (mol/mol)
+ 0.000004 CO_2 conc.
(vol% of CO_2 in carrier)*CO_2 conc.(vol% of CO2 in carrier)
+ 0.000001 1st stage Temp (C)*2nd stage Temp (C)
- 0.000385 1st stage Temp (C)*S/C (mol/mol) + 0.000007 1st stage Temp (C)*CO_2 conc.
(vol% of CO_2 in carrier) + 0.000777 2nd stage Temp (C)*S/C (mol/mol)
- 0.000033 2nd stage Temp (C)*CO2 conc.(vol% of CO_2 in carrier)
- 0.001041 S/C (mol/mol)*CO_2 conc.(vol% of CO_2 in carrier)

CCE (%) = -10.4 - 0.0190 1st stage Temp (C) + 0.2259 2nd stage Temp (C)
+ 2.568 S/C (mol/mol) + 0.0003 CO2 conc.(vol% of CO2 in carrier)
+ 0.000012 1st stage Temp (C)*1st stage Temp (C)
- 0.000129 2nd stage Temp (C)*2nd stage Temp (C) - 0.5340 S/C (mol/mol)*S/C (mol/mol)
- 0.000202 CO_2 conc. (vol% of CO_2 in carrier)*CO_2 conc.(vol% of CO2 in carrier)
+ 0.000007 1st stage Temp (C)*2nd stage Temp (C)
+ 0.00006 1st stage Temp (C)*S/C (mol/mol) + 0.000031 1st stage Temp (C)*CO_2 conc.
(vol% of CO_2 in carrier) + 0.002842 2nd stage Temp (C)*S/C (mol/mol)
+ 0.000044 2nd stage Temp (C)*CO_2 conc.(vol% of CO_2 in carrier)
- 0.00467 S/C (mol/mol)*CO_2 conc.(vol% of CO_2 in carrier)

CGE (%) = -109.0 + 0.036 1st stage Temp (C) + 0.3527 2nd stage Temp (C)
+ 8.65 S/C (mol/mol) - 0.184 CO_2 conc.(vol% of CO_2 in carrier)
- 0.000054 1st stage Temp (C)*1st stage Temp (C)
- 0.000193 2nd stage Temp (C)*2nd stage Temp (C) - 0.510 S/C (mol/mol)*S/C (mol/mol)
- 0.000250 CO_2 conc.(vol% of CO_2 in carrier)*CO_2 conc.(vol% of CO2 in carrier)
+ 0.000049 1st stage Temp (C)*2nd stage Temp (C)
- 0.00017 1st stage Temp (C)*S/C (mol/mol) - 0.000027 1st stage Temp (C)*CO_2 conc.
(vol% of CO_2 in carrier) - 0.01203 2nd stage Temp (C)*S/C (mol/mol)
+ 0.000312 2nd stage Temp (C)*CO_2 conc.(vol% of CO_2 in carrier)
- 0.00437 S/C (mol/mol)*CO_2 conc.(vol% of CO_2 in carrier)

PE (%) = -208.5 + 0.075 1st stage Temp (C) + 0.5416 2nd stage Temp (C)
+ 9.75 S/C (mol/mol) - 0.104 CO_2 conc.(vol% of CO2 in carrier)
- 0.000101 1st stage Temp (C)*1st stage Temp (C)
- 0.000287 2nd stage Temp (C)*2nd stage Temp (C) - 1.8187 S/C (mol/mol)*S/C (mol/mol)
- 0.000217 CO_2 conc.
(vol% of CO_2 in carrier)*CO_2 conc.(vol% of CO_2 in carrier)
+ 0.000017 1st stage Temp (C)*2nd stage Temp (C)
+ 0.00360 1st stage Temp (C)*S/C (mol/mol) - 0.000030 1st stage Temp (C)*CO_2 conc.
(vol% of CO_2 in carrier) - 0.00146 2nd stage Temp (C)*S/C (mol/mol)
+ 0.000212 2nd stage Temp (C)*CO_2 conc.(vol% of CO_2 in carrier)
- 0.00630 S/C (mol/mol)*CO_2 conc.(vol% of CO_2 in carrier)

Appendix D Database used in the processes in the LCA

Processes	**Reference units**	**Based on Ecoinvent database or else**
Steam methane reforming	1 kg of H_2	hydrogen production, steam reforming, 3.9.1, cutoff, RER
Conventional coal gasification	1 kg of H_2	(Wiatowski and Kapusta, 2020, Ocampo et al., 2003, Pohořelý et al., 2006)
Conventional biomass gasification	1 kg of H_2	(Li et al., 2004)
Conventional municipal solid waste gasification	1 kg of H_2	(Arena et al., 2010)
Partial oxidation of oil products (POX)	1 kg of H_2	hydrogen cracking, APME, 3.9.1, cutoff, RoW
Electrolysis (PEM)	1 unit	fuel cell production, polymer electrolyte membrane, 2kW electrical, future, 3.9.1, cutoff, RoW
Electricity from coal	1 kWh	heat production, wood chips from industry, at furnace 1000kW, state-of-the-art 2014, 3.9.1, cutoff, RoW
Heat from biomass	1 MJ	heat production, wood chips from industry, at furnace 1000kW, state-of-the-art 2014, 3.9.1, cutoff, RoW
Heat from waste	1 MJ	heat, from municipal waste incineration to generic market for heat district or industrial, other than natural gas, 3.9.1, cutoff, RoW

Electricity from wind	1 kWh	electricity production, wind, >3MW turbine, offshore, 3.9.1, cutoff, RoW
Electricity from solar	1 kWh	electricity production, solar thermal parabolic trough, 50 MW, 3.9.1, cutoff, RoW
Electricity from nuclear	1 kWh	electricity production, nuclear, pressure water reactor, 3.9.1, cutoff, RoW
Ship-transportation	1 ton*km	transport, freight, sea, container ship, 3.9.1, cutoff, RoW
Transportation	1 ton*km	transport, freight, lorry, all sizes, EURO4 to generic market for transport, freight, lorry, unspecified, 3.9.1, cutoff, RoW
Compression	1 m^3	compressed air production, 1000 kPa gauge, <30kW, optimised generation, 3.9.1, cutoff, RoW
PSA	1 m^3	biogas purification to biomethane by pressure swing adsorption, 3.9.1, cutoff, RoW
Flu gas treatment	1 MJ	treatment of coal gas, in power plant, 3.9.1, cutoff, RoW
Pelletisation	1 kg	wood pellet production, 3.9.1, cutoff, RoW
Steam production	1 kg	steam production, in chemical industry, 3.9.1, cutoff, RoW

Plant unit	1 unit	chemical factory construction, organics, 3.9.1, cutoff, RoW